# **UNCLASSIFIED**

# AD NUMBER AD841155 LIMITATION CHANGES TO: Approved for public release; distribution is unlimited. FROM: Distribution authorized to U.S. Gov't. agencies and their contractors; Administrative/Operational Use; AUG 1968. Other requests shall be referred to Air Force Flight Dynamics Lab., Wright-Patterson AFB, OH 45433. AUTHORITY AFFDL ltr 29 Oct 1973

# AD 841155

AFFDL-TR-68-2

# STRUCTURAL-ACOUSTIC RESPONSE, NOISE TRANSMISSION LOSSES AND INTERIOR NOISE LEVELS OF AN AIRCRAFT FUSELAGE EXCITED BY RANDOM PRESSURE FIELDS

J. A. COCKBURN A. C. JOLLY

Wyle Laboratories Research Staff Huntsville, Alabama

TECHNICAL REPORT AFFDL-1R-68-2

**AUGUST 1968** 



This document is subject to special export controls and each transmittal to foreign governments or foreign nationals may be made only with prior approval of the Air Force Flight Dynamics Laboratory, FDDA, Wright-Patterson Air Force Base, Ohio 45433.

AIR FORCE FLIGHT DYNAMICS LABORATORY AIR FORCE SYSTEMS COMMAND WRIGHT-PATTERSON AIR FORCE BASE, OHIO

### NOTICE

When Government drawings, specifications, or other data are used for any purpose other than in connection with a definitely related Government procurement operation, the United States Government thereby incurs no responsibility nor any obligation whatsoever; and the fact that the Government may have formulated, furnished, or in any way supplied the said drawings, specifications, or other data, is not to be regarded by implication or otherwise as in any manner licensing the holder or any other person or corporation, or conveying any rights or permission to manufacture, use, or sell any patented invention that may in any way be related thereto.

This document is subject to special export controls, and each transmittal to goreign governments or foreign nationals may be made only with prior approval of the AF Flight Dynamics Laboratory (FDDA), Wright-Patterson AFB, Ohio.

The distribution of this report is limited because it contains design methods for aircraft.



Copies of this report should not be returned unless return is required by security considerations, contractual obligations, or notice on a specific document.

200 - Sept. 1968 - CO455 - 51-1129

# BLANK PAGE

# STRUCTURAL-ACOUSTIC RESPONSE, NOISE TRANSMISSION LOSSES AND INTERIOR NOISE LEVELS OF AN AIRCRAFT FUSELAGE EXCITED BY RANDOM PRESSURE FIELDS

J. A. COCKBURN

A. C. JOLLI

This document is subject to special export controls and each transmittal to foreign governments or foreign nationals may be made only with prior approval of the Air Force Flight Dynamics Laboratory, FDDA, Wright-Patterson Air Force Base, Ohio 45433.

#### FOREWORD

The research effort reported herein was performed by the Testing Division of Wyle Laboratories, Huntsville, Alabama for the Aero-Acoustics Branch, Vehicle Dynamics Division, Air Force Flight Dynamics Laboratory, Wright-Patterson Air Force Base, Ohio, under Contract F33(615)-67-C-1287. This contract was initiated under Project 1471, "Aero-Acoustic Problems", Task 147102, "Prediction and Control of Noise." The work described herein, a part of Air Force Systems Command's exploratory development program, was undertaken to provide methods to predict and control the aero-acoustic environment of flight vehicles. Mr. D. L. Smith is the project engineer.

This report covers work performed during the period of January 1967 to January 1968 and concludes the work on Contract F33(615)-67-C-1287. Previous work also conducted under this contract provided a prediction method for noise generated in turbulent boundary layers. It is presented in AFFDL-TR-67-167 entitled "Prediction of Boundary Layer Pressure Fluctuations."

The authors wish to extend their appreciation to the following members of the Wyle Research Staff: Mr. R. W. White, for contributions to the coupled response theory; Mr. R. C. Potter, for his contribution to the jet noise theory; Dr. M. V. Lowson, for the work on boundary layer turbulence; Dr. B. Sharp for his contribution in the sound transmission and noise reduction areas; Dr. C. A. Mercer, for assistance in developing the computer program for the determination of the panel group natural frequencies; and to Messrs. D. J. Bozich, Principal Investigator for this contract and L. C. Sutherland, Director of Huntsville Research Staff, for their valued advice and encouragement throughout the course of this research.

The Wyle Laboratories Report Number is WR 67-16. The manuscript was released by the authors in April 1968 for publication.

This technical report has been reviewed and is approved.

Valle of Bushylow WALTER J. MIKYTOW

Asst. for Research & Technology Vehicle Dynamics Division

AF Flight Dynamics Laboratory

#### **ABSTRACT**

A theoretical and empirical study of the structural-acoustic response and sound transmission properties of fuselage structures is described. The external fluctuating pressure environments discussed are boundary layer turbulence, jet noise and reverberant acoustic fields. In order to investigate the complete behavior of the fuselage, equivalent structural models are analyzed whose combined characteristics represent the complex fuselage structure throughout the entire frequency response range of interest. The structure and interior sound field are treated throughout as a coupled dynamic system whose response is describable in terms of the system's normal modes. Prediction methods are developed for structural responses, noise reduction and internal acoustic fields of untreated and acoustically treated fuselage structures. The results of this study have been programmed for computer solution, thus allowing the significant parameters affecting sound transmission to be determined. In addition to the computer programs, empirical design charts are presented for carrying out pre-design estimates of the external fluctuating loads due to boundary layer turbulence and jet noise and overall noise reduction of typical acoustic treatments.

# TABLE OF CONTENTS

SECTION			PAGE	
I.	INTRODUCTION			
II.	DESCR	EFTION OF THE FUSELAGE STRUCTURE	3	
	1.	Equivalent Structural Models	3	
		a. Low Frequency Range	3	
		b. High Frequency Range	3	
		c. Intermediate Frequency Range	4	
		d. Special Case of a Double-Walled Fuselage	4	
		e. Acoustic Treatment	7	
	2.	Mode Shapes and Natural Frequencies	8	
		a. Circular Stiffened Cylinder	8	
		b. Simply-Supported Panel	13	
		c. Panel Group	16	
	LIST	OF SYMBOLS USED IN SECTION II	24	
· п.		CTURAL-ACOUSTIC COUPLING OF THE FUSELAGE ID THE CABIN VOLUME	27	
	1.	Coupling of the Overali, or Low Frequency, Modes	27	
		a. The Internal Acoustic Field	27	
		b. Response of the Dynamically Coupled System	34	
		<ul> <li>Total Response of the Coupled System to External Fluctuating Pressure Fields</li> </ul>	36	
		d. Computation of the Internal Acoustic Field from the Structural Response	40	
	2.	Coupling of the Individual Panel, or High Frequency, Modes	44	
		a. The Internal Acoustic Field Induced by Arbitrary	44	

SECTION				PAGE
		ь.	Rigid Shell With a Single Radial Piston	52
		c.	Rigid Shell With Two or More Radia! Pistons	52
		d.	Computation of the Internal Acoustic Field from the Structural Response	53
	3.	Cou	pling of the Intermediate Modes	56
	LIST	OF SY	MBOLS USED IN SECTION III	57
IV.			ristics of the fluctuating pressure nments	61
	1.	Aero	odynamic Turbulence	61
		c.	Overall Level	61
		Ь.	Spectral Distribution	63
		c.	Narrow-Band Space Correlation Coefficients	65
		d.	Correlation Length and Coincidence	69
	2.	The	Jet Noise Environment	70
		α.	Introduction	<i>7</i> 0
		Ь.	Overall Acoustic Power Level	71
		c.	Frequency Spectra	<i>7</i> 2
		d.	Prediction of the Free-Field Sound Pressure Levels	<i>7</i> 3
		e.	Pressure Levels on Fuselage Structures	75
		f.	Narrow-Band Pressure Correlation Patterns	<i>7</i> 8
		9.	Correlation Length	82
	3.	Reve	erberant Acoustic Field Environment	83
		a.	Equivalent Reverberant Field, Overall Level and Frequency Spectra	83
		Ь.	Narrow-Band Pressure Correlation Coefficients	83
		c.	Correlation Length	85

SECTION					PAGE
	LIST C	OF SY	MBOL	S USED IN SECTION IV	86
٧.	THE RESPONSE EQUATIONS				89
	1.	Resp	onse o	f the Overal! Fuselage Modes	<b>8</b> 9
		a.	•	lacement and Acceleration Power Spectral	89
		b.	Join	t Acceptances for the Various Environments	98
			(1)	Boundary Layer Turbulence	102
			(2)	Reverberant Acoustic Field	103
			(3)	Jet Noise	105
	2.	Resp	onse o	f the Individual Panel Modes	107
		a.		lacement and Acceleration Power Spectral ensities	107
		Ь.	Join	t Acceptances for the Various Environments	109
			(1)	Boundary Layer Turbulence	110
			(2)	Reverberant Acoustic Field	111
			(3)	Jet Noise	113
	3.	Resp	onse o	of the Panel Group Modes	114
		a.		Placement and Acceleration Power Spectral ensities	114
		ь.	Join	at Acceptances for the Various Environments	118
			(1)	Boundary Layer Turbulence	118
			(2)	Reverberant Acoustic Field	119
			(3)	Jet Noise	119
	LIST (	OF SY	MBOL	S USED IN SECTION V	120

SEC1101	4		PAGE
VI.	NOI	se reduction	124
	1.	Introduction	124
	2.	Derivation of Transmission Coefficient for Multi-Layered Acoustic Treatment	125
		a. Pressure Ratio Across A Single Pane!	126
		b. Pressure Ratio Across a Septum	127
		c. Pressure Ratio Across a Porous Blanket	128
		d. Pressure Ratio Across an Airgap	129
		e. Determination of Overall Transmission Coefficient	130
	3.	Computation of Noise Reduction Using the Modal Approach	130
		<ul> <li>a. Increase in Transmission Loss Through the Acoustic Treatment</li> </ul>	130
		<ul> <li>Increase in Noise Reduction Due to Internal Absorption</li> </ul>	132
	4.	Computation of Noise Reduction for a Diffuse Internal Sound Field	134
	5.	Equivalent Reverberant Field	13∈
	6.	The Effect of Flanking Transmission	138
	7.	Transmission Loss Through Isolated Capsule Compartments	140
	8.	Panel Damping Material	141
	9.	Summary	143
		a. Modal Method	144
		b. Diffuse Field Method	744

SECTION	1		PAGE
	LIST OF SYMBO	DLS USED IN SECTION VI	146
VII.	DISCUSSION		149
	APPENDIX I.	GENERA ON OF THE ACOUSTIC- STRUCTURE COUPLING OF CYLINDRICAL SHELLS AND INTERNAL ACOUSTIC FIELDS	152
	APPENDIX II.	THE COMPUTER PROGRAM	170
	APPENDIX III.	DESIGN CHARTS	219
	APPENDIX IV.	PRESSURE RATIOS AND INPUT IMPEDANCES FOR ACOUSTIC TREATMENT	233
	REFÉRENCES		239

### LIST OF ILLUSTRATIONS

FIGURE		PAGE
1	Double-Wall Fuselage; Low Frequency Model	245
2	Double-Wall Fuselage; High Frequency Model	245
3	Geometry of the Reinforced Cylindrical Shell	246
4	Geometry and Coordinate Axes of the Panel Group	247
5	Panel Group; Stringer Details	248
6	Resonant Deflection Shapes of a Cylindrical She!!	249
7	Typical Circumferential and Racial Acoustic Wave Patterns and the Corresponding Circumferential Structural Wave Patterns	250
8	Rigid Shell with a Single Radial Piston	251
9	Graph of Radial Displacement of a Rigid Shell with Radial Pistons	252
10	Rigid Shell with Two or More Radial Pistons	253
11	Fluctuating Pressure Non-Dimensionalized by Dynamic Head Versus Mach Number	254
12	Fluctuating Pressure Non-Dimensionalized by Wall Shear Stress Versus Mach Number	255
13	Comparison of Empirical Curve with Data From Bies	256
14	Comparison of Pressure Fluctuation Spectra	257
15	Narrow-Band Longitudinal Space Correlation Coefficient for Boundary Layer Turbulence	258
16	Narrow-Band Lateral Space Correlation Coefficient for Boundary Layer Turbulence	259
17	Narrow-Band Longitudinal Space-Time Correlation Coefficients for Wall Pressure Field from Boundary Layer Turbulence	260
18	Narrow-Band Lateral Space-Time Correlation Coefficients for Wall Pressure Field from Boundary Layer Turbulence	261
19	Turbulent Boundary Layer Convection Velocity Derived from Narrow-Band Longitudinal Space-Time Correlation Measurements	262
20	Asymptotic Values of Narrow-Band Longitudinal Pressure Correlation Coefficient at $[\omega \zeta/U_c(\omega)] = 0$	263
21	Asymptotic Values of Narrow-Band Lateral Pressure Correlation	<b>0</b> / /

# LIST OF ILLUSTRATIONS (Continued)

FIGURE		PAGE
22	Comparison of Longitudinal, Broadband Correlation Coefficients at	265
	Two Mach Numbers	266
23	Jet Noise Fields	200
24	Overall Jet Sound Power Per Unit Nozzle Area Versus Exhaust Velocity	267
25	Spectrum of Overall Sound Produced by a Jet	268
26	Normalized Power Spectra in Core Region	269
27	Normalized Power Spectra in Downstream Region	270
28	Overall Acoustic Power Per Unit Axial Distance and Per Unit Nozzle Area	271
29	Jet Geometry	272
30	Calculated Directivity as a Function of Position in the Jet with $\theta_i$ , the Angle from Upstream, as a Parameter	273
31	Fuselage and Engine	274
32	The Coardinate System; Wing-Mounted Engine	275
33	Geometry and Pressure Distribution; Fuselage-Mounted Engine	276
34	Narrow-Band Pressure Correlation Points	277
	Summary of Narrow-Band Longitudinal Correlation Data	278
35 24	Summary of Narrow-Band Lateral Correlation Data	279
36	Near Field Longitudinal Correlations	280
37 38	Numerical Values of the Constant B Appearing in the Longitudinal Correlation Coefficient;	
	$C(\zeta;\omega) = \exp\left[-0.0955 \frac{\omega \zeta}{c}\right] \cos\left\{\frac{B\omega \zeta}{c}\right\}$	281
39	Longitudinal Narrow-Band Correlation Coefficient; $C(\zeta;\omega) = e^{-0.0955} \left(\frac{\omega\zeta}{c}\right) \cdot \cos \beta \frac{\omega\zeta}{c}$	282
40	Narrow-Band Langitudinal Space Correlation Coefficient on the Surface of a Cylinder Immersed in a Reverberant Acoustic Field	283

### LIST OF ILLUSTRATIONS (Continued)

FIGURE		PAGE
41	Narrow-Band Longitudinal and Lateral Space Correlation Coefficients on the Surface of a Cylinder Immersed in a Reverberant Acoustic Field	284
42	Transformation of the Region of Integration for Joint Acceptances	285
43	Separation of the Behavior of a Typical Structure into Three Frequency Regions	286
44	Shell Resonances, $\omega_{mn}$ , and Coupled System Resonances, $\Omega_{mns}$ , for Axial Mode number m = 1	287
45	Shell Resonances, $\omega_{mn}$ , and Coupled System Resonances, $\Omega_{mns}$ , for Axial Mode number m = 12	288
46	Shell Resonances, $\omega_{mn}$ , and Coupled System Resonances, $\Omega_{mns}$ , for Axial Mode number m = 25	289
47	Boundary Layer Noise at a Position 40 Feet Along Fuselage	290
48	Jet Exhaust Noise Variation Along the Fuselage	291
49	Noise Reduction for the Untreated Fuselage	292
<i>5</i> 0	Incremental Transmission Loss of Acoustic Treatment and Interior Noise Reduction	293
51	Equivalent Reverberant Fields for Jet Noise and Boundary Layer Turbulence	295
52	Fuselage Internal Noise Levels due to Transmitted Boundary Layer Noise	296
53	Computer Program Organization	297
54	Conversion Chart for p <sub>rms</sub> /q to dB as a Function of Mach Number	298
55	Noise Sources as a Function of Aircraft Geometry and Speed	299
56	Conversion Chart for p <sub>rms</sub> /q to dB	300
<b>57</b>	Boundary Layer Thickness	301
58	Design Chart for Octave Band Sound Pressure Level Versus Nondimensional Center Frequency – Turbulent Boundary Layer Pressure Fluctuations	302
59	Overall Sound Field for J57-P21 Turbojet Engine at 100 Percent Military Power	303
60	Sound Field Grid in Nozzle Digmeters for J57-P21 Turbojet Engine	304

THE RESERVE OF THE PROPERTY OF

# LIST OF ILLUSTRATIONS (Continued)

FIGURE		PAGE
61	Relative Sound Pressure Levels in Octave Bands for J57–P21 Turbojet	305
62	Overall SPL Velocity Exponent Field	311
63	Effective Transmission Loss (Random Incidence)	312
<b>64</b>	Design Chart for the Change in Effective Transmission Loss of Single Untroated Panels to Include the Effect of Coincidence	313
65	Incremental Attenuation due to Adding the Absorbing Structure to the Basic Plate	314
66	Noise Reduction Versus Absorption Coefficient and Either Average Transmission Coefficient or Average Transmission Loss of Cabin Walls	319
67	Typical Acoustic Treatments	320
<b>68</b>	Calculated Combined Loss Factors for Three Typical Unconstrained Commercial Damping Materials Applied to a Uniform Aluminum Plate (Temp. 65°F, Frequency – 75 Hz)	321
69	Design Chart for Optimum Constrained Layer Damping Treatment	322
70	Variation of Combined Loss Factor with the Ratio; Weight of Treatment to Weight of Basic Plate	323

### LIST OF TABLES

TABLE		PAGE
I	Numerical Values of $\overline{R}_{ns}/\pi$ for $J_n^*(\overline{R}_{ns})=0$	324
11	Coefficients of the Rational Fraction Approximations for Sine and Cosine Integrals	325
Ш	Test Case Input Data	326
IV	Absorption Coefficients	328

# BLANK PAGE

# SECTION I

Cabin noise during cruising flight of modern aircraft is caused largely by vibration of the pressurized fuselage shell and floor. The fuselage vibrations are caused by a combination of air pressure fluctuations and forces of mechanical origin. The former find their source in propeller noise, turbojet or turbine exhaust and compressor waise, and in the turbulence of the air flow over the fuselage surface, while the latter derive mainly from the prime movers. The present trend towards almost complete dependence upon turbojet propulsion and rearward location of the power units alleviates the jet exhaust problem somewhat, but the boundary layer induced noise is unaffected by this trend. Supersonic cruising flight will tend to eliminate the jet noise problem but severely increase the boundary layer induced noise since the intensity of the pressure fluctuations increases approximately as the fourth power of the airspeed.

Cabin designs for minimum noise levels usually rely heavily on in-flight measurements in the first instance, and subsequent application of acoustic treatment to reduce the noise levels to meet some pre-determined cabin noise criteria; in other words, the noise problem is resolved after final structural design. The foregoing method has in the past been reasonably efficient in practice, but with current trends in aircraft design towards maximum structural efficiency, the need has arisen for optimization studies of the weight of acoustic treatment versus its effectiveness at the preliminary design stage.

Fundamental studies of sound transmission through fuselage structures have been largely concerned with the sound field radiated by single finite panels excited by boundary layer turbulence (References 1 - 6), and emphasis has been placed on the development of theoretical models for comparison with experimental results. However, the complete solution to the problem is much more complex since the interior sound field is set up by the response of the entire structural-pressurized cabin volume system to external pressure fluctuations.

The interaction between plane sound waves and a flexible structure was originally considered by Junger (Reference 7) in relation to the problem of sound scattering by thin elastic shells. Starting from the general solution of the wave equation and the Lagrange equations of the shell in vacuo, application of the boundary condition governing the radial particle deflection and expression of the exchange of energy between the shell and the medium in terms of generalized forces led to a solution for the scattered sound pressure, though the transmitted interior field was not discussed. More recently this work was extended by Foxwell and Franklin (Reference 8), who investigated the interior sound field set up in an infinitely long stiffened cylinder subjected to plane account on the effects of scattering, though the problem was solved for the two-dimensional case only.

In the present investigation the three-dimensional problem of a finite stiffened fuselage is studied by considering three equivalent structural models to represent the entire frequency range of interest. The response of the fuselage at low frequencies is determined by the characteristics of a stiffened cylindrical shell, while the fuselage responses at intermediate and high frequencies

are determined by the characteristics of a stiffened panel group and a single fuselage panel respectively; this structural equivalence according to frequency is compatible with the modal behavior of typical fuselage structures.

Studying each equivalent structural model in turn, the free vibration characteristics of the structural-acoustic coupled system are first derived and then expressions are developed for the internal sound pressure in terms of external fluctuating pressures. By adopting the classical modal analysis method, the power spectral density of the response is expressed in terms of the power spectral density of the external pressure fluctuations caused by boundary layer turbulence, jet noise, and reverberant acoustic fields. Thus, expressions for the internal sound field in terms of the structural response to external fluctuating pressure environments are defined. Finally, the noise reduction of the untreated fuselage structure is determined simply from the ratio of the power spectral densities of the internal acoustic field and the external pressure fluctuations. Adding this noise reduction to the incremental transmission loss of the acoustic treatment and computation of the absorption due to internal furnishings yields the overall noise reduction of the acoustically treated structure. Conversion of the power spectral density of the external pressure fluctuations to an equivalent reverberant field and subtraction of the overall noise reduction leads directly to the internal acoustic field. The noise reduction of the untreated fuselage is calculated simply from its transmission loss and the absorption of the bare metal walls and internal air volume. Fuseloge-acoustic treatment configurations discussed in this report, in addition to the bare fuselage, are; (1) bare fuselage with an inner structural wall, (2) bare fuselage with a single absorptive lining, (3) a composite structure consisting of bare fuselage, acoustical blankets, septa, air gaps and panels, and (4) a floating inner capsule suspended within and isolated from the main fuselage structure.

Computer programs have been developed for the determination of the applied fluctuating pressures, sound transmission losses, and interior acoustic fields occurring in the foregoing fuseloge-treatment configurations. The frequency range for each of the three structural models can be selected arbitrarily, so as to provide flexibility in analyzing responses and transmission losses, and involves some degree of overlap.

Since the geometry of the fuselage, properties of the acoustic treatments, and aircraft flight configuration are variable input parameters, these programs may be used to determine the significant parameters affecting sound transmission loss and thus to optimize acoustic treatments within the scope of specific structural design variations. Of particular importance here is the ability to perform optimization studies with regard to the weight of acoustic treatment versus overall noise reduction.

In addition to the computer programs, a number of preliminary design charts are presented in Appendix III for determining; (1) the active-band sound pressure levels due to boundary layer turbulence and jet noise, (2) the incremental transmission losses for a number of typical acoustic treatments, (3) absorption of internal furnishings, and (4) overall noise reduction. These charts provide a means of carrying out simple pre-design calculations prior to a more detailed investigation using the computer programs.

#### SECTION II

### DESCRIPTION OF THE FUSELAGE STRUCTURE

In this section a brief description of the structural design details of a typical fuselage is presented. Since the classical modal analysis method is adopted to treat a complex coupled fuselage – internal air mass system, it is necessary to have certain structural idealizations, or equivalents, in order that the entire frequency range of interest can be accurately represented. Once the equivalent structures are defined, the free vibration characteristics are determined, namely, the mode shapes, generalized masses and the resonant frequencies.

### 1. EQUIVALENT STRUCTURAL MODELS

A typical fuselage structure can be considered ideally as a closed-ended circular cylindrical shell uniformly reinforced by transverse ring frames and longitudinal stringers. Further stiffening is provided by the floor section, which runs the whole length of the fuselage, and by the in-plane stresses introduced by any pressure differential which exists across the fuselage wall. Temperature stresses introduced by aerodynamic heating are ignored in the present study.

The characteristics of the vibratory modes of the fuselage are dependent, of course, on the excitation frequency and can generally be considered to fall into three groups covering the low, high and intermediate frequencies.

#### a. Low Frequency Range

This frequency range is dominated by overall fuselage modes, or modes having axial half wavelengths significantly larger than the distance between transverse ring frames. It will include the fuselage "breathing" modes, where the middle surface of the shell stretches, as well as the "radial – axial" modes, where both stretching and bending take place, having circumferential half wavelengths greater than the distance between stringers.

The equivalent structural model for this frequency range is therefore a closed circular shell reinforced by uniform, equi-spaced ring frames and stringers.

### b. High Frequency Range

This frequency range is dominated by individual panel modes, the transverse ring frames and longitudinal stringers acting as node points. The individual panel motion is substantially uncorrelated with its neighboring panels; thus the equivalent structural model for this frequency range is assumed to be a single panel simply supported at the ring frame and stringer boundaries. This model is particularly useful in determining the localized effects caused by windows and hatches in the fuselage walls.

### c. Intermediate Frequency Range

This frequency range has, of course, the overall modes as a lower bound and the individual panel modes as an upper bound. Typically it will be characterized by axial half wavelengths approaching the distance between ring frames and circumferential wavelengths greater than the distance between stringers. Panel motion for these modes will, unlike the high frequency region, be correlated over several panel bays and stringer bending and torsion will play a dominant role. Thus the equivalent structural model for the intermediate frequency region is represented by a group of panels with attached stringers and bounded by ring frames. Clarkson and Ford (Reference 9) have shown experimentally that for groups of panels the ring frames act as node points. The actual number of panels considered in any group will be a function of the typical correlation length for the particular fluctuating pressure environment. The correlation lengths associated with each fluctuating pressure environment considered in this investigation are discussed in detail in Section IV.

### d. Special Case of a Double-Walled Fuselage

It is of interest to consider the effects of an additional stiffening wall, placed inside the fuselage, on the sound transmission properties of the total structure. Provided that certain simplifying assumptions are acceptable, it is possible to consider the three structural models in an approximate manner.

### Low Frequency Model

It is assumed that the effects of the inner wall, shown diagrammatically in Figure 1, it can be accounted for by modifying the moments of inertia of the stiffeners (i.e., the coupling of adjacent panels formed between adjacent ring frames and stringers is effectively ignored). Thus the added structural wall has the following dimensions, per stiffener; thickness t, length  $\ell$ , and width d, where  $\ell$  and d are the ring frame and stringer pitches, respectively.

Consider first the case where the inner wall is absent. Then the relevant moments of inertia, about the stiffener shown in Figure 1, are I and the polar moment J. Now, by definition;

$$J = I_{xx} + I_{yy}$$
 (2.1)

Considering now, the addition of the inner wall, the above relationship will be modified to,

$$J' = I'_{xx} + I'_{yy}$$
 (2.2)

Thus, it is first necessary to evaluate  $I'_{xx}$  and  $I'_{yy}$  as follows:

$$I'_{xx} = I_{xx} + \frac{bt_0^3}{12} + bt_0\bar{x}^2$$
 (2.3)

$$I'_{yy} = I_{yy} + \frac{t_0 b^3}{12}$$
 (2.4)

where the symbols are as defined in Figure 1. Thus it follows that,

$$j' = J + \frac{bt_0^3}{12} + \frac{t_0b^3}{12} + bt_0\bar{x}^2$$
 (2.5)

Finally, the moments of inertia can be re-defined;

$$J_{s}^{i} = J_{s} + K_{1} \left[ \frac{dt_{0}^{3}}{12} + \frac{t_{0}d^{3}}{12} + dt_{0}\bar{x}^{2} \right]$$
 (2.6)

$$J_r' = J_r + K_2 \left[ \frac{\ell r_0^3}{12} + \frac{t_0 \ell}{12} + \ell r_0 \vec{x}^2 \right]$$
 (2.7)

$$I_{s}^{1} = I_{s} + K_{1} \left[ \frac{dr_{0}^{3}}{12} + dr_{0} \bar{x}^{2} \right]$$
 (2.8)

$$l_r' = l_r + K_2 \left[ \frac{\ell_0^3}{12} + \ell_0 \bar{x}^2 \right]$$
 (2.9)

where d and  $\boldsymbol{l}$  are the stringer and ring frame pitches, s and r denote stringer and ring frame,  $t_0$  denotes the thickness of the inner wall, and  $K_1$ ,  $K_2$  are

defined as;

$$K_1 = K_2 = t_0 = 0$$
 for a single fuselage wall

$$K_{2} = 0$$
,  $K_{1} = 1$  for a double wall, attachment to stringers only

$$K_2 = 1$$
,  $K_1 = 0$  for a double wall, attachment to ring frames only.

### High Frequency Model

In this frequency range a double panel model is used. It is emphasized however that this model is used only to define the motion of the fuselage wall at high frequencies and is not used in calculating transmission loss. Assuming that the motion of the double panel shown in Figure 2 can be considered as a single unit (a relatively crude assumption though it by-passes the complex problem of panel-ring frame - air volume coupling), the distance of the neutral axis from one of the outer faces is given by the expression

$$d_{o} = \frac{h \left( h_{o} - h/2 \right) + h_{i}^{2}/2}{h + h_{i}}$$
 (2.10)

where the symbols are defined by the geometry of Figure 2.

The in-plane extensional stiffness is defined by

$$K_e = E(h + h_1)$$
 per unit panel width and length for (2.11)

panels of the same material.

Now, the resonant frequencies of a simply-supported panel are given by,

$$\omega_{mn} = \pi^2 \sqrt{\frac{D}{\mu}} \left( \frac{m^2}{\alpha^2} + \frac{n^2}{b^2} \right)$$
(2.12)

where  $\mu$  = mass per unit area

and D = 
$$\frac{Eh^3}{12(1-v^2)}$$

The plate bending rigidity can be written in an equivalent form as,

$$D = \frac{EI}{(1-v^2)}$$

where

$$I = h \left[ h_o - d_o - \frac{h}{2} \right]^2 + h_1 \left[ d_o - \frac{h_1}{2} \right]^2$$
 (2.13)

in4 per inch width.

Thus the resonant frequencies of the equivalent plate are determined from the relation,

$$\omega_{mn} = \pi^2 \left[ \frac{m^2}{a^2} + \frac{n^2}{b^2} \right] \sqrt{\frac{EI}{\mu(1-\nu^2)}}$$
 (2.14)

where

$$\mu = \rho(h + h_1)$$
 for panels of the same material and I is determined from Equation (2.13).

### Intermediate Frequency Model

It is assumed that the effects of a double wall on the characteristics of this model can be determined by modifying the properties of the stiffeners in the same way as was done for the low frequency model.

### e. Acoustic Treatment

Since internal noise criteria are established largely from a consideration of the aircraft type and primary function, e.g., military, cargo, or commercial transport, a number of noise reduction methods, employing various accustic treatments, are available to the aircraft designer. The acoustic treatments considered in the present study are as follows:

(1) A single absorbing layer attached to the inside surface of the bare fuselage.

- (2) A composite layer consisting of the bare fuselage plus acoustical blankets, septa, air gaps and panels.
- (3) A floating inner capsule suspended within the main fuselage structure by springs.

The above three cases together with the bare fuselage and the special case of a double structural wall make a total of five cases of primary interest. The foregoing accustic treatment cases are dealt with more fully in Section VI.

# 2. MODE SHAPES AND NATURAL FREQUENCIES

### a. Circular Stiffened Cylinder

The geometry of a typical circular cylinder reinforced by ring frames and stringers is shown in Figure 3. If the cylinder is assumed to be simply supported at the ends then the radial and circumferential components of the mode shapes are given by;

Radial; 
$$\phi_{mn1}(\vec{x}, \vec{y}) = \sin m\pi \vec{x} \sin 2\pi n \vec{y}$$

$$\phi_{mn2}(\vec{x}, \vec{y}) = \sin m\pi \vec{x} \cos 2\pi n \vec{y}$$
(2.15)

Circumferential; 
$$\psi_{mn1}(\bar{x}, \bar{y}) = \sin m\pi \bar{x} \cos 2\pi n\bar{y}$$
 (2.16) 
$$\psi_{mn2}(\bar{x}, \bar{y}) = \sin m\pi \bar{x} \sin 2\pi n\bar{y}$$

where m = number of elastic half-waves along the cylinder axis (= 1, 2, 3, .....)

n = number of elastic full waves around the circumference

= 0 for breathing or extensional ring mode

1 for translational ring mode

= 2, 3, 4, ..... for circumferential bending modes.

 $x = axial coordinate <math>0 \le x \le L_x$ 

y = circumferential coordinate  $0 \le y \le L_v$ .

$$\bar{x} = \frac{x}{L_x}, 0 \le \bar{x} \le 1$$

$$\bar{y} = \frac{y}{L_y}, \quad 0 \leq \bar{y} \leq 1$$

L = Axial length of cylinder.

 $L_{\nu}$  = Circumferential length of cylinder =  $2\pi R$ .

R = Radius to the middle surface of the cylinder.

A single structural mode shape can be denoted by the pair of functions

$$\left[\phi_{\min}(\bar{x},\bar{y}),\psi_{\min}(\bar{x},\bar{y})\right]$$
 where (mni) is a triplet of integers with  $i=1$  or 2.

Orthogonality between two different modes (mni) and (rsj) is expressed by the relation;

$$\int_{\bar{\mathbf{x}}=0}^{1} \int_{\bar{\mathbf{y}}=0}^{1} \mu \left[ \phi_{mni}(\bar{\mathbf{x}}, \bar{\mathbf{y}}) \phi_{rsj}(\bar{\mathbf{x}}, \bar{\mathbf{y}}) + \psi_{mni}(\bar{\mathbf{x}}, \bar{\mathbf{y}}) \psi_{rsj}(\bar{\mathbf{x}}, \bar{\mathbf{y}}) \right] d\bar{\mathbf{x}} d\bar{\mathbf{y}} = 0 \quad (2.17)$$

provided that  $(mni) \neq (rsj)$ .

The mode shapes defined by equations (2.15) and (2.16) clearly satisfy this orthogonality condition.

Because of the symmetry of the cylinder cross-section there is no preferred location for the origin of the y-axis and thus the two sets of orthogonal ring modes,  $\sin 2\pi n \bar{y}$  and  $\cos 2\pi n \bar{y}$ , are required to specify the complete response of the ring modes. For a particular external loading of the cylinder, these two sets of ring modes will combine so as to produce a single set where the node points of the modes are determinable with respect to the loading. For example, a radial point force acting on the cylinder will cause the two sets of ring modes to combine, resulting in an anti-node at the point of force application, while a random pressure loading on the cylinder will cause the node points to rotate around the cylinder in a random fashion.

For each mode of vibration (mni), there is a generalized or effective modal mass  $M_{mni}$  which can be defined by the integral;

$$M_{\text{med}} = \mu A \int_{\bar{x}=0}^{1} \int_{\bar{y}=0}^{1} \left[ \left\{ \phi_{\text{mni}}(\bar{x}, \bar{y}) \right\}^{2} + \left\{ \psi_{\text{mni}}(\bar{x}, \bar{y}) \right\}^{2} \right] d\bar{x} d\bar{y}$$

$$= M_{0} \xi_{\text{mni}} \qquad (2.18)$$

where  $M_0$  denotes the total mass of the cylinder and  $\xi_{mni}$  denotes the generalized mass fraction for the (mni) mode.

Thus: 
$$M_0 = \mu A$$
 (2.19)

and

$$\xi_{\text{mni}} = \int_{\bar{\mathbf{x}}=0}^{1} \int_{\bar{\mathbf{y}}=2}^{1} \left\{ \phi_{\text{mni}}(\bar{\mathbf{x}},\bar{\mathbf{y}}) \right\}^{2} + \left\{ \psi_{\text{mni}}(\bar{\mathbf{x}},\bar{\mathbf{y}}) \right\}^{2} d\bar{\mathbf{x}} d\bar{\mathbf{y}}$$
 (2.20)

Substituting equations (2.15) and (2.16) in equation (2.20) and performing the integration shows that  $\xi_{mni} = 1/2$  for all modes. It follows from equations (2.18) and (2.19) that for the (mni) mode;

$$M_{mni} = \frac{M_0}{2} = \frac{\mu A}{2}$$
 (2.21)

where A is the surface area of the cylinder and  $\mu$  is the mass per unit area (lb. sec<sup>2</sup> per in<sup>3</sup>).

The equation for the resonant frequencies of a ring frame and stringer stiffened cylindrical shell, simply supported at each end is;

$$\frac{\overline{M} \, L_{X}^{4} \omega^{2}}{\pi^{4} \, D} = m^{4} \left(1 + \overline{\beta}^{2}\right)^{2} + m^{4} \left[ \frac{E_{S} I_{S}}{D \, d} + \overline{\beta}^{2} \left( \frac{G_{S} J_{S}}{D \, d} + \frac{G_{r} J_{r}}{D \, \ell} \right) \right]$$

$$+ \overline{\beta}^{4} \frac{\overline{E}_{r} \overline{I}_{r}}{D \underline{I}} + \frac{12z_{n}^{2}}{\pi^{4}} \left[ \frac{1 + \overline{S}\Lambda_{s} + \overline{R}\Lambda_{r} + \overline{R}\overline{S}\Lambda_{rs}}{\Lambda} \right]$$

$$- pR\overline{\beta}^{2} \frac{m^{2}L_{x}^{2}}{\pi^{2}D} \qquad (2.22)$$

where;

$$\Lambda_{s} = 1 + 2\overline{\alpha}^{2} (\overline{z}_{s}/R) (\overline{\beta}^{2} - v) + \overline{\alpha}^{4} (\overline{z}_{s}/R)^{2} (1 + \overline{\beta}^{2}) 
\Lambda_{r} = 1 + 2n^{2} (\overline{z}_{r}/R) (1 - \overline{\beta}^{2}v) + n^{4} (\overline{z}_{r}/R)^{2} (1 + \overline{\beta}^{2})^{2} 
\Lambda_{rs} = n^{2} \cdot \alpha^{2} (\overline{z}_{r}/R)^{2} \left[ \overline{\beta}^{2} (1 - v^{2}) + 2(1 + v) \right] + n^{4} \left[ 1 - v^{2} + 2\overline{\beta}^{2} (1 + v) \right] 
= (\overline{z}_{r}/R)^{2} + 2n^{2} (1 - v^{2}) (\overline{z}_{s}/R) + 2n^{2} (1 - v^{2}) (\overline{z}_{r}/R) 
+ 2n^{4} (1 + v)^{2} (\overline{z}_{r}/R) (\overline{z}_{s}/R) + 1 - v^{2} 
\Lambda = (1 + \overline{\beta}^{2})^{2} + 2\overline{\beta}^{2} (1 + v) (\overline{R} + \overline{S}) + (1 - v^{2}) \left[ \overline{S} + \overline{R}\overline{\beta}^{4} + \left( 2\overline{\beta}^{2} \overline{R}\overline{S} \right) \right] 
= (1 + v) 
\sigma = \frac{L_{x}^{4} (1 - v^{2})}{R^{2} h^{2}} 
\overline{\beta} = \frac{nL_{x}}{m\pi R} 
\overline{\alpha} = \frac{m\pi R}{L_{x}} 
\overline{S} = \frac{E_{s}A_{s}}{Ehd}$$
(2.24)

$$\widetilde{R} = \frac{\widetilde{E}_{r}A_{r}}{\widetilde{E}h\ell}$$

(2.24 Continued)

p = p - p

p = extensal pressure

p. = internal pressure.

M = Total mass/unit area of stiffened cylinder

u = circular frequency of vibration.

D = Flexural rigidity of the isotropic cylinder wall

$$= \frac{Et^3}{12(1-v^2)}$$

h = cylinder wall thickness

v = Poisson's Ratio

E = Young's Modulus

G = shear modulus

= moment of inertia of stiffener about its centroid.

J = torsional constant (i.e., Polar Moment of Inertia) for the stiffener.

r,s = subscripts referring to stiffening in the y and x d'.ections respectively

 $d_{\bullet}L$  = stringer spacing, ring frame spacing (see Figure 3).

A,A = cross-sectional areas of stringer and ring frame

 $\vec{z}_r$ ,  $\vec{z}_s$  = distance from the middle surface of the cylinder to the centroid of the ring frame and stringer respectively.

Note: The quantities  $\vec{z}_s$  and  $\vec{z}_r$  are positive when the stiffeners are located on the external surface of the cylinder and negative when the stiffeners are on the inner surface.

Equation (2.22) is a closed-form expression for determining the resonant frequencies of a stiffened cylinder subjected to a differential pressure, thus allowing an investigation of fuselage pressurization effects to be carried out. The equation was first derived by Mr.Elman, Mickulas and Stein (Reference 10) with the usual assumption that axial in-plane inertia forces are negligible. It should be noted that while the discrete properties of the stiffeners are required to solve for natural frequencies, their effects on the modal behavior have been accounted for by averaging them over the cylinder surface.

### b. Simply Supported Panel

For a simply supported panel, the mode shape of the (m,n) mode can be expressed as:

$$\phi_{mn}(x,y) = \sin \frac{m\pi x}{a} \sin \frac{n\pi y}{b}$$
 (2.25)

where;

m = number of elastic half-waves in the x direction

n = number of elastic half-waves in the y direction

x =longitudinal coordinate  $0 \le x \le a$ 

y = lateral (or circumferential) coordinate 0 < y < b

a, b = panel length and dith respectively.

Orthogonality between the modes (m,n) and (r,s) is expressed by the condition;

$$\int_{x=0}^{\alpha} \int_{y=0}^{b} \mu \left[ \phi_{mn}(x,y) \cdot \phi_{rs}(x,y) \right] dxdy = 0$$
 (2.26)

provided that  $(m,n) \neq (r,s)$ .

The mode shape defined by equation (2.25) clearly satisfies the orthogonality condition.

Corresponding to each mode of vibration (m,n), the generalized effective mass  $M_{mn}$  is defined by the integral;

$$M_{mn} = \mu \int_{x=0}^{a} \int_{y=0}^{b} \phi_{mn}^{2}(x, y) dxdy \qquad (2.27)$$

where

$$\xi_{\text{min}} = \int_{\bar{\mathbf{x}}=0}^{1} \int_{\bar{\mathbf{y}}=0}^{1} \phi_{\text{min}}^{2}(\bar{\mathbf{x}}, \bar{\mathbf{y}}) d\bar{\mathbf{x}} d\bar{\mathbf{y}}$$
 (2.28)

= generalized mass fraction for the (m,n) mode

and  $M_0 = total mass of the panel.$ 

Substituting equation (2.25) in (2.28) shows that  $\xi_{mn} = \frac{1}{4}$  for all modes. It therefore follows from equation (2.27) that the generalized mass for the (m,n) mode is:

$$M_{mn} = \frac{M_0}{4} = \frac{\mu A}{4} \tag{2.29}$$

where A denotes the surface area of the panel and  $\mu$  denotes the mass per unit area (lb. sec.2/in.3).

The resonant frequencies of a simply supported panel may be computed from the relation (Reference 11);

$$u_{mn} = \pi^2 \left[ \frac{m^2}{\sigma^2} + \frac{n^2}{b^2} \right] \sqrt{\frac{Eh^2 g}{12\rho(1 - v^2)}}$$
 (2.30)

where:

h = panel thickness

E = Young's modulus

v = Poisson's ratio

 $\rho = \text{density of panel (lb./in}^3).$ 

For simply supported panels under the combined action of lateral loads and forces acting in the middle plane it can be shown from simple theory (Reference 12) that the frequency equation is:

$$f_{mn} = \frac{1}{2} \left[ \frac{g}{\rho h} \left\{ N_{x} \frac{m^{2}}{\sigma^{2}} + N_{y} \frac{n^{2}}{b^{2}} + 2N_{xy} \frac{mn}{\alpha b} \right\} + \frac{D\pi^{2}g}{\rho h} \left( \frac{m^{2}}{\sigma^{2}} + \frac{n^{2}}{b^{2}} \right)^{2} \right]^{\frac{1}{2}}$$
(2.31)

where

 $N_{x'}$ ,  $N_{y'}$  = direct forces in the middle plane/unit length  $N_{xy}$  = shear force in the middle plane  $D = \frac{Eh^3}{12(1 - v^2)}$ , the bending rigidity of the panel.

In the absence of in-plane loads, equation (2.31) of course, reduces to equation (2.30). This latter form is particularly useful for studying the response of individual panels of a pressurized fuselage. In this case, if p denotes the difference in pressure between the inside and the outside of the fuselage, then the longitudinal load per unit panel width is

and the circumferential load per unit width is given by;

$$N_{y} = \frac{pR}{h} \times \frac{\mathbf{L}h}{\mathbf{L}} = pR \qquad (2.33)$$

where;

R = mean fuselage radius

h = cylinder wall thickness

and L = iength.

The shear force in the middle plane is, of course, zero for the case of uniform

fuseloge pressurization. Substitution of (2.32) and (2.33) in (2.31) and putting  $N_{xy} = 0$  leads to the approximate panel resonant frequencies occurring in a pressurized fuselage.

### c. Panel Group

The panel group consists of a row of N flat panels supported by N+1 intermediate stringers between two ring frames as shown in Figure 4. The entire panel row is assumed to be simply-supported at the ring frames, i.e., x = 0 and x = L, and a normal mode of vibration is given by

$$y_{i}(\vec{y}) \sin \frac{m\pi x}{L} \tag{2.34}$$

where m is the number of halfwaves in the x(axial) direction. The general solution for  $y_i$  can be shown to be, (Reference 13);

$$Y_1(\vec{y}) = A_1 \cosh k_1 \vec{y} + A_2 \sinh k_1 \vec{y} + A_3 \cos k_2 \vec{y} + A_4 \sin k_2 \vec{y}$$
 (2.35)

where  $A_1$ ,  $F_2$ ,  $A_3$  and  $A_4$  are unknown constants

and

$$k_{1} = b_{1} \left\{ u \left( \frac{h\rho}{D} \right)^{\frac{1}{2}} + \left( \frac{m\pi}{L} \right)^{2} \right\}^{\frac{1}{2}}$$
(2.36)

$$k_2 = b_i \left\{ \omega \left( \frac{h\rho}{D} \right)^{\frac{1}{2}} - \left( \frac{m\pi}{L} \right)^2 \right\}^{\frac{1}{2}}$$

and the non-dimensional local coordinate its expressed as,

$$\bar{y} = \frac{1}{b_i} \left( y - \sum_{k=1}^{i-1} b_k \right)$$
 (2.37)

with 
$$\sum_{k=1}^{i-1} b_k \le y \le \sum_{k=1}^{i} b_k$$
.

In the above expressions;

 $b_i, b_k$  = width of the i-th and k-th panels respectively

h = panel thickness

P = mass density of panel material

D = bending rigidity =  $\frac{E h^3}{12(1 - v^2)}$ 

 $\mathbf{L}$  = panel dimension between ring frames, (i.e., the x direction)

4 = resonant frequency

 $\bar{y}$  = non-dimensional coordinate,  $0 \le \bar{y} \le 1$ .

Now, the equation of motion for the undamped free vibration of any panel, say the i-th, is given by;

$$\frac{\partial^4 w}{\partial x^4} + \frac{2}{b_i^2} \frac{\partial^4 w}{\partial x^2 \partial \bar{y}^2} + \frac{1}{b_i^4} \frac{\partial^4 w}{\partial \bar{y}^4} + \frac{h_i \rho_i}{D_i} \quad \dot{w} = 0 \qquad (2.38)$$

where the dats refer to differentiation with respect to time.

Since the two edges, x=0 and x=1 are simply supported, a solution to equation (2.38) is

$$w(x,y;t) = Y_i(\vec{y}) \sin \frac{m \pi x}{f} \cdot e^{i\omega t} . \qquad (2.39)$$

By differentiating equation (2.35) with respect to  $\tilde{y}$ , the derivatives can be written in matrix form as;

$$\begin{bmatrix} Y \\ Y^1 \\ Y^2 \\ Y^{12} \end{bmatrix}_{\bar{y}} = \begin{bmatrix} \cosh k_1 \bar{y} & \sinh k_1 \bar{y} & \cos k_2 \bar{y} & \sin k_2 \bar{y} \\ k_1 \sinh k_1 \bar{y} & k_1 \cosh k_1 \bar{y} & -k_2 \sin k_2 \bar{y} & k_2 \cos k_2 \bar{y} \\ k_1^2 \cosh k_1 \bar{y} & k_1 \sinh k_1 \bar{y} & -k_2^2 \cos k_2 \bar{y} & -k_2^2 \sin k_2 \bar{y} \\ k_1^2 \sinh k_1 \bar{y} & k_1^2 \cosh k_1 \bar{y} & k_2^2 \sin k_2 \bar{y} & -k_2^2 \cos k_2 \bar{y} \end{bmatrix}_{\bar{i}} \begin{bmatrix} A_1 \\ A_2 \\ A_4 \\ A_4 \end{bmatrix}$$

$$(2.40)$$

or, in matrix notation,

$$\left[ Y(\vec{y}) \right] = \left[ B_{i}(\vec{y}) \right] A_{i}$$

Since,

$$\Theta = \frac{\partial w}{\partial y}$$

$$M = D \left[ \frac{\partial^2 w}{\partial y^2} + v \frac{\partial^2 w}{\partial x^2} \right]$$
and
$$Q = D \left[ \frac{\partial^3 w}{\partial y^3} + (2 - v) \frac{\partial^3 w}{\partial x^2 \partial y} \right]$$

The vector Y may be translated into the state vector Z with components

$$\left\{w,\,b_0^{}\,e,\,\frac{b_0^2\,M}{D_0}\,,\,\frac{b_0^3\,Q}{D_0}\right\},\,\,\,\text{where}\,\,\,b_0^{}\,\,\,\text{is a reference panel width and}$$

 $D_{\rm q}$  is a reference rigidity. Furthermore, it can be shown (Reference 13) that for a chain of panels the state vectors at the extreme ends of the row are related by a total transfer matrix T, as follows,

$$\overline{Z}_{n}^{R} = T \overline{Z}_{n}^{L} \qquad (2.42)$$

where the subscripts of and in denote the O-th and in-th stringers and the superscripts R and L denote positions immediately to the right and left of a

particular stringer. If both ends of the row of panels are free then equation (2.42) may be written as,

$$\begin{bmatrix} \mathbf{w} \\ \mathbf{b}_0 \\ \mathbf{0} \\ \mathbf{0} \end{bmatrix}_{\mathbf{0}}^{\mathbf{R}} = \begin{bmatrix} \mathbf{T} \end{bmatrix} \cdot \begin{bmatrix} \mathbf{w} \\ \mathbf{b}_0 \\ \mathbf{0} \\ \mathbf{0} \end{bmatrix}_{\mathbf{0}}^{\mathbf{L}}$$
 (2.43)

where,

$$\begin{bmatrix} T \end{bmatrix} = \begin{bmatrix} t_{11} & t_{12} & t_{13} & t_{14} \\ t_{21} & t_{22} & t_{23} & t_{24} \\ t_{31} & t_{32} & t_{33} & t_{34} \\ t_{41} & t_{42} & t_{43} & t_{44} \end{bmatrix}$$
(2.44)

$$= \begin{bmatrix} F \end{bmatrix} \begin{bmatrix} 1 & 0 & 0 & 0 \\ 0 & 1 & 0 & 0 \\ e & t & 1 & 0 \\ -k - e & 0 & 1 \end{bmatrix}$$
 (2.45)

and the matrix  $\begin{bmatrix} \mathbf{F} \end{bmatrix}$  is given by,

$$\begin{bmatrix} \mathsf{F} \end{bmatrix} = \begin{bmatrix} \mathsf{C}_0 + \beta^2 \eta \mathsf{C}_{-2} \,, & \beta \mathsf{S}_{-1} + \beta^3 \xi \mathsf{S}_{-3} \,, & \frac{\beta^2}{\alpha} \mathsf{C}_{-2} \,, & \frac{\beta^3}{\alpha} \mathsf{S}_{-3} \\ \frac{\mathsf{S}_1}{\beta} + \beta \eta \, \mathsf{S}_{-1}^1 \,, & \mathsf{C}_0 + \beta^2 \xi \mathsf{C}_{-2} \,, & \frac{\beta}{\alpha} \, \mathsf{S}_{-1}^1 \,, & \frac{\beta^2}{\alpha} \, \mathsf{C}_{-2} \\ \frac{\alpha}{\beta^2} \, \mathsf{C}_2 + \alpha \beta^2 \eta \, \xi \, \mathsf{C}_{-2}^1 \,, & \frac{\alpha}{\beta} \, \mathsf{S}_1 + \alpha \beta (\xi \mathsf{S}_{-1}^1 - \eta \mathsf{S}_{-1}^1) \,, & \mathsf{C}_0^1 - \beta^2 \eta \mathsf{C}_{-2}^1 \,, & \beta \mathsf{S}_{-1}^1 - \beta^3 \eta \, \mathsf{S}_{-3}^1 \\ -\alpha \beta^3 \eta \, \xi \, \tilde{\mathsf{S}}_{-3}^2 \,, & \frac{\alpha \mathsf{C}_2}{\beta^2} + \alpha \beta^2 \eta \, \xi \, \mathsf{C}_{-2}^1 \,, & \frac{\mathsf{S}_1^1}{\beta} - \beta \, \xi \, \mathsf{S}_{-1}^1 \,, & \mathsf{C}_0^1 - \beta^2 \xi \, \mathsf{C}_{-2}^2 \\ -\alpha \beta \eta \, \xi \, \tilde{\mathsf{S}}_{-1}^1 \,, & \mathbf{S}_1^1 + \alpha \, \beta^2 \eta \, \xi \, \mathsf{C}_{-2}^1 \,, & \frac{\mathsf{S}_1^1}{\beta} - \beta \, \xi \, \mathsf{S}_{-1}^1 \,, & \mathsf{C}_0^1 - \beta^2 \xi \, \mathsf{C}_{-2}^2 \\ -\alpha \, \beta \eta \, \xi \, \tilde{\mathsf{S}}_{-1}^1 \,, & \mathsf{C}_0^1 - \beta^2 \, \xi \, \mathsf{C}_{-2}^1 \,, & \mathsf{C}_0^1 - \beta^2$$

(2.46)

In the above relations;

$$\begin{split} e &= \frac{b_0^2}{D_0} \left\{ EI_{\eta} S_z \left( \frac{m\pi}{L} \right)^4 - \rho A C_{\gamma} \omega^2 \right\} \\ k &= \frac{b_0^2}{D_0} \left\{ EI_{\eta} \left( \frac{m\pi}{L} \right)^4 - \rho A \omega^2 \right\} \\ t &= \frac{b_0^3}{D_0} \left\{ EC_{\omega S} \left( \frac{m\pi}{L} \right)^4 + GC \left( \frac{m\pi}{L} \right)^2 - \rho I_S \omega^2 \right\} \\ \alpha &= \frac{D_1}{D_0} \\ \beta &= \frac{b_1}{b_0} \\ \eta &= \nu \left( \frac{m\pi b_0}{L} \right)^2 \\ \xi &= (2 - \nu) \left( \frac{m\pi b_0}{L} \right)^2 \\ C_{-2} &= \cosh k_1 - \cos k_2 \\ C_0 &= k_2^2 \cosh k_1 + k_1^2 \cos k_2 \\ C_0' &= k_1^2 \cosh k_1 + k_2^2 \cos k_2 \\ C_2 &= k_1^2 k_2^2 C_{-2} \\ S_{-3} &= \frac{1}{k_1} \sinh k_1 - \frac{1}{k_2} \sin k_2 \end{split}$$

$$S_{-1} = \frac{k_2^2}{k_1} \sinh k_1 + \frac{k_1^2}{k_2} \sin k_2$$

$$S_{-1}^{1} = k_{1} \sinh k_{1} + k_{2} \sin k_{2}$$

$$S_1 = k_1^2 k_2^2 S_{-3}$$

$$S_1' = k_1^3 \sinh k_1 - k_2^3 \sin k_2$$

$$S_3 = k_1^2 k_2^2 S_{-1}^4$$

 $C_{ws} = C_w + \frac{1}{2}S_z$ , the warping constant of the stringer cross-section with respect to S as the center of twist.

 $I_s = I_c + A^2 C_y + A(C_z - S_z)^2$ , the polar moment of inertia of the stringer cross-section with respect to S. (See Figure 5.)

A = cross-sectional area of the stringer.

C = Saint Venant constant of uniform torsion for the stringer crosssection

G = stringer shear modulus = E/2(1 + v)

 $I_{\xi'}I_{\eta}$  = moments of inertia of stringer cross-section about its centroidal axes

 $C_z$ ,  $C_y$  = distances from the centraidal axes to the shear center O (see Figure 5).

S<sub>z</sub> = distance from skin surface to shear center

I = polar moment of inertia of the stringer cross-section about its

C<sub>w</sub> = warping constant of the stringer cross-section with respect to its centroid.

Returning to equations (2.43) and (2.45); it is possible to extract the following relationship,

$$\begin{bmatrix} t_{31} & t_{32} \\ t_{41} & t_{42} \end{bmatrix} \begin{bmatrix} w \\ b_0 \theta \end{bmatrix} \begin{bmatrix} L \\ 0 \end{bmatrix} = \begin{bmatrix} 0 \\ 0 \end{bmatrix}$$
 (2.47)

provided that the determinant of

$$\begin{bmatrix} t_{31} & t_{32} \\ t_{41} & t_{42} \end{bmatrix} = 0 (2.48)$$

Equation (2.48) is thus the frequency equation, the solution of which gives the values of the natural frequencies. By use of equations (2.44) and (2.46) it can be shown that the coefficients of equation (2.48) evaluate as;

$$\begin{split} t_{31} &= e \left\{ C_0 + \beta^2 \eta C_{-2} \right\} + t \left\{ \frac{S_1}{\beta} + \beta \eta S_{-1}^{1} \right\} + \left\{ \frac{\alpha}{\beta^2} C_2 + \alpha \beta^2 \eta \xi C_{-2} \right\} \\ t_{32} &= e \left\{ \beta S_{-1} + \beta^3 \xi S_{-3} \right\} + t \left\{ C_0 + \beta^2 \xi C_{-2} \right\} + \left\{ \frac{\alpha}{\beta} S_1 + \alpha \beta (\xi S_{-1}^{1} - \eta S_{-1}^{1}) - \alpha \beta^3 \eta \xi S_{-3} \right\} \\ t_{41} &= -k \left\{ C_0 + \beta^2 \eta C_{-2} \right\} - e \left\{ \frac{S_1}{\beta} + \beta \eta S_{-1}^{1} \right\} + \left\{ \frac{\alpha S_3}{\beta^3} + \frac{\alpha}{\beta} (\eta S_{-1}^{1} - \xi S_1^{1}) - \alpha \beta \eta \xi S_{-1}^{1} \right\} \\ t_{42} &= -k \left\{ \beta S_{-1} + \beta^3 \xi S_{-3} \right\} - e \left\{ C_0 + \beta^2 \xi C_{-2} \right\} + \left\{ \frac{\alpha C_2}{\beta^2} + \alpha \beta^2 \eta \xi C_{-2} \right\} \end{split}$$

Equations (2.49)

Having obtained a value for the natural frequency, then by use of equation (2.47), it follows that

 $b_0 \theta_0^L = -\frac{t_{31}}{t_{32}} w_0^L \qquad (2.50)$ 

Allowing unit deflection at the left hand end of the panel row, the vector  $Z_0^{\mathbf{L}}$ 

in equation (2.42) becomes equal to  $\left\{1,-\frac{t_{31}}{t_{32}},0,0\right\}$  and premultiplying this vector by the appropriate transfer matrix leads to the vector  $\overline{Z}_i^R$ , again in terms of unit deflection at the left hand end of the panel row. Transfer no fine vector  $\overline{Z}_i^R$ , by use of equations (2.41) leads to the vector

 $A_1$ ,  $A_2$ ,  $A_3$ ,  $A_4$ , the elements of which are the coefficients of cash  $k_1 \bar{y}$ ,  $\sinh k_1 \bar{y}$ ,  $\cos k_2 \bar{y}$  and  $\sin k_2 \bar{y}$ , respectively, in the expression for the normal mode over the i-th span, i.e., equations (2.35) and (2.39). Consequently, the normal mode can be calculated at any point on the panel group.

## LIST OF SYMBOLS

# LIST OF SYMBOLS USED IN SECTION II

0	panel length
Ь	panel width
d	distance between stringers
ď	distance from extreme fiber surface to neutral axis
f mn	natural frequency of the (m, n)-mode
mn h	cylinder wall or panel thickness
h	double panel thickness
k <sub>1</sub> , k <sub>2</sub>	constants given by Equation (2.36)
£ 2	distance between ring frames
m	number of elastic axial half waves
n	number of elastic full waves around the circumference or half waves along the panel width
p = p <sub>o</sub> - p;	the pressure difference across the fuselage wall
r,\$	subscripts denoting ring frame and stringer respectively
to, h	inner wall thickness
₩ •	panel displacement
×	axial coordinate
у	circumferential, or lateral, coordinate
, X	nondimensional axial coordinate
<del>y</del>	nondimensional circumferential, or lateral, coordinate
z	radial coordinate
z <sub>o</sub>	constant defined by Equation (2.24)
Ξ <sub>r</sub> , Ξ <sub>s</sub>	distance from middle surface of cylinder to centroid of the ring frame and stringer respectively
A	surface area
A <sub>1,2,3,4</sub>	constants
C	Saint Venant constant of uniform tarsion for the stringer cross-section
C <sub>ws</sub>	warping constant of the stringer-crass-section with respect to S as the center of twist

$c_y, c_z$	distances from centroidal axes to the shear center 0 (see Figure 5).
D	flexural rigidity
E	Young's modulus of elasticity
G	modulus of rigidity
$I_s, I_r$	moment of inertia of stiffeners about centroid
I <sub>xx</sub> , I <sub>yy</sub>	moment of inertia about x and y axes
J	polar moment of inertia
K <sub>1</sub> , K <sub>2</sub>	constants baving numerical values of 0 or 1
K <sub>e</sub>	extensional stiffness of double panel
L <sub>x</sub> , i <sub>y</sub>	length in the x and y directions
M	bending moment
Mo	total mass
M <sub>mn</sub> , M <sub>mni</sub>	generalized mass of the (mn) and (mni) modes
M	total mass per unit area of stiffened cylinder
N <sub>x</sub> , N <sub>y</sub>	direct forces in the middle plane per unit length
N <sub>xy</sub>	shear force in the middle plane
Q	shear force resultant
<b>R</b>	shell mean radius
R	shell constant defined by Equation (2.24)
\$	shell constant defined by Equation (2.24)
T	transfer matrix for the panel group
Y; (y)	component of the panel group mode shape in the circumferential direction
Z	state vector for the panel group

α	panel group constant (Equation 2.46)
ā	shell constant defined by Equation (2,24)
β	panel group constant (Equation 2.46)
β	shell constant defined by Equation (2.24)
8	slope
μ	mass per unit area
ν	Poisson's ratio
ξ <sub>mn</sub> , ξ <sub>mn</sub> ;	generalized mass fractions for the (mn) and (mni)-modes respectively
ρ	density
• <sub>mni</sub> (x, y)	radial component of the shell mode shape
φ <sub>m n</sub> (x, y)	panel mode shape for the (m n)-mode
Ψ <sub>mni</sub> (x, y)	circumferential companent of the shell mode shape
မ	circular frequency
e m n	resonant frequency of the (mn)-mode
$ \begin{array}{c} \Lambda \\ \Lambda_r \\ \Lambda_s \\ \Lambda_{re} \end{array} $	shell constants defined by Equations (2.23)

#### SECTION III

## STRUCTURAL-ACOUSTIC COUPLING OF THE FUSELAGE AND THE CABIN VOLUME

### 1. COUPLING OF THE OVERALL OR LOW FREQUENCY MODES

Consider the equivalent structural model for the low frequency region, i.e., a stiffened cylinder of length  $L_{\chi}$  and mean radius R, simply supported at the ends.

Let w(x,y,t) denote the radially outward displacement of the shell and let  $\phi_{mn}(x,y)$  denote the normalized (to unity) component deflection shape of the (m,n) mode of the shell. Then if  $q_{mn}(t)$  denotes the time variation of the radial displacement in the (m,n) mode;

$$w(x,y,t) = \sum_{m=1}^{\infty} \phi_{mn}(x,y) q_{mn}(t)$$
 (3.1)

where m denotes the number of axial halfwaves and n denotes the number of full circumferential waves. The mode shape, defined previously in Section 11-2a is;

$$\phi_{mn}(\vec{x}, \vec{y}) = \sin m\pi \vec{x} (\sin 2\pi n \vec{y} + \cos 2\pi n \vec{y})$$
or,
$$\phi_{mn}(x, y) = \sin \frac{m\pi x}{L} (\sin n\phi + \cos n\phi)$$
(3.2)

where  $\phi = y/R$ , and the character of the first few modes are shown graphically in Figure 6.

The modes for which n=1 correspond to beam like bending of the shell in which the circular cross-section translates without distortion. Since these modes introduce essentially no sound waves within the cavity of the cylinder, they can usually be neglected.

#### a. The Internal Acoustic Field

The internal acoustic field is defined by the wave equation;

$$\nabla^2 e = \frac{1}{c^2} \frac{\partial^2 e}{\partial t^2} = -\left(\frac{\omega}{\epsilon}\right)^2 e = -K^2 e \qquad (3.3)$$

where 
$$\nabla^2 = \frac{\partial^2}{\partial r^2} + \frac{1}{r} \frac{\partial}{\partial r} + \frac{1}{r^2} \frac{\partial^2}{\partial \phi^2} + \frac{\partial^2}{\partial x^2}$$
 (3.4)

and e = dilatation

ω = steady state frequency of the acoustic field

 $K = \frac{\omega}{c} = acoustic wave number$ 

c = speed of sound in the medium.

The acoustic pressure p, and the particle displacement components in the radial tangential and axial directions can be expressed in terms of the dilatation as follows;

$$p = -p_0 c^2 e$$

$$w = -\frac{1}{K^2} \frac{\partial e}{\partial \tau}$$

$$v = -\frac{1}{K^2 \tau} \frac{\partial e}{\partial \phi}$$

$$v = -\frac{1}{K^2} \frac{\partial e}{\partial x}$$
(3.5)

where  $\rho_n$  is the ambient density of the medium.

The general form of the solution to the wave equation, determined by the method of separation of variables, can be shown to be;

$$e = \left[A \quad J_n(\vec{r}) + \alpha Y_n(\vec{r})\right] \left[\cos n\phi + b\sin n\phi\right] \left[\sin \phi x + d\cos \phi x\right] e^{i\omega t} \quad (3.6)$$

where A,a,b,d,a, are constants of integration.

 $J_n(\vec{r}) = n$ -th order Bessel function of the first kind.

 $Y_n(\vec{r})$  = n-th order Bessel function of the second kind.

n = 0,1,2,3,....

and, 
$$\bar{r} = Kr \left[1 - \left(\frac{\phi}{K}\right)^2\right]^{\frac{1}{2}}$$
 (3.7)

The primitive solution, equation 3.6, will satisfy only certain ideal boundary conditions imposed on the acoustic field. One such condition is that the ends of the cylinder are open, and if this is assumed to be the case then the analysis is simplified considerably, since the acoustic pressures at x=0 and  $x=L_x$  will be zero.

The case of a closed-closed cylinder is treated in Appendix 1, where it is seen that an exact result is considerably more complicated than the open-open case. It is shown that in general the (m,n) structural modes of the closed cylinder couple with all of the acoustic modes, whereas, as shown here, the (m,n) structural modes of the open cylinder couple only with the corresponding (m,n) acoustic modes. For purposes of noise reduction calculations the open cylinder equations derived here are used because of their relative simplicity. In practice, no doubt, the end conditions will lie somewhere between the two extremes of open and closed.

From the first of equations (3.5), we can conclude that the dilatation must be zero for x = 0 and  $x = L_x$ . For zero dilatation, compatibility with equation

(3.6) yields 
$$\phi = \frac{m\pi}{L_x}$$
 and  $d = 0$ .

Now the radial component of the particle deflection must be equal to the radial deflection of the cylinder at r=R. Since the radial deflection of the cylinder has both a  $\sin n \phi$  and  $\cos n \phi$  variation with  $\phi$ , and the particle deflection (from 3.6) is proportional to  $(\cos n \phi + b \sin n \phi)$ , then it follows that the constant b must be equal to unity.

The Bessel functions Y(r) tend to infinity at r=0; and since this is a physically meaningless condition, then it follows that the constant, a, must be equal to zero. Thus, the resulting dilatation component of the acoustic field can be written in the following manner; substituting the values of the constants in (3.6) yields,

$$e = A \left[ J_n(\vec{r}) \right] \left[ \cos n \phi + \sin n \phi \right] \sin \frac{m\pi x}{L_x} e^{i\omega t}$$
 (3.8)

Now, from equation (3.5),

$$\mathbf{w} = -\frac{1}{K^2} \frac{\partial \mathbf{e}}{\partial \mathbf{r}} = \frac{-1}{K} \cdot \frac{1}{K} \cdot \frac{\partial \mathbf{e}}{\partial \mathbf{r}}$$
 (3.9)

differentiating (3.7) with respect to r and re-arranging gives;

$$\frac{1}{K} = \frac{\partial \tau}{\partial r} \left[ 1 - \left( \frac{\phi}{K} \right)^2 \right]^{\frac{1}{2}}$$
 (3.10)

Substituting (3.10) into (3.9)

$$w = -\frac{1}{K} \left[ 1 - \left( \frac{\phi}{K} \right)^2 \right]^{\frac{1}{2}} \cdot \frac{\partial r}{\partial \hat{r}} \cdot \frac{\partial e}{\partial r}$$
 (3.11)

Equating (3.1) and (3.11) for compatibility of radial deflection at r=R, and cancelling through,

$$q_{mn}(t) = -\frac{A}{K} \left[ 1 - \left( \frac{\Phi}{K} \right)^2 \right]^{\frac{1}{2}} J_n^r(\overline{R}) e^{i\omega t}$$
 (3.12)

where 
$$J_n^*(\overline{R}) = \frac{d}{d\overline{r}} \left\{ J_n(r) \right\}_{r=R}$$

or the constant, A, can be defined by;

$$A = \frac{-q_{mn}(t) K}{\left[1 - \left(\frac{\psi}{K}\right)^2\right]^{\frac{1}{2}} J_n'(\vec{R}) e^{i\omega t}}$$
(3. 13)

Also, by definition,

$$\frac{\Phi}{K} = \frac{m\pi}{KL_{x}} = \frac{m\pi\epsilon}{\omega L_{x}} = \frac{\omega_{m}}{\omega}$$
 (3-14)

where  $\omega_{m} = \frac{m\pi c}{L}$ , the m-th resonant frequency of open-open axial modes.

It should be noted that when  $\omega_m > \omega$ , both the radical and the argument of the Bessel Function appearing in equations (3.12) and (3.13) become imaginary. For this condition the constant A is replaced by A' and the Bessel Function by definition becomes a modified Bessel Function of order n.

Thus when  $\omega_m > \omega$ ,  $J_n(\vec{r})$  and  $J_n'(\vec{R})$  are replaced by  $I_n(\vec{r}) = J_n(\vec{r})$  and  $I_n'(\vec{R}) = \frac{d}{d\vec{r}} \left\{ I_n(\vec{r}) \right\}_{r=R}^{n}$  respectively, and the constant given by equation (3.13) is re-defined,

$$A = \frac{q_{mn}(t) K}{\left[\left(\frac{\Phi}{K}\right)^{2} - 1\right]^{\frac{1}{2}} \prod_{n}^{i} (\overline{R}) e^{i\omega t}}$$

Substituting for  $\phi/K$  in equation (3.13);

$$A = \frac{-q_{mn}(t) K}{\left[1 - \left(\frac{\omega_{m}}{\omega}\right)^{2}\right]^{\frac{1}{2}} J_{n}^{i}(\overline{R}) e^{i\omega t}}$$
(3.15)

Having satisfied the boundary conditions for vibrations of the shell in the (m-n) mode at frequency  $\omega$ , the dilatation e, acoustic pressure distribution, p, and component deflections of the field can be defined by use of equations (3.5), (3.8) and (3.15) as follows;

$$e_{mn}(r,\phi,x;t) = \frac{-q_{mn}(t) K}{\sqrt{1-\left(\frac{\omega_{m}}{\omega}\right)^{2}}} \cdot \frac{J_{n}(\bar{r})}{J_{n}(\bar{R})} (\cos n\phi + \sin n\phi) \cdot \sin \frac{m\pi x}{L}$$
 (3.16)

$$P_{mn}(r, \phi, x;t) = + \left\{ \frac{q_{mn}(t) p_o \omega c}{\sqrt{1 - \left(\frac{\omega_m}{\omega}\right)^2}} \cdot \left\{ \frac{J_n(\overline{r})}{J_n^*(\overline{R})} (\cos n\phi + \sin n\phi) \sin \frac{m\pi x}{L} \right\} \right\}$$
(3.17)

$$w_{mn}(r,\phi,x;t) = q_{mn}(t) \frac{J_n'(\bar{r})}{J_n'(\bar{R})} (\cos n \phi + \sin n \phi) \sin \frac{m\pi x}{L_x}$$
 (3.18)

$$v_{mn}(r,\phi,x;t) = q_{mn}(t) - \frac{n}{r} - \frac{J_n(r)}{J_n^*(R)} (\cos n\phi - \sin n\phi) \sin \frac{m\pi x}{L_x}$$
 (3.19)

$$u_{mn}(r,\phi,x;t) = q_{mn}(t) \cdot \frac{m\pi}{KL_{x}} \cdot \frac{J_{n}(\bar{r})}{J_{n}^{t}(\bar{R})} \cdot \frac{(\cos n\phi + \sin n\phi)}{\sqrt{1 - \left(\frac{\omega_{m}}{\omega}\right)^{2}}} \cos \frac{m\pi x}{L_{x}}$$
(3.20)

Inspection of equations (3.16) - (3.20) shows that another set of system resonances can occur, defined by the equation;

$$J_{n}^{*}(\overline{R}) = 0 \tag{3.21}$$

At these frequencies,  $e_{mn}$ ,  $P_{mn}$ , w, v, and u become infinitely large when  $q_{mn}$  (t) is non-zero. The only exception is the radial particle deflection at the shell wall where r = R. For this case,

$$w_{mn} = q_{mn}(t) \sin \frac{m\pi x}{L_x} (\sin n\phi + \cos n\phi);$$

however, when r < R the  $w_{mn}$ 's are unbounded. For each integer n there are an infinite number of roots,  $\overline{R}_{ns}$ , to equation (3.21), where  $s = 0, 1, 2, 3, \dots$ . For each root  $\overline{R}_{ns}$  there will be an infinite set of resonant frequencies  $w_{mns}$  corresponding to  $m = 1, 2, 3, \dots$ . An equation for the complete set of "system"

resonances can be derived from equation (3.7) by replacing r by R and noting from (3.14) that

$$\frac{\Phi}{K} = \frac{\omega_m}{\omega}$$

However, the system resonant frequency, previously defined by  $\omega$  (acoustic field) or  $\omega_{mn}$  (shell resonance), because of equation (3.21) is now denoted  $\omega_{mns}$ , so that;

$$\frac{\Phi}{K} = \frac{\omega}{\omega}$$

or 
$$K = \left(\frac{K}{\phi}\right) \cdot \phi = \frac{m\pi}{L} \cdot \frac{\omega_{mns}}{\omega_{m}}$$
 (3.22)

Substituting (3.22) in (3.7) and putting r=R,  $\overline{r}=\overline{R}$ , gives

$$\overline{R}_{ns} = m \pi \left(\frac{R}{L}\right) \left(\frac{\omega_{mns}}{\omega_{m}}\right) \left[1 - \left(\frac{\omega_{m}}{\omega_{mns}}\right)^{2}\right]^{\frac{1}{2}}$$
(3.23)

Squaring equation (3.23) and solving for  $\omega_{mns}$ ;

$$\omega_{\text{mns}} = \omega_{\text{m}} \sqrt{1 + \frac{1}{m^2} \left(\frac{L_x}{R}\right)^2 \left(\frac{\overline{R}_{\text{ns}}}{\pi}\right)^2}$$
 (3.24)

where  $\overline{R}_{ns}$  are the  $\overline{R}$ 's which satisfy equation (3.21). Numerical values of  $\overline{R}_{ns}$  are listed in Morse (Reference 14) and several of these values are listed in Table 1. Notice from (3.24) that  $\omega_{mns} > \omega_{m}$ . Furthermore, note that the root  $\overline{R}_{oo} = 0$  is associated with purely axial resonant frequencies,  $\omega_{m}$ .

Typical circumferential and radial acoustic wave patterns are shown in Figure 7 along with the corresponding structural wave patterns. A structural mode having n elastic wavelengths around the circumference can only excite those acoustic

modes which have n circumferential wavelengths. Similarly, the m-th order shell mode can excite only m-th order acoustic waves.

Thus, in general, the (mn) shell mode can excite only the (mn) acoustic mode, regardless of the excitation frequency. However, the exciting frequency will determine the degree to which the s-th order radial mode is excited. At any given (mn)-mode frequency, all corresponding radial modes (s = 0, 1, 2, 3, --) will be excited; however, the amplitude of the response of a particular (mns) mode will depend on how closely the excitation frequency  $\omega$  matches the resonant frequency,  $\omega_{\rm mns}$ .

Now that the (uncoupled) resonant frequencies and mode shapes of both the structure and the internal acoustic field are known, it is possible to dynamically couple the acoustic field and the structure and to obtain a set of (coupled) system resonances and mode shapes.

### b. The Response of the Dynamically Coupled System

Treating each (mn) mode of the structure as a single degree of freedom system, the equation of motion for the (mn) mode is;

$$M_{mn}q_{mn}(t) + \omega_{mn}^2 M_{mn}q_{mn}(t) = F_{mn}(t)$$
 (3.25)

where  $M_{mn}$  = generalized mass of the (mn) shell mode

$$= A_0 \mu \int_0^1 \int_0^1 \phi_{mn}^2(\vec{x}, \vec{y}) d\vec{x} d\vec{y} = \frac{M_0}{2}$$

M\_ = total mass of 抗心 shell

y = mass/unit area

F (t) = generalized force for the (mn) mode, due to internal reaction pressures on the shell.

$$= A_{c} \int_{\bar{x}=0}^{1} \int_{\bar{y}=0}^{1} P_{mn}(R,\bar{x},\bar{y};t) \phi_{mn}(\bar{x},\bar{y}) d\bar{x} d\bar{y}$$
 (3.26)

 $P_{mn}(\hat{\kappa}, \bar{x}, \bar{y}; t) = Acoustic reaction pressure at a point on the shell wall for the (mn) acoustic mode.$ 

External pressures acting on the shell have been neglected so that the system vibrates freely. Assuming that such a free vibration is periodic at frequency  $\Omega$ , then equations (3.25) and (3.26) can be combined and solved for the amplitude  $q_{mn}(t)$ ;

$$q_{mn}(t) = \frac{A_o \int_{\overline{x}=0}^{1} \int_{\overline{y}=0}^{1} P_{mn}(R_{r}\overline{x}_{r}\overline{y}_{r}t) \phi_{mn}(\overline{x}_{r}\overline{y}) d\overline{x} d\overline{y}}{M_{mn}(\omega_{mn}^{2} - \Omega^{2})}$$
(3.27)

Now, the amplitude of the acoustic pressure,  $P_{mn}(R, \mathcal{Z}, \tilde{y}; t)$ , can be determined from equation (3.17) by substituting  $\Omega$  for  $\omega$  at r = R;

$$P_{mn}(R,\bar{x},\bar{y};t) = + \frac{q_{mn}(t) \rho_0 \Omega c}{\sqrt{1 - \left(\frac{\omega_m}{\Omega}\right)^2}} \cdot \frac{J_n(\bar{R})}{J_n^{\dagger}(\bar{R})} - \sin m \bar{x}$$

$$\cdot (\cos 2\pi n \bar{y} + \sin 2\pi n \bar{y}) \qquad (3.28)$$

Also, from equation (3.24) we note that;

$$\Omega = \omega_{\rm m} \sqrt{1 + \left(\frac{\overline{R}}{m\pi}\right)^2 - \left(\frac{L_{\rm x}}{R}\right)^2}$$
 (3.29)

Notice that when  $\overline{R}=\overline{R}_{ns}$ ; then  $\Omega=\omega_{mns}$ , which is a "hard wall" acoustic resonant frequency. Substituting equation (3.28) in (3.27), performing the integration, cancelling  $q_{mn}(t)$  from the expression and re-arranging, we obtain;

$$\left[1-\left(\frac{\Omega}{\omega_{mn}}\right)^{2}\right]\left[1-\left(\frac{\omega_{m}}{\Omega}\right)^{2}\right]^{\frac{1}{2}}J_{n}^{*}(\overline{R})-\frac{\rho_{o}c\Omega J_{n}(\overline{R})}{\mu\omega_{mn}^{2}}=0$$
(3.30)

The above equation is the expression for the coupled resonant frequencies of the system. Notice that if the second term of (3.30) were omitted, the resonant frequencies would consist of the shell resonances, the axial acoustic resonances,

and the radial acoustic resonances. Also note that there will exist a set of coupled resonant frequencies,  $\Omega_{mns}$ , for each pair of intégers (m,n).

The magnitudes of the various acoustic field parameters, such as dilatation, pressure and particle velocity, at the system resonant frequencies can be obtained by setting  $\omega = \Omega_{mns}$  in equations (3.16) – (3.20). It should be noticed that these magnitudes are proportional to the structural deflection amplitude,  $q_{mn}(t)$ , at the system resonance. For example, the pressure  $P_{mn}$  at resonance ( $\omega = \Omega_{mns}$ ) can be written:

$$P_{mn}(R, \tilde{x}, \tilde{y}; t) = + q_{mn}(t) \frac{\rho_0 c \Omega_{mns}}{\sqrt{1 - \left(\frac{\omega_m}{\Omega_{mns}}\right)^2}} \cdot \frac{J_n(\tilde{R})}{J_n^1(\tilde{R})} \cdot \sin m \pi \tilde{x} \left(\sin 2\pi n \tilde{y} + \cos 2\pi n \tilde{y}\right)$$

Now, from equation (3.30);

$$-\frac{J_{n}(\overline{R})}{J_{n}^{*}(\overline{R})} \rho_{n} c \Omega_{mns} = \mu \omega_{mn}^{2} \left[ \left( \frac{\Omega_{mns}}{\omega_{mn}} \right)^{2} - 1 \right] \left[ 1 - \left( \frac{\omega_{m}}{\Omega_{mns}} \right)^{2} \right]^{\frac{1}{2}}$$
(3.31)

By combining the above two equations;

$$P_{mn}(R, \overline{x}, \overline{y}, t) = q_{mn}(t) \mu \omega_{mn}^{2} \left[ 1 - \left( \frac{\Omega_{mns}}{\omega_{mn}} \right)^{2} \right] \sin m \pi \overline{x} \left( \sin 2\pi n \overline{y} + \cos 2\pi n \overline{y} \right)$$

$$(3.32)$$

#### c. Total Response of the Coupled System to External Fluctuating Pressure Fields

The total response to an external fluctuating pressure field is equal to the sum of the responses of the individual modes to the pressure field. Treating each system mode independently, the equation of motion for the (mns) mode is;

$$\ddot{q}_{mns}(t) + \frac{\Omega_{mns}}{Q_{mns}} \dot{q}_{mns}(t) + \Omega_{mns}^2 q_{mns}(t) = \frac{F_{mns}(t)}{M_{mns}}$$
 (3.33)

where:

 $q_{mns}(t) = generalized shell deflection for the (mns) mode$ 

Q = effective dynamic magnification factor for the (mns) made

 $M_{mns}$  = generalized mass for the (mns) mode =  $\frac{M_0}{2}$  +  $M_{mns}^{(a)}$ 

 $M_{mns}^{(a)}$  = generalized acoustic mass for the (mns) mode

 $F_{mins}(t)$  = generalized force for the (mns) mode at time t

$$= A_0 \int_{\overline{x}=0}^{1} \int_{\overline{y}=0}^{1} P_e(\overline{x}, \overline{y}; t) \phi_{mn}(\overline{x}, \overline{y}) d\overline{x} d\overline{y}$$
 (3.34)

 $P_{\mathbf{x}}(\bar{\mathbf{x}},\bar{\mathbf{y}},t)=$  external pressure on the shell at the point  $(\bar{\mathbf{x}},\bar{\mathbf{y}})$ .

The generalized acoustic mass can be computed as follows; the system generalized stiffness  $K_{mns}$  and generalized mass  $M_{mns}$  are related by the equation:

$$K_{mns} = \Omega_{mns}^2 M_{mns}$$
 (3.35)

$$= 2^2_{mns} \left[ \frac{M_o}{2} + M_{mns}^{(a)} \right]$$

$$= K_{mn}^{(s)} + K_{mns}^{(a)}$$
 (3.36)

where  $K_{mn}^{(s)}$  = generalized stiffness of the (mn) shell make

$$= \omega_{\rm mn}^2 \frac{M_{\odot}}{2} \tag{3.37}$$

and  $K_{mns}^{(a)}$  = generalized stiffness of the (mns) acoustic mode

$$= \frac{\rho_{o}c^{2}}{q_{mns}^{2}} \int_{r=0}^{R} \int_{\phi=0}^{2\pi} \int_{x=0}^{L_{x}} e_{mns}^{2} \langle r, \phi, x \rangle r dr d\phi dx \qquad (3.38)$$

Note: The generalized stiffness is defined as  $K_r$ , the stiffness of a linear spring which when displaced by an amount q from an unrestrained position has the same potential energy stored as the actual system when displaced by an amount  $q_r \phi_r(x)$ , where  $\phi_r(x)$  is the mode shape. The potential energy stored is equal to one-half the force times the deflection,

i.e. 
$$\frac{K_r q^2}{2}$$
.

Now for the coupled system, the work done per unit volume,  $U_{\epsilon}$  is equal to one-half the stresses times the strains, so that;

$$U = U_0 dx dy dz = \frac{1}{2} \int_{\text{volume}} (\text{pressure}) \cdot (\text{volumetric strain}) dV$$
$$= \frac{1}{2} \int_{\text{volume}} \rho_0 c^2 e_{\text{mns}}^2 dV$$

Equating the potential energy stored;

$$K_r q_{mns}^2$$
 =  $\int_{\text{volume}} \rho_o c^2 e_{mns}^2 dV$ 

which leads to equation (3.38).

Notice that  $e_{mns}(r,\phi,x)$  is the dilatation associated with the (mns) system mode, obtainable from equation (3.16) by setting  $\omega$  equal to  $\Omega_{mns}$  and  $q_{mn}$  equal to  $q_{mns}$ . Equation (3.38) may be re-written as;

$$K_{mns}^{(a)} = \frac{\rho_0 c^2}{q_{mns}^2} \int_{y=0}^{2\pi r} \int_{r=0}^{R} \int_{x=0}^{L_x} e_{mns}^2(y,r,x) \, dy \, dr \, dx \qquad (3.39)$$

Substituting (3.16) in (3.38), the generalized stiffness of the (mns) acoustic mode becomes;

$$K_{mns}^{(o)} = \rho_o c^2 \int_{r=0}^{R} \int_{\phi=0}^{2\pi} \sum_{x=0}^{L_x} \frac{K^2}{\left[1 - \left(\frac{\omega_m}{Q_{mns}}\right)^2\right]} \cdot \left\{\frac{J_n(\vec{r})}{J_n^*(\vec{R})}\right\}^2 \left(\cos n\phi + \sin n\phi\right)^2.$$

$$\cdot \sin^2 \frac{m\pi x}{L_x} \left(r \cdot dr \cdot d\phi \cdot dx\right). \tag{3.40}$$

Now, from (3.7) and (3.14);

$$\frac{d\vec{r}}{dr} = K \left[ 1 - \left( \frac{\omega_m}{\Omega_{mns}} \right)^2 \right]^{\frac{1}{2}}$$

Thus, rdr =  $\frac{\vec{r} d\vec{r}}{K^2 \left[1 - \left(\frac{\omega_m}{\Omega_{mns}}\right)^2\right]}$ , so that equation (3.40) reduces to;

$$K_{mns}^{(a)} = \frac{\rho_0 c^2}{\left[1 - \left(\frac{\omega_m}{\Omega_{mns}}\right)^2\right]^2} \int_{\vec{r}=0}^{\vec{R}} \int_{\phi=0}^{2\pi} \int_{x=0}^{L_x} \left\{ \frac{J_n(\vec{r})}{J_n^1(\vec{R})} \right\}^2 \cdot (1 + \sin 2n\phi) \cdot \sin^2 \frac{m\pi x}{L_x}.$$

$$\cdot \vec{r} d\vec{r} d\phi dx \qquad (3.41)$$

Finally, we have that,

$$K_{mns}^{(c)} = \frac{\pi \rho_{o} c^{2} L_{x} \bar{R}^{2} \left[ J_{n}^{2}(\bar{R}) - J_{n-1}(\bar{R}) \cdot J_{n+1}(\bar{R}) \right]}{2 \left\{ J_{n}^{*}(\bar{R}) \right\}^{2} \left\{ 1 - \left( \frac{\omega_{m}}{\Omega_{mns}} \right)^{2} \right\}^{2}}$$
(3.42)

Thus the generalized acoustic mass can be obtained from equations (3.29) and (3.36). The analysis presented so far has demonstrated that the internal acoustic field can be combined with the structure to produce a system whose modal response equations are identical to those of a single degree of freedom system. Thus the response of an acoustic – structural system follows the same analytical procedure as the response of a purely structural system. The only additional detailed computations which must be made are determination of coupled system resonances and the generalized mass and stiffness of the acoustic field.

# d. Computation of the Internal Acoustic Field from the Structural Response

The acoustic pressure distribution within the cylindrical shell can be expressed by the equation;

$$P_{mn}(r,\vec{x},\vec{y},t;\omega) = \frac{+q_{mn}(t) P_{o} \omega c}{\left[1 - \left(\frac{\omega_{m}}{\omega}\right)^{2}\right]^{\frac{1}{2}}} \cdot \frac{J_{n}(\vec{r})}{J_{n}^{*}(\vec{R})} \cdot \phi_{mn}(\vec{x},\vec{y})$$

$$\text{where; } \vec{r} = \frac{\omega r}{c} \left[1 - \left(\frac{\omega_{m}}{\omega}\right)^{2}\right]^{\frac{1}{2}}$$

and  $\phi_{mn}(\bar{x},\bar{y})$  is the normalized mode shape of the (mn) structural mode.

Substituting the shell displacement,  $w(\bar{x},\bar{y},t;\omega)$  for the term  $q_{mn}(t) \phi_{mn}(\bar{x},\bar{y})$  in equation (3.43) leads to;

$$P_{mn}(r,\bar{x},\bar{y},t;\omega) = + w_{mn}(\bar{x},\bar{y},t;\omega) \left[\frac{\rho_{o}\omega c}{\left\{1 - \left(\frac{\omega_{m}}{\omega}\right)^{2}\right\}^{\frac{1}{2}}} \cdot \left[\frac{J_{n}(\bar{r})}{J_{n}^{1}(\bar{R})}\right]$$
(3.44)

Consider now, the mean-square values of the above quantities, i.e.,

$$\overline{P_{\text{tnn}}^{2}(r, x, y; \omega)} = \overline{w_{\text{mn}}^{2}(x, y; \omega)} \cdot \left[ \frac{\rho_{o} \omega c}{\left\{1 - \left(\frac{\omega_{m}}{\omega}\right)^{2}\right\}^{\frac{1}{2}}} \right]^{2} \cdot \left[ \frac{J_{n}(\bar{r})}{J_{n}^{*}(\bar{R})} \right]^{2}$$
(3.45)

The excitation pressures acting on the exterior of the fuselage are, in general, random with respect to time and are thus most conveniently expressed in terms of spectral densities. Consequently it is also convenient to express the structural displacement response and internal pressure response in terms of the spectral densities  $S_{\mathbf{w}}(\bar{\mathbf{x}},\bar{\mathbf{y}};\omega)$  and  $S_{\mathbf{p}}(\mathbf{r},\bar{\mathbf{x}},\bar{\mathbf{y}};\omega)$  respectively.

$$S_{p_{i_{mn}}}\left[r,\bar{x},\bar{y};\omega\right] = S_{mn}\left[\bar{x},\bar{y};\omega\right] \cdot \left[\frac{\rho_{o}\omega c}{\left\{1 - \left(\frac{\omega_{m}}{\omega}\right)^{2}\right\}^{\frac{1}{2}}} - \frac{J_{n}(\bar{r})}{J_{n}^{r}(\bar{R})}\right]^{2}$$
(3.46)

Space-averaging over the internal cylindrical volume;

$$S_{p_{\tilde{i}}}(\omega) = S_{\mathbf{w}}(\omega) \cdot \left[\frac{p_{0}\omega c}{J_{n}^{i}(\tilde{R})}\right]^{2} - \frac{1}{\left\{1 - \left(\frac{\omega_{m}}{\omega}\right)^{2}\right\}} \cdot \frac{1}{R^{2}} \int_{0}^{R} J_{n}^{2}(\tilde{r}) - r dr$$
(3.47)

Now, the space-averaged displacement power spectral density of the response to external pressure fluctuations for the coupled modes can be shown to be given by

(see Section V) the relation;

$$\frac{S_{\mathbf{w}}(\omega)}{S_{\mathbf{p}}(\omega)} = A_{o}^{2} \sum_{\mathbf{mns}} \frac{\gamma_{\mathbf{mn}} H^{2} \left(\frac{\omega}{\Omega_{\mathbf{mns}}}\right) J_{\mathbf{mni}}^{2}(\omega)}{M_{\mathbf{mns}}^{2} \Omega_{\mathbf{mns}}^{4}}$$
(3.48)

where  $S_{\mathbf{p}}(\omega)$  is the power spectral density of the external pressure fluctuations.

Dividing both sides of equation (3.47) by  $S_p(\omega)$  and evaluating the integral leads to the equation;

$$\frac{S_{\mathbf{p}_{i}^{(\omega)}}}{S_{\mathbf{p}^{(\omega)}}} = \left[\frac{S_{\mathbf{w}^{(\omega)}}}{S_{\mathbf{p}^{(\omega)}}} (\mathbf{p}_{0}\omega c)^{2}\right] \sum_{m=1}^{\infty} \frac{\left[J_{n}^{2}(\overline{R}) - J_{n-1}(\overline{R}) \cdot J_{n+1}(\overline{R})\right]}{\left[J_{n}^{2}(\overline{R})\right]^{2} \left[1 - \left(\frac{\omega_{m}}{\omega}\right)^{2}\right]}$$
(3.49)

Thus the ratio of the internal acoustic field to the external fluctuating pressure field is obtained directly by substituting the numerical results obtained from Equation (3.48) into Equation (3.49)

For the case where  $\omega_{m}>\omega$ , it can be shown that Equation (3.49) is modified to,

$$\frac{S_{p_{i}}(\omega)}{S_{p}(\omega)} = \begin{bmatrix} S_{w}(\omega) & (\rho_{o}\omega c)^{2} \end{bmatrix} \sum_{m=1}^{\infty} \frac{\begin{bmatrix} I_{n}^{2}(\overline{R}) - I_{n-1}(\overline{R}) \cdot I_{n+1}(\overline{R}) \end{bmatrix}}{\begin{bmatrix} I_{n}^{1}(\overline{R}) \end{bmatrix}^{2} \begin{bmatrix} (\frac{\omega m}{\omega})^{2} - 1 \end{bmatrix}}$$

Equation (3.49) represents the space averaged noise reduction coefficient of a cylindrical shell in the absence of acoustical damping. It may be observed that the summation term on the right-hand side of the equation expresses the modification to the acoustic input impedance of semi-infinite space,  $_{\rm O}$  , due to the enclosed cylindrical volume.

The denominator under the summation sign in (3.49) may be considered as an acoustic dynamic magnification factor and zeros of this term represent resonances of the acoustic system. In order to introduce the effect of acoustic damping into the system, it is convenient to consider an acoustic "Q" denoted by  $\mathbf{Q}_{ac}$  and expand the denominator in the form of an infinite series in the neighborhood of a zero. It can be shown (Reference 14) that

$$J_{n}^{+}(\vec{R}) = J_{n}^{+}(\vec{R}_{ns}) + (\vec{R} - \vec{R}_{ns}) J_{n}^{+}(\vec{R}_{ns}) + \frac{1}{2}(\vec{R} - \vec{R}_{ns})^{2} J_{n}^{++}(\vec{R}_{ns}) + \dots$$

If  $\overline{R}_{ns}$  is a zero of  $J^{*}(\overline{R})$ , and neglecting higher order terms, then

$$J_{n}^{*}(\overline{R}) \approx (\overline{R} - \overline{R}_{n_{S}}) J_{n}^{**}(\overline{R}_{n_{S}})$$

and for small values of  $(\bar{R} - \bar{R}_{ns})$ ,

$$\overline{E} - \overline{R}_{ns} \approx \frac{K^2 R^2 \left[1 - \left(\frac{\omega_{ns}}{\omega}\right)^2\right]}{2\overline{R}_{ns}}$$

Thus, using the above relationships together with the definition of  $\,\overline{R}\,$  gives the following result,

$$\frac{1}{J_{n}^{12}(\vec{R}) \left\{ 1 - \frac{\omega_{m}}{(\omega)^{2}} \right\}^{2}} \approx \frac{4}{K^{2} R^{2} J_{n}^{112}(\vec{R}_{ns}) \left\{ 1 - \frac{\omega}{(\omega_{ns})^{2}} \right\}^{2}}$$

when  $\omega = \omega$  . If we insert the acoustic dynamic magnification factor at resonance,  $Q_{ac}$ , into the above and allow  $\omega = \omega$  then the above equation becomes

$$\frac{1}{J_n^{\prime 2} (\overline{R}) \left\{ I - \left( \frac{\omega_{m}}{\omega_{ns}} \right)^2 \right\}} \approx \frac{4 Q_{qc}^2}{K^2 R^2 \left[ J_n^{\prime\prime} (\overline{R}_{ns}) \right]^2}$$
(3.49a)

The choice of a value of Q as a function of the absorption characteristics of the interior of the cylinder is discussed in Section VI.

#### COUPLING OF THE INDIVIDUAL PANEL, OR HIGH FREQUENCY MODES 2.

## The Internal Acoustic Field Induced by Arbitrary Wall Motion

Consider an infinitely long cylindrical shell of radius R, containing a uniform homogeneous fluid medium. The cylindrical wall is assumed to vibrate radially in an arbitrary pattern with respect to the polar angle  $\phi$ . It is assumed that this motion is uniform with respect to the cylinder axis, and harmonic in time at frequency w. The acoustic field generated within the medium is considered as a twodimensional field; and in the following analysis equations are developed for the distributions and amplitudes of the acoustic pressure and particle velocities in terms of the (assumed known) motions of the wall. Deflection amplitudes of the wall are assumed to be small, and linear accustic theory is employed. Once the general equations are developed, several special cases are considered including a rigid cavity wall with one or more radial pistons driving the fluid medium. Consideration is also given to the sound field generated by random motions of the wall, particularly when two different parts of the wall vibrate in a statistically uncorre-

The accoustic pressure distribution in the fluid is governed by the cylindrical form of the two-dimensional wave equation,

$$\nabla^2 P - \frac{1}{e^2} \frac{\partial^2 P}{\partial t^2} = 0 ag{3.50}$$

where, 
$$\nabla^2 = \frac{\partial^2}{\partial r^2} + \frac{1}{r} \frac{\partial}{\partial r} + \frac{1}{r^2} \frac{\partial^2}{\partial \phi^2}$$

 $P(r, \phi, t)$  = acoustic pressure in the fluid medium

speed of sound in the medium.

The particle displacements in the fluid are expressed in terms of the spatial variations of the acoustic pressure by the equations

$$U_r = U_r(r,\phi,t) = +\frac{1}{\rho_o} \frac{\partial P}{\partial r} = \text{radial component of displacement}$$
(3.51)

$$U_{\phi} \equiv U_{\phi}(r,\phi,t) = +\frac{1}{\rho_{c}r} \frac{\partial P}{\partial \phi} = \text{tangential component of displacement.}$$

Since linearity is assumed, a small amplitude radial vibration of the wall at frequency w will produce an internal acoustic field at frequency w. Thus let

$$P(r,\phi,t) = P(r,\phi,\omega) - e^{i\omega t}$$

$$U_{r}(r,\phi,t) = U_{r}(r,\phi,\omega) - e^{i\omega t} = + \frac{1}{\rho_{o}\omega^{2}} \frac{\partial P(r,\phi,\omega)}{\partial r} \cdot e^{i\omega t}$$
(3.52)

$$U_{\phi}(r,\phi,t) = U_{\phi}(r,\phi,\omega) \cdot e^{i\omega t} = + \frac{1}{p_{\phi}\omega^{2}r} \frac{\partial P(r,\phi,\omega)}{\partial \phi} \cdot e^{i\omega t}$$

Substituting the first of equations (3.52) into (3.50) gives,

$$\nabla^2 P(\mathbf{r}, \mathbf{\varphi}, \omega) + K^2 P(\mathbf{r}, \mathbf{\varphi}, \omega) = 0$$
(3.53)

where,  $K = \omega/c =$  acoustic wave number.

ω = steady state frequency of the acoustic field.

Furthermore, the pressure amplitude must be periodic with respect to the polar angle  $\phi$ , so that,

$$P(r,\phi,\omega) = P(r,\omega) + \Phi_{\mathbf{n}}(\phi)$$

$$\Phi_{\mathbf{n}}(\phi) = a_{\mathbf{n}} \cos n\phi + b_{\mathbf{n}} \sin n\phi \qquad n = 0, 1, 2, 3, ....$$
(3.54)

where a and b are coefficients to be determined from the boundary conditions. Substituting (3.54) into (3.53) leads to Bessel's equation for the pressure component  $P(r, \omega)$ ; namely,

$$\frac{d^2 P(r,\omega)}{dr^2} + \frac{1}{r} \frac{d P(r,\omega)}{dr} + \left[K^2 - \frac{n^2}{r^2}\right] P(r,\omega) = 0$$

or, in terms of a non-dimensional radial coordinate

$$\frac{d^2 P(\hat{r}, \omega)}{d\hat{r}^2} + \frac{1}{\hat{r}} \frac{d P(\hat{r}, \omega)}{d\hat{r}} + \left[\alpha^2 - \frac{n^2}{\hat{r}^2}\right] P(\hat{r}, \omega) = 0 \qquad (3.55)$$

$$\begin{array}{rcl}
\hat{r} & = r/R \\
\alpha & = KR = \omega R/c
\end{array}$$
(3.56)

Neglecting solutions of (3.55) which are infinity at  $\hat{r} = 0$ , the general solution can be written as

$$P(\hat{r},\omega) = P_{n}(\omega) + J_{n}(\alpha \hat{r})$$
 (3.57)

where  $P_n(\omega)$  = amplitude of pressure component at frequency  $\omega$ .

Combining (3.54) and (3.57) gives the pressure for a single integer n; and noting that the general expression for the pressure consists of a summation of these pressure components over all integers n, then,

$$P(r,\phi,\omega) = \sum_{n=0}^{\infty} P_n(\omega) + J_n(\alpha r) + \Phi_n(\phi)$$
 (3.58)

The primary concern in the present analysis is with the radial displacement component,  $U_r(r,\phi,\omega)$ . Substituting (3.58) into the second of equation (3.52) gives

$$U_{r}(r,\phi,\omega) = + \frac{\alpha}{\rho_{n}^{R}\omega^{2}} \sum_{n=0}^{\infty} P_{n}(\omega) \cdot J_{n}^{i}(\alpha_{r}^{A}) + \Phi_{n}(\phi)$$

$$= + \frac{1}{\rho_{C}\omega} \sum_{n=0}^{\infty} P_{n}(\omega) \cdot J_{n}^{i}(\alpha_{r}^{\Lambda}) \cdot \Phi_{i}(\phi) \qquad (3.59)$$

where, 
$$J_n^i(\alpha_r^{\Lambda}) = dJ_n(\alpha_r^{\Lambda})/d(\alpha_r^{\Lambda}) = \left(\frac{R}{\alpha}\right) \cdot dJ_n(\alpha_r^{\Lambda})/dr$$
 (3.60)

At the boundary of the fluid, where r = R or r = 1, the radial deflection is, from (3.59)

$$U_{r}(R,\phi,\omega) = + \frac{1}{P_{o}c\omega} \sum_{n=0}^{\infty} P_{n}(\omega) \cdot J_{n}^{i}(\alpha) \cdot \Phi_{n}(\phi)$$
 (3.61)

Now, the radial deflection of the wall can be expanded in a Fourier series,

$$U_{r}(R,\phi,\omega) = U_{Q}(\omega) \qquad \sum_{n=0}^{\infty} \Phi_{n}(\phi)$$
 (3.62)

where  $U_0(\omega)$  denotes the wall amplitude at frequency  $\omega$ . Thus it can be assumed that the Fourier coefficients  $a_n$  and  $b_n$  in (3.54) are known and are determinable from a knowledge of the wall motion. Comparing (3.61) and (3.62), term by term, shows that the pressure amplitudes  $P_n(\omega)$  must be equal to

$$P_{n}(\omega) = + \omega P_{o} c \frac{U_{o}(\omega)}{J_{n}^{\prime}(\alpha)}$$
(3.63)

Thus, substituting (3.63) into (3.58) and (3.59) gives the following equations

for the amplitudes and distributions of the accustic pressure and radial particle displacement component in terms of the known wall motion:

$$P(r,\phi,\omega) = + \omega \rho_{\mathcal{S}} \quad U_{\mathcal{S}}(\omega) \qquad \sum_{n=0}^{\infty} \frac{J_{n}(\alpha \hat{r})}{J_{n}^{'}(\alpha)} \quad \Phi_{n}(\phi)$$
 (3.64)

$$U_{r}(r,\phi,\omega) = U_{Q}(\omega) \sum_{n=0}^{\infty} \frac{J_{n}^{1}(\alpha_{r}^{r})}{J_{n}^{r}(\alpha)} \phi_{n}(\phi)$$
 (3.65)

Notice that at the boundary where  $\hat{r}=1$ , equation (3.65) reduces to the assumed form (3.62). The above two equations show that when the amplitude,  $U_{o}(\omega)$ , of the wall motion approaches zero, so that the wall becomes completely rigid, non-zero acoustic pressure and particle displacement can exist only for frequencies which satisfy the equations,

$$J_{n}^{1}(\alpha) = J_{n}^{1}(\alpha_{ns}) = 0$$
(3.66)

$$\omega_{ns} = \frac{c}{R} \alpha_{ns} = \frac{c}{a}$$
 resonant frequencies for two-dimensional acoustic field with rigid cylindrical wall.

Thus, when the wall vibrates at the frequencies  $\omega_{ns}$ , the "hard wall" acoustic resonances in the fluid are excited. A table of values of the "hard wall" resonant frequencies can be found in Reference 14.

Inspection of equation (3.64) shows that the frequency appears in the arguments of both Bessel Functions. This is an inconvenience for subsequent numerical evaluations and hence, it is necessary to rewrite this expression. To do this, it is first noted that

(a) 
$$J_n(\alpha_{ns}^{A}) - \Phi_n(\phi) = \text{mode shape of (ns)-acoustic mode}$$

(b) 
$$\left[1 - (\omega/\omega_{ns})^2\right]^{-1} = \left[1 - (\alpha/\alpha_{ns})^2\right]^{-1} =$$
 undamped dynamic magnification factor for the  $(n,s)$ -mode.

(c) the total pressure is the summation of all of the modal pressure components.

Thus it is reasonable to assume that  $P(r,\phi,\omega)$  can be written in the form:

$$P(r,\phi,\omega) = +\omega \rho_0 c \ U_0(\omega) \sum_{n=0}^{\infty} \sum_{s=1}^{\infty} A_{ns} \left[ 1 - \left( \frac{\alpha}{\alpha_{ns}} \right)^2 \right]^{-1}$$

$$\cdot J_n(\alpha_{ns} \hat{r}) \cdot \Phi_n(\phi)$$
(3.67)

where the  $A_{\rm ns}$  are coefficients to be determined such that (3.64) and (3.67) are identical. Comparing (3.64) and (3.67), term by term, it is clear that

$$\frac{J_{n}(\alpha_{n}^{\Lambda})}{J_{n}^{L}(\alpha)} = \sum_{s=1}^{\infty} A_{ns} \left[1 - \left(\frac{\alpha}{\alpha_{ns}}\right)^{2}\right]^{-1} \cdot J_{n}(\alpha_{ns}^{\Lambda})$$
(3.68)

Multiplying both sides of (3.68) by  $\left[ {\stackrel{\wedge}{r}} J_n(\alpha_{nx} {\stackrel{\wedge}{r}}) - d^{\stackrel{\wedge}{r}} \right]$  and integrating over  ${\stackrel{\wedge}{r}}$  from  ${\stackrel{\wedge}{r}} = 0$  to  ${\stackrel{\wedge}{r}} = 1$ , we obtain;

$$\frac{1}{J_n^{\prime}(\alpha)} \int_0^{1} r^{\alpha} J_n^{\prime}(\alpha_r^{\alpha}) \cdot J_n^{\prime}(\alpha_{nx}^{\alpha}) dr^{\alpha} =$$

$$= \sum_{s=1}^{\infty} A_{ns} \left[ 1 - (\alpha/\alpha_{ns})^{2} \right]^{-1} \int_{0}^{1} \hat{r} J_{n}(\alpha_{ns} \hat{r})$$

$$J_{n}(\alpha_{nx} \hat{r}) d\hat{r} \qquad (3.69)$$

In the evaluation of the two integrals in (3.69), it is convenient to employ the following general relationship for Bessel functions,

$$J_{n}^{t}(\alpha) = \frac{n}{\alpha} J_{n}(\alpha) - J_{n+1}(\alpha)$$
 (3.70)

and to obtain from this expression and the first of equations (3.66) the special relationship, that when  $\alpha = \frac{\alpha}{ns}$ 

$$nJ_{n}(\alpha_{ns}) = \alpha_{ns} J_{n+1}(\alpha_{ns})$$
 (3.71)

Standard expressions for the integrals in (3.69), together with the simplifications provided by (3.66), (3.70) and (3.71) lead to;

$$\int_{0}^{1} \int_{r}^{\Lambda} J_{n}(\alpha_{n}^{\Lambda}) J_{n}(\alpha_{nx}^{\Lambda}) d_{r}^{\Lambda} = \frac{\alpha/\alpha_{nx}^{2}}{\left[1 - \left(\frac{\alpha}{\alpha_{nx}}\right)^{2}\right]} J_{n}(\alpha_{nx}) J_{n}^{1}(\alpha) \quad (3.72)$$

$$\int_{0}^{1} \hat{r} J_{n}(\alpha_{ns}\hat{r}) \cdot J_{n}(\alpha_{nx}\hat{r}) d\hat{r} =$$

$$= \frac{n}{\alpha_{ns}^{2} - \alpha_{nx}^{2}} \left[ J_{n}(\alpha_{nx}) J_{n}(\alpha_{ns}) - J_{n}(\alpha_{ns}) J_{n}(\alpha_{nx}) \right]$$

$$= 0, \quad x \neq n$$
(3.73)

$$\int_{0}^{1} \int_{r}^{\Lambda} \left[ J_{n}(\alpha_{nx}^{\Lambda}) \right]^{2} dr^{\Lambda} = \frac{1}{2} \left[ 1 - (n/\alpha_{nx})^{2} \right] \cdot \left[ J_{n}(\alpha_{nx}) \right]^{2} (3.74)$$

Substituting (3.72) - (3.74) into (3.69) shows that only one non-zero term on the right-hand side of (3.69) is obtained, namely that term for which s = x, and thus, that,

$$A_{ns} = \frac{2\alpha/\alpha_{ns}^2}{\left[1 - (n/\alpha_{ns})^2\right]} \cdot \frac{1}{J_n(\alpha_{ns})} =$$

$$= \frac{2R\omega/c\alpha_{ns}^2}{\left[1 - (n/\alpha_{ns})^2\right]} \cdot \frac{1}{J_n(\alpha_{ns})}$$
(3.75)

Substituting (3.75) into (3.67) leads to the desired modal expression of the pressure field at frequency  $\omega$ . Substitution of (3.67) into the second of equations (3.52) gives the modal expansion of the radial displacement component. The resulting expressions are:

$$P(r,\phi,\omega) = + 2\omega^{2}\rho R U_{o}(\omega) \sum_{n=0}^{\infty} \sum_{s=1}^{\infty} \frac{J_{n}(\alpha_{ns}\hat{r})}{J_{n}(\alpha_{ns})} \frac{\Phi_{n}(\phi)}{\left[\alpha_{ns}^{2} - n^{2}\right] \cdot \left[1 - \left(\frac{\omega}{\omega_{ns}}\right)^{2}\right]}$$

$$U_{r}(r,\phi,\omega) = + 2U_{o}(\omega) \sum_{n=0}^{\infty} \sum_{s=1}^{\infty} \frac{J_{n}^{1}(\alpha_{ns}\hat{r})}{J_{n}(\alpha_{ns})} \frac{\alpha_{ns} \cdot \Phi_{n}(\phi)}{\left[\alpha_{ns}^{2} - n^{2}\right] \cdot \left[1 - \left(\frac{\omega}{\omega_{ns}}\right)^{2}\right]}$$

$$(3.76)$$

$$J_{n}^{1}(\alpha_{ns}\hat{r}) = dJ_{n}(\alpha_{ns}\hat{r})/d(\alpha_{ns}\hat{r})$$
 (3.78)

(3.77)

Notice that from (3.76) the pressure,  $P(R,\phi,\omega)$ , which acts on the wall is,

$$P(R,\varphi,\omega) = +2\omega^{2} \rho_{R} U_{\underline{n}}(\omega) \sum_{n=0}^{\infty} \sum_{s=1}^{\infty} \frac{\Phi_{\underline{n}}(\varphi)}{\left[\alpha^{2}_{\underline{n}s} - n^{2}\right] \cdot \left[1 - \left(\frac{\omega}{\omega_{\underline{n}s}}\right)^{2}\right]}$$
(3.79)

In equations (3.76), (3.77) and (3.79), the frequency  $\omega$  appears explicitly, whereas in (3.64) and (3.65) the frequency is implicit in the arguments of the Bessel functions.

#### b. Rigid Shell with a Single Radial Piston

Assume that the cylindrical wall is rigid and fixed except for a radially moving piston which subtends an angle  $\phi_0$ , as shown in Figure 8. Assume also that the piston lies in the range  $-\phi_0/2 < \phi < \phi_0/2$ . If  $U_0(\omega)$  denotes the amplitude of the piston displacement, then the wall motion can be described as shown in Figure 9. The Fourier series of the radial deflection shown in this figure can be written in the form given by equation (3.62) where the n-th Fourier component  $\Phi_n(\epsilon)$  is

$$\Phi_{n}(\phi) = 2\phi_{o} \left[ \frac{\sin(n\phi_{o}/2)}{(n\phi_{o}/2)} \right] \cdot \cos n\phi_{o}$$
 (3.80)

Substitution of (3.80) into (3.76), (3.77) and (3.79) will yield the desired expressions which describe the internal acoustic field for a single radial piston mounted in an otherwise rigid wall. It is interesting to note that as  $\phi_0$  approaches zero, all of the (lower order) Fourier components  $\phi_n(\phi)$  tend toward  $2\phi_0$ , independent of n. This case corresponds to a point radial source, or a line source with respect to the entire cylinder.

#### c. Kigid She!! with Two or More Radial Pistons

Consider the case shown in Figure 10 in which the cylinder wall is rigid except for two radial pistons which subtend angles  $\phi_1$  and  $\phi_2$ , and which are centered at  $\phi=0$  and  $\phi=\beta$  respectively. Assume that the two pistons oscillate harmonically at frequency  $\omega_1$  either in-phase or out-of-phase, with amplitudes  $U_{0,1}(\omega)$  and

 ${\rm U_{0}}_{2}(\omega)$  respectively. The Fourier series for the radial wall motion in this case is

$$U_{r}(R,\phi,\omega) = \sum_{n=0}^{\infty} \left[ U_{01}(\omega) \Phi_{n1}(\phi) + U_{02}(\omega) \Phi_{n2}(\phi) \right]$$
 (3.81)

$$\Phi_{ni}(\phi) = 2\phi_i \left[ \frac{\sin(n\phi_i/2)}{(n\phi_i/2)} \right] \cos n\phi \qquad (3.82)$$

$$\Phi_{nz}(\phi) = 2\phi_2 \left[ \frac{\sin(n\phi_2/2)}{(n\phi_2/2)} \right] \cos n(\phi - \beta)$$
 (3.83)

Substituting (3.81) into (3.76), (3.77) and (3.79) leads to the necessary equations which describe the acoustic field generated in this case. It is important to note that the total wall motion can be described as the linear summation of two motions, one for each piston; and hence the acoustic field will simply be the summation of the acoustic fields generated by each piston. Clearly then, for multiple pistons, the net acoustic field is the linear summation of the acoustic fields generated by each piston.

#### d. Computation of the Internal Acoustic Field from the Structural Response

The pressure at a point in the interior of a cylindrical shell due to the motion of part of the wall can be expressed by equation (3.76). At high frequencies of external pressure excitation, where the pressure correlation lengths are less than the dimensions of an individual panel, the total response of an aircraft fuselage to random pressure fields will be in the form of uncorrelated motion of individual panels with frames and stringers acting as nodal lines. If the panel motion is converted to that of an equivalent piston then the internal pressure response can be obtained directly fram equation (3.76). Conversion of panel motion to an equivalent piston is carried out by averaging the square of the motion amplitude over the panel area; the panel motion can be calculated assuming simply supported edges and this can be shown to be given by (see Section V);

$$\frac{S_{w}(\omega)}{S_{p}(\omega)} = A_{o}^{2} \sum_{mns} \frac{\gamma_{mn} H^{2} \left(\frac{\omega}{\omega_{ns}}\right) J_{\alpha\alpha}^{2} (\omega)}{M_{mn}^{2} \omega_{ns}^{4}}$$
(3.84)

where  $S_{p}(\omega)$  is the power spectral density of the external pressure fluctuations and  $S_{\mathbf{w}}(\omega)$  is the power spectral density of the panel motion. Converting equation (3.76) to a power spectral density and dividing both sides by  $S_p(\omega)$  leads to the definition of the internal acoustic field;

$$\frac{S_{p_{ns}}(r,\phi;\omega)}{S_{p}(\omega)} = 4\rho_{0}^{2}\omega^{4}R^{2} \frac{S_{w}(\omega)}{S_{p}(\omega)} \cdot \frac{J_{n}^{z}(\alpha_{ns}^{A}) \Phi_{n}^{z}(\phi)}{J_{n}^{z}(\alpha_{ns}^{z}-n^{2})\left[1-\left(\frac{\omega}{\omega_{ns}}\right)^{z}\right]^{2}}$$
(3.85)

The Fourier coefficients  $a_k$  and  $b_k$  which occur in  $\phi_n$  may be evaluated by Fourier analysis since from Figure 9  $f(\phi) = 1 \text{ when } \frac{-\phi_0}{2} \le \phi \le \frac{\phi_0}{2}$ and zero elsewhere, giving;

$$a_0 = \frac{b}{2\pi R} \tag{3.86}$$

$$b_0 = 0 (3.87)$$

$$a_{n} = \frac{1}{n\pi} \sin \frac{nb}{R}$$

$$b_{n} = \frac{2}{n\pi} \sin^{2} \frac{nb}{2R}$$
(3.88)

$$b_n = \frac{2}{n\pi} \sin^2 \frac{nb}{2R}$$
 (3.89)

where b is the panel dimension in the circumferential direction.

The average pressure of the two-dimensional acoustic field within the fuselage may be obtained by integrating over the area and carrying out the modal summation to give;

$$\frac{S_{p_i}(\omega)}{S_{p}(\omega)} = \left[\frac{S_{w}(\omega)}{S_{p}(\omega)} \cdot (\rho_{o}\omega c)^2\right] \cdot 2\left(\frac{\omega R}{c}\right)^2.$$

$$\cdot \sum_{\substack{n=0\\s=0}}^{\infty} \frac{-\epsilon_{s} \left[ J_{n}^{2} (\alpha_{ns}) - J_{n-1} (\alpha_{ns}) \cdot J_{n+1} (\alpha_{ns}) (\alpha_{n}^{2} + b_{n}^{2}) - J_{n}^{2} (\alpha_{ns}) (\alpha_{n}^{2} - n^{2})^{2} \left[ 1 - \left( \frac{\omega}{\omega_{ns}} \right)^{2} \right]^{2}$$
 (3.90)

where e is a Neumann factor having the values;

$$\epsilon_s = 2$$
,  $s = 0$ 

Equation (3.90) represents the space-averaged noise reduction coefficient of a twodimensional circular shell in the absence of acoustical damping. As in the threedimensional case, acoustic damping may be introduced through a value of the dynamic magnification factor at resonance. Thus the third term in the denominator under the summation sign becomes

$$\left\{1 - \left(\frac{\omega}{\omega_{ns}}\right)^2\right\}^2 + \frac{1}{Q_{ac}^2} \left(\frac{\omega}{\omega_{ns}}\right)^2$$

when w-wns.

It should be noted that the mode number in above corresponds to the mode number in the circumferential direction used in the response equations in Section V, and that the mode number is above is the other mode number required to define a two-dimensional acoustic mode.

It was shown in Section 2.c that the total internal pressure may be obtained by the linear summation of the effects of all the panels forming the bounding wall. Thus, the total internal pressure power spectral density is obtained by multiplying equation (3.90) by the number of skin panels around the circumference of the fuselage, between two adjacent ring frames. Allowance may be made for the effect

of a floor in the fuselage by reducing the number of panels. The effect of fuselage windows may be introduced by calculating the structural response of the windows (i.e., panels having modified structural characteristics) and the resulting internal pressure and summing to give the total internal pressure power spectral density.

# 3. COUPLING OF THE INTERMEDIATE MODES

The theoretical treatment of the coupling of the panel groups with the internal air mass of the fuselage is carried out in exactly the same manner as for the individual panels of the previous case. In the present case, a single piston vibrating in the wall of the shell now represents a panel group composed of N panels supported by N + 1 intermediate stringers between two adjacent ring frames. The motion of each panel group is assumed to be uncorrelated with its neighboring group, in the same way that the individual panels of the previous case were assumed to be uncorrelated.

Converting the average motion of the panel group (the equation for which is developed in Section V and is similar in form to equation (3.84)) into an equivalent piston and substitution into equation (3.76) allows the definition of the internal pressure response. It should be noted that the total length of a particular panel group is dependent on the typical correlation lengths for the fluctuating pressure environments, and these lengths are discussed in detail in Section IV. The average pressure of the acoustic field within the fuselage is again obtained from equation (3.90), the only difference being that the b's used for the evaluation of the Fourier coefficients (equations (3.86 - 3.89)) now represent the total circumferential length of the panel group. The total internal pressure power spectral density is obtained by multiplying equation (3.90) by the number of panel groups around the circumference of the fuselage, which in fact is also the number of individual panels around the circumference.

## LIST OF SYMBOLS

# LIST OF SYMBOLS USED IN SECTION III

α	constant in the wave equation,
ak'an	Fourier coefficients
Ь	constant in the wave equation
b <sub>k</sub> ,b <sub>n</sub>	Fourier coefficients
c	speed of sound
d	constant in the wave equation
e,e <sub>mn</sub> ,e <sub>mns</sub>	dilatation
h	thickness of shell wall
m	integer, number of axial half wavelengths along the cylinder or panel
n	integer, number of circumferential waves around the cylinder, or number of panel halfwaves
P	pressure
$q_{mn}(t), q_{mns}(t)$	time variation of the radial displacement in the (m-n)-mode or (mns)-mode.
r	radial coordinate
ī =	$Kr\left[1-\left(\frac{\Phi}{K}\right)^2\right]^{1/2}$
<b>^</b> =	r R
s	acoustic mode number, or an integer
t	time
υ	axial component of displacement
v	tangential component of displacement
w	radial component of displacement
×	axial coordinate, or integer

×	non-dimensional axial coordinate
У	circumferential coordinate
<del>ጀ</del>	non-dimensional circumferential coordinate
A	constant
A <sub>0</sub> .	area
A ns	coefficient defined by Equation (3.75)
$F_{mn}(t)$ , $F_{mns}(t)$	generalized forces for the (mn) and (mns) modes at time t
$H\left(\frac{\omega}{\Omega_{mns}}\right)$	dynamic magnification factor for the (mns) coupled mode
J <sub>n</sub> (α <sup>^</sup> )	n -th order Bessel function of the first kind and argument $\alpha$ $\stackrel{\Lambda}{r}$
J <sub>n</sub> (α <sub>nx</sub> <sup>A</sup> )	n —th order Bessel function of the first kind and argument a $\overset{\Lambda}{\text{nx}}$
j <sup>2</sup> (u)	joint acceptance for the (mni) shell mode
J <sub>n</sub> (F)	n—th order Bessel function of the first kind and argument $(\overline{r})$
$J_{\alpha\alpha}^{2}(\omega)$	joint acceptance for the (mn) panel mode
$K = \frac{u}{c}$	acoustic wave number
Kmns	generalized stiffness of the structural-acoustic system
K <sup>(s)</sup>	generalized stiffness of the (mn) shell mode
K <sup>(a)</sup> mns	generalized stiffness of the (mns) acoustic mode
L <sub>x</sub>	axial length of the shell
M <sub>o</sub>	total mass of the shell
Mmn	generalized mass of the (m n)—shell made
M <sub>mns</sub>	generalized mass for the (mns) coupled mode
M <sub>mns</sub>	generalized acoustic mass for the (mns) mode
N	number of panels in a row

$P_{e}(\overline{x}, \overline{y}; t)$	external pressure on the shell at the point $(\overline{x}, \overline{y})$
P <sub>n</sub> (ω)	amplitude of internal pressure component at frequency w
P <sub>mn</sub> (r, φ, x; ω	
Q <sub>mns</sub>	effective dynamic magnification factor for the (mns) coupled mode
Q <sub>ac</sub>	effective acoust , dynamic magnification factor
R	shell radius
R	dimensionless radial coordinate
=	$KR\left[1-\left(\frac{\phi}{K}\right)^2\right]^{1/2}$ for the three-dimensional acoustic field
Rns	roots of Equation (3.21)
S <sub>ρ</sub> (ω)	power spectral density of the external pressure fluctuations at frequency $\boldsymbol{\omega}$
.S <sub>p<sub>1</sub></sub> (ω)	power spectral density of the internal acoustic field at frequency $\omega$
$S_{p_i}(r, \overline{x}, \overline{y}; \omega)$	power spectral density of the internal acoustic field at the point (r, $\overline{x}$ , $\overline{y}$ ) and frequency $\omega$
S <sub>w</sub> (ω)	power spectral density of the displacement response at frequency $\omega$
S <sub>w</sub> (x, ȳ; ω)	power spectral density of the displacement response at the point $(\overline{x},\overline{y})$ and frequency $\omega$
υ <sub>ο</sub>	work done per unit volume
U <sub>O</sub> (ω)	amplitude of radial displacement at frequency w
u <sub>r</sub>	redial component of particle displacement for the two-dimensional acoustic field
U <sub>p</sub>	tangential component of particle displacement for the two-dimensional acoustic field
Y <sub>n</sub> (ፑ)	n-th order Bessel function of the second kind and argument 7
<b>;</b> =	<u>mπ</u>
<b>x</b> =	$KR = \frac{\omega R}{c}$

<sup>a</sup> ns	value of the constant a for the (ns)-resonant mode of the two-dimensional acoustic field enclosed by a rigid wall (see Equation 3.66)
α <sub>nx</sub>	value of the constant $\alpha$ for the (nx)-resonant mode of the two-dimensional acoustic field (note that $x$ is an integer which may or may not be equal to $s$ )
β	angle subtended by two radial pistons
γ <sub>m n</sub>	space average constant for the (m n)-mode shape of the cylinder and panel, defined by Equations (5.8) and (5.62) respectively
ć s	Neumann factor defined by Equation (3.90)
μ	mass per unit area
Po	ambient density of the cabin medium
φ	circumferential coordinate $\left(=\frac{y}{R}\right)$
ф <sub>m n</sub>	normalized component deflection shape of the (mn) shell mode
	$(=\phi_{mn_1}+\phi_{mn_2})$
Ф <sub>0</sub>	angle subtended by a single radial piston
မ	steady state frequency
ω <sub>m</sub>	the resonant frequency of the m-th axial acoustic mode of a cylindrical shell
ш m п	resonant frequency of the (min)-structural mode
ယ ns	resonant frequency of two dimensional acoustic field
ω mns	acoustic resonant frequency (in the absence of the shell)
Φ <sub>n</sub> (φ)	periodic component of the pressure amplitude for the two-dimensional acoustic field
Ω	Acoustic resonant frequency of the shell-airmass system ( = $\omega_{m.n.s}$ when $R = R_{n.s}$ )
$\Omega_{ exttt{mns}}$	resonant frequency of the dynamically coupled system
()	denotes mean square

#### SECTION IV

#### CHARACTERISTICS OF THE FLUCTUATING PRESSURE ENVIRONMENTS

When computing the response of structures to fluctuating pressures, it is necessary to describe the fluctuating pressure environment in terms of;

- i) Overall Level
- ii) The Power Spectrum
- iii) The Narrow-Band Space Correlation Coefficients

In the following sections, each of the above properties is discussed for the aerodynamic turbulence environment, the jet noise environment, and a reverberant acoustic field environment.

### 1. AERODYNAMIC TURBULENCE ENVIRONMENT

The aerodynamically induced pressure fluctuations acting on the exterior surface of an aircraft in flight are an important source of cabin noise and can also be of sufficient intensity to cause fatigue failure of parts of the structure. Over a considerable portion of the aircraft only the attached boundary layer sources are significant, and these are the only sources considered in the present investigation.

The prediction methods put forward here for the overall level, power spectrum and narrow-band space correlation functions are those suggested by Lowson (Reference 15), who carried out an extensive study of the basic mechanisms underlying the turbulence phenomenon.

### a. Overall Level

Experimental and theoretical information on the overall level, particularly at supersonic speeds, is fragmentary and not in particularly good agreement. However, reasonably good correlation has been found using  $p_{\rm rms}/q$  as a parameter (Reference 16), where  $p_{\rm rms}$  is the root mean square pressure fluctuation, and q is the dynamic head (= 0.5 p Uo), though the accuracy of this prediction is reduced at supersonic speeds. Theory (Reference 17) suggests that  $p_{\rm rms}/\tau_{\rm w}$  would be a suitable non-dimensionalized parameter, where  $\tau_{\rm w}$  is the wall shear stress, but this theoretical prediction is dependent on the similarity of the boundary layer velocity profiles. Neither the effects on pressure fluctuations of roughness nor those of pressure gradient are found to be predicted on a  $\tau_{\rm w}$  basis. Thus, the use of  $\tau_{\rm w}$  increases the complexity of prediction without offering any advantages in increased applicability.

A comparison of the data for the above two schemes is shown in Figures 11 and 12, and some scatter is apparent. An advantage of using  $\tau_w$  is that  $\tau_w = 3.0$  does give a line which is approximately a mean of the various results at both subsonic and supersonic speeds (see Figure 12). However, there is every reason to expect

that  $p_{rms}$  would be a function of Mach number, so that a graph of  $p_{rms}/q$  versus M would be an acceptable predictor if the data could be shown to collapse.

The basic mechanism underlying the production of the surface pressure fluctuations beneath a turbulent boundary layer, at least in subsonic flows, appears to be two-fold. Firstly, there is a component associated with the eddies at the edge of the laminar sublayer, tentatively associated with the laminar sublayer "eruption" process (Reference 18). This component is relatively intense, is typically of high frequency, ( $\omega \, \delta_b / U_o > 1$ ) and has a convection speed of about 0.5 - 0.6 of the free stream velocity. The second component is associated with the eddies in the outer intermittent parts of the boundary layer. The intensity of this component appears to be markedly affected by upstream conditions such as roughness or protuberances, is typically of low frequency ( $\omega \, \delta_b / U_o < 0.2$ ) and has a convection speed of about 0.8 of the free-stream velocity. The experimental data which shows these effects in the clearest manner is that of Bull (Reference 19).

At subsonic speeds the wall layer is generally the most effective source of fluctuating pressures. The assumption that this will be true at supersonic speeds leads to an interesting result for the intensity. At subsonic speeds the available data suggests that the fluctuating pressure intensity is given approximately by

$$p_{rms} = 0.006 \times (0.5 \rho_o U_o^2)$$
 (4.1)

where  $0.5 \, \rho_0 \, U^2$  is the dynamic head,  $\rho_0$  is the free stream density and  $U_0$  is the free stream velocity. Assuming that the wall layer is the principal source of fluctuating pressure at supersonic speeds, leads to the following universal formula

$$P_{\text{rms}} = 0.006 \times (0.5 \, \rho_1 \, U_0^2)$$
 (4.2)

where  $\rho_{i}$  is the density near the wall at the site of the most intense eddies. Maintaining U as the free stream velocity implies a subsidiary assumption that the turbulent velocities are always proportional to  $U_{o}$ , and that there is no change of relative scale; this feature agrees with arguments put forward by Morkovin (Reference 20). Since the temperature increases and the density decreases near the wall, Equation (4.2) suggests a reduction in the value of  $\rho_{rms}/q$  at supersonic speeds; this observation has been the subject of unpublished work by both Eldred and Houbolt. Following this argument, Lowson (Reference 15) has suggested that

$$p_{rms}/q = \frac{0.006}{(1+0.14 \text{ M}^2)} \tag{4.3}$$

be used as an empirical curve for the fluctuating pressure intensity beneath an attached turbulent boundary layer. This curve is also plotted in Figure 11, and can be seen to be a fairly good, slightly conservative fit to the available data.

Figures 11 and 12 show that there is reasonable agreement between the prediction curve suggested here and that using  $p_{rms}/\tau_w = 3.0$ , based on Bies methods for predicting  $\tau_w$  (Reference 21).

Equation (4.3) may be rewritten,

$$P_{rms} = \frac{0.0042 \text{ p}_{o}}{M^{-2} + 0.14} \tag{4.4}$$

where  $p_{o}$  is the free stream static pressure. Thus as M becomes very large  $p_{rms}$  becames equal to 0.03  $p_{o}$ . Although use of a formula such as (4.1) would suggest intensities several orders of magnitude greater than this, it seems reasonable that the limiting intensity of the fluctuating pressure sources would be proportional to the static pressure.

## b. Spectral Distribution

The frequency spectra of attached turbulent boundary layer pressure fluctuations are found to scale on a Stroubal number basis; that is the frequency is non-dimensionalized by multiplying by a typical length and dividing by a typical velocity. However, the choice of correct typical lengths and velocities is far from easy. Free stream velocity is generally used for the non-dimensionalized velocity, aithough the use of a typical eddy convection velocity, itself a function of frequency, would correspond more closely with the physical situation. For simplicity, free stream velocity will be used here.

Definition of a typical length is more difficult. Boundary layer thickness  $\delta_i$ , displacement thickness  $\delta^*$ , and momentum thickness  $\overline{\theta}$  have all been used by various aumors. For subsonic boundary layers most results have been taken for equilibrium flows with a similar ratio of these characteristic lengths, so that non-dimensionalization using any of these gives very similar collapse. In supersonic flows the typical lengths do vary widely with Mach number, but no final conclusion can be drawn on the relative merits of the collapse against any particular length. Perhaps the most generally used typical length is  $\delta^*$ , the displacement thickness. However, in this report the boundary layer thickness  $\delta_b$  will be used for three reasons; firstly, it is easier to predict, secondly, it is related to a physical characteristic of the flow, the size of the largest eddies; and thirdly, it gives a slightly improved collapse of the only available supersonic data.

The principal problem in predicting subsonic spectra under any scheme is estimation at the low frequencies. Experiment, both in flight and in wind tunnels, shows considerable low frequency scatter from the very low values reported by Hodgson (Reference 22) for a glider, to the high values reported by Gibson (Reference 23) and Maestrello (Reference 24) for full scale aircraft, although Hodgson's results were

taken at low Reynolds number on a far from equilibrium boundary layer, and are therefore not considered relevant here. It is extremely difficult to define any single curve from the available data. Bies has recently published a detailed review of spectral measurements in a wind tunnel and in flight (Reference 21) and suggested the curves shown in Figure 13 as means through the data. The scatter about these curves is about  $\pm 5$  dB. These curves have been converted to the present basis by assuming that the wind tunnel results were taken at a typical Mach number of 0.5 and a typical Reynolds number of 10 $^7$ , while the flight results were typified by the values M=0.8 and  $Re=10^8$ . Values of the boundary layer parameters were estimated from the curves given by Bies, using the above figures.

では、100mmの

Since it is desired to apply the empirical results from the present study to the supersonic case, and there are, at present, no reliable in flight supersonic measurements, the supersonic wind tunnel data of Speaker and Ailman (Reference 25)—have been reviewed carefully. Figure 14—shows a re-plot of the Speaker and Ailman data on the present basis. Overall level has been non-dimensionalized by dividing by  $q/(1+0.14\ M^2)$ , and the Stroubal number is based on free stream velocity and boundary layer thickness.

An empirical curve fit for the frequency spectrum which is close to the mean empirical curves derived from Bies results and is a good representation of the Speaker and Ailman data for the supersonic cases is given by Lowson (Reference 15) as:

$$\frac{p^{2}(\omega)}{q^{2}} = \left\{ \frac{0.006}{1 + 0.14 \, M^{2}} \right\}^{2} - \frac{1}{\omega_{o} \left\{ 1 + \left( \frac{\omega}{\omega_{o}} \right)^{2} \right\}^{3/2}}$$
(4.5)

where the typical frequency  $\omega_0$  has been taken as equal to  $8U_0/\delta_0$ . This curve is shown in both Figures 13 and 14 and has the advantage of being analytical as well as matching the data. As can be seen, the curve is probably conservative at the high frequencies for the highest Mach numbers.

There is a definite trend noticeable in Figure 14, which was also pointed out by Speaker and Ailman. The slope of the high frequency portion of the curves for M>0.8 is greater than that of the lower Mach number spectra. Furthermore the curve for M=0.42 agrees closely with that of Bull (Reference 19) in the high frequency region. Typically, low Mach number wind tunnel spectra decay at 20 dB per decade at high frequencies, while the present high Mach spectra decay at 40 dB per decade. Little independent data is available to substantiate this trend, although Macstrello's results (Reference 24) taken at 0.63 < M < 0.78 do show some increase in decay rate. Since the trend to increased rates of decay above a Mach number of about 0.8 cannot be conclusively verified, it seems desirable to exercise some caution in making predictions, and this is reflected in the empirical curve in Figure 14. It may be noted that while the empirical curve does lie below the low speed wind tunnel

data at high frequencies it appears to match the subsonic flight data well (see Figure 13). It is thought that the empirical curve may be used with some confidence for aircraft predictions unless extraneous low frequency effects are present.

Since the formulae given here requires a knowledge of the boundary layer thickness,  $\delta_b$ , the empirical equation suggested by Bies (Reference 21) is recommended here, namely,

$$\frac{\delta_{b}}{x} = 0.37 \text{ Re}_{x}^{-0.2} \left\{ 1 + \left( \frac{R_{e}}{x} \right)^{2} \right\}^{0.1}$$

where x is the distance from the leading edge of the body and  $Re_{x} = U_{0}x/v$ , where v is the kinematic viscosity.

## c. Narrow-Band Space Correlation Coefficients

The key parameter needed to describe an impinging pressure field is the narrow-band space correlation function, often referred to as the cross power spectral density, which can be written as the product of the mean square (or power) spectral density of the pressures and a narrow-band cross correlation coefficient.

Consider two points (x,y) and (x',y') on the surface of the structure and let P(x,y,t) and P(x',y',t) denote the instantaneous pressures at these two points. In addition, assume that these pressures are passed through a narrow-band filter of bandwidth  $\Delta\omega$  and centered on frequency  $\omega$ ; and let  $P(x,y,t;\omega)$  and  $P(x',y',t;\omega)$  denote the filtered outputs. The narrow-band space correlation function is denoted by  $R(x,y;x',y';\omega)$  and is defined functionally as (in the limit as  $\Delta\omega$  approaches zero)

$$R(x, y; x', y'; \omega) = \frac{1}{\Lambda \omega} \overline{P(x, y, t; \omega) P(x', y', t; \omega)}$$
(4.7)

where the bar ( ) denotes time average. When the points (x, y) and  $(x^1, y^1)$  are coincident, this correlation function reduces to the mean square pressure spectral density, at the point (x, y) for instance, and such a quantity can be denoted simply as  $R(x, y; \omega)$ . The narrow-band space correlation coefficient is denoted as  $C(x, y; x^1, y^1; \omega)$  and is defined as

$$C(x, y; x', y'; \omega) = \frac{R(x, y; x', y'; \omega)}{R(x, y; \omega)}$$
(4.8)

Thus, as defined, the numerical values of  $C(x, y; x', y'; \omega)$  lie between  $\pm 1$ .

A simplified form of the correlation coefficient is assumed throughout this work, namely that the correlation coefficient can be written in separable form with respect to the coordinate axes of the structure. Thus,

$$C(x, y; x', y'; \omega) = C(x, x'; \omega) \cdot C(y, y'; \omega)$$
 (4.9)

In addition it is assumed that the x-component and the y-component of the pressure field are homogeneous, in the sense that the correlation coefficients  $C(x, x^i; \omega)$  and  $C(y, y^i; \omega)$  are even functions only of the separation distance (and of course frequency) along their respective coordinate axes so that they are independent of the actual position of either of the points (x, y) or  $(x^i, y^i)$ . Thus in simplified form the pressure correlation coefficient reduces to:

$$C(x, y; x', y'; \omega) = C(\zeta; \omega) \cdot C(\eta; \omega)$$

$$C(\zeta; \omega) = C(-\zeta; \omega) \qquad \zeta = x - x'$$

$$C(\eta; \omega) = C(-\eta; \omega) \qquad \eta = y - y'$$
(4.10)

Wind tunnel measurements of narrow-band pressure correlations have been obtained for subsonic speeds but are quite scarce for supersonic speeds. However, a limited amount of broadband correlation data exists for the supersonic case, which indicate, as a first approximation that the subsonic pressure correlations can be used for the higher speed range.

Measurements of longitudinal and lateral correlations in wind tunnels have been made by Bull (Reference 19) and others (References 22 - 27). The correlation data obtained by these investigators are presented in Figures 15 and 16 where it is observed that the data have been collapsed on correlation Strouhal numbers  $\zeta_{\rm W}/U_{\rm c}$  and  $\eta_{\rm W}/U_{\rm c}$ . In comparing these data, it is observed that good agreement exists for the longitudinal correlation, while the lateral correlations exhibit significant scatter.

From these data, mean empirical expressions have been derived for the space correlation coefficients, as follows;

$$C (\zeta; \omega) = \exp \left[ -0.1 \left| \zeta \right| \omega / U_c \right] \cdot \cos (\zeta \omega / U_c)$$
 (4.11)

$$C(\eta; \omega) = \exp \left[-0.720 \mid \eta \mid \omega/U_c\right]$$
 (4.12)

The above correlation coefficients may be obtained by direct averaging and normalizing of the narrow-band pressure components as indicated by the deficitions (4.7) and (4.8). Alternatively, they may be obtained as special cases of the space-time correlation functions. Experimental measurements of the longitudinal space-time correlation coefficients are approximated reasonably well by the equation

$$\frac{P(x, y, t; \omega) \cdot P(x + \zeta, y, t + \tau; \omega)}{R(x, y; \omega)} = C(\zeta, \tau; \omega)$$

$$= \left| C(\zeta; \omega) \right| \cos \omega (\tau - \zeta/U_c)$$
(4.13)

where the point  $(x + \zeta, y)$  is downstream of the point (x, y) by a distance  $\zeta, \tau$  denotes a time delay in the downstream pressure, the ratio  $\zeta/U_C$  denotes the time for the flow to traverse the distance  $\zeta$ , and  $|C(\zeta;\omega)|$  denotes the maximum value of the space-time correlation coefficient. The quantity  $|C(\zeta;\omega)|$  can be obtained experimentally by adjusting the delay times  $\tau$  so as to maximize the space-time correlation. In Equation (4.12) this delay time would be  $\tau = \zeta/U_C$ . For a fixed value of  $\zeta$ , the delay time for maximum correlation will vary somewhat with frequency. Equation (4.13) can be treated as exact however, by assuming that the convection velocity  $U_C$  is a function of frequency  $\omega$  and the distance  $\zeta$ , that is  $U_C = U_C(\zeta;\omega)$ . The spatial correlation coefficient  $C(\zeta;\omega)$  is obtained from Equation (4.13) by setting  $\tau = 0$ , thus;

$$C(\zeta; \omega) = |C(\zeta; \omega)| \cos \zeta \omega/U_c$$
 (4.14)

Measurements of  $|C(\zeta;\omega)|$  have been made by Bull (Reference 19) for different Mach numbers and boundary layer displacement thicknesses,  $\delta^*$ , and these results are presented in Figure 17. The exponential function in Equation (4.11) is a close approximation to this curve. Similar data are presented in Figure 18 for the maximum lateral space-time correlation and Equation (4.12) closely approximates this curve. It should be noted that Equations (4.11) and (4.12) indicate that the area over which the pressures can be considered correlated is large for low frequency components and small for high frequency components; and hence, the correlation varies inversely with convection velocity  $U_c$ .

A typical value of  $U_c$  for the larger eddies, or low frequency components, is 0.9  $U_c$  and for the smaller eddies, associated with the high frequency pressure components is 0.6  $U_c$ .

Although convection velocity has been found to vary with both frequency and spatial separation, in the present study it is recommended that Bies formula be used (Reference 21) which ignores spatial separation;

$$\frac{U_c}{U_o} = \left[0.6984\right] \left(\frac{U_o}{\omega \delta^*}\right)^{0.09} \qquad (4.15)$$

where;

$$\delta^{*} = \frac{\delta_{b}}{8} \quad \text{for} \quad M < 1 \tag{4.16}$$

$$\delta^{*} = \frac{(1.3 + 0.43 \text{ M}^2) \delta_{b}}{10.4 + 0.5 \text{ M}^2 \left[1 + 2 \times 10^{-8} \text{ Re}_{x}\right]^{1/3}} \text{ for M > 1}$$
 (4.17)

and  $\delta_0$  is as defined by Equation (4.6). A curve, based on this empirical formula is shown in Figure 19.

It is important to note that the narrow-band correlation data obtained by Maestrello have not been measured at values of  $\omega \, \delta_D/U_C < 0.2$ . It can be seen that if these small values were substituted in Equations (4.11) and (4.12), very large correlation lengths would result. In physical terms, a correlation length greater than the boundary layer thickness would not be expected, therefore low frequency correction factors must be applied to these two equations. Bull, (Reference 19) has presented measured asymptotic values of the narrow band longitudinal and lateral correlation coefficients for small values of  $\zeta \, \omega/U_C$  and  $\eta \, \omega/U_C$ . These data are presented in Figures 20 and 21, and based on this, the corrected expressions for the space correlation coefficients are (Reference 15)

$$C \left(\zeta;\omega\right) = \exp\left[-\left\{\left(0.1 \frac{|\zeta| \omega}{U_{c}}\right)^{2} + \left(0.27 \frac{|\zeta|}{\delta_{b}}\right)^{2}\right\}^{0.5}\right] \cos \frac{\omega \zeta}{U_{c}}$$
(4.18)

$$C (\eta; \omega) = \exp \left[ - \left\{ \left( 0.72 \frac{\omega |\eta|}{U_c} \right)^2 + \left( 1.95 \frac{|\eta|}{\delta_b} \right)^2 \right\}^{0.5} \right]$$
 (4.19)

A comparison of the broadband longitudinal space correlation coefficient for Mach 0.59 and Mach 3.45, obtained by Kistler and Chen (Reference 28) is shown in Figure 22, the data having been corrected for momentum thickness and convection velocity. The close agreement obtained for the two Mach numbers suggests that the range of velocity expressed in Equations (4.18) and (4.19) can be extended to include supersonic flows.

In order to generalize the mathematical relationships developed so far, it is convenient to rewrite Equations (4.18) and (4.19) in general functional forms and to express these correlation coefficients in terms of non-dimensional separation distances  $\frac{1}{\zeta}$  and  $\frac{1}{\eta}$ . The resulting expressions are;

$$C(\overline{\zeta}; \omega) = \exp \left[-\delta_{\chi} |\overline{\zeta}|\right] \cos \gamma_{\chi} \overline{\zeta}$$

$$C(\overline{\eta}; \omega) = \exp \left[-\delta_{\chi} |\overline{\eta}|\right]$$
(4.20)

where;

$$\delta_{x} = \left\{ \left( 0.1 \frac{L_{x} \omega}{U_{c}} \right)^{2} + \left( 0.27 \frac{L_{x}}{\delta_{b}} \right)^{2} \right\}^{1/2}$$

$$\gamma_{x} = \frac{L_{x} \omega}{U_{c}}$$

$$\delta_{y} = \left\{ \left( 0.72 \frac{L_{y} \omega}{U_{c}} \right)^{2} + \left( 1.95 \frac{L_{y}}{\delta_{b}} \right)^{2} \right\}^{1/2}$$

$$\overline{\zeta} = \zeta/L_{x}$$

$$\overline{\eta} = \eta/L_{y}$$
(4.21)

### d. Correlation Length and Coincidence

The narrow band space correlation function  $R\left(\zeta,\eta;\omega\right)$  can be thought of physically as a measure of the time average value of the relative phase between pressures acting at two points (x,y) and (x',y') which are separated by component distances  $\zeta$  and  $\eta$ . This implies that the pressure acting at any point (x',y') within the central region of positive correlation will, over a long time average, be in-phase for an R fraction of this time with the pressure acting at the center (x,y) of the region. The correlation length,  $C_L$ , is defined as equal to that length over which the excitation may be considered as perfectly correlated in space, i.e., the correlation length times unit correlation is equal to the area under the normalized space correlation curve. Thus for boundary layer turbulence the correlation length in the flow direction is,

$$C_{L} = \frac{2 S_{X}}{S_{X}^{2} + \gamma_{X}^{2}} \cdot L_{X}$$
 (4.22)

and the correlation length at right angles to the flow is,

$$C_{L} = \frac{2}{\delta_{v}} \cdot L_{y} \tag{4.23}$$

where,  $\delta_{_{_{\boldsymbol{y}}}}$ ,  $\delta_{_{_{\boldsymbol{x}}}}$ , and  $\gamma_{_{_{\boldsymbol{x}}}}$  are as defined by Equation (4.21).

When the pressure correlation lengths are equal to the bending half wave lengths of the structure for a particular mode, the pressures are on the average spatially

correlated with the bending deflection shape of that mode. This condition results in a maximum joint acceptance for the mode, and when this condition also occurs at ar near the resonant frequency of the mode, the modal response is a maximum, thus producing what is commonly called coincidence. It can be shown that wave length matching at resonance for a finite panel causes the bending wave propagation velocity to be equal to the surface pressure convection velocity; this is often used as the basic definition of coincidence.

The typical pressure wave length can be denoted by  $\lambda_p = U_c/f$ , where  $U_c$  is the convection velocity and f some arbitrary excitation frequency. Now, if the elastic wavelength of the m-th axial mode is defined as  $\lambda_e = 2 \, L_\chi/m$ , where  $L_\chi$  is the structural dimension in the x-direction, then the elastic-to-pressure wavelength ratio is

$$\frac{\lambda_{e}}{\lambda_{p}} = \frac{2 L_{x} f}{m U_{c}}.$$

The condition of coincidence occurs when the elastic and pressure wavelengths are equal, i.e., when;

$$\frac{\lambda_{e}}{\lambda_{p}} = \frac{2 L_{x} f}{m U_{c}} = \frac{\gamma_{x}}{m \pi} = 1 \qquad (4.24)$$

### 2. THE JET MOISE ENVIRONMENT

### a. Introduction

The noise field produced by a jet engine can be divided into three broadly distinct regions, described, with the aid of Figure 23, as follows:

### (1) Close to the Jet Boundary

The pressure fluctuations in this region are strongly influenced by the convection of the hydrodynamic turbulent field. The region extends to approximately two jet diameters out from the boundary and downstream to a plane about 15 diameters down the nazzle exit plane.

## (2) The Near Field

The near field includes not only outwardly propagating waves, but also local reciprocating motions and pressure fluctuations, such as may be directly induced by fluctuating vartex movements in the turbulent gas flow. The region extends to about ten diameters out from the jet boundary, twenty diameters downstream and ten diameters upstream of the nozzle exit plane. The position of the outer surface of this region is not clearly defined and is thought to be frequency dependent (Reference 29).

## (3) The Far Field

In this region the pressure and particle velocity are in-phase, or very nearly in phase, and the acoustic intensities fall off in proportion to the inverse square of the distance. Within a particular narrow band of frequencies, the far field of any noise source is the region whose distance from it substantially exceeds two wavelengths (Reference 30).

## b. Overall Acoustic Power Level

Classical aerodynamic noise theory, developed by Lighthill (Reference 31) and 32), shows that the overall sound power of a circular stationary jet is proportional to  $\rho_0 V^8 D^2/c^5$  where  $\rho_0$  is the ambient density, V the nazzle velocity, D the nazzle diameter and c the ambient speed of sound. This expression was derived for subsonic flow but, experimentally, it has shown remarkable validity for exhaust velocities up to twice the ambient speed of sound. At velocities higher than this, the exponent begins to decrease, reaching a minimum of about 3 at velocities greater than 4,000-5,000 f.p.s.

It will be noticed that Lighthill's expression contains only one exhaust gas parameter, namely velocity; two further exhaust gas parameters of some importance are density and temperature. Theory gives a multiplicative factor  $(p/p_0)^2$  for the noise emission from unit volume of turbulence, where p is the mean gas density, while jet noise has been found experimentally to vary approximately as  $(p_1/p_0)^2$  for different exhaust gases, where  $p_1$  is the nozzle flow density. However, for velocities up to approximately twice the ambient sound speed, the noise appears to be independent of any density variations caused by a temperature change. The exact effect of temperature on the overall sound power is not clear, although it is known to have an important effect upon the spectrum and directivity, (References 33, 34, and 35). Rollin, in Reference 35, has shown that the effects of a temperature increase, with a resulting density decrease, tend to cancel so that the overall level of acoustic power is a function of velocity alone. However, the SAE Prediction Method (Reference 36) includes a density correction based on the square of the density; this result was determined from experimental measurements and agrees with Lighthill's analysis.

These uncertainities have led to many attempts to collapse experimental sound power data against numerous normalizing parameters, many of which are based upon Lighthill's parameter, but which include jet stream energy, momentum and mass flow. These parameters have resulted in varying degrees of collapse of the data but none shows any particular advantage and any method can be expected to accurately predict power levels to within 2 or 3 dB for conventional jet geometries.

Some typical experimental results for jet flow are shown in Figure 24, which describes the total acoustic power generated by the jet flow as a function of the jet exhaust gas velocity. These results, obtained by Eldred (Reference 37) show that the acoustic power generated is proportional to the eighth power of the jet velocity

for exit speeds up to 2,000 f.p.s., but that above this exit speed, the power levels conform more to a velocity cubed law as predicted by Ffowcs Williams and Lighthill (References 38 and 39).

The SAE prediction method (Reference 36) was developed from experimental measurements for application to a wide range of conventional and afterburning turbojet engines. This method leads to an estimate of the maximum octave band sound pressure levels observed along a 200 ft. sideline. A normalized curve of Overall Sound Power Level, corrected for jet density and nozzle area is also presented in Figure 24, for comparison with Eldred's results. This curve was calculated on the assumption that the maximum overall directivity, at 45° to the jet axis, is 8 dB. It is apparent that for velocities less than 2,500 f.p.s. the SAE method over-estimates the overall power level while for velocities greater than 2,500 f.p.s. it under-estimates the overall power level; however, the difference between the two empirical curves does not exceed approximately 3 dB for practical turbojet operating conditions. The SAE method has been found to predict the octave band sound pressure level for jet engines to within 5 dB. It should be noted that this is the maximum sideline noise level and the method does not attempt to include actual variation of the frequency spectrum with radiation angle.

For jet exit velocities less than 2,000 f.p.s. the experimental results of Figure 24 can be fitted by the equation;

OAPWL/unit nozzle exit area = 
$$77.5 \log_{10} V - 85.5$$
 (4.25)

where the nozzle exit area is in ft<sup>2</sup> and V is the exit jet velocity in f.p.s. For speeds above 2,000 f.p.s. the results can be fitted by the equation;

OAPWL/unit nozzle exit area = 
$$32.3 \log_{10} V + 62.3$$
 (4.26)

If the density of the jet exhaust flow is significantly different from that of a typical current engine then the result should be modified by adding the factor, (Reference 36),  $20 \log_{10}(\rho/\rho_{\rm T})$  where  $\rho_{\rm T}$  is a typical current engine gas density (assumed to be about  $0.001 \, {\rm slug/fr}^2$ ) and  $\rho$  is the density of a non-typical gas flow.

The effect of aircraft motion on the sound produced is simply allowed for by substituting the relative exhaust velocity in Equations (4.25) and (4.26).

### c. Frequency Spectra

The overall sound field of a jet engine shows maximum sound pressure levels along an axis making an angle of approximately 35 degrees to the jet-flow direction. This angle is found to increase with increasing jet exit velocity. However, the high frequency sound exhibits a peak at a greater angle than the overall, and conversely, the low frequency sound pattern peaks closer to the jet axis. This "directivity" is

caused by the acoustic sources (pressure fluctuations) in the exhaust being convected along in the flow. The variation in angle for different sources is due to their location in the exhaust flow; the higher frequency sources corresponding to fluctuations near the nozzle exit, and the low frequency sources to fluctuations from the slower downstream flow. Thus the directivities of the individual sources are determined by their location in the exhaust flow and the individual distribution of each frequency band of sources must be considered in the prediction of the near field.

The normalized jet noise spectrum adopted for the present study is based on the results of Howes, et al (Reference 40) and is shown in Figure 25. The figure describes the total acoustic power generated by a single jet engine as a function of the Strouhai number, the actual levels occurring at specific points around the jet being dependent, of course, on the direction of radiation.

### d. Prediction of the Free-Field Sound Pressure Levels

The prediction technique is based on division of the exhaust flow into a series of uncorrelated source regions, and the allocation of a spectrum of sources in each region. This breakdown is complex, but because it is based on boundary and near field measurements, does appear to give a satisfactory description of the resultant noise field. This technique was originally used to study the near field noise of jets (Reference 41) and the acoustic loading on space vehicles due to exhaust flow noise (Reference 42). The source allocation is given by the two normalized spectra shown in Figures 26 and 27, from Reference 41). These spectra are for the two basic flow regions of the jet; the upstream region near the nozzle where the jet is driven by the core flow, and the downstream transition region. The results for the upstream flow show a normalization on the basic jet flow parameters and the distance downstream from the nozzle. The results for the transition region show that the spectrum is independent of downstream position in the jet flow. The latter result is limited to the transition region, following the initial core region, and must not be confused with the downstream fully developed flow which begins some 40 jet exit diameters downstream of the nozzle exit plane. Analytical studies of this latter region (References 43 and 44) have shown that the sound power per unit jet length is inversely proportional to the seventh power of the distance. For the transition region which is the region of interest here, it has been shown that the sound power generated is inversely proportional to the third power cothe distance (Reference 41).

Before being able to make use of the normalized spectra it is first necessary to determine the total acoustic power generated per unit length. The total power per segment in terms of the care length of the jet is described in Figure 28. This care length is given by an empirical expression derived by Eldred (Reference 41) as follows;

$$x_{t} = \left[6.9 \left(1 + 0.38 \,\mathrm{M_{e}}\right)^{2} \,\mathrm{r_{e}}\right] \left[\frac{1 + \epsilon}{1 - \epsilon}\right]$$
 (4.27)

where;

x is the distance from the nozzle exit plane to the core tip

M\_ is the exit Mach number

is the radius of the jet nazzle

and e is the ratio of the aircraft to jet velocity.

The free-field sound pressure level at a point 0 can be calculated as follows (see Figure 29);

- (1) Define the jet mixing pattern in terms of the core length x,
- (2) Divide the jet into at least twelve segments each of length, say  $x_{+}/3$ . (It is recommended that the core be divided into at least 3 segments).
- (3) Determine the variation of the overall acoustic power per unit axial distance and per unit nozzle area, as a function of the downstream position in the jet, using Figure 28. Thus, determine the overall acoustic power in each segment.
- (4) Compute the normalized power spectra for each source in the jet flow and for each octave band center frequency, using Figures 26 and 27. Since these spectra are of one cycle bandwidth, it is necessary to add the appropriate corrections to convert them to full octave band spectra.
- (5) Finally, the sound pressure level at a point in the free-field is obtained from the relation (Reference 41);

$$SPL^{(k)} = L \sum_{i=1}^{12} \left\{ PWL_i^{(k)} + 10 \log_{10} f_i(\theta_i) - 10 \log_{10} 4 \pi R_i^2 + 0.5 \right\} dB. re: 0.0002 dynes/cm2 (4.28)$$

where;

 $PWL_{i}^{(k)}$  = acoustic power of the i-th segment for the k-th octave (dB, re:  $10^{-13}$  watts).

10 log  $f_i(\theta_i)$  = directivity for the appropriate position in the jet flow, obtained directly in dB from Figure 30, (Reference 41) as a function of  $x/\lambda_0$ , the modified axial Stroubal number, and the angle  $\theta_i$  from the forward axis (see Figure 29).

R<sub>i</sub> = the distance between the center of the i-th segment and the point 0 in the free-field.

Notice that the summation is a logarithmic summation of the dB results. The overall sound pressure level is obtained by adding the results for the individual octave bands.

The foregoing procedure allows the free-field sound pressure levels to be calculated at points near to the jet. In order to predict structural response, it is necessary to convert the free-field levels to actual structural pressure loadings and this is described in the following section.

# e. Pressure Levels on Fuselage Structures

One immediate effect of placing a fuselage structure in a free-field is that of pressure-doubling at the structural surface directly facing the source. In the following discussion two cases are considered separately; aircraft having wing mounted engines, and aircraft having fuselage mounted engines. It should be noted that multi-engine cases are solved by considering the summation of the pressure fields for each engine calculated individually.

# Wing-Mounted Engines

A typical fuselage and engine configuration for this case is shown in figure 31. The distance between the center lines of the fuselage and engine is assumed to be at least fifteen jet diameters and the location of a typical source in the exhaust flow is indicated in the figure. The initial problem is to define the sound field for a single source of frequency in the jet flow, S, and determine the sound field at a point on the fuselage surface, Q. The coordinate system adapted is shown in Figure 32. The acoustic wave—is considered to be a plane wave of strength  $P_{\rm O}$  at the point where it reaches the fuselage, and the pressure fluctuations, without scattering effects are given by;

$$P = P_0 e^{i k (x-ct)}$$
 (4.29)

where

k is the wave number of the particular source =  $2\pi/\lambda$ 

 $\lambda$  is the wavelength = c/f

c is the speed of sound

t is time

and x is the distance in the direction of propagation (see Figure 32)

The wave direction is such that the normal to the wave makes an angle  $\,\beta\,$  to the normal to the axis of the fuselage. The point on the surface of the fuselage is given

by  $(a, z, \phi)$ , where a is the radius of the fuselage, z is the dimension along the axis, and  $\phi$  is the angle around the fuselage measured from the projection of the line joining the source to the fuselage on the perpendicular cross-section. When the angle  $\phi$  is zero, the point is on the far side of the fuselage, completely hidden from the source.

The solution for the scattering case can be shown to be (Reference 42);

$$P = \frac{4P_0}{\pi k a \cos \beta} \sum_{m=0}^{\infty} \left\{ \frac{\cos m^{\frac{m}{2}}}{C_m'} e^{i(-\gamma_m + \frac{\pi m}{2})} \right\} e^{i k z \sin \beta} e^{-2\pi i ft}$$
(4.30)

where  $C_{m}^{i}$  and  $\gamma_{m}^{i}$  are functions of  $k = \cos \beta$ ,

$$C_{o}^{t} = 2\left[\int_{1}^{2} (k\alpha \cos \beta) + N_{t}^{2}(k\alpha \cos \beta)\right]^{\frac{1}{2}}$$

$$(4.31)$$

$$C_{m}^{\epsilon} = \frac{1}{2} \left[ \left\{ J_{m+1}^{\epsilon} \left( ka \cos \beta \right) - J_{m-1}^{\epsilon} \left( ka \cos \beta \right) \right\}^{2} + \left\{ N_{m-1}^{\epsilon} \left( ka \cos \beta \right) \right\}^{2} \right]$$

$$-N_{m+1} (ka cos \beta) \begin{cases} 2 \\ 1 \end{cases}$$
 (4.32)

$$\gamma_{o}^{i} = T_{an}^{-1} \left[ \frac{-J_{1}(k\alpha \cos \beta)}{N_{1}(k\alpha \cos \beta)} \right]$$
(4.33)

$$\gamma'_{m} = T_{cm}^{-1} \left[ \frac{J_{m+1} (ka\cos\beta) - J_{m+1} (ka\cos\beta)}{N_{m-1} (ka\cos\beta) - N_{m+1} (ka\cos\beta)} \right]$$
 (4.34)

where

J and N are first and second kind of Bessel functions

- z is the axial distance along the fuselage
- is the angle around the fuselage from the projected direction of propagation of the wave on a circular section (i.e., the wave impinges directly on the cylinder at the angular point • = \*\* radians).

This result was developed from that given by Morse in Reference 14; for a normally incident plane wave scattered by a cylinder, by Potter in Reference 42 and proved mathematically by Wenzel in Reference 45.

The actual pressure variation on the fuselage surface is given by the real part of Equation (4.30). It should be noted that this expression cannot be used for the case of fuselage mounted engines since in this case the acoustic sources are very close to the structure. It is only applicable to wing-mounted engines where the sound field for a given source can be approximated to a plane wave at the point where it strikes the fuselage. The equation describing the pressure fluctuations is limited to some extent by the fact that the effects of spherical radiation have not been included. Furthermore, the surface of the fuselage was assumed to be perfectly rigid, which is not the case in practice. The complete solution, involving the scattering of an obliquely incident spherical radiation by a finite non-rigid structure will be extremely complicated and is not considered in the present study.

Equation (4.30) can be reduced to a simpler basic form as follows;

The pressure at a point on the fuselage surface, due to an obliquely incident plane wave of frequency  $\, f \, \, is \,$ 

$$P = A \cos (2 \pi f t + \Phi)$$
 (4.35)

where;

$$A = (x^2 + y^2)^{1/2}$$

$$\Phi = \operatorname{Tan}^{-1}\left(\frac{y}{x}\right)$$

$$\times = D_o(EG - FH)$$

$$D_0 = \frac{4 P_0}{\pi k a \cos \beta}$$

$$E = \sum_{m=0}^{\infty} \frac{\cos m \, \phi}{C_m^i} \sin \left(-\gamma_m^i + \frac{\pi \, m}{2}\right) \tag{4.36}$$

$$F = \sum_{m=0}^{\infty} \frac{\cos m \, \phi}{C_m^t} \cos \left(-\gamma_m^t + \frac{z \, m}{2}\right)$$

$$H = \sin(kz\sin\beta)$$

and  $P_0$  = free-field pressure calculated from the distributed source theory.

## Fuselage Mounted Engines

In this case the engines will be so close to the fuselage that the technique of scattering is not suitable. However, since the structure adjacent to the jet is leaded by the sources in the immediate vicinity, the source allocation method can be used for determining the free-field sound pressure level and conversion to fuselage pressure loadings may be achieved by use of a simple equation. For an abliquely incident wave, as shown in Figure 33, the pressure at a point on the fuselage surface may be determined from the equation;

$$P = P_0 \left( \frac{\cos 2\alpha + 3}{2} \right) \tag{4.37}$$

where  $\alpha$  is the angle between the wavefront and the tangent to the surface,  $-\pi/2 \le \alpha \le \pi/2$ , and  $P_0$  is the free-field pressure calculated from the distributed source theory. The resulting pressure loading on the fuselage, obtained from Equation (4.37) is shown in Figure 33.

## f. Narrow-Band Pressure Correlation Patterns

Two methods of describing the correlations are presented in this section; an analytical representation based on the calculated pressure levels occurring at the fuselage surface, and an empirical representation based on experimental measurements in the near field.

### (1) Analytical Definition

The expression developed by Potter (Reference 42) for the pressure acting on the fuselage surface, i.e., Equation (4.35), can be used to define the pressure correlation pattern simply by comparing the pressures at any two points on the surface. Consider two points on the fuselage, say X and X<sup>1</sup>; the correlation coefficient of the acoustic pressure (for the scattered case) for one source is;

$$R = \frac{\int_{0}^{1/f} A \cos(2\pi f t + \Phi) A^{T} \cos(2\pi f t + \Phi^{T}) dt}{\left\{\int_{0}^{1/f} A^{2} \cos^{2}(2\pi f t + \Phi) dt\right\}^{1/2} \left\{\int_{0}^{1/f} A^{T^{2}} \cos^{2}(2\pi f t + \Phi^{T}) dt\right\}^{1/2}}$$

$$= \frac{A A^{T} \cos(\Phi - \Phi^{T})}{\left\{A^{2}\right\}^{1/2} \left\{A^{T^{2}}\right\}^{1/2}}$$
(4.38)

Now, if

$$A = A'$$
, then  $R = \frac{A^2 \cos (\Phi - \Phi')}{A^2} = \cos (\Phi - \Phi')$  (4.40)

For a series of n uncorrelated sources of the same frequency;

$$R = \frac{\sum_{m=1}^{n} A_{m}^{2} \cos (\Phi_{m} - \Phi_{m}^{*})}{\sum_{m=1}^{n} A_{m}^{2}}$$
(4.41)

i.e., each correlation curve for each source is weighted by its overall pressure and then the covariances are added and the result normalized.

A final simplification is possible in calculating the correlation patterns from these expressions by determining the carrelation coefficient in two directions, one longitudinally along the fuselage parallel to the axis, and the other, laterally around the fuselage. For the case of the longitudinal correlations the angle  $\Phi$  is fixed for all points. Then if the sources in the stream are far enough away from the fuselage that the inclination angle  $\beta$  can be assumed constant, the same values for the factors D, E, and F, can be used for all sources of the same frequency.

Similarly, when the lateral correlations around the fuselage are calculated, the angle  $\,\beta\,$  can again be assumed constant, and it will be possible to fix the values of the factors  $\,D_{\!_{\!4}}$ ,  $\,G_{\!_{\!4}}$ , and  $\,H_{\!_{\!4}}$  for a series of sources at the same frequency.

### (2) Empirical Definition

The experimental narrow-band pressure correlation data obtained to date are summarized in Figure 34, which shows the positions relative to the jet nozzle plane where the measurements were carried out. These data were obtained by Howes, et al. (Reference 46), Cox, et al., (Reference 47), and Clarkson and Ford (Reference 48). While the narrow-band longitudinal pressure correlations are available at most of the points indicated in Figure 34, the correlations in the lateral direction (i.e., along an axis perpendicular to the plane of the figure) are available only at two points, both of which lie on the jet boundary.

In the above references, all the correlation data were plotted with the ratio of separation distance to nazzle exit diameter as abscissa. If the longitudinal correlation data are re-plotted as a function of a non-dimensional frequency parameter  $\omega \zeta / c$ , (where  $\omega$  is the center frequency,  $\zeta$  is the longitudinal separation distance and c is the speed of sound in ambient air), a relatively high degree of collapse is obtained, as shown in Figure 35. In some cases, where the original longitudinal correlation axis was

parallel to the jet boundary, the results were projected so that the axis was parallel to the jet centerline. Similarly, the lateral correlation data display a reasonable degree of collapse when plotted as a function of  $\omega\eta/c$ , (where  $\eta$  is the lateral separation distance), as shown in Figure 36. It is noticed in Figure 35 that all the correlation data lie predominantly along a single curve except for point number 5 on the near field boundary. The equation to this curve, which may be regarded as the average narrow-band longitudinal correlation coefficient in the near field, is;

$$C(\zeta;\omega) = \exp\left[-0.0955 \frac{\omega \zeta}{c}\right] \cos\left\{0.715 \frac{\omega \zeta}{c}\right\}$$
(4.42)

The marked difference in correlation exhibited by point number 5 is due substantially to the effects of spherical radiation; in other words the longitudinal correlation scale depends upon the angle, 0, which the correlation traverse line makes with the line joining the reference point to the source, (see Figure 34). Consequently, the carrelation lengths increase as the correlation reference point moves around to a point on the normal to the jet centerline. Typical values of the distance to the first zero crossing,  $f\zeta/c$ , are plotted in Figure 37 as a function of the angle between the line joining the correlation reference point and the source region, and the jet centerline; for convenience the source region is assumed to be a point located five jet nozzle exit diameters downstream on the jet centerline. The data shown in this figure were obtained from References 46, 47, and 48 and the scatter is due to filtering in the measurements. Also shown in the figure are the Fa. Field approximation,  $f\zeta/c = 0.25/\cos\theta$ , and an empirical curve fit to the data,  $f\zeta/c = 0.29/1.16 - \sin^2\theta$ . The empirical curve fit is shown for values of  $\theta$ between 0 and 180°; it is thus assumed that longitudinal correlation lengths are symmetrical about a line at right angles to the jet axis some five jet diameters downstream.

Replacing Equation (4.42) by the more general form;

$$C (\zeta; \omega) = \exp \left[ -A \frac{\omega \zeta}{c} \right] \cos \left\{ B \frac{\omega \zeta}{c} \right\}$$

it can be seen that the first zero crossing of the correlation coefficient occurs when the argument of the cosine term is equal to  $\pi/2$ , or when  $\omega$   $\zeta/c = \pi/2B$ . Using this condition, in conjunction with the curve of  $f\zeta/c$  versus  $\theta$  shown in Figure 37, values of the constant B were computed as a function of  $\theta$  for angles between 0 and  $180^{\circ}$  as shown in Figure 38. From this figure it can be seen that as  $\theta$  approaches  $90^{\circ}$ , a minimum value of B and thus a maximum correlation length occurs.

To verify the dependence of correlation length on the angle  $\theta$ , values of the constant, B, were computed for correlation reference points 1, 2, and 5 in the near field (see Figure 34). The correlation curves,

$$C (\zeta; \omega) = \exp \left[ -0.0955 \frac{\omega \zeta}{c} \right] \cos \left\{ B \frac{\omega \zeta}{c} \right\}$$
 (4.43)

for these particular values of B are shown in Figure 39. It can be seen from this figure that there is fair agreement between the empirical curves and the experimental data, suggesting that Equation (4.43) is a suitable form for the longitudinal correlations.

The narrow-band lateral correlation coefficients shown in Figure 36 are similar in form to the longitudinal correlations but differ in that the correlation lengths are somewhat greater (by a factor of approximately two). A suitable approximation for the equation to the curve describing the correlation coefficient is;

$$C (\eta; \omega) = \exp \left[ -0.1193 \frac{\omega \eta}{c} \right] \cos \left\{ 0.382 \frac{\omega \eta}{c} \right\}$$
 (4.44)

Rewriting Equations (4.43) and (4.44) in terms of non-dimensional separation distances  $\overline{\zeta}$  and  $\overline{\eta}$ , gives,

$$C(\overline{\zeta};\omega) = \exp\left[-\delta_{\mathbf{x}}|\overline{\zeta}|\right] \cos \gamma_{\mathbf{x}}|\overline{\zeta}|$$
 (4.45)

$$C(\overline{\eta};\omega) = \exp \left[-\frac{\delta}{\gamma} \left| \overline{\eta} \right| \right] \cos \gamma_{\gamma} \left| \overline{\eta} \right| \qquad (4.46)$$

where;

$$\delta_{x} = 0.0955 \frac{\omega L_{x}}{c}$$

$$\gamma_{x} = B \frac{\omega L_{x}}{c}$$

$$\delta_{y} = 0.1193 \frac{\omega L_{y}}{c}$$

$$\gamma_{y} = 0.382 \frac{\omega L_{y}}{c}$$

$$\overline{\zeta} = \frac{\zeta}{L_{x}}$$

$$\overline{\eta} = \frac{\eta}{L_{y}}$$
(4.47)

and the constant, B, is determined from the structure-jet exit geometry.

Since, (a) the use of the analytical forms (Equations 4.39 and 4.41) would necessitate lengthy computations, particularly in determining the joint acceptances, and, (b) the accuracy of the scattering technique has not been verified experimentally, it is recommended that the empirical correlation coefficients be used in view of their simplicity and the fact that they represent practical noise fields.

Moreover, it is suggested that when predicting the response of the whole fuselage to jet noise, the average longitudinal carrelation coefficient, defined by Equation (4.42), be used since the joint acceptance of the whole fuselage can be determined only when the carrelation pattern is homogeneous. When predicting the response of discrete sections of the fuselage, such as the intermediate and high frequency models, the dependence of the correlation length on the respective position of the reference point in the near field must, of course, be taken into account by use of Equation (4.43).

Finally, it should be barne in mind that the empirical correlations put forward here have been based on the available experimental data, which is confined to the near field. Longitudinal correlation data in the region,  $45^{\circ} \le \theta \le 135^{\circ}$ , and more extensive measurements of lateral correlations are two essential requirements needed to substantiate the present predicted correlations.

# g. Correlation Length

The correlation length, C<sub>L</sub>, was previously defined as equal to that length over which the excitation may be considered as perfectly correlated in space, i.e., the correlation length times unit correlation is equal to the area under the normalized space correlation curve. Thus for the jet noise environment, the correlation length in the axial direction is,

$$C_{L} = \frac{2 \delta_{x}}{\delta_{x}^{2} + \gamma_{x}^{2}} \cdot L_{x} \qquad (4.48)$$

and the correlation length in the circumferential direction is;

$$C_{L} = \frac{2\delta_{y}}{\delta_{y}^{2} + \gamma_{y}^{2}} \cdot L_{y}$$
 (4.49)

where  $\delta_{x}$ ,  $\delta_{y}$ ,  $\gamma_{x}$ , and  $\gamma_{y}$  are defined by Equations (4.46).

### 3. REVERBERANT ACOUSTIC FIELD ENVIRONMENT

## a. Equivalent Reverberant Field, Overall Level and Frequency Spectra

Since the final response equations, developed in Section V are in the form of a ratio of displacement power spectral density to excitation pressure spectral density, it is possible to define an equivalent reverberant field which replaces aerodynamic turbulence or jet noise, yet produces identical structural responses. This concept is particularly useful when simulating fluctuating pressure environments in the laboratory a when studying transmission loss characteristics, since the theory for the latter is based on reverberant field acoustics. For example, subtracting logarithmically the ratio of displacement power spectral density to excitation pressure power spectral density for the boundary layer turbulence environment from a similar ratio for the reverberant acoustic field environment, with the condition that the displacement power spectral densities are identical, results in the equivalent reverberant field, expressed as a dB ratio of the exciting pressures, i.e.,

10 
$$\log \frac{S}{\frac{S}{p}(\omega)} = 10 \log \frac{S}{p} = 10 \log \frac{S}{p}$$

Thus, provided the spectrum of the fluctuating pressures is known for boundary layer turbulence or jet noise the computation of the equivalent reverberant field is straightforward. This technique has previously been used (Reference 49) to demonstrate that a reverberant field is, in general, more efficient than boundary layer turbulence in exciting a fuselage structure, especially above coincidence frequencies at subsonic flight speeds.

## b. Narrow-Band Pressure Correlation Coefficients

In describing the pressure correlation patterns on a fuselage in a reverberant field, the effects of diffraction should be included for exactness. Theoretical expressions for the pressure correlations on an isotropic cylinder in a reverberant field, which include the effects of diffraction, have been developed by Wenzel (Reference 45); however, the numerical analysis required is prohibitively long and extension of this theory to cover the case of a stiffened fuselage structure is therefore not justified.

In order to obtain tractable mathematical expressions for the joint acceptances and generalized forces, it is assumed that the pressure correlation functions may be approximated by those of an infinite flat plate. The magnitude of the error introduced by this assumption is inversely proportional to frequency, though it is shown later that in general it can be disregarded.

The pressure space correlation  $C(r;\omega)$  for a diffuse field acting on an infinite plate, as derived by Eckart (Reference 50), is;

$$C(\tilde{r};\omega) = \frac{\sin(2\pi \tilde{r})}{2\pi \tilde{r}}$$
 (4.51)

where

$$\bar{r} = \frac{r}{\lambda}$$

 $\lambda$  = acoustic wavelength = c/f

r = distance between two points on the flat surface.

It will be noticed from the above equation that the correlation pattern about a point on the surface is circular since the equation is independent of the polar orientation on the line between the points. The cylindrical geometry of the structure and the circular symmetry of the correlation pattern also leads to lengthy expressions for the generalized forces. Consequently, further simplification is afforded by separating Equation (4.51) into;

$$C(\overline{r};\omega) = C(\overline{\zeta};\omega) - C(\overline{\eta};\omega)$$
 (4.52)

$$C(\overline{\zeta};\omega) = \frac{\sin\left(2\pi\frac{L}{\lambda}\overline{\zeta}\right)}{2\pi\frac{L}{\lambda}\overline{\zeta}}$$
(4.53)

$$C(\overline{\eta}; \omega) = \frac{\sin\left(2\pi \frac{L}{\lambda} \frac{y}{\overline{\eta}}\right)}{2\pi \frac{L}{\lambda} \overline{\eta}}$$
(4.54)

where 
$$\overline{\zeta} = \zeta/L_{x}$$
;  $\overline{\eta} = \eta/L_{y}$ ;  $\zeta = x - x^{t}$ ;  $\eta = y - y^{t}$ .

In justifying the use of these approximate forms for the correlation coefficients, it is of interest to compare numerically Equations (4.53) and (4.54) with the more exact forms obtained by Wenzel (Reference 45). The narrow-band longitudinal and lateral pressure correlation coefficients on the surface of a cylinder, obtained by use of the above equations, are compared with the results of Wenzel in Figures 40 and 41 respectively. It is noticed that the lateral correlations display some sensitivity to diffraction effects, while the longitudinal correlations do not. However, the lateral correlation coefficient does follow the general frequency variation indicated in Equation (4.54) and the resulting error caused by the simplifying assumptions is not considered to be significant for structural response predictions.

## c. Correlation Length

Applying the definition that the correlation length times unit correlation is equal to the area under the normalized space correlation curve; the correlation length in the longitudinal direction is

$$C_{L} = \frac{\pi c}{\omega L_{x}} \cdot L_{x} \tag{4.55}$$

and the correlation length in the circumferential direction is

$$C_{L} = \frac{\pi c}{\omega L_{y}} \cdot L_{y}$$
 (4.56)

A typical pressure wavelength is denoted by  $\lambda_p = c/f$ , where c is the speed of sound and f some arbitrary excitation frequency. Now, the elastic wavelength of the m-th axial mode is defined as,

$$\lambda_e = \frac{2L_x}{m}$$

where  $L_{\chi}$  is the structural length in the x-direction and m is the number of axial half-wavelengths. Then, coincidence is defined as

$$\frac{\lambda_{e}}{\lambda_{p}} = 1$$

Thus,

$$\frac{\lambda_e}{\lambda_p} = \frac{2L_x f}{mc} = 1$$

So that the coincidence frequency may be defined as,

$$f = \frac{mc}{2L_x}$$

# LIST OF SYMBOLS

# LIST OF SYMBOLS USED IN SECTION IV

```
fuselage radius
                 ambient speed of sound
                 frequency - Hz
                 directivity index
                 wavenumber (= 2\pi/\lambda)
                 axial mode number or integer
m
                 free stream static pressure
\mathsf{P}_{\mathsf{rms}}
                 root mean square level of fluctuating pressure
                 dynamic head (= 0.5 \rho_0 U_0^2)
q
                 separation distance for a plate in a reverberant acoustic field
                 radius of jet nozzle
                     a dimensionless separation distance
                 time
                 Cartesian coordinates
Do
E
                 constants defined by Equation 4.36
G
Н
                 a constant
C(\delta_{\xi^*, k}), C(\eta; u) narrow-band space correlation coefficients
                 a function of ka \cos \beta (defined by Equation 4.32)
                 correlation length
                 jet nozzle exit diameter
```

J	Bessel function of the first kind
L <sub>x</sub> , L <sub>y</sub>	structural dimensions in the x and y directions
М	Mach number
M <sub>e</sub>	exit Mach number
N	Bessel function of the second kind
P	instantaneous pressure
Po	free field sound pressure
PWL	acoustic power level
R	correlation function
Re <sub>x</sub>	Reynolds number based on distance from the leading edge
R,	distance between the center of the i-th segment and a reference point in the free field
U <sub>o</sub>	free stream velocity
U <sub>c</sub>	convection velocity
٧	jet exit velocity
α	angle between the wavefront and a tangent to the surface (for fuselage mounted engines) (see 1 gure 33)
β	angle between the normal to the wave and the normal to the axis of the fuselage (see Figure 32)
δ <sub>x</sub> δ <sub>y</sub> γ <sub>x</sub> γ <sub>y</sub>	correlation parameters defined by Equations (4.21) and (4.46)
γ <mark>m</mark>	function of $ka$ cas $\beta$ (defined by Equation 4.34)
δ <sub><b>b</b></sub>	boundary layer thickness
δ* .	boundary layer displacement thickness
ć	ratio of aircraft to jet exhaust velocity

5, 9	spatial separations in x and y directions respectively
ξ, <del>η</del>	non-dimensional spatial separations
Ө	angle which correlation traverse line makes with the line joining the correlation reference point to the source (see Figure 34)
θ,	angle between the forward jet axis and the line joining the i-th segment to a point on the structure (see Figure 29)
Θ	momentum thickness
λ	acoustic wavelength
$\lambda_{\mathbf{e}}$	elastic wavelength
λ <sub>P</sub>	pressure wavelength
ν	kinematic viscosity
p	mean gas density
Po	free stream air density
P <sub>1</sub>	air density near sites of most intense eddies
ρ <sub>j</sub>	nozzle flow density
P <sub>T</sub>	typical engine gas density
τ	time delay
τ <b>w</b>	wall shear stress
ψ	angular distance around fuselage (see Figure 32)
ω	circular frequency (rads/sec)
<sup>ယ</sup> ဝ	typical circular frequency
Δω	frequency bandwidth
()	time average
11	modulus
Φ	function defined by Equation (4.36)

Eligny harmstonian about a con-

### SECTION V

### THE RESPONSE EQUATIONS

When analyzing the vibration response of linear structures to ascillatory applied loads, it is convenient to express the total response as the summation of the responses of the individual modes and to assume that each mode responds independently of all other modes. Once the natural frequencies and deflection shapes are known for all modes, the problem reduces to one of determining the responses of a set of generalized single degree of freedom systems, each of which is excited by a generalized applied load.

In a rigorous sense, this classical method is valid only if coupling between the modes of vibration does not take place. When the resonance frequencies of adjacent modes are well separated and the damping is relatively small, it is usually assumed that the damping coupling between modes is sufficiently small to be neglected.

When the modal response bandwidths overlap, such as for the higher order modes of a complex structure, significant damping coupling between modes can occur. However, the total energy associated with any two such modes is very nearly the same with or without damping coupling, particularly if the modes are excited to approximately the same response level. The primary influence of the damping coupling is to create a significant cross-coupling or cross-correlation between the instantaneous response amplitudes of any two such modes.

In the present analysis, the classical method is adopted to treat systems having a large number of modes whose natural frequencies are closely spaced and whose bandwidths may overlap. It is assumed that the mean square response amplitude of each mode can be obtained independently, and that the summation of these mean square responses is insensitive to damping coupling between modes. The total mean square response of a structure at any point depends upon the summation of the mean square modal responses and upon the summation of the cross-correlations between pairs of modes. The latter term is in some cases significant; however, each term in this summation becomes equal to zero when the space average of the mean square response is obtained. The cancellation of modal cross-correlations for space average response is due to orthogonality between the modes.

Thus, in the following sections expressions for the space average of the mean square structural responses are developed for each of the equivalent structural models.

# RESPONSE OF THE OVERALL FUSELAGE MODES

Displacement and Acceleration Power Spectral Densities

Consider the structural response of a stiffened cylinder in the absence of any coupling with the internal air mass. The instantaneous radial acceleration  $\hat{w}(x,y,t)$ 

at a point (x,y) on the cylinder surface can be written as the linear summation,

$$\hat{\mathbf{w}}(\mathbf{x},\mathbf{y},\mathbf{t}) = \sum_{\mathbf{mni}} \phi_{\mathbf{mni}}(\mathbf{x},\mathbf{y}) \, \hat{\mathbf{q}}_{\mathbf{mni}}(\mathbf{t}) \tag{5.1}$$

where i = 1 or 2 and (mn) denotes all the modes of interest. The mode shape  $\phi_{mni}$  is as defined by equation (2.15) in Section 11. Writing the product  $[\ddot{w}(x,y,t).~\dot{w}(x,y,t+\tau)]$  in series form;

$$\hat{w}(x,y,t).\hat{w}(x,y,t+\tau) = \sum_{mni} \sum_{rsj} \phi_{mni}(x,y) \phi_{rsj}(x,y) \ddot{q}_{mni}(t) . \ddot{q}_{rsj}(t) \qquad (5.2)$$

Time-averaging this equation leads to the autocorrelation function for the acceleration at the point (x,y) in terms of the modal cross correlation function,

$$R\left[\ddot{w}(x,y,t);\tau\right] = \sum_{mni} \sum_{rsj} \phi_{mni}(x,y) \phi_{rsj}(x,y) R\left[\ddot{q}_{mni}(t),\ddot{q}_{rsj}(t);\tau\right]$$
(5.3)

Notice that when (mni) = (rsj), the modal cross correlation function reduces to the autocorrelation function  $R\left[\ddot{q}_{mni}(t);\tau\right]$  for the (mni) mode.

Taking the Fourier transform of each term in the above equation gives the power spectral density of the acceleration at (x,y) in terms of the modal cross spectral density function,

$$S\left[\ddot{w}(x,y,t);\omega\right] = \sum_{mni} \sum_{rsi} \phi_{mni}(x,y) \phi_{rsj}(x,y) S\left[\ddot{q}_{mni}(t), \ddot{q}_{rsj}(t);\omega\right] (5.4)$$

When (mni) = (rsj), the modal cross spectral density function reduces to the power spectral density function for the (mni) mode, namely  $S[\ddot{q}_{mni}(t);\omega]$ 

Now the space-average,  $S\left[\tilde{w};\omega\right]$  of the acceleration spectral density is given by,

$$S\left[\tilde{w};\omega\right] = \int_{\tilde{x}=0}^{1} \int_{\tilde{y}=0}^{1} S\left[\tilde{w}(x,y,t);\omega\right] d\bar{x} d\bar{y}$$
 (5.5)

$$=\sum_{mni}\sum_{rsj}\left[\int_{\bar{x}=0}^{1}\int_{\bar{y}=0}^{1}\phi_{mni}(x,y)\cdot\phi_{rsj}(x,y)\,d\bar{x}\,d\bar{y}\right]\cdot S\left[\ddot{q}_{mni}(t),\ddot{q}_{rsj}(t);\omega\right]$$
(5.6)

Unless (rsj) = (mni) the space-average indicated in the brackets is equal to zero because of the orthogonality of the modes. Hence, the above equation reduces to the form,

$$S\left[\vec{w};\omega\right] = \sum_{mn} \gamma_{mn} \left\{ S\left[\vec{q}_{mn1}(t);\omega\right] + S\left[\vec{q}_{mn2}(t);\omega\right] \right\}$$

$$= \sum_{mn} \gamma_{mn} S\left[\vec{q}_{mn}(t);\omega\right]$$

$$= \sum_{n=0}^{1} \int_{\vec{y}=0}^{1} \left[\phi_{mni}(x,y)\right]^{2} d\vec{x} d\vec{y}$$

$$= \frac{1}{2} ; m = 1,2,3,...; n = 0 ; i = 2$$

$$= 0 ; m = 1,2,3,...; n = 0 ; i = 1$$

$$= \frac{1}{4} ; m = 1,2,3,...; n = 1,2,3,...; i = 1,2 .$$
(5.8)

and  $\ddot{q}_{mn}(t)$  denotes the summation of  $\ddot{q}_{mn1}(t)$  and  $\ddot{q}_{mn2}(t)$ .

The equation describing the response of the (mni) mode has the general form of the equation of motion for a single degree of freedom system, namely

$$\ddot{q}_{mni}(t) + \frac{\omega_{mn}}{Q_{mn}} \dot{q}_{mni}(t) + \omega_{mn}^2 q_{mni}(t) = \frac{F_{mni}(t)}{M_{mni}}$$
 (5.9)

where  $Q_{mn}$  denotes the dynamic magnification factor at resonance for the (mn) mode,  $M_{mni}$  is the generalized mass defined by equation (2.21) and  $F_{mni}(f)$  is the generalized force defined by,

$$F_{mni}(t) = A \int_{\bar{x}=0}^{1} \int_{\bar{y}=0}^{1} P(\bar{x}, \bar{y}, t) \cdot \phi_{mni}(\bar{x}, \bar{y}) d\bar{x} \cdot d\bar{y}$$
 (5.10)

where A is the surface area of the structure.

Assuming that both the modal acceleration and the generalized force are harmonic at frequency  $\omega$ , the solution to the latter equation is;

$$\ddot{q}_{mni}(t) = \left[\frac{\omega}{\omega_{mn}}\right]^2 \frac{H(\omega/\omega_{mn})}{M_{mni}} e^{-\theta(\omega/\omega_{mn})} F_{mni}(t)$$
 (5.11)

where

$$H(\omega/\omega_{mn}) = \left[ \left\{ 1 - \left( \frac{\omega}{\omega_{mn}} \right)^2 \right\}^2 + \frac{1}{Q_{mn}^2} \left( \frac{\omega}{\omega_{mn}} \right)^2 \right]^{-\frac{1}{2}}$$

$$\theta(\omega/\omega_{mn}) = T_{an}^{-1} \left[ \frac{(\omega/\omega_{mn})}{Q_{mn} \left\{ 1 - (\omega/\omega_{mn})^2 \right\}} \right]$$
(5.12)

From equation (5.11) it follows that the power spectral density of the modal acceleration is,

$$S\left[\ddot{q}_{mni}(t);\omega\right] = \left[\frac{\omega}{\omega_{mn}}\right]^{4} \frac{H^{2}(\omega/\omega_{mn})}{M^{2}_{mni}} \cdot S\left[F_{mni}(t);\omega\right]$$
(5.13)

Now, the power spectral density of the generalized force is obigined from the autocorrelation by the relation,

$$S\left[F_{mni}(t);\omega\right] = \int_{-\infty}^{\infty} R\left[F_{mni}(t);\tau\right] e^{-i\omega\tau} d\tau \qquad (5.14)$$

The autocorrelation of the generalized force may easily be shown to be given by,

$$R\left[F_{mni}(t);\tau\right] = A^2 \int_{\overline{x}=0}^{t} \int_{\overline{y}=0}^{t} \int_{\overline{x}'=0}^{t} R\left[P(\overline{x},\overline{y},t),P(\overline{x}',\overline{y}',t);\tau\right].$$

$$- \phi_{mni}(\bar{x}, \bar{y}) \cdot \phi_{mni}(\bar{x}', \bar{y}') d\bar{x} d\bar{y} d\bar{x}' d\bar{y}'$$
 (5.15)

The correlation function within the integrand of this equation is a space-time correlation between the fluctuating applied pressures at the two points (x,y) and (x',y'). Substituting (5.15) into (5.14),

$$S\left[F_{mni}(t);\omega\right] = A^{2} \int_{\bar{x}=0}^{1} \int_{\bar{y}=0}^{1} \int_{\bar{x}'=0}^{1} \int_{\bar{y}'=0}^{1} \left\{ \int_{-\infty}^{\infty} R\left[P(\bar{x},\bar{y},t),P(\bar{x}',\bar{y}',t);\tau\right] \right.$$

$$\left. \cdot e^{-i\omega\tau} d\tau \right\} \cdot \phi_{mni}(\bar{x},\bar{y}) \cdot \phi_{mni}(\bar{x}',\bar{y}') \cdot d\bar{x} \cdot d\bar{y} \cdot d\bar{x}' \cdot d\bar{y}' \qquad (5.16)$$

The cross-correlation of the pressures is a real quantity; however, the Fourier integral of this function will, in general, have non-zero real and imaginary parts. If the applied pressure P(x,y,t) is a stationary function then the space average of the imaginary part of this Fourier transform is equal to zero. To show this, it is first noted that the statistical properties of stationary functions are invariant with respect to time translations. Thus, we can write,

$$R\left[P(\vec{x},\vec{y},t),P(\vec{x}',\vec{y}',t);\tau\right] = R\left[P(\vec{x}',\vec{y}',t),P(\vec{x},\vec{y},t);-\tau\right]$$
(5.17)

The Fourier transform of the pressure correlation can be written, (Reference 56),

$$S\left[P(\vec{x},\vec{y},t),\ P(\vec{x}^{\scriptscriptstyle \dagger},\vec{y}^{\scriptscriptstyle \dagger},t);\omega\right] = \int\limits_{-\infty}^{\infty} R\left[P(\vec{x},\vec{y},t),P(\vec{x}^{\scriptscriptstyle \dagger},\vec{y}^{\scriptscriptstyle \dagger},t);\tau\right]$$

$$= \int_{-\infty}^{\infty} R\left[P(\bar{x}, \bar{y}, t), P(\bar{x}', \bar{y}', t); \tau\right] \left\{\cos \omega \tau - i \sin \omega \tau\right\} d\tau$$

$$= \int_{0}^{\infty} \left\{ R\left[P(\vec{x}^{*}, \vec{y}^{*}, t), P(\vec{x}, \vec{y}, t); \tau\right] + R\left[P(\vec{x}, \vec{y}, t), P(\vec{x}^{*}, \vec{y}^{*}, t); \tau\right] \right\} \cos \omega \tau \, d\tau$$

+ i 
$$\int_{0}^{\infty} \left\{ R \left[ P(\vec{x}^{*}, \vec{y}^{*}, t), P(\vec{x}, \vec{y}, t); \tau \right] - R \left[ P(\vec{x}, \vec{y}, t), P(\vec{x}^{*}, \vec{y}^{*}, t); \tau \right] \right\} \sin \omega \tau \, d\tau$$
(5.18)

It is obvious that the double space averages, indicated in equation (5.16), of the two terms in the first integral of equation (5.18) are equal; and similarly, the double space averages of the two terms in the second integral are equal. Therefore, the double space average of the second integral in equation (5.18) is equal to zero. Substituting equation (5.18) in (5.16) leads to,

$$S\left[F_{mni}(t);\omega\right] = A^{2} \int_{\bar{x}=0}^{1} \int_{\bar{y}=0}^{1} \int_{\bar{x}'=0}^{1} \int_{\bar{y}'=0}^{1} S_{c}\left[P(\bar{x},\bar{y},t),P(\bar{x}',\bar{y}',t);\omega\right] \cdot \phi_{mni}(\bar{x},\bar{y})$$

$$-\phi_{mni}(\bar{x}',\bar{y}') - d\bar{x}d\bar{y}d\bar{x}'d\bar{y}'$$
 (5.19

where  $S = \left[ P(\bar{x}, \bar{y}, t), P(\bar{x}', \bar{y}', t); \omega \right]$  is the cross-spectrum of the applied pressures and is defined,

$$S_{c}\left[P(\bar{x},\bar{y},t),P(\bar{x}',\bar{y}',t);\omega\right] = 2 \int_{0}^{\infty} R\left[P(\bar{x},\bar{y},t),P(\bar{x}',\bar{y}',t);\tau\right] \cdot \cos \omega \tau \,d\tau$$
(5.20)

Assuming that the fluctuating pressure field is homogeneous, i.e., the power spectral density of the applied pressure,  $S\left[P(x,y,t);\omega\right]$ , is constant at all points on the structure, and can thus be written as  $S\left[P;\omega\right]$ . This assumption leads to the definition of a narrow-band space correlation coefficient,

$$C(\bar{x},\bar{y};\bar{x}',\bar{y}';\omega) = \frac{S_{c}\left[P(\bar{x},\bar{7},t), P(\bar{x}',\bar{y}'t);\omega\right]}{S\left[P_{z\omega}\right]}$$
(5.21)

Therefore, equation (5.19) may be written as

$$S\left[F_{mni}(t);\omega\right] = A^2 S\left[P;\omega\right] - J_{mni}^2(\omega) \qquad (5.22)$$

where  $J_{mni}^{2}(\omega)$  is termed the joint-acceptance and is defined by the integral,

$$J_{mni}^{2}(\omega) = \int_{\bar{x}=0}^{1} \int_{\bar{y}=0}^{1} \int_{\bar{x}'=0}^{1} \int_{\bar{y}'=0}^{1} C(\bar{x},\bar{y};\bar{x}',\bar{y}';\omega) \cdot \phi_{mni}(\bar{x},\bar{y}) \cdot \phi_{mni}(\bar{x}',\bar{y}')$$

$$- d\bar{x} d\bar{y} d\bar{x}' d\bar{y}' \qquad (5.23)$$

Substituting (5.22) into (5.13) yields the equation for the power spectral density of the modal acceleration,

$$S\left[\ddot{q}_{mni}(t);\omega\right] = A^{2}\left[\frac{\omega}{\omega_{mn}}\right]^{4} \cdot \frac{H^{2}(\omega/\omega_{mn})}{M^{2}_{mni}} \cdot S\left[P;\omega\right] \cdot J_{mni}^{2}(\omega) \qquad (5.24)$$

Finally, substitution of the above equation into equation (5.7) gives the space average of the spectral density of the acceleration response,

$$\frac{S[\tilde{w};\omega]}{S[P;\omega]} = A^2 \sum_{mn} \gamma_{mn} \left[ \frac{\omega}{\omega_{mn}} \right]^4 \cdot \frac{H^2(\omega/\omega_{mn})}{M_{mni}^2} \cdot J_{mni}^2(\omega)$$
 (5.25)

Since the mean square displacement and acceleration spectral densities are related by the equation,

$$S[\tilde{w};u] = u^4 S[w;u]$$

the space average of the spectral density of the displacement response is,

$$\frac{S[w;\omega]}{S[P;\omega]} = A^2 \sum_{mn} \gamma_{mn} \left[ \frac{1}{\omega_{mn}} \right]^4 \frac{H^2(\omega/\omega_{mn})}{M^2_{mni}} \cdot J^2_{mni}(\omega)$$
 (5.26)

Further, the power spectral density of the displacement at a point (x,y) on the structure may be shown from equations (5.5), (5.8) and (5.26) to be,

$$\frac{S\left[w(x,y),\omega\right]}{S\left[P;\omega\right]} = A^{2} \sum_{mn} \phi_{mni}^{2}(x,y) \left[\frac{1}{\omega_{mn}}\right]^{4} \cdot \frac{H^{2}(\omega/\omega_{mn})}{\frac{M^{2}}{mni}} \cdot J_{mni}^{2}(\omega) \qquad (5.27)$$

For the case of structural coupling with the internal air mass, equations (5.25), (5.26) and (5.27) are modified by replacing  $\omega_{\rm mn}$  by  $\Omega_{\rm mns}$ , the coupled resonance frequency, and M by M the generalized mass of the coupled system; the summations being extended, of course, over m,n and s. Thus, for example, the power spectral density of the displacement at a point (x,y) may be written,

$$\frac{S\left[w(x,y);\omega\right]}{S\left[P;\omega\right]} = A^{2} \sum_{mns} \phi_{mni}^{2}(x,y) \left[\frac{1}{\Omega_{mns}}\right]^{4} \frac{H^{2}(\omega/\Omega_{mns})}{M_{mns}^{2}} \cdot J_{mni}^{2}(\omega) \quad (5.28)$$

A final point concerns the power spectral density of the applied pressure. In the foregoing analysis it was assumed that this quantity was identical at all points on the structure. However, for the case of jet noise, the fluctuating pressure field cannot be assumed homogeneous. Therefore, when analyzing the structural response to jet noise it is essential to have a knowledge of the power spectral densities at all points on the structure; this may be obtained by use of the prediction technique described in Section IV. Knowing the distribution of the applied pressures, the response at a particular point may be determined from equation (5.27) or alternatively, the space averaged response may be determined from equation (5.26) provided that the power spectral density of the applied pressures is space averaged with respect to an arbitrary reference pressure.

#### b. Joint Acceptances for the Various Environments

The derivation of the joint acceptance expressions is based on the assumption that the pressure correlation coefficient can be written in a separable form such as,

$$C(\bar{x},\bar{y},\bar{x}',\bar{y}';\omega) = C(\bar{x},\bar{x}';\omega) \cdot C(\bar{y},\bar{y}';\omega)$$
(5.29)

It is also assumed that along each coordinate axis the pressure distribution is statistically homogeneous so that the space correlation coefficients are even functions only of the separation distance along their respective axes. We can thus write,

$$C(\bar{x}, \bar{x}^{i}; \omega) = C(\bar{\zeta}; \omega) \qquad \bar{\zeta} = \bar{x} + \bar{x}^{i}$$

$$C(\bar{y}, \bar{y}^{i}; \omega) = C(\bar{\eta}; \omega) \qquad \bar{\eta} = \bar{y} - \bar{y}^{i}$$
(5.30)

Since the mode shapes may be written in separable form, the joint acceptance can similarly be written in separable form (Reference 57),

$$J_{mni}^{2}(\omega) = J_{m}^{2}(\omega) - J_{ni}^{2}(\omega)$$
 (5.31)

$$J_{m}^{2}(\omega) = \int_{\bar{x}=0}^{1} \int_{\bar{x}'=0}^{1} C(\bar{\zeta};\omega) \cdot \sin m\pi \bar{x} \cdot \sin m\pi \bar{x}' d\bar{x} d\bar{x}' \qquad (5.32)$$

$$J_{n1}^{2}(\omega) = \int_{\bar{y}=0}^{1} \int_{\bar{y}'=0}^{1} C(\bar{\eta};\omega) \cdot \sin 2n\pi \bar{y} \cdot \sin 2n\pi \bar{y}' d\bar{y}d\bar{y}' \qquad (5.33)$$

$$J_{n2}^{2}(\omega) = \int_{\overline{y}=0}^{1} \int_{\overline{y}'=0}^{1} C(\overline{\eta}_{i}\omega) \cdot \cos 2n\pi \overline{y} \cdot \cos 2n\pi \overline{y}' d\overline{y}d\overline{y}' \qquad (5.34)$$

Thus we can define,

$$J_{ni}^{2}(\omega) = J_{n1}^{2}(\omega) + J_{n2}^{2}(\omega)$$

$$= \int_{\bar{y}=0}^{1} \int_{\bar{y}'=0}^{1} C(\bar{\eta};\omega) \cos 2n\pi \bar{\eta} d\bar{y} d\bar{y}' \qquad (5.35)$$

The joint acceptance expressions (5.32) and (5.35) involve double integration over one of the coordinate axes of the cylinder. Since, in both cases, the correlation coefficient is a function of separation distance and since the modal deflection functions are spatially harmonic, the double integration can be reduced to a single integration, for an arbitrary correlation coefficient, by a transformation of the variables of integration.

Consider the expression for  $J_{m}^{2}(\omega)$  given by equation (5.32). The product

[sīn max · sin max i] can be written as,

$$\frac{1}{2} \left[ \cos m\pi \bar{\zeta} - \cos m\pi \left( 2\bar{\xi} + 1 \right) \right] \tag{5.36}$$

where; 
$$\bar{\xi} = \frac{1}{2}(\bar{x} + \bar{x}' - 1)$$

and 
$$\bar{\zeta} = \bar{x} - \bar{x}'$$
 (5.37)

Now, in equation (5.32) the region of integration is  $0 \le \bar{x} \le 1$ , and this region is shown in Figure 42(a). If  $\bar{\xi}$  and  $\bar{\zeta}$  represent the new variables of integration, the transformed region over which the integration is performed is indicated in Figure 42(b).

The element of area  $d\vec{x} d\vec{x}^t$  is transformed according to the Jacobian equation,

$$d\vec{x} d\vec{x}' = \begin{vmatrix} \frac{\partial \vec{\xi}}{\partial x} & \frac{\partial \vec{\xi}}{\partial x'} \\ \frac{\partial \vec{\zeta}}{\partial x} & \frac{\partial \vec{\zeta}}{\partial x'} \end{vmatrix} \cdot d\vec{\xi} \cdot d\vec{\zeta}$$
 (5.38)

$$= \begin{vmatrix} 1/2 & 1/2 \\ 1 & -1 \end{vmatrix} \cdot d\bar{\xi}d\bar{\zeta} = \begin{vmatrix} -1 \end{vmatrix} d\bar{\xi}d\bar{\zeta} = d\bar{\xi} - d\bar{\zeta}$$
 (5.39)

By integrating first with respect to  $\bar{\xi}$ , the limits of the first integral are

 $\vec{\xi} = -\frac{1}{2} \left[ 1 - \left| \vec{\zeta} \right| \right]$  and  $\vec{\xi} = \frac{1}{2} \left[ 1 - \left| \vec{\zeta} \right| \right]$ . The limits of integration for the variable  $\vec{\zeta}$  are -1 and +1. Thus, equation (5.32) can be written as:

$$J_{m}^{2}(\omega) = \frac{1}{2} \int_{0}^{1} C(\bar{\zeta}; \omega) \int_{0}^{1} \left[ \cos m\pi \bar{\zeta} - \cos m\pi (2\bar{\xi} + 1) \right] d\bar{\xi} \cdot d\bar{\zeta}$$

$$\bar{\zeta} = -1 \qquad \bar{\xi} = -\frac{1}{2} \left[ 1 - |\bar{\zeta}| \right]$$
(5.40)

Performing the first integration gives;

$$J_{m}^{2}(\omega) = \frac{1}{2} \int_{\overline{\zeta}=-1}^{1} C(\overline{\zeta}; \omega) \left[ (1 - |\overline{\zeta}|) \cos m\pi \overline{\zeta} + \frac{1}{m\pi} \sin m\pi |\overline{\zeta}| d\overline{\zeta} \right]$$
 (5.41)

However,  $C(\overline{\zeta};\omega)$  is an even function of  $\overline{\zeta}$  so that the latter equation reduces to;

$$J_{m}^{2}(\omega) = \int_{\overline{\zeta}=0}^{1} C(\overline{\zeta}; \omega) \left[ (1-\overline{\zeta}) \cos m\pi \overline{\zeta} + \frac{1}{m\pi} \sin m\pi \overline{\zeta} d\overline{\zeta} \right] \qquad (5.42)$$

The transformation of equation (5.35) is achieved as follows;

Substituting  $\bar{\eta} = \bar{y} - \bar{y}'$  and putting  $\bar{\xi} = \frac{1}{2}(\bar{y} + \bar{y}' - 1)$ , we have;

$$d\bar{y} \cdot d\bar{y}' = d\bar{\xi} \cdot d\bar{\eta} \tag{5.43}$$

and the limits of integration are;

$$- \; \frac{1}{2} \left[ 1 - \left| \; \bar{\eta} \; \right| \; \right] \leq \bar{\xi} \leq \; \frac{1}{2} \left[ 1 - \left| \; \bar{\eta} \; \right| \; \right] \; ; \quad -1 \leq \bar{\eta} \leq \; + \; 1$$

Rewriting equation (5.35) with the appropriate substitutions, and omitting the subscript i, gives;

$$J_{n}^{2}(\omega) = \int_{0}^{1} C(\bar{\eta}; \omega) \int_{0}^{1} \frac{1}{2} \left[ 1 - |\bar{\eta}| \right] d\bar{\eta}$$

$$= \int_{0}^{1} C(\bar{\eta}; \omega) \cos 2\pi n \bar{\eta} \left[ 1 - |\bar{\eta}| \right] d\bar{\eta}$$

$$= \int_{0}^{1} C(\bar{\eta}; \omega) \cos 2\pi n \bar{\eta} \left[ 1 - |\bar{\eta}| \right] d\bar{\eta}$$
(5.44)

However, since  $C(\overline{\eta};\omega)$  is an even function of  $\overline{\eta}$ , the latter equation becomes:

$$J_{\eta}^{2}(\omega) = 2 \int_{\bar{\eta}=0}^{1} (1 - \bar{\eta}) C(\bar{\eta}; \omega) \cos 2\pi n \bar{\eta} d\bar{\eta}$$
 (5.45)

Notice that for breathing modes (n=0) the above equation reduces to;

$$J_0^2(\omega) = 2 \int_{\bar{\eta}=0}^1 (1 - \bar{\eta}) C(\bar{\eta}; \omega) d\bar{\eta}$$
 (5.46)

#### (1) Boundary Layer Turbulence

The joint acceptance of the axial modes of the fuselage for boundary layer turbulence is obtained by substituting the first of equations (4.20), for the correlation coefficient in the x direction into equation (5.42), performing the integration and simplifying the algebraic expressions, giving

$$J_{m}^{2}(\omega) = \frac{2}{(m\pi)^{2} \Delta_{x}^{2}} \left[ P_{x} \left\{ 1 - (-1)^{m} e^{-\delta_{x}} \cos \gamma_{x} \right\} + 4(-1)^{m} q_{x} e^{-\delta_{x}} \right.$$

$$\left. - \sin \gamma_{x} + \frac{m\pi}{2} r_{x} \Delta_{x} \right]$$
 (5.47)

where;

$$\Delta_{x} = \left[1 + \left(\frac{\gamma_{x}}{m\pi}\right)^{2} + \left(\frac{\delta_{x}}{m\pi}\right)^{2}\right]^{2} - 4\left(\frac{\gamma_{x}}{m\pi}\right)^{2}$$

$$P_{x} = \left[1 - \left(\frac{\gamma_{x}}{m\pi}\right)^{2} + \left(\frac{\delta_{x}}{m\pi}\right)^{2}\right]^{2} - 4\left(\frac{\gamma_{x}}{m\pi}\right)^{2}\left(\frac{\delta_{x}}{m\pi}\right)^{2}$$

$$q_{x} = \left(\frac{\gamma_{x}}{m\pi}\right)\left(\frac{\delta_{x}}{m\pi}\right)\left[1 - \left(\frac{\gamma_{x}}{m\pi}\right)^{2} + \left(\frac{\delta_{x}}{m\pi}\right)^{2}\right]$$

$$r_{x} = \left(\frac{\delta_{x}}{m\pi}\right)\left[1 + \left(\frac{\gamma_{x}}{m\pi}\right)^{2} + \left(\frac{\delta_{x}}{m\pi}\right)^{2}\right]$$
(5.48)

and the quantities  $\delta_{x}$ ,  $\gamma_{x}$ , are as defined by equation (4.21) in Section IV.

This expression is in agreement with that derived by Wilby (Reference 58).

The joint acceptance of the circumferential ring modes is obtained by substituting the second of equations (4.20), for the correlation coefficient in the y direction, into equation (5.45), performing the integration and simplifying the final expression, giving

$$J_{n}^{2}(\omega) = \frac{2\delta_{y}}{\left[(2\pi n)^{2} + \delta_{y}^{2}\right]} + 2 \cdot \frac{(2\pi n) - \delta_{y}\left[1 - e^{-\delta_{y}}\right]}{\left[(2\pi n)^{2} + \delta_{y}^{2}\right]^{2}}$$
(5.49)

where  $\delta_y$  is defined by equation (4.21) in Section IV.

#### (2) Reverberant Acoustic Field

The joint acceptance expression for the axial modes of the cylinder to a reverberant acoustic field is obtained by substituting equation (4.53), for the correlation coefficient in the x- direction, into equation (5.42). The resulting integral contains three terms in the integrand. The first term can be written in terms of cosine integrals, the second term can be integrated directly, and the third term can be written in terms of sine integrals. The joint acceptance equation can thus be expressed as follows;

$$J_{m}^{2}(\omega) = \frac{1}{(2\pi)^{2} m L_{x}/\lambda} \left[ \text{Cin} \left\{ \pi(m + 2L_{x}/\lambda) \right\} - \text{Cin} \left\{ \pi(m - 2L_{x}/\lambda) \right\} \right]$$

$$+ \frac{1}{4\pi L_{x}/\lambda} \left[ \text{Si} \left\{ \pi(m + 2L_{x}/\lambda) \right\} - \text{Si} \left\{ \pi(m - 2L_{x}/\lambda) \right\} \right]$$

$$+ \frac{1}{(m\pi)^{2}} \frac{1 - (-1)^{m} \cos(2\pi L_{x}/\lambda)}{1 - (2L_{x}/m\lambda)^{2}}$$
(5.50)

where;

Ci (z) = 
$$\int_0^z \frac{1-\cos x}{x} dx$$
 (cosine integral)

$$Si(z) = \int_0^z \frac{\sin x}{x} dx$$
 (sine integral)

The joint acceptance of the circumferential modes to a reverberant acoustic field is obtained by substituting equation (4.54) into (5.45), as follows;

$$J_{n}^{2}(\omega) = \frac{1}{2\pi(L_{y}/\lambda)} \left[ Si \left\{ 2\pi(n + L_{y}/\lambda) \right\} - Si \left\{ 2\pi(n - L_{y}/\lambda) \right\} \right]$$

$$+ \frac{1}{2(n\pi)^{2}} \cdot \frac{1 - \cos(2\pi L_{y}/\lambda)}{1 - (L_{y}/n\lambda)^{2}} \text{ at } n \neq 0 \qquad (5.51)$$

$$= \frac{Si \left\{ 2\pi L_{y}/\lambda \right\}}{\pi L_{y}/\lambda} - \frac{1 - \cos(2\pi L_{y}/\lambda)}{2\pi^{2}(L_{y}/\lambda)^{2}} \text{ at } n = 0.$$

The sine and cosine integrals can be evaluated numerically by using power series expansions for small values of z (0 < z < 1) (see Reference 59), rational fraction approximations for intermediate values of z (1 < z < 50), and asymptotic expansions for large values of z (z < 50). The approximate expression used in the numerical evaluations are summarized below;

$$Si(z) = \sum_{n=0}^{\infty} \frac{(-1)^n z^{2n+1}}{(2n+1)(2n+1)!}$$

$$Ci(z) = \sum_{n=0}^{\infty} \frac{(-1)^{n+1} z^{2n}}{(2n)(2n)!}$$
(5.52)

$$Si(z) = \frac{\pi}{2} - f(z) \cos z - g(z) \sin z$$

Ci(z) = f(z) sin z - g(z) cos z = 
$$\int_0^z \frac{1-\cos t}{t} \cdot dt$$

$$Cin(z) = \gamma + Lnz - Ci(z)$$

$$\gamma$$
 = Eulers Constant = 0.5772156649

$$f(z) = \int_0^{\infty} \frac{e^{-zt}}{t^2+1} dt \approx \frac{1}{z} \cdot \frac{a_8 z^8 + a_6 z^6 + a_4 z^4 + a_2 z^2 + a_0}{b_8 z^8 + b_6 z^6 + b_4 z^4 + b_2 z^2 + b_0} / 1 < z < \infty$$

$$g(z) = \int_0^\infty \frac{t e^{-zt}}{x^3 + 1} dt \approx \frac{1}{z^2} \frac{c_8 z^8 + c_6 z^6 + c_4 z^4 + c_2 z^2 + c_0}{d_8 z^9 + d_6 z^6 + d_4 z^4 + d_2 z^2 + d_0}, 1 < z < \infty$$

$$f(z) = \frac{1}{2} \left[ 1 - \frac{2!}{z^2} + \frac{4!}{z^4} - \dots \right]$$
  $i < z$ 

$$g(z) = \frac{1}{z^2} \left[ 1 - \frac{3!}{z^2} + \frac{5!}{z^4} - \dots \right]$$

Numerical values for the constants  $a_i$ ,  $b_i$ ,  $c_i$  and  $d_i$  appearing in the expressions f(z) and g(z) are tabulated in Table II.

#### (3) Jet Noise

The joint acceptance of the axial modes of the fuselage for jet noise is obtained by substituting equation (4.45), for the correlation coefficient in the x direction, into equation (5.42), performing the integration and simplifying the algebraic expressions, giving,

$$J_{m}^{2}(\omega) = \frac{2}{(m\pi)^{2} \Delta_{x}^{2}} \left[ P_{x} \left\{ 1 - (-1)^{m} e^{-\delta_{x}} \cos \gamma_{x} \right\} + 4 (-1)^{m} q_{x} e^{-\delta_{x}} \right].$$

$$-\sin \gamma_{x} + \frac{m\pi r_{x} \Delta_{x}}{2}$$
 (5.53)

This expression is identical in form to  $J_m^2(\omega)$  for boundary layer turbulence, except for the magnitude of the quantities  $\delta_{\mathbf{x}}$  and  $\gamma_{\mathbf{x}}$ , which for this case are given by equations (4.47). In the above expression,  $\Delta_{\mathbf{x}}$ ,  $P_{\mathbf{x}}$ ,  $q_{\mathbf{x}}$  and  $r_{\mathbf{x}}$  are determined from equations (5.48) with the appropriate values for  $\delta_{\mathbf{x}}$  and  $\gamma_{\mathbf{x}}$  substituted.

The joint acceptance of the circumferential modes of the fuselage for jet noise is obtained by substituting equation (4.46), for the correlation coefficient in the y direction, into equation (5.45), performing the integration and simplifying,

$$J_n^2(\omega) = F(\gamma_y + 2n\pi) + F(\gamma_y - 2n\pi)$$
 (5.54)

where;

$$F(\gamma_y \pm 2n\pi) = \frac{e^{-\delta_y} \left[ \left\{ \delta_y^2 - (\gamma_y \pm 2n\pi)^2 \right\} - \cos \left( \gamma_y \pm 2n\pi \right) \right]}{\left[ \delta_y^2 + (\gamma_y \pm 2n\pi)^2 \right]^2}$$

$$\frac{-2\delta_{y}\left(\gamma_{y}\pm2n\pi\right)\sin\left(\gamma_{y}\pm2n\pi\right)\right]-\left[\delta_{y}^{2}-\left(\gamma_{y}\pm2n\pi\right)^{2}\right]+\delta_{y}\left[\delta_{y}^{2}+\left(\gamma_{y}\pm2n\pi\right)^{2}\right]}{\left[\delta_{y}^{2}+\left(\gamma_{y}\pm2n\pi\right)^{2}\right]^{2}}$$

and the magnitudes of  $\gamma_y$  and  $\delta_y$  are defined by equations (4.47) in Section IV. For the special case of fuselage breathing modes (i.e., when n=0, then substitution of equation (4.46) into equation (5.46) leads to the expression;

$$J_{(n=e)}^{2}(\omega) = 2 \left[ \frac{\delta_{y}}{(\delta_{y}^{2} + \gamma_{y}^{2})} - \frac{(\delta_{y}^{2} - \gamma_{y}^{2})(1 - e^{-\delta_{y}} \cos \gamma_{y})}{(\delta_{y}^{2} + \gamma_{y}^{2})^{2}} \right]$$

$$\frac{-2e^{-\delta_y}\gamma_y\delta_y\sin\gamma_y}{(\delta_y^2+\gamma_y^2)^2}$$
 (5.56)

# 2. RESPONSE OF THE INDIVIDUAL PANEL MODES

# a. Displacement and Acceleration Power Spectral Densities

The equation of motion governing the response of each panel mode is

$$\ddot{q}_{mn}(t) + \frac{\omega_{mn}}{Q_{mn}} \dot{q}_{mn}(t) + \omega_{mn}^2 q_{mn}(t) = \frac{F_{mn}(t)}{M_{mn}}$$
 (5.57)

The displacement of any point on the panel at time t may be expressed by the sum

$$w(\bar{x},\bar{y},t) = \sum_{m,n} q_{mn}(t) \phi_{mn}(\bar{x},\bar{y}) \qquad (5.58)$$

where  $\phi_{mn}(\vec{x},\vec{y})$  is the normalized mode shape of the panel and is equal to  $\sin m\pi \vec{x} \sin n\pi \vec{y}$ , where  $\vec{x}=\frac{x}{a}$ ,  $\vec{y}=\frac{y}{b}$ .

By the same theoretical arguments as discussed previously in 1a, for the overall fuselage modes, it can be shown that by summing over all modes, the power spectral density of the displacement at a point  $(\bar{x},\bar{y})$  is given by,

$$\frac{S\left[w(\bar{x},\bar{y});\omega\right]}{S\left[P;\omega\right]} = A^{2} \sum_{m,n} \frac{\Phi_{mn}^{2}(\bar{x},\bar{y}) H^{2}\left(\frac{\omega}{\omega_{mn}}\right) J_{\alpha\alpha}^{2}(\omega)}{M_{mn}^{2} \omega_{mn}^{4}}$$
(5.59)

where;

A = Surface area of the panel.

M = Generalized mass of the (m, n) mode  $= \frac{M}{A} = \text{for a simply supported panel.}$ 

M = Total mass of the panel.

= Resonant frequency of the (m,n) made.

$$H\left(\frac{\omega}{\omega_{mn}}\right) = \left[\left\{1 - \left(\frac{\omega}{\omega_{mn}}\right)^{2}\right\}^{2} + \frac{1}{Q_{mn}^{2}}\left(\frac{\omega}{\omega_{mn}}\right)^{2}\right]^{-\frac{1}{2}}$$

Q = Dynamic magnification factor at resonance.

 $J_{\alpha\alpha}^{2}(\omega)$  = Joint acceptance for the (mn) mode and is defined as

$$\int_{\overline{x}=0}^{1} \int_{\overline{x}=0}^{1} \int_{\overline{x}'=0}^{1} \int_{\overline{x}'=0}^{1} C(\overline{x}, \overline{y}; \overline{x}', \overline{y}'; \omega) \cdot \phi_{mn}(\overline{x}, \overline{y}) \phi_{mn}(\overline{x}', \overline{y}') d\overline{x} d\overline{y} d\overline{x}' d\overline{y}' \quad (5.60)$$

and,  $C(\bar{x}, \bar{y}; \bar{x}', \bar{y}'; \omega)$  = Narrow-band space correlation coefficient for the particular environment.

The power spectral density of the acceleration can again be obtained by use of the relation

$$S\left[\vec{w}(\vec{x}, \vec{y}); \omega\right] = \omega^4 - S\left[w(\vec{x}, \vec{y}); \omega\right]$$

Finally, the space-averaged spectral density of the displacement response can be shown to be given by the expression,

$$\frac{S[w;\omega]}{S[P;\omega]} = A^2 \sum_{mn} \gamma_{mn} \left[ \frac{1}{\omega_{mn}} \right]^4 \cdot \frac{H^2(\omega/\omega_{mn}) J_{\alpha\alpha}^2(\omega)}{M_{mn}^2}$$
 (5.61)

where 
$$\gamma_{mn} = \int_{\bar{x}=0}^{1} \int_{\bar{y}=0}^{1} \varphi_{mn}^{2}(\bar{x},\bar{y}) d\bar{x} d\bar{y}$$
  

$$= 0 ; m = 1,2,3,...; n = 0$$

$$= \frac{1}{4} ; m = 1,2,3,...; n = 1,2,3,...$$
(5.62)

# b. Joint Acceptances for the Various Environments

The derivation of the joint acceptance expressions is based on the same arguments as used for the overall modes in 1b above, namely that the correlation coefficients, mode shapes and thus joint acceptances are separable. Thus, we can define,

$$J_{\alpha\alpha}^{2}(\omega) = J_{m}^{2}(\omega) - J_{n}^{2}(\omega) \qquad (5.63)$$

$$J_{m}^{2}(\omega) = \int_{\bar{x}=0}^{1} \int_{\bar{x}'=0}^{1} C(\bar{\zeta};\omega) \sin m\pi \bar{x} \cdot \sin m\pi \bar{x}' d\bar{x}d\bar{x}' \qquad (5.64)$$

$$J_{n}^{2}(\omega) = \int_{\bar{y}=0}^{1} \int_{\bar{y}'=0}^{1} C(\bar{\eta};\omega) \sin n\pi \bar{y} \cdot \sin n\pi \bar{y}' d\bar{y}d\bar{y}' \qquad (5.65)$$

where; 
$$\vec{\zeta} = \vec{x} - \vec{x}'$$
 and  $\vec{\eta} = \vec{y} - \vec{y}'$ 

Note that the axial joint acceptance of the panel modes  $J_m^2(\omega)$  is of identical form to the axial joint acceptance of the overall fuselage modes (see equation (5.32)). Thus, by transforming the variables of integration, it can be shown that,

$$J_{m}^{2}(\omega) = \int_{\zeta=0}^{1} C(\overline{\zeta};\omega) \left[ (1-\overline{\zeta}) \cos m\pi \overline{\zeta} + \frac{1}{m\pi} \sin m\pi \overline{\zeta} \right] d\overline{\zeta} \quad (5.66)$$

Similarly, it can be shown that,

$$\mathbf{J}_{\mathbf{n}}^{2}(\boldsymbol{\omega}) = \int_{\bar{\eta}=0}^{1} C(\bar{\eta}; \boldsymbol{\omega}) \left[ (1-\bar{\eta}) \cos n\pi \bar{\eta} + \frac{1}{n\pi} \sin n\pi \bar{\eta} \right] d\bar{\eta} \qquad (5.67)$$

# (1) Boundary Layer Turbulence

The joint acceptance of the axial modes of the panel for boundary layer turbulence is obtained by substituting the first of equations (4.20) for the correlation coefficient in the x - direction into equation (5.66), performing the integration and simplifying,

$$J_{\mathbf{m}}^{2}(\omega) = \frac{2\Phi_{\mathbf{x}}}{m^{2}\tau^{2}} \tag{5.68}$$

where;

$$\Phi_{X} = \frac{1}{\Delta_{X}^{2}} \left\{ P_{X} \left[ 1 - (-1)^{m} e^{-\delta_{X}} \cos \gamma_{X} \right] + 4 (-1)^{m} q_{X} e^{-\delta_{X}} \sin \gamma_{X} \right. \\
+ \frac{m\pi}{2} r_{X} \Delta_{X} \right\} \cdot \\
\Delta_{X} = \left[ 1 + \left( \frac{\delta_{X}}{m\pi} \right)^{2} + \left( \frac{\gamma_{X}}{m\pi} \right)^{2} \right]^{2} - 4 \left( \frac{\gamma_{X}}{m\pi} \right)^{2} \\
P_{X} = \left[ 1 + \left( \frac{\delta_{X}}{m\pi} \right)^{2} - \left( \frac{\gamma_{X}}{m\pi} \right)^{2} \right]^{2} - 4 \left( \frac{\gamma_{X}}{m\pi} \right)^{2} \left( \frac{\delta_{X}}{m\pi} \right)^{2} \\
q_{X} = \left( \frac{\delta_{X}}{m\pi} \right) \left( \frac{\gamma_{X}}{m\pi} \right) \left[ 1 + \left( \frac{\delta_{X}}{m\pi} \right)^{2} - \left( \frac{\gamma_{X}}{m\pi} \right)^{2} \right] \\
r_{X} = \left( \frac{\delta_{X}}{m\pi} \right) \left[ 1 + \left( \frac{\delta_{X}}{m\pi} \right)^{2} + \left( \frac{\gamma_{X}}{m\pi} \right)^{2} \right]$$
(5.69)

$$\delta_{x} = \left\{ \left( G.1 \frac{\alpha \omega}{U_{c}} \right)^{2} + \left( 0.27 \frac{\sigma}{\delta_{b}} \right)^{2} \right\}^{\frac{1}{2}}$$

$$\gamma_{x} = \frac{\alpha \omega}{U_{c}}$$

a = panel dimension in the x direction

δ<sub>b</sub> = boundary layer thickness

U<sub>c</sub> = convection velocity.

The joint acceptance of the circumferential panel modes is obtained by substituting the second of equations (4.20), for the correlation coefficient in the y - direction, into equation (5.67), performing the integration and simplifying.

$$J_n^2(\omega) = \frac{2\Phi}{n^2\pi^2} \tag{5.70}$$

where;  $\Phi_y$ ,  $\Delta_y$ ,  $P_y$ ,  $q_y$  and  $r_y$ , are given by equations (5.69) with the subscript y replacing the subscript x, and  $\delta_y$ ,  $\gamma_y$  are as follows;

$$\delta_{y} = \left\{ \left(0.72 \frac{b \omega}{U_{c}}\right)^{2} + \left(1.95 \frac{b}{E_{o}}\right)^{2} \right\}^{\frac{1}{2}}$$

(5.71)

b = panel dimension in the y - direction

 $\gamma_y = 0$ 

### (2) Reverberant Acoustic Field

The joint acceptance of the axial modes of the panel to a reverberant acoustic field is obtained by substituting equation (4.53), for the correlation coefficient in the x-direction, into equation (5.66) and performing the integration. The resulting expression can be written,

$$J_{m}^{2}(\omega) = I_{1}(m) + I_{2}(m) + I_{3}(m)$$
 (5.72)

$$I_1 = \frac{1}{4\pi^2 L_{\infty}^1 m} \left\{ \operatorname{Cir} \left[ \pi (2L_{\times}^1 + m) \right] - \operatorname{Cir} \left[ \pi (m - 2L_{\times}^7) \right] \right\}$$

$$I_{2} = \frac{1}{4\pi L_{x}^{1}} \left\{ \operatorname{Si} \left[ \pi \left( 2L_{x}^{1} + m \right) \right] - \operatorname{Si} \left[ \pi \left( m - 2L_{x}^{1} \right) \right] \right\}$$
(5.73)

$$I_{3} = \frac{1}{(m\pi)^{2}} - \frac{1 - (-1)^{m} \cos(2\pi L_{X}^{1})}{1 - (2 L_{X}^{1}/m)^{2}}$$

where  $L_x^1 = \frac{a}{\lambda}$ 

λ = wave length of sound

 $\alpha$  = panel dimension in the x-direction.

The joint acceptance of the circumferential modes to a reverberant accustic field is obtained by substituting equation (4.54) into equation (5.67), performing the integration and simplifying,

$$J_n^2(\omega) = I_1(n) \div I_2(n) + I_3(n)$$
 (5.74)

where  $I_1(n)$ ,  $I_2(n)$  and  $I_3(n)$  are given by equations (5.73) with the substitutions, n for m and  $L^1_y$  for  $L^1_x$ , where

$$L_y^1 = \frac{b}{\lambda}$$

b = panel dimension in the y-direction.

#### (3) Jet Noise

The joint acceptance of the axial modes of the panel to jet noise is obtained by substituting equation (4.45), for the correlation coefficient in the x - direction, into equation (5.66), performing the integration and simplifying,

$$J_{m}^{2}(\omega) = \frac{2}{(m\pi)^{2}\Delta_{x}^{2}} \left[ P_{x} \left\{ 1 - (-1)^{m} e^{-\delta_{x}} \cos \gamma_{x} \right\} + 4(-1)^{m} q_{x} e^{-\delta_{x}} \right]$$

$$\cdot \sin \gamma_{x} + \frac{m\pi r \Delta_{x}}{2}$$
(5.75)

where  $\Delta_x$ , P,  $q_x$  and  $r_x$  are as defined by equation (5.69), and

$$\delta_{x} = 0.0955 \frac{\omega \sigma}{c}$$

$$\gamma_{x} = 0.715 \frac{\omega \sigma}{c}$$
(5.76)

c = panel dimension in the x-direction.

It should be noted that the above expression is identical to the joint acceptance for boundary layer turbulence except for the numerical values of  $\delta_{_{\mathbf{X}}}$  and  $\gamma_{_{\mathbf{X}}}$ .

The joint acceptance of the circumferential modes of the panel to jet noise is obtained by substituting equation (4.46) for the correlation coefficient in the y - direction, into equation (5.67). Performing the integration and simplifying gives,

$$J_{\eta}^{2}(\omega) = \frac{2}{(n\pi)^{2}\Delta_{y}^{2}} \left[ p_{y} \left\{ 1 - (-1)^{n} e^{-\delta} y \cos \gamma_{y} \right\} + 4(-1)^{n} q_{y} e^{-\delta} y \right]$$

$$\cdot \sin \gamma_{y} + \frac{n\pi r_{y} \Delta_{y}}{2}$$
(5.77)

where;  $\Delta_y$ ,  $P_y$ ,  $q_y$  and  $r_y$  are given by the relations

$$\Delta_{y} = \left[1 + \left(\frac{\delta_{y}}{n\pi}\right)^{2} + \left(\frac{\gamma_{y}}{n\pi}\right)^{2}\right]^{2} - 4\left(\frac{\gamma_{y}}{n\pi}\right)^{2}$$

$$P_{y} = \left[1 + \left(\frac{\delta_{y}}{n\pi}\right)^{2} - \left(\frac{\gamma_{y}}{n\pi}\right)^{2}\right]^{2} - 4\left(\frac{\delta_{y}}{n\pi}\right)^{2}\left(\frac{\gamma_{y}}{n\pi}\right)^{2}$$

$$q_{y} = \left(\frac{\delta_{y}}{n\pi}\right)\left(\frac{\gamma_{y}}{n\pi}\right)\left[1 + \left(\frac{\delta_{y}}{n\pi}\right)^{2} - \left(\frac{\gamma_{y}}{n\pi}\right)^{2}\right]$$

$$r_{y} = \left(\frac{\delta_{y}}{n\pi}\right)\left[1 + \left(\frac{\delta_{y}}{n\pi}\right)^{2} + \left(\frac{\gamma_{y}}{n\pi}\right)^{2}\right]$$

$$\delta_{y} = 0.1193 \frac{\omega b}{c}$$

$$\gamma_{y} = 0.382 \frac{\omega b}{c}$$
(5.78)

panel dimension in the y-direction.

#### RESPONSE OF THE PAN'EL GROUP MODES ٦.

Displacement and Acceleration Power Spectral Densities

The displacement at any point on the panel group at time t may be expressed as;

$$w(x,y,t) = \sum_{mn} q_{mn}(t) \varphi_{mn}(x,y) \qquad (5.79)$$

and the mode shape  $\phi_{mn}(x,y)$  may be written for each of the panels in the row,

$$\phi(x, \vec{y}) = (A_1 \cosh k_1 \vec{y} + A_2 \sinh k_1 \vec{y} + A_3 \cosh k_2 \vec{y} + A_4 \sin k_2 \vec{y}) \sin \frac{m\pi x}{2}$$
(5.80)

where  $\bar{y} = \frac{y}{b}$  and a and b are the panel length and width respectively.

The spectral density of the displacement response may be shown to be given by,

$$\frac{S\left[w(x,y);\omega\right]}{S\left[P;\omega\right]} = A^{2} \sum_{mn} \frac{H^{2}\left(\frac{\omega}{\omega_{mn}}\right) \phi_{mn}^{2}(x,y) \cdot J_{mn}^{2}(\omega)}{\widetilde{M}_{mn}^{2} \omega_{mn}^{4}}$$
(5.81)

where in this particular case, m = 1, 2 or 3 and n depends on the number of panels in the row, N. To obtain the average displacement of the panel group it is necessary to integrate over the total area and divide by the area, i.e., the average displacement of each panel may be obtained and then the average over the number of panels.

For the i-th panel,

$$\vec{\phi}_{1}^{2} = \int_{C}^{1} \int_{0}^{\alpha} (A_{1} \cosh k_{1} \tilde{y} + A_{2} \sinh k_{1} \tilde{y} + A_{3} \cos k_{2} \tilde{y} + A_{4} \sin k_{2} \tilde{y})^{2} \cdot \left(\sin \frac{m \pi x}{\alpha}\right)^{2} \frac{d \tilde{y} d x}{\alpha}$$

$$= \frac{1}{2} \int_{0}^{1} (A_{1} \cosh k_{1} \tilde{y} + A_{2} \sinh k_{1} \tilde{y} + A_{3} \cos k_{2} \tilde{y} + A_{4} \sin k_{2} \tilde{y})^{2} d \tilde{y}$$
(5.82)

Squaring and integrating the above expression gives;

$$\begin{split} \Phi_{1}^{2} &= \frac{1}{2} \left\{ \frac{A_{1}^{2}}{2} \left( \frac{1}{2k_{1}} \sinh 2k_{1} + 1 \right) + \frac{A_{2}^{2}}{2} \left( \frac{1}{2k_{1}} \sinh 2k_{1} - 1 \right) \right. \\ &+ \frac{A_{1}A_{2}}{2k_{1}} \left( \cosh 2k_{1} - 1 \right) + \frac{A_{3}^{2}}{2} \left( \frac{1}{2k_{2}} \sin 2k_{2} + 1 \right) \\ &+ \frac{A_{4}^{2}}{2} \left( 1 - \frac{1}{2k_{2}} \sin 2k_{2} \right) + \frac{A_{3}A_{4}}{2k_{2}} \left( 1 - \cos 2k_{2} \right) \\ &+ \frac{2A_{1}A_{3}k_{2}}{k_{1}^{2} + k_{2}^{2}} \left( \cosh k_{1} \sin k_{2} + \frac{k_{1}}{k_{2}} \sinh k_{1} \cos k_{2} \right) \\ &+ \frac{2A_{1}A_{4}k_{2}}{k_{1}^{2} + k_{2}^{2}} \left( \frac{k_{1}}{k_{2}} \sinh k_{1} \sin k_{2} - \cosh k_{1} \cos k_{2} + 1 \right) \\ &+ \frac{2A_{2}A_{3}k_{2}}{k_{1}^{2} + k_{2}^{2}} \left( \sinh k_{1} \sin k_{2} + \frac{k_{1}}{k_{2}} \left( \cosh k_{1} \cos k_{2} - 1 \right) \right) \\ &+ \frac{2A_{2}A_{4}k_{2}}{k_{1}^{2} + k_{2}^{2}} \left( \frac{k_{1}}{k_{2}} \cosh k_{1} \sin k_{2} - \sinh k_{1} \cos k_{2} \right) \right\} \tag{5.83} \end{split}$$

The generalized mass may be approximated by

$$\overline{M}_{mn} = M_o \frac{\iint \phi_{mn}^2(x,\overline{y}) dx d\overline{y}}{A} = M_o \sum_{i=1}^N \overline{\phi}_i^2$$
 (5.84)

where  $M_0$  = Total panel group mass and A = surface area. If M' is the mass of each panel and M'' is the mass of each stringer, then,

$$M_{\odot} = N(M' + M'') + M''$$
 (5.85)

i.e., 
$$\overline{M}_{mn} = \overline{\phi}^2 \left\{ N(M' + M'') + M'' \right\}$$
where  $\overline{\phi}^2 = \sum_{i=1}^N \overline{\phi}_i^2$  (5.86)

Thus, assuming that the joint acceptance is separable, the space average of the displacement response is given by,

$$\frac{S[w;\omega]}{S[P;\omega]} = A^{2} \sum_{mn} \frac{H^{2}\left(\frac{\omega}{\omega_{mn}}\right) J_{m}^{2}(\omega) \cdot J_{n}^{2}(\omega)}{\overline{\phi}^{2} \left\{ N(M' + M'') + M'' \right\}^{2} \omega_{mn}^{4}}$$
(5.87)

Substituting Equations (5.85) and (5.86) together with the relation A = Nab,

$$\frac{S[w;\omega]}{S[P;\omega]} = \left(\alpha b N\right)^{2} \sum_{mn} \frac{H^{2}\left(\frac{\omega}{\omega_{mn}}\right) J_{m}^{2}(\omega) \cdot J_{n}^{2}(\omega)}{\overline{\Phi}^{2} M_{0}^{2} \omega_{mn}^{4}}$$
(5.88)

The power spectral density of the acceleration response can again be found by use of the relation,

$$S\left[\overline{w};\omega\right] = \omega^4 S\left[w;\omega\right]$$

#### b. Joint Acceptances for the Various Environments

Since the mode shape varies as  $\sin \frac{m\pi x}{a}$  in the axial direction, the joint

acceptance of the axial modes can be determined from equation (5.66). Due to the complexity of the mode shapes in the circumferential direction, the joint acceptance is more conveniently evaluated by use of numerical techniques such as Simpson or Trapezoidal integration. The number of panels considered in the panel group is a function of the typical correlation length of the environment, which is in turn frequency dependent, but will lie between the values  $3 \le N \le N'$ .

#### (1) Boundary Layer Turbulence

Substituting the first of equations (4.20) into equation (5.66) and performing the integration,

$$J_m^2(\omega) = \frac{2\Phi}{(m\pi)^2} \tag{5.89}$$

where  $\phi_x$  is as defined by equation (5.69)

The joint acceptance of the circumferential modes is obtained by numerical evaluation of the expression,

$$J_{n}^{2}(\omega) = \int_{\overline{y}=0}^{1} \int_{\overline{y}'=0}^{1} C(\overline{\eta}; \omega) \phi(\overline{y}) \phi(\overline{y}') d\overline{y} d\overline{y}'$$

where  $C(\bar{\eta}; \omega) = \exp \left[-\delta_y |\bar{\eta}|\right]$ 

 $\phi(\vec{y}), \phi(\vec{y}')$  = mode shape components in the y-direction.

and  $\delta_y$  is given by Equation 5.71

The evaluation of the above expression by trapezoidal integration is described in detail in Appendix II.

#### (2) Reverberant Acoustic Field

The joint acceptance of the axial modes of the panel group is obtained by substituting equation (4.53), for the correlation coefficient in the  $\times$ -direction, into equation (5.66) and integrating. The resulting joint acceptance is the same as given by Equations (5.72) and (5.73).

The joint acceptance of the circumferential modes of the panel group to a reverberant accoustic field is obtained by numerical evaluation of the expression

$$J_{n}^{2}(\omega) = \int_{\overline{y}=0}^{1} \int_{\overline{y}'=0}^{1} C(\overline{\eta}; \omega) \phi(\overline{y}) \phi(\overline{y}') d\overline{y} d\overline{y}'$$

where 
$$C(\bar{\eta};\omega) = \frac{\sin \left(2\pi \frac{b}{\lambda} \bar{\eta}\right)}{2\pi \frac{b}{\lambda} \bar{\eta}}$$

The evaluation of the above expression by trapezoidal integration is described in detail in Appendix II.

#### (3) Jet Noise

The joint acceptance of the axial modes of the panel group to jet noise is obtained by substituting equation (4.45), for the correlation coefficient in the x - direction, into equation (5.66) and integrating. The resulting joint acceptance expression is identical to equations (5.75) and (5.76).

The joint acceptance of the circumferential modes of the panel group to jet noise is obtained by numerical evaluation of the expression

$$\mathbf{J}_{\mathbf{n}}^{2}(\omega) = \int_{\overline{\mathbf{y}}=\mathbf{0}}^{\mathbf{I}} \int_{\overline{\mathbf{y}}'=\mathbf{0}}^{\mathbf{I}} C(\overline{\eta}; \omega) \phi(\overline{y}) \phi(\overline{y}') d\overline{y} d\overline{y}'$$

where;

$$C(\bar{\eta}; e) = \exp \left[ -\frac{\delta}{y} \left| \bar{\eta} \right| \right] \cos \gamma_{y} \left| \bar{\eta} \right|$$

and  $\delta_{y}$ ,  $\gamma_{y}$  are as given by equations (5.78).

The evaluation of the above expression by trapezoidal integration is described in detail in Appendix II.

#### LIST OF SYMBOLS

# LIST OF SYMBOLS USED IN SECTION V

a panel length (x-direction)  a <sub>1</sub> , b <sub>1</sub> , c <sub>1</sub> , d <sub>1</sub> polynomial coefficients in the rational fraction approximations of the auxiliary functions f(z) and g(z)  b panel width (y-direction)  c ambient speed of sound  f excitation frequency (fiz)  fmn resonant frequency of the (mn) mode  f(z), g(z) auxiliary functions used to define sine and cosine integrals  i, j integers  m number of elastic full waves along the x-axis  n number of elastic full waves around the circumference of a shell, or number of elastic half waves along the panel y-axis  q <sub>x</sub> , q <sub>y</sub> coefficients used to define the joint-acceptance of the structure to aerodynturbulence and jet noise.  q <sub>mni</sub> (t), q <sub>mn</sub> (t)  generalized deflection of the (mni) and (mn) modes  r  x', r <sub>y</sub> coefficients used to define the joint-acceptance of the structure to aerodynaturbulence and jet noise.  t time (sec)  w(x,y) radial displacement at the point (x,y)  x axial coordinate  nondimensional axial coordinate, o ≤ x ≤ 1  circumferential coordinate  y circumferential coordinate, or a dummy variable  A <sub>y</sub> , A <sub>y</sub> , A <sub>x</sub> , A <sub>x</sub> modal constants for the panel group	
b panel width (y-direction)  c ambient speed of sound  f excitation frequency (fiz)  fmn resonant frequency of the (mn) mode  f(z), g(z) auxiliary functions used to define sine and cosine integrals  i, j integers  m number of elastic half waves along the x-axis  n number of elastic full waves around the circumference of a shell, or number of elastic half waves along the panel y-axis  coefficients used to define the joint-acceptance of the structure to aerodynturbulence and jet noise.  qmni(t), qmn(t)  generalized deflection of the (mni) and (mn) modes  fx, ry coefficients used to define the joint-acceptance of the structure to aerodynturbulence and jet noise.  t time (sec)  w(x,y) radial displacement at the point (x,y)  x axial coordinate  x nondimensional axial coordinate, o ≤ x ≤ 1  circumferential coordinate  y circumferential coordinate, o cordinate, o cordinate, o cordinate, or a dummy variable  A surface area	
ambient speed of sound  f excitation frequency (fiz)  fun resonant frequency of the (mn) mode  f(z), g(z) auxiliary functions used to define sine and cosine integrals  i, j integers  m number of elastic half waves along the x-axis  n number of elastic full waves around the circumference of a shell, or number of elastic half waves along the panel y-axis  q <sub>x</sub> , q <sub>y</sub> : coefficients used to define the joint-acceptance of the structure to aerodynt turbulence and jet noise.  q <sub>mni</sub> (t), q <sub>mn</sub> (t) generalized deflection of the (mni) and (mn) modes  r distance between two points on a flat surface  f <sub>x</sub> , r <sub>y</sub> coefficients used to define the joint-acceptance of the structure to aerodynaturbulence and jet noise.  t time (sec)  w(x,y) radial displacement at the point (x,y)  x axial coordinate  x̄ nondimensional axial coordinate, o ≤ x ≤ 1  y circumferential coordinate  ȳ nondimensional circumferential coordinate, o ≤ y ≤ 1  z radial coordinate, or a dummy variable  A surface area	
f resonant frequency (Fiz)  fmn resonant frequency of the (mn) mode  f(z), g(z) auxiliary functions used to define sine and cosine integrals  i, j integers  m number of elastic half waves along the x-axis  n number of elastic full waves around the circumference of a shell, or number of elastic half waves along the panel y-axis  ax, ay: coefficients used to define the joint-acceptance of the structure to aerodynturbulence and jet noise.  qmni(t), qmn(t)  generalized deflection of the (mni) and (mn) modes  distance between two points on a flat surface  fx, fy coefficients used to define the joint-acceptance of the structure to aerodynaturbulence and jet noise.  t time (sec)  w(x,y) radial displacement at the point (x,y)  x axial coordinate  nondimensional axial coordinate, o ≤ x ≤ 1  y circumferential coordinate  nondimensional circumferential coordinate, o ≤ y ≤ 1  radial coordinate, or a dummy variable  A surface area	
resonant frequency of the (mn) mode  f(z), g(z) auxiliary functions used to define sine and cosine integrals  i, j integers  m number of elastic half waves along the x-axis  n number of elastic full waves around the circumference of a shell, or number of elastic half waves along the panel y-axis  ax, ay coefficients used to define the joint-acceptance of the structure to aerodynturbulence and jet noise.  amni(t), amn(t) generalized deflection of the (mni) and (mn) modes  f distance between two points on a flat surface  fx, fy coefficients used to define the joint-acceptance of the structure to aerodynaturbulence and jet noise.  the time (sec)  w(x,y) radial displacement at the point (x,y)  x axial coordinate  x nondimensional axial coordinate, o < x < 1  y circumferential coordinate  y nondimensional circumferential coordinate, o < y < 1  radial coordinate, or a dummy variable  A surface area	
integers  number of elastic half waves along the x-axis  number of elastic full waves around the circumference of a shell, or number of elastic half waves along the panel y-axis  qx, qy  coefficients used to define the joint-acceptance of the structure to aerodynturbulence and jet noise.  qmni(t), qmn(t)  generalized deflection of the (mni) and (mn) modes  r  coefficients used to define the joint-acceptance of the structure to aerodynturbulence and jet noise.  r  x, r  y  coefficients used to define the joint-acceptance of the structure to aerodynaturbulence and jet noise.  t  time (sec)  w(x,y)  radial displacement at the point (x,y)  x  axial coordinate  nondimensional axial coordinate, o ≤ x ≤ 1  y  circumferential coordinate  nondimensional circumferential coordinate, o ≤ y ≤ 1  z  radial coordinate, or a dummy variable  A  surface area	
integers  number of elastic half waves along the x-axis  number of elastic full waves around the circumference of a shell, or number of elastic half waves along the panel y-axis  qx, qy  coefficients used to define the joint-acceptance of the structure to aerodynturbulence and jet noise.  qmni(t), qmn(t)  generalized deflection of the (mni) and (mn) modes  r  coefficients used to define the joint-acceptance of the structure to aerodynturbulence and jet noise.  r  x, r  y  coefficients used to define the joint-acceptance of the structure to aerodynaturbulence and jet noise.  t  time (sec)  w(x,y)  radial displacement at the point (x,y)  x  axial coordinate  nondimensional axial coordinate, o ≤ x ≤ 1  y  circumferential coordinate  nondimensional circumferential coordinate, o ≤ y ≤ 1  z  radial coordinate, or a dummy variable  A  surface area	
number of elastic half waves along the x-axis  number of elastic full waves around the circumference of a shell, or number of elastic half waves along the panel y-axis  qx, qy coefficients used to define the joint-acceptance of the structure to aerodynturbulence and jet noise.  qmni(t), qmn(t) generalized deflection of the (mni) and (mn) modes  r distance between two points on a flat surface  rx, ry coefficients used to define the joint-acceptance of the structure to aerodynaturbulence and jet noise.  t time (sec)  w(x,y) radial displacement at the point (x,y)  x axial coordinate  \overline{x} nondimensional axial coordinate, o < x < 1  y circumferential coordinate  nondimensional circumferential coordinate, o < y < 1  radial coordinate, or a dummy variable  A surface area	
number of elastic full waves around the circumference of a shell, or number of elastic half waves along the panel y-axis  q_x, q_y: coefficients used to define the joint-acceptance of the structure to aerodynaturbulence and jet noise.  q_mni(t), q_mn(t) generalized deflection of the (mni) and (mn) modes  distance between two points on a flat surface  r_x, r_y coefficients used to define the joint-acceptance of the structure to aerodynaturbulence and jet noise.  t time (sec)  w(x,y) radial displacement at the point (x,y)  x axial coordinate  \overline{x} nondimensional axial coordinate, o < x < 1  y circumferential coordinate  radial coordinate, or a dummy variable  A surface area	
of elastic half waves along the panel y-axis  q <sub>x</sub> , q <sub>y</sub> : coefficients used to define the joint-acceptance of the structure to aerodynaturbulence and jet noise.  q <sub>mni</sub> (t), q <sub>mn</sub> (t) generalized deflection of the (mni) and (mn) modes  r distance between two points on a flat surface  r <sub>x</sub> , r <sub>y</sub> coefficients used to define the joint-acceptance of the structure to aerodynaturbulence and jet noise.  time (sec)  w(x,y) radial displacement at the point (x,y)  x axial coordinate  \overline{x} nondimensional axial coordinate, o < x < 1  y circumferential coordinate  radial coordinate, or a dummy variable  A surface area	
turbulence and jet noise.  q <sub>mni</sub> (t), q <sub>mn</sub> (t) generalized deflection of the (mni) and (mn) modes  r distance between two points on a flat surface  r <sub>x</sub> , r <sub>y</sub> coefficients used to define the joint-acceptance of the structure to aerodynaturbulence and jet noise.  t time (sec)  w(x,y) radial displacement at the point (x,y)  x axial coordinate  \( \tilde{x} \) nondimensional axial coordinate, o \( \infty \) x \( \infty \) 1  y circumferential coordinate  y nondimensional circumferential coordinate, o \( \infty \) y \( \infty \) 1  z radial coordinate, or a dummy variable  A surface area	
r distance between two points on a flat surface  r_x, r_y coefficients used to define the joint-acceptance of the structure to aerodynaturbulence and jet noise.  t time (sec)  w(x,y) radial displacement at the point (x,y)  x axial coordinate  \overline{x} nondimensional axial coordinate, o < x < 1  y circumferential coordinate  y nondimensional circumferential coordinate, o < y < 1  z radial coordinate, or a dummy variable  A surface area	ami c
coefficients used to define the joint-acceptance of the structure to aerodynaturbulence and jet noise.  time (sec)  w(x,y) radial displacement at the point (x,y)  x axial coordinate  \overline{x} nondimensional axial coordinate, o < x < 1  y circumferential coordinate  nondimensional circumferential coordinate, o < y < 1  z radial coordinate, or a dummy variable  A surface area	
turbulence and jet noise.  time (sec)  w(x,y) radial displacement at the point (x,y)  x axial coordinate  \overline{x} nondimensional axial coordinate, o < x < 1  y circumferential coordinate  y nondimensional circumferential coordinate, o < y < 1  z radial coordinate, or a dummy variable  A surface area	
w(x,y)  radial displacement at the point (x,y)  x  axial coordinate  \overline{\pi}  nondimensional axial coordinate, o < x < 1  y  circumferential coordinate  nondimensional circumferential coordinate, o < y < 1  z  radial coordinate, or a dummy variable  A  surface area	mic
x axial coordinate  \overline{\pi} nondimensional axial coordinate, o < x < 1  y circumferential coordinate  \overline{\pi} nondimensional circumferential coordinate, o < y < 1  z radial coordinate, or a dummy variable  A surface area	
nondimensional axial coordinate, o ≤ x ≤ 1  y circumferential coordinate  y nondimensional circumferential coordinate, o ≤ y ≤ 1  z radial coordinate, or a dummy variable  A surface area	
y circumferential coordinate  y nondimensional circumferential coordinate, o ≤ y ≤ 1  z radial coordinate, or a dummy variable  A surface area	
y nondimensional circumferential coordinate, o ≤ y ≤ 1  z radial coordinate, or a dummy variable  A surface area	
z radial coordinate, or a dummy variable  A surface area	
A surface area	
A A A A model constants for the agreet annual	
UN USTUSTA import extensions to the batter Brook	
narrow-band, longitudinal space correlation coefficient of fluctuating pressured = $C(x, x'; \omega)$	ıre
C(ζ,τμ) narrow-band, longitudinal space-time correlation coefficient for a fluctuatir pressure field.	1g

```
(ديزر)⊃
                      narrow-band, circumferential space correlation coefficient of fluctuating
                      pressure field = C(y, y'; e)
 C(x,y;x',y';\omega)
                     naπow-band, space correlation coefficient between pressures acting at
                     points (x,y) and (x', y').
 C(r;u)
                      narrow-band, space correlation coefficient between pressures acting at
                     two points, a distance in apart, on a flat surface exposed to a reverberant
                      acoustic field
 Ci(z)
                     modified cosine integral
 Cin(z)
                      cosine integral = \gamma + Ln(z) - Ci(z)
 F(\gamma_v \pm 2 n \pi)
                     function used in defining joint acceptance to jet noise
 F (t), F (t)
                     generalized force for the (mni) and (mn) modes
                     dynamic magnification factor, at frequency w, of the (mn) mode
 J<sup>2</sup> (ω)
J<sup>2</sup> (ω)
J<sup>2</sup> (ω)
J<sup>2</sup> (ω)
                     joint-acceptance of the m-th axial mode
                     joint-acceptance of the i-th component of the n-th ring mode
                     net joint acceptance of the n-th ring mode
 ,___(ω)
mni
                     joint acceptance of the (mni) cylinder mode.
 J_{\alpha\alpha}^{z}(\omega)
                     joint acceptance of the (mn) panel made
 Lx, Ly
                     structural lengths in the x and y directions
 L'x
                     α/λ
 M١
                     panel mass
М"
                     stringer mass
                     total panel group mass
Mmi, Mmn
                     generalized masses of the (mni) and (mn) modes
Ν
                    number of panels in an array or group
P(x, y, t)
                    instantaneous pressure acting at the point (x, y)
Px, Py
                    coefficients used to describe the joint acceptance of the structure to aero-
                    dynamic turbulence and jet noise
Q
                    dynamic magnification factor at resonance for all modes
\mathbf{Q}_{\mathbf{mn}}
                    dynamic magnification factor at resonance for the (mn) mode
R[f(t); \tau]
                    autocorrelation of the time function f(t)
R[f(t),g(t);\tau]
                    cross-correlation of the time functions f(t) and g(t)
                    narrow-band pressure correlation function for pressures at point (x,y) and
R(x, y; x', y'x)
                    point (x1, y1)
```

```
[سر ۲] S
                    mean-square (power)spectral density of the pressure - (psi)<sup>2</sup>/Hz
S [f(t); ω]
                    mean-square spectral density of the function f(t)
5 [f(t), g(t);ພ]
                    cross-power spectral density of the functions f(t) and g(t)
S [w;ω]
                    space overage of the mean-square acceleration spectral density; g^2/H_Z
S_{p}[P(x,y,t),P(x',y',t):c] cross-spectrum of pressures P(x,y,t) and P(x',y',t)
Si(z)
                    sine integral
Uc
                    boundary layer convection velocity
                    Free stream velocity
Y,(y)
                    y-component of the panel group made shape
                    Eulers constant (0.5772156649)
γ
δx
                    correlation parameters for the turbulent boundary layer and jet noise
                    pressure fluctuations
γ<sub>mn</sub>
                    space average constant for the (mn) made shape
ВЬ
                    boundary layer thickness
Δ,; Δ,
                    coefficients used in describing the joint acceptances to boundary layer
                    and jet noise pressure fluctuations.
                    axial separation distance, x - x^t
                    nondimensional axial separation distance, \zeta/L_{_{\mathbf{X}}}
η
                    circumferential separation distance, y - y'
                    nondimensional circumferential separation distance, \eta/L_y
η
6 (u/u<sub>mn</sub>)
                    phase angle between excitation and response at frequency \omega for the (mn)
                    acoustic wavelength, \frac{c}{t}
                    mass per unit area
                    variable of integration for joint acceptances = (\bar{x} + \bar{x} - 1)/2
                    generalized mass fractions for the (mni) and (mn) modes
ξ<sub>mni</sub>, ξ<sub>mn</sub>
                    time delay
ቒ. (፳,፶)
                    normalized made shape for the i-th panel of the panel group
\phi_{mni}(x,y)
                    radial component of cylinder mode shape for the (mni)-mode
```

<sup>ф</sup> х′ <sup>ф</sup> у	parameter used to define the joint acceptance of the panel and panel group to boundary layer turbulence
φ <sub>mni</sub> (x,y)	tangential component of cylinder mode shape for the (mni)-mode
ជ	excitation frequency, rad/sec
ω mn	resonant frequency for the (m,n)-mode
Δευ	band-width of vanishingly small frequency band, rad/sec
Ω mes	resonant frequency of the coupled cylinder-internal air mass system
11	absolute value
( <sup>*</sup> )	time derivative

#### SECTION VI

#### NOISE REDUCTION

#### 1. INTRODUCTION

The previous sections have described classical modal methods for computing the sound pressure inside a bare cylindrical fuselage for a given external excitation. It is now necessary to illustrate how these expressions are utilized to determine the noise reduction provided by the fuselage and its internal acoustic treatment. In this context, it should be understood that the term noise reduction implies the reduction in noise level due to the transmission loss through the structure together with the reduction due to any absorption inside the fuselage. These two mechanisms can be treated separately.

The fundamental property that describes the transmission loss of a structure is the transmission coefficient  $\tau$ , defined for this report as the fraction of the excitation energy that is transmitted

$$\tau = \frac{E_2}{E_1}$$

where  $\frac{E_1}{1}$  and  $\frac{E_2}{2}$  are the energy densities on the incident and transmitting sides of the structure respectively. If the incident excitation is a plane wave, then

$$\tau = \left| \frac{P_t}{P_1 + P_r} \right|^2 = \left| \frac{P_2}{P_1} \right|^2$$
 (6.1)

where

$$P_2 = P_1$$

$$P_i + P_r = P_1$$

and P<sub>i</sub>, P<sub>r</sub>, P<sub>t</sub> are the incident, reflected and transmitted sound pressures respectively.

In general, these are complex quantities and phase is eliminated by taking the absolute value of the pressure ratio to determine  $\tau$ . (Note that the definition used here for transmission loss necessarily differs from the standard form (Reference 60) in that it includes the reflected pressure  $P_r$ . This is computed to account for diffraction effects of the cylindrical fuselage in a jet noise field.

In the case of boundary layer noise excitation, the excitation pressure  $P_{ij}$  is the fluctuating pressure at the surface of the fuselage. To provide a common basis for defining the effective

transmission loss for excitation by a jet noise field or by boundary layer noise, both forms of excitation will be defined in terms of an equivalent reverberant field. This is the sound pressure that would exist on a <u>rigid</u> fuselage in a reverberant sound field which would produce the same structural response as the jet noise or boundary layer noise when the fuselage is allowed to move.

As discussed in Section IV, a reverberant field consists of an infinite number of plane waves traveling in all possible directions. The effect of varying angle of incidence on sound transmission loss must therefore be considered.

It is to be expected of course, that  $\tau$  is a function of the angle of incidence  $\theta$  with respect to a normal to the structure. To account for random incidence, the value of  $\tau$  used must be averaged over all angles of incidence

$$\bar{\tau} = 2 \cdot \frac{\int_{0}^{\theta'} \tau(\theta) \sin 2\theta \, d\theta}{(1 - \cos 2\theta')}$$
 (6.2)

where  $\theta^{i}$  is a limiting angle of incidence (Reference 61).

Since the value of  $\tau$  is always less than unity, it is usual to quote the transmission loss in terms of  $1/\tau$ , the actual definition being

Transmission loss = 
$$TL = 10 \log \left(\frac{1}{\overline{\tau}}\right)$$
 dB. (6.3)

# 2. DERIVATION OF TRANSMISSION COEFFICIENT FOR MULTI-LAYERED ACOUSTIC TREATMENT

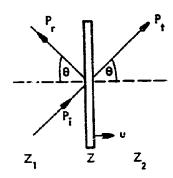
The derivation of an expression for the transmission coefficient  $\tau$  through the acoustic treatment inside a structure can be obtained most conveniently by employing an impedance approach. In the case of complex structures, it is proposed to determine  $\tau$  for each individual section in this manner, and then combine these various values of  $\tau$  to obtain an overall coefficient. Thus any combination of elements can be treated as long as the expression for the transmission coefficient of each element is known. In practice it is found that acoustic treatment of conventional aircraft fuselages consist of combinations of the following:

- (i) panels
- (ii) impervious septa (having negligible stiffness)
- (iii) poraus blankets
- (iv) airgaps.

In this section, the value of the complex pressure ratio, for an incident plane wave will be evaluated for each of the four above cases. The overall transmission coefficient for any combination of these basic elements is then found by taking the square of the absolute value of the product of the corresponding pressure ratios.

#### a. Pressure Ratio Across a Single Panel

The first case to be considered is that of a single panel having both mass and stiffness exposed to a plane wave incident at an angle  $\theta$  with the normal as shown in the following sketch.



If Z is the normal impedance of the panel, defined as the ratio of net pressure acting on the panel to the panel velocity, u, then

$$P_i + P_r - P_t = Z_U \cos \theta$$

Hence

$$\frac{P_1}{P_2} = \frac{P_1 + P_r}{P_t} = \left[1 + \frac{Z\cos\theta}{Z_2}\right] \tag{6.4}$$

where  $Z_2$  is the terminating impedance on the transmitting side of the panel. The most general expression for the normal impedance of the panel, which includes a stiffness term to represent the panel impedance below the fundamental resonance frequency, is given by

$$Z = \omega_{O}^{m\eta} + \frac{\omega^{3}D\eta}{c^{4}}\sin^{4}\theta + j\left[\omega_{m} - \frac{\omega_{O}^{2}m}{\omega} - \frac{\omega^{3}D}{c^{4}}\sin^{4}\theta\right] \qquad (6.5)$$

where

$$\omega_{o} = \pi^{2} \sqrt{\frac{D}{m}} \left( \frac{1}{\sigma^{2}} + \frac{1}{b^{2}} \right)$$
, resonance frequency of panel

$$D = \frac{E h^3}{12} , \text{ panel stiffness}$$

 $m = \rho h$  , surface mass density

and

ρ = density of panel

h = thickness of panel

E = Young's modulus of the material of the panel.

a,b = lateral dimensions of the panel.

 $\eta$  = loss factor of the panel

 $=\frac{1}{Q}$ 

### b. Pressure Ratio Across a Septum

In a conventional aircraft fuselage one element of the acoustic treatment usually consists of a lightweight septum having mass but negligible stiffness. In this case, the impedance is purely a function of the mass

and

$$\left|\frac{P_1}{P_2}\right|^2 = \frac{1}{\tau} = \left[1 + \left(\frac{\omega m \cos \theta}{Z_2}\right)^2\right] \tag{6.7}$$

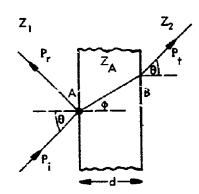
where

$$m = ph$$

and

Z, is the terminating impedance as before.

### c. Pressure Ratio Across a Porous Blanket



The sound pressure P<sub>1</sub> at point A is given by (References 62, 63)

$$P_{1} = Z_{A} \cosh \left[ \frac{bd}{\cos \phi} + \phi \right]$$
 (6.8)

where

$$\phi = \coth^{-1}\left[\frac{Z_2}{Z_\Delta}\right] \tag{6.9}$$

$$\cos \phi = \left[1 - \left(\frac{c_A}{c_1}\right)^2 \sin^2 \theta\right]^{\frac{1}{2}} \tag{6.10}$$

 $Z_A$  = characteristic impedance of the porous material,

b = propagation constant of the porous material which may be complex,

c<sub>1</sub>, c<sub>A</sub> = the velocity of sound in the incident region and the porous blanket respectively.

At point B, the pressure P2 is given by

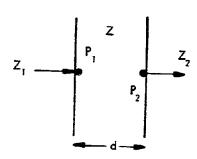
$$P_2 = Z_A \cosh \phi$$

$$\frac{P_1}{P_2} = \left[ \frac{\cosh\left(\frac{b \ d}{\cos \phi} + \phi\right)}{\cosh \phi} \right]$$
 (6.11)

The input impedance  $Z_1$  at the point A is given by

In Appendix IV, expressions for b,  $Z_A$  and  $\frac{P_1}{P_2}$  are given in terms of the basic properties of the material.

### d. Pressure Ratio Across an Air-Gap



In this case, the characteristic impedance of the material  $Z_A = \rho_o c$ , and the propagation constant  $b = j \frac{\omega}{c}$ . Therefore in a similar manner to that used in 2.c. above it can be shown that, (References 62, 63)

$$\frac{P_1}{P_2} = \frac{\cosh\left[\left(\frac{j\omega d}{c\cos\theta}\right) + \coth^{-1}\left(\frac{Z_2}{\rho_0 c}\right)\right]}{\cosh\left[\coth^{-1}\left(\frac{Z_2}{\rho_0 c}\right)\right]}$$
(6.13)

and the input impedance  $Z_1$  at the interface is given by

$$Z_{1} = \rho_{o} c \coth \left[ \left( \frac{j \omega d}{c \cos \theta} \right) + \coth^{-1} \left( \frac{Z_{2}}{\rho_{o} c} \right) \right]$$
 (6.14)

As before,  $\frac{P_1}{P_2}$  and  $Z_1$  are expressed in terms of basic quantities in Appendix IV.

#### e. Determination of Overall Transmission Coefficient

In each of the four cases described above, expressions to: the input and terminating impedances have been developed together with the sound pressure ratios. When the various elements are combined in a conventional structure, the overall transmission coefficient  $\tau$  is obtained from

$$\tau = \left| \frac{P_2}{P_1} \cdot \frac{P_3}{P_2} \cdot \dots \cdot \frac{P_n}{P_{n-1}} \right|^2$$
 (6.15)

where the terminating impedance of one element is the input impedance to the next and so on.

To account for random incidence of the reverberant field excitation, the overall transmission coefficient  $\tau$  is computed from Equation (6.15) for incidence angles from 0 to a limiting angle  $\theta'$  of 85 degrees in steps of approximately 5 degrees. The incidence angle is assumed to be the same for each layer since the incident and transmitted angles are also assumed to be equal. This overall  $\tau(\theta)$  for a given angle is then used in Equation (6.2) to determine an average transmission coefficient  $\tilde{\tau}$  for all angles of incidence. This procedure is considered more realistic for defining transmission loss through porous blanket elements. For low angles of incidence, the longer path length through the blanket results in a greater attenuation which tends to provide a result similar to, but more conservative than, the approach used in Reference 62 where only normal incidence is considered. This refinement is considered practical since it is readily carried out by the computer program.

### 3. COMPUTATION OF NOISE REDUCTION USING THE MODAL APPROACH

The noise reduction of a fuselage, treated with acoustic material, is computed by the modal approach in two basic steps in the following manner.

### a. Increase in Transmission Loss Through the Acoustic Treatment

The fractional noise reduction for the bare fuselage, using any one of the three structural models outlined in Section III, is defined by an equation of the form (see Equation 3.49 or 3.90)

$$\frac{S_{P_i}(\omega)}{S_{P}(\omega)} = \left[\frac{S_w(\omega) (\rho_0 c \omega)^2}{S_{P}(\omega)}\right] \cdot C_A(\omega)$$
 (6.16)

where

 $C_A(\omega)$  = an acoustic coupling factor defined by the summation terms in Equation (3.49 or 3.90)

 $S_{p}(\omega)$  = spectral density of external pressure at frequency  $\omega$ 

 $S_{p}(\omega)$ ,  $S_{w}(\omega)$  = space averaged spectral densities of internal pressure and wall displacement respectively.

The bracketed quantity in this expression can be recognized as a form of transmission coefficient  $\tau$ . The numerator represents the mean square pressure transmitted by a wall, with a velocity spectral density  $\omega^2 S_{\omega}(\omega)$ , which is radiating into a characteristic impedance  $\rho_{\omega}c$ .

The denominator represents the mean square external pressure. Thus, this term represents the modal form of the transmission coefficient for radiation into free space by the bare fuselage wall.

The comparable expression for a single bare flat wall is obtained from Equation (6.4) as

$$\tau_{w} = \left| \frac{\rho_{1}}{P_{1}} \right|^{2} = \left| 1 + \frac{Z \cos \theta}{\rho_{0} c} \right|^{-2}$$
 (6.17)

where

Z = normal impedance of wall (including stiffness) given by Equation (6.5).

It is assumed that if the same type of acoustic treatment is added to the fuselage and to the single flat wall, the incremental transmission loss due to the treatment is the same and is given in decibel form by

$$\Delta TL = 10 \log (1/\bar{\tau}_{ow}) - 10 \log (1/\bar{\tau}_{w})$$
 (6.18)

where

ow overall transmission coefficient for any form of treatment computed from Equation (6.15) and integrated over angle by Equation (6.2).

= average transmission coefficient for a single bare wall computed from Equation (6.17) and integrated over angle by Equation (6.2).

The incremental transmission loss is then added to the noise reduction for the bare fuselage to account for the increased transmission loss of the acoustic treatment. The noise reduction for the bare fuselage is obtained from Equation (6.16) in decibel form as

$$NR_{o} = 10 \log \left[ S_{p}(\omega) / S_{p}(\omega) \right]$$
 (6.19)

where

$$S_p(\omega)/S_p(\omega) = \text{pressure ratio given by Equation (3.49) or (3.90)}.$$

### b. Increase in Noise Reduction Due to Internal Absorption

Consider now the acostic coupling term  $C_{\mathbf{A}}(\omega)$  in Equation (6.16). This term modifies the radiation load  $\rho$  c to account for the actual acoustic modal impedance inside the cylindrical fuselage.

As shown in Section III, by Equation (3.49 or 3.90), this term is defined by a summation of the acoustic modes of the cylinder. For an excitation frequency  $\omega$  in the vicinity of one of the acoustic resonance frequencies, this coupling term is controlled by the resonant amplification factor  $\mathbf{Q}_{ac}$ . The latter, in turn, is controlled by the acoustic absorption inside the fuseloge.

For a three-dimensional cylindrical acoustic field with relatively low enform damping on all walls, the resonant amplification factor is approximately equal to (Reference 14)

$$Q_{oc} = \frac{4V\omega}{c\bar{\alpha}_{n}} \left[ \frac{1}{\frac{S_{x} + \frac{S_{R}/2}{1 - (n/\pi\psi_{ns})^{2}}}} \right]$$
 (6.20)

where  $V = \pi R^2 L_X^2$  volume of cylinder c = speed of sound a = average normal absorption coefficient at walls

 $S_x = 2 \pi R^2$  - area of end walls

 $S_R = 2\pi R L_x - area of side walls$ 

n = radial mode number

 $\psi_{ns} = \text{roots of } \mathcal{J}_{n}^{r}(\overline{R}) = 0$  as defined by Equation (3.21).

For the important range of acoustic modal frequencies, and for typical fuselage sizes, this can be roughly estimated by

$$Q_{ac} \approx \frac{4V\omega}{c\bar{\alpha}S_{R}}$$
 (6.21)

Making the further approximation that the average random incidence absorption coefficient  $\alpha$  is equal to about  $2\tilde{\alpha}_n$  for typical absorbing materials, then

$$Q_{ac} \approx \frac{8 V_{\omega}}{ca}$$
 (6.22)

and

a = 
$$\sum_{i} \alpha_{i} S_{i}$$
 - the total square feet of absorption

Values for  $\alpha$  may be determined for typical surfaces inside aircraft from the data in Table IV. A typical value for Q in the low frequency range, where the modal approach is realistic, is about 25.

To summarize the modal approach for computing noise reduction

- Without any treatment, the noise reduction is computed by the modal approach from Equation (6.19) using an appropriate value for Q in the program as computed from Equation (6.22).
- With added treatment, the increased absorption inside the fuselage is determined by modifying the value of Q and adding the incremental transmission loss for the treatment defined by Equation (6.18).

#### 4. COMPUTATION OF NOISE REDUCTION FOR A DIFFUSE INTERNAL SOUND FIELD

The method of the previous section considers the modal response of the internal acoustic field, and an expression for the noise reduction is obtained by a modal summation. However, at high frequencies where the modal density is high, this involves some lengthy calculations even for a computer and so it is preferable to simplify the approach in this region and use more conventional methods for computing noise reduction. This can be done if the modal density is sufficiently high so that the invalid field can then be considered to be uniform both in space and spectral content. A mode of the internal acoustic field is (Reference 14)

$$N(f) = \frac{4\pi f^2 V}{c^3} + \frac{\pi f A}{2c^2} + \frac{L}{8c}$$
 (6.23)

where 
$$V = \pi R^2 L_X$$

$$A = 2\pi R (R + L_X)$$

$$L = 4\pi R + 4L_X$$

and R = radius of cylinder

L = length of cylinder

Thus if  $\Delta f$  is the bandwidth of a mode having a fundamental frequency f Hz, the condition for a uniform or diffuse sound field can be written as

$$N(f) \cdot \Delta f \geq 10 \tag{6.24}$$

If Equation (6.23) is approximated by considering the first term only, the frequency at which the above condition is satisfied is given by

$$f_{D} \approx c \left[ \frac{10^{Q}_{oc}}{4 \pi^{2} R^{2} L_{v}} \right]^{\frac{1}{3}}$$
 Hz (6.25)

where  $\mathbf{Q}_{\mathbf{ac}}$  is the magnification factor of the acoustic mode given by

$$Q_{ac} = \frac{f}{\Delta f}$$

Therefore, above this frequency, the sound field can be considered essentially diffuse and can be treated by statistical methods. In this case the total noise reduction is given as

$$NR_{D} = 10 \log \left[ 1 + \frac{\bar{\alpha} \bar{S}}{\bar{\tau}_{ow} S_{t}} \right]$$
 (6.26)

 $\bar{\alpha} = (\Sigma \alpha_i S_i)/\Sigma S_i$ , the average absorption coefficient

 $\bar{S} = \Sigma S_{\hat{i}}$ , the total absorbing surface area

 $\alpha_{i}$  = the absorption coefficient associated with area  $S_{i}$ 

and

 $\bar{\tau}_{ow}$  = the overall transmission coefficient of the structure through the transmitting area  $S_{+}$ .

The values of  $\alpha_i$  are found from Table IV and  $\bar{\alpha}$  computed as indicated above to provide an appropriate input for the program. The value of  $\bar{\tau}_{ow}$  is computed by the program using equations (6.15 and 6.2). Any set of elements from a single panel on up to complex double wall construction can be evaluated using the various expressions covered in Section 2. above.

The criterion for application of this statistical or diffuse field method for computing noise reduction was stated earlier in terms of an acoustical modal density. (See Equation (6.25.)) Two additional criteria may also be used to define a lower limiting frequency, below which the modal approach should be used.

In order that the plate curvature can be neglected, the diffuse field approach should only be used above the first breathing mode given by

$$f_b \approx \frac{C_L}{2\pi R}$$
 (6.27)

where

 $C_L$  = the longitudinal wave velocity in the cylinder.

Also, since the effect of the supporting frames has been neglected, the approach should only be used above the fundamental panel resonance frequency where the frames can be considered to be nodal points. This frequency is given by (see Equation (6.5) for definition of symbols)

$$f_o = \frac{\pi}{2} \sqrt{\frac{D}{m}} \left( \frac{1}{a^2} + \frac{1}{b^2} \right)$$
 (6.28)

Thus combining these conditions it can be stated that the simple statistical approach should only be used in the frequency region greater than the highest of the limiting frequencies defined by Equations (6.25, 6.27, and 6.28). This insures that the internal field is diffuse, curvature effects are negligible, and the structure is equivalent to single panels vibrating above their first mode.

In summary, the noise reduction for a diffuse internal sound field is computed directly by Equation (6.26). This expression is evaluated by routine TRLSS in the computer program. It is important to note that this routine is also used to compute the incremental transmission loss  $\Delta TL$  (Equation 6.18) for the modal approach.

### 5. EQUIVALENT REVERBERANT FIELD

It has been assumed up to this point that the noise reduction is computed for an external reverberant sound field driving the structure.

It is necessary now to define the spectral intensity of this equivalent reverberant field which produces the same structural response as does excitation by jet noise or boundary layer turbulence.

The space average pressure spectral density inside the fuselage  $S_{p_i}(\omega)$  can be defined by

$$S_{p_{i}}(\omega) = S_{p}(\omega) \cdot \frac{S_{p_{i}}(\omega)}{S_{p}(\omega)} = S_{p}(\omega) \cdot \frac{S_{p_{i}}(\omega)}{S_{p_{i}}(\omega)} \cdot \left[\frac{S_{p_{i}}(\omega)}{S_{p_{i}}(\omega)}\right]$$

where

\*\*\*\*\*\*\*

 $S_p(\omega)$  = pressure spectral density of the jet noise or boundary layer noise field  $S_p(\omega)$  = pressure spectral density of equivalent reverberant field.

Dividing the numerator and denominator of the bracketed term in the above expression by the respective structural displacement spectral densities and expressing the result in decibel form, the space average internal pressure spectrum level  $SL_i(\omega)$  is given by

$$SL_{i}(\omega) = SL(\omega) - NR_{r} + C(\omega)$$
 (6.29)

where

$$SL_i(\omega) = 10 \log S_{p_i}(\omega)/P_{ref}^2$$
 - internal pressure spectrum level  
 $SL(\omega) = 10 \log S_{p_i}(\omega)/P_{ref}^2$  - true external pressure spectrum level

$$NR_r = 10 \log S_P(\omega)/S_P(\omega) - \text{noise reduction for reverberant field}$$
  
 $r = 10 \log S_P(\omega)/S_P(\omega) - \text{noise reduction for reverberant field}$ 

$$C(\omega) = 10 \log \frac{S_{p_r}(\omega)/S_{w_r}(\omega)}{S_{p_r}(\omega)/S_{w_r}(\omega)}$$
 relative correction factor for equivalent reverberant field.

$$P_{ref}^2 = (0.0002 \text{ dynes/cm}^2)^2$$

If by definition, the displacement spectral densities  $S_{w}(\omega)$  and  $S_{w}(\omega)$  for the reverberant

and true excitation (jet noise or boundary layer noise) are identical, then the correction factor  $C(\omega)$  has the value necessary to correct the noise reduction, computed for reverberant field excitation, so that it corresponds to the actual noise reduction for the true excitation.

Thus, the noise reduction for either jet noise or boundary noise excitation is given by

$$NR = NR_r - C(\omega) \tag{6.30}$$

where

NR<sub>r</sub> = noise reduction for reverberant field excitation which is computed by either the modal approach (Section VI.3.) or the diffuse field approach (Section VI.4.)

The value of  $C(\omega)$  may be computed from the print-out provided by the program of the ratios  $S_{w}(\omega)/S_{p}(\omega)$  and  $S_{w}(\omega)/S_{p}(\omega)$  where the former refers to a reverberant field excitation and

the latter to either jet noise or boundary layer is se excitation. Note that this ratio of normalized response functions and hence the equivalent reverberant field correction  $C(\omega)$  can be computed for any of the three basic structural models (i.e. – cylinder, coupled or single panel) over the entire frequency range. However, the following practical limiting frequency range is suggested as a rough criteria for the frequency range of each model.

c For cylinder model — compute C(w) from the program print-out from the lowest frequency of interest to an upper limit equal to the breathing mode frequency f<sub>b</sub> given by Equation (6.27)

o For coupled panel model — compute C( $\omega$ ) from the program listing from 1/2 the the breathing mode frequency  $f_b$  to approximately  $\frac{4}{b}$   $f_b$  .

For single panel model - compute C(ω) from the program listing from approximately 2 times the panel fundamental frequency for given by Equation (6.28) to the highest frequency of interest.

These are approximate guidelines which can also be used to define the upper and lower frequency bounds for the structural response covered by these three structural models. However, these limiting frequencies, which are required as input parameters for the program, can be selected by the user to meet any desired range. The above criteria are suggested as covering a practical range of validity for computing an equivalent reverberant field.

### 6. THE EFFECT OF FLANKING TRANSMISSION'

The previous sections have not considered the fact that sound is radiated at high frequencies by the circumferential frames. This source of flanking loss is treated here in terms of sound radiation by an infinite strip. In the frequency range when flanking loss is significant, the circumferential bending wavelength of the frame  $\lambda_{\rm bn}$  will be greater than the acoustic wavelength  $\lambda_{\rm d}$  so that lengthwise, bending vibrations of the frame will couple efficiently to the interior sound field. (Reference 60.) However, in the width direction, for frequencies below

$$f_{\ell} \approx \frac{4300}{W} \text{ Hz} \tag{6.31}$$

where w is the width of the frame in inches, the acoustic radiation on a vibrating load begins to decrease proportional to  $f^{3/2}$ . Thus it can be assumed that the frame becomes an efficient radiator only above this frequency. In order to obtain an estimate for the limiting value of the noise reduction, it is assumed that sound transmission through the frame follows a mass-law. Providing the noise reduction for either the treated fuselage (without any flanking loss) or through the flanking path is greater than about 20 db, the decrease in noise reduction due to the flanking loss is estimated by

$$\Delta NR_{f} = -10 \log \left[ 1 + \frac{\tau_{f} S_{f}}{\bar{\tau}_{ow} S_{f}'} \right] \qquad (6.32)$$

where

τ<sub>f</sub> = transmission coefficient for flanking path

ow = average transmission coefficient for treated fuselage (from Equation (6.15)

S<sub>f</sub> = surface area of flanking path

S' = transmitting surface area of fuselage minus area of flanking path.

The transmission coefficient for the flanking loss is estimated by

$$\tau_{f} \simeq \begin{cases} 0.3 (\omega_{f}/\rho_{o}c)^{2}, & f > f_{f} \\ 0.3 (\omega_{f}/\rho_{o}c)^{2} \left(\frac{f}{f_{f}}\right)^{3/2}, & f < f_{f} \end{cases}$$
(6.33)

where

m<sub>t</sub> = total surface mass density of bare cylinder.

This represents an approximate expression for the field incidence mass law transmission coefficient of a limp mass. Other types of flanking loss can occur such as vent holes or leaks to unpressurized areas. In this case, Equation (6.32) can also be applied where the transmission coefficient for the flanking path  $\tau_{\rm f}$  can be taken as unity.

It will be noticed that stiffness effects (and hence coincidence) of the frames have been ignored. However, since the frames are relatively thick and are stiffer than an equivalent beam on account of their curvature, the critical frequency will occur at low frequencies, in the majority of cases, lower than  $f_{\ell}$ . Hence the assumption of mass behavior for the frame results in a conservative value for the transmission coefficient and hence for the limitation of the effect of flanking.

The situation also occurs in the case of a double panel i.e., outer skin plus inner septum. The previous theory has assumed there is no connection between the two, whereas in practice there is strong coupling due to the presence of the frames. To account for this flanking transmission, the mass law is again assumed and the separate values of  $\tau$  summed according to area as before. However, the effective mass of the skin is now the sum of the masses of the skin and the septum. From this an upper limiting value for the transmission loss is determined.

In general, observed values of overall noise reduction at high frequencies (above 5000 Hz) for conventional acoustic treatment of aircraft, will be limited to 40 to 60 dB.

#### TRANSMISSION LOSS THROUGH ISOLATED CAPSULE COMPARTMENTS

A design requirement for very high transmission loss into a special compartment within an airplane will lead to the use of a vibration-isciated inner capsule to eliminate or reduce the effects of flanking loss. This will generally consist of one of two types:

- 1) An inner shell of the same basic shape as the fuselage with comparable dimensions for crew or equipment spaces or
- A smaller equipment capsule located anywhere inside the aircraft.

Because of the complex sound and vibration transmission paths involved for this case,  $\alpha$  detailed calculation of the effective sound transmission loss for such capsules is not attempted here. Rather, a simplified method is suggested as a guide for evaluating preliminary design concepts. Final verification of the actual transmission loss achieved for such special structure will ordinarily require experimental tests.

### Isolated, Inner Cylindrical Crew Capsule

Since the principal benefit of isolating an inner capsule is to effectively eliminate any significant transmission of sound by flanking paths, an upper bound for the noise reduction can be computed by neglecting any flanking transmission loss and treating the wall of the isolated capsule as the inner wall of a double wall fuselage with no interconnecting transmission paths. The noise reduction for this case can then be computed by the same methods outlined previously using the modal approach for the noise reduction at low frequencies, including any corrections for transmission loss through acoustic treatment between the walls (see Section VI.3.a.) and internal absorption inside the inner capsule (see Section VI.3.b.) For high frequencies above the limiting value specified by Equation (6.25), the diffuse field approach would be employed, and transmission loss through both walls would be computed as explained in Section VI.4.

### Small Isolated Equipment Capsule

In this case, where the capsule diameter is much less than the basic fuselage diameter, the total noise reduction would be computed by first defining the noise field inside the fuselage, neglecting the presence of the equipment capsule, and then computing the noise reduction for the inner capsule. Depending on the size of the capsule, and accuracy required for the computation, either of two methods are recommended to campute the noise reduction for a small capsule.

 Use the same computer program developed for the entire fuselage but assuming a reverberant field outside the capsule. The appropriate structural parameters for the capsule would be used in the computer program in place of the fuselage parameters.

Use the simplified design method covered in Appendix III.

### 8. PANEL DAMPING MATERIAL

The effects of applying a damping treatment to a fuselage panel are twofold; firstly, the values of the structural Q-factor and the generalized mass are modified, and secondly, the sound transmission properties of the composite panel are also modified. The structural Q-factor is, by definition,

$$Q = \frac{1}{2\delta} = \frac{1}{\eta} \tag{6.34}$$

where

 $\delta$  = the damping ratio =  $\frac{C}{C_c}$ 

C = panel viscous damping coefficient

 $C_c = panel critical viscous damping coefficient$ 

 $\eta = loss$  factor of the panel.

A typical value of Q for a fuselage panel is approximately 15. The problem of panel damping by the application of unconstrained and constrained layer treatments has received considerable attention and is well reported in the literature (References 64,65, and 66).

For a typical unconstrained visco-elastic damping layer applied to a panel, Oberst (Reference 65) has shown that,

$$\frac{\overline{\eta}}{\eta} = \frac{k_2 \left[ 12 h_{21}^2 + h_2^2 (1 + k_2)^2 \right]}{\left[ 1 + k_2 \right] \left[ 12 k_2 h_{21}^2 + (1 + k_2) (1 + k_2 h_2^2) \right]}$$
(6.35)

where,

 $\overline{\eta}$  = loss factor of the composite panel

 $\eta$  = extensional loss factor of the visco-elastic material

k<sub>2</sub> = extensional stiffness of the visco-elastic layer relative to that for the untreated panel

h<sub>21</sub> = distance between the neutral axes of the basic panel and the viscoelastic layer divided by the thickness of the basic panel h, = damping layer thickness divided by basic panel thickness.

For a typical constrained layer, Kerwin (Reference 66) has shown that the damping is given by,

$$\frac{\bar{\eta}}{\beta} = \frac{12\left(\frac{h_o}{h_1}\right)^2 \left(\frac{k_3}{k_1}\right) \left[g_o/(1+g_o)^2\right]}{\left[1+\left\{12\left(\frac{h_o}{h_1}\right)^2+2\right\} \left(\frac{k_3}{k_1}\right) \left\{g_o/(1+g_o)\right\}\right]}$$
(6.36)

for small values of  $k_3/k_1$ , and the condition that  $E_3 = E_1$ 

where;

 $\bar{\eta} = loss$  factor of the composite panel

 $\beta$  = shear loss factor of the visco-elastic material

h<sub>o</sub> = distance between the neutral axes of the basic panel and the constraining layer

 $k_1, k_3$  extensional stiffness of the basic panel and constraining layer respectively =  $E_1 h_1, E_2 h_3$ 

h, = thickness of the basic panel

h<sub>a</sub> = thickness of constraining layer

E<sub>1</sub> = modulus of elasticity of the basic panel

E = modulus of elasticity of the constraining layer

$$g_{o} = \frac{1}{4\pi\sqrt{3}!} \left(\frac{E_{1}}{\rho_{1}}\right)^{1/2} \cdot \frac{1}{f} \cdot \frac{G/E_{1}}{(k_{3}/k_{1}) h_{2}}$$
 (6.37)

 $\rho_1 = \text{density of the panel}$ 

G = flexural rigidity of the damping layer

h, = thickness of the damping layer.

For given values of  $h_0/h_1$  and  $k_3/k_1$ , a maximum value of  $\eta/\beta$  occurs as the shear parameter,  $g_0$ , is varied between 0.5 and 1.0. In this region the maximum value of the loss – factor ratio depends primarily on  $(k_3/k_1)$ .

Modification of the generalized mass used in the response equations is carried out simply by computing the added weight due to the treatment and adjusting the mass per unit area accordingly.

It should be noted that the foregoing theory is only applicable to thin damping layers and to the individual panels, i.e., the high frequency region of the fuselage response. When considering the overall fuselage modes, the predominant effect of the treatment is to modify the structural response via the generalized mass.

For thicker constrained damping treatment, values for the overall loss factor  $\eta$  may be estimated from the design charts in Appendix III. The latter also show the relative weight of damping treatment versus loss factor. Thus the effect of damping treatment may be accounted for by computing the overall loss factor from Equation (6.36 or 6.37) or by obtaining values from Appendix III. In either case, the structural loss factor is inserted into the computer program as input data.

### 9. SUMMARY

The conventional types of aircraft fuselage that are met with in practice are as follows:

- (a) Bare cylinder
- (b) Cylinder with absorbent lining
- (c) Bare cylinder with septum and absorbent linings
- (d) Simple double concentric cylinders
- (e) Inner capsule.

Two basic methods have been outlined in this section for digital computation of the noise reduction for these various types of aircraft structure. The common element for both procedures is the use of a complex impedance approach for computing the average transmission loss through any arbitrary acoustic treatment. This approach is applied in a different manner for each of the two basic methods for computing noise reduction. The methods are applied

• Upper Frequency Range - Specified by highest value of:

f<sub>D</sub> from Equation (6.25) (Lower limit for diffuse field)

f<sub>b</sub> from Equation (6.27) (Breathing mode or ring frequency)

f fr m Equation (6.28) (Panel fundamental frequency)

Structural Models for Modal Method

Cylinder Model - Applied for frequencies up to the breathing mode

frequency fb.

Coupled Panel Model - Applied from about 1/2 fb to 4 fb.

Single Panel Model - Applied above about 2 times panel fundamental

frequency

Noise Reduction for Untreated Fuselage

Cylinder Model

- Computed by program from Equation (3, 49)

Coupled or Single Panel Model - Compute by program from Equation (3.90)

Noise Reduction for Treated Fuselage

Additional transmission loss due to treatment computed by program from Equation (6.18).

Increase in noise reduction due to absorption computed by program by inserting acoustic  $Q_{\rm ac}$  determined from Equation (6.22).

#### (b) Diffuse Field Method

- Lower Frequency Limit Equal to upper frequency limit for modal method as defined above.
- Structural Models for Diffuse Field Method Applicable to any uniform composite fuselage plus treatment.
- Transmission Loss Computed by program using Equations (6.15 and 6.2).

Noise Reduction

Computed by program using Equation (6.26) with input table of average absorption coefficients computed from data such as in Table IV.

For either method, an equivalent reverberant sound field is assumed for computing noise reduction. A correction factor  $C(\omega)$ , as specified with Equation (6.29), is used to correct the reverberant field noise reduction to correspond to the actual jet noise or boundary layer noise to determine the actual internal sound level.

The case of the inner capsule can be treated in two distinct ways as explained in Section 7., depending on its size, position and frequency range under consideration.

If flanking transmission is to be taken into account then the effective value of the transmission coefficient for the flanking path has to be calculated. This provides an upper limit for the transmission coefficient and hence for the noise reduction available. A correction to account for the decrease in noise reduction is given by Equations (6.32 and 6.33).

Increased structural damping of the fuselage skin panels can be accounted for using the methods outlined in Section 8.

### LIST OF SYMBOLS

### LIST OF SYMBOLS FOR SECTION VI

α	Total square feet of absorption, or panel length					
b	Propagation constant of porous material, or panel width					
c	Speed of sound					
<sup>c</sup> A	Speed of sound in porous blanket					
f	Frequency - Hz					
90	Structural factor in Equation 6.37 for damping loss factor					
h	Thickness of panel					
h <sub>2</sub>	Relative thickness of damping layer specified in Equation 6.35					
h <sub>21</sub>	Relative distance defined for Equation 6.35					
m	Surface mass density = ph					
n	Radial mode number					
V	Particle or panel velocity					
w	Width of frame flange - in.					
С	Viscous damping coefficient for panel					
C <sub>A</sub> (ω)	Acoustic coupling factor					
cL	Longitudinal wave velocity in cylinder					
D	Panel stiffness = $Eh^3/12$					
E	Young's modulus of elasticity					
E1, E2	Energy dessities on incident and transmitting sides of a structure, respectively					

G Flexural rigidity of damping layer  $J_{ns}^{'}(\overline{R})$ First derivative of Bessel function (see List of Symbols - Section III) Lx Length of cylinder N(f) Modal density of the internal acoustic field NR Noise reduction Incident, reflected, and transmitted pressures, respectively  $P_i$ ,  $P_r$ ,  $P_t$ Excitation and transmitted pressures, respectively  $P_1, P_2$ Q Resonant amplification factor (structural)  $\mathbf{Q}_{\mathbf{ac}}$ Resonant amplification factor (acoustic) Radius of cylinder Si, S ith absorbing surface and total obsorbing surface  $S_{p}(\omega), S_{p_{i}}(\omega)$ Spectral densities of external and internal pressures, respectively  $S_{W}(\omega)$ ,  $S_{W_{\Gamma}}(\omega)$ Space averaged displacement spectral densities for excitation and reverberant field excitation, respectively SL(w) Pressure spectrum level  $S_{x}$ Area of end walls =  $2 \pi R^2$  $S_R$ Area of side wall = 2 m R L V Volume of cylinder =  $\pi R^2 L_x$  $Z, Z_1, Z_2$ Normal input and terminating impedances  $Z_A$ Characteristic impedance Greek Symbols

## Sound absorption coefficient (random incidence)

α

œ

$\overline{\alpha}_{n}$	Average normal absorption coefficient
. <b>3</b>	Shear loss factor of damping material
8	Critical damping ratio
η	Loss factor
η	Overall loss factor of panel treated with damping material
в	Angle of incidence of plane wave re: normal to surface
$\lambda_{\mathbf{q}}$	Acoustic wavelength = c/f
$\lambda_{bn}$	Circumferential bending wavelength in frames = $2\pi R/n$
ρ	Density
ф	Transmitting angle of refracted plane wave through porous blanker
<b>φ</b> τ	Transmitting angle of refracted plane wave through porous blanker  Transmission coefficient
•	
τ	Transmission coefficient  Transmission coefficient for single panel, averaged over incidence angles
τ τ̄ <sub>w</sub>	Transmission coefficient  Transmission coefficient for single panel, averaged over incidence angles from 0 to 85°  Overall transmission coefficient for any treatment, averaged over incidence
T Tw	Transmission coefficient  Transmission coefficient for single panel, averaged over incidence angles from 0 to 85°  Overall transmission coefficient for any treatment, averaged over incidence angles from 0 to 85°
T Tw Tow	Transmission coefficient  Transmission coefficient for single panel, averaged over incidence angles from 0 to 85°  Overall transmission coefficient for any treatment, averaged over incidence angles from 0 to 85°  Phase angle for propagation through porous blankets

#### SECTION VII

#### DISCUSSION

In predicting fuselage interior noise, the low frequency range poses the most difficult problem, since the relatively low modal density of the structural shell coincides with a low acoustic modal density within the fuselage. Because of this, conventional reverberant-field acoustics is not applicable since it assumes a high acoustic modal density in the receiving space. This mismatch problem is illustrated by Figure 43(a) which describes the respective modal densities for a cylindrical shell. In the low frequency region the acoustic modal density is considerably less than the structural modal density. The modal densities coincide at about 800 Hz and a peak in the structural modal density coincides with the shell breathing mode of about 550 Hz. Above 800 Hz the structural modal density can be approximated reasonably well by an equivalent flat plate. Two additional lines are shown in Figure 43(a), corresponding to the upper bounds to the modal densities of two fuselage panels of different area. In these two cases the structural shell was assumed to consist of 20 equal panels and 200 equal panels. This result shows that when the structural and acoustic modal densities are both low, then there is a low probability of having a structural mode couple with an acoustic mode of the same frequency. In practice, a single shell resonance will couple with several adjacent acoustic resonances, to produce coupled system resonances, the degree of coupling depending primarily on the proximity of the acoustic mode with respect to the shell mode.

#### Effect of End-Closure on Noise Reduction

The analytical approach to the coupled structural-acoustic response for a cylinder required an assumption of acoustically open ends to make the computer program manageable. A general derivation of the coupled response for open- or closed-end conditions is covered in Appendix I. To provide a qualitative indication of the effect of changing the end conditions, a simple one-dimensional analysis was carried out for the noise reduction through a spring-mounted rigid piston driving a tube which is either open, rigidly closed, or terminated with a pure acoustic resistance equal to 5 p.c. The results of this analysis, carried out by standard methods covered in Reference 14, are illustrated in Figure 43(b). For convenience, the structural resonance in vacuo was set equal to the fundamental clased-end acoustic resonance frequency. This case differs from the cylinder model in that the axial acoustic modes are not the same for open or closed ends while open-open vs. closed-closed axial acoustic modes of the cylinder are the same. Keeping this in mind, it is apparent that the principle difference for the open vs. closed tube is the noise reduction below the first axial mode. Below this frequency, the closed case exhibits a cavity stiffness effect which limits the noise reduction to a finite value at low frequency. Above this frequency, the average noise reduction has an approximate upper bound similar to the "mass law" transmission loss for the piston. The principal effect of varying the closure is to change the magnitude of the minima and slightly alter the resonance Trequencies. The latter effect is not considered significant for engineering analysis of fuselage noise reduction. What is significant is the general trend in the structural-acoustic coupling and the ability of the program developed here to account for these trends in a systematic fashion.

#### Test Case Results

Preliminary results have been obtained for the hypothetical aircraft fuselage described by the test input data in Table III.

The coupled structural-acoustic system resonances for the low frequency cylinder model are shown in Figures 44, 45 and 46 for axial mode numbers m=1, m=12 and m=25 respectively. In each of these figures the intersection of constant n and constant s lines define the (mns) coupled fuselage-internal air mass system modes for the particular value of m. The shell resonances (m,n) are also denoted in these figures for the purposes of comparison. The figures show that as the axial mode number m is increased, the coupled system resonance frequencies also increase for given values of n and s. Also, in general, for a given mode number, n, the number of coupled system modes lying below the (mn) shell mode increases as the mode number m increases. These results point to the fact that the (mn) shell resonances couple only with the corresponding (m,n) acoustic mode numbers so that a given shell mode has strong coupling only with those acoustic modes in close proximity.

The computed octave band sound pressure levels for boundary layer noise and jet noise are shown in Figures 47 and 48 respectively. The boundary layer noise spectrum shown corresponds to a point 40 ft from the leading edge and an aircraft forward speed of 350 ft/sec. The jet naise spectra correspond to points 10 ft, 30 ft and 50 ft from the leading edge on a line 45 degrees around from the horizontal and were computed using the scattering technique.

The noise reduction through the bare fuselage is shown in Figure 49 for the case of fuselage excitation by boundary layer turbulence. The average noise reduction obtained from the modal summation response theory is shown for each of the three structural models. The importance of including an adequate number of modes in the summations is shown in Figure 49, where the rapid increase in noise reduction at the upper end of each frequency range may be due in part to the particular number of modes used. Two noise reduction curves computed from Field Incidence Mass Law are also shown in the figure for comparison purposes. The mass densities used in computing these curves correspond to the cylinder and single panel models and the effects of the coupled structural-acoustic resonances on the noise reduction can be clearly seen in the 10 Hz - 100 Hz region.

The incremental transmission losses of two typical fuselage acoustic treatments and the corresponding interior noise reduction are shown in Figure 50. Details of the acoustic treatment are given in the figure and in Table III.

The equivalent reverberant fields for boundary layer turbulence and jet noise are shown in Figure 51 which was constructed from the normalized structural response results for the three structural models. This figure shows that in general the reverberant field is more efficient than boundary layer turbulence in exciting the structure at low frequencies. It is emphasized that the equivalent reverberant field for boundary layer noise is highly dependent upon the cerodynamic parameters as well as the type of structure considered.

The untreated fuselage Internal Noise Level is shown in Figure 52 for the case of boundary layer turbulence. This figure was constructed by subtracting the average noise reduction shown in Figure 49 from the external pressure spectrum.

### Summary

The results of the foregoing theory were programmed for computer solution and an overall program has been developed to provide detailed design trade-off studies of aircraft acoustic treatments. Complete details of the computer program are presented in Appendix II, but the principal elements can be summarized as follows:

- 1. Coupled resonant frequencies for the fuselage cylinder modes.
- 2. Coupled resonant frequencies for the panel group and single panel modes.
- 3. Joint acceptances of the cylinder, panel group and single panel models to boundary layer turbulence, jet noise and reverberant acoustic fields.
- 4. Overall levels and frequency spectra for boundary layer turbulence and jet noise.
- 5. Structural-Acoustic response of the three models to the external environments.
- Noise reduction for untreated and acoustically treated fuselage structures and the resulting interior noise levels.

### APPENDIX I

# GENERALIZATION OF THE ACOUSTIC-STRUCTURAL COUPLING OF CYLINDRICAL SHELLS AND INTERNAL ACOUSTIC FIELDS

In Section III, a method of analysis is set forth in which the acoustic field of an open ended cylindrical cavity is dynamically coupled with a thin cylindrical shell enclosure having tangentially pinned ends. It is shown in Section V how the dynamic response of this coupled acoustic-structural system can be obtained for external fluctuating pressure loads. Also treated in Section III is the two-dimensional acoustic field generated by a vibrating panel, or a group of panels, mounted in the shell wall. These analyses can be generalized to cylindrical sound fields with closed ends, and to three-dimensional sound fields generated by a single panel, or a group of panels. The purpose of the following discussion is to set forth the essential concepts and methodology involved in this generalization.

Consider a cylindrical cavity of length L and radius R; and let (x,y,r) denote the axial, circumferential and radial coordinates, respectively, of the cavity, where  $y = R\phi$  and  $\phi$  is the circumferential angular coordinate. The internal sound field is governed by the wave equation

$$\left[\nabla^2 - \frac{1}{c^2} \frac{\partial^2}{\partial t^2}\right] P(x,y,r,t) = 0 \tag{1}$$

$$\nabla^2 = \frac{\partial^2}{\partial x^2} + \frac{1}{r^2} \frac{\partial^2}{\partial \phi^2} + \frac{\partial^2}{\partial r^2} + \frac{1}{r} \frac{\partial}{\partial r}$$

c = speed of sound.

For harmonic response of this sound field at frequency  $\omega$ , the solution of (1) is

$$P(x,y,r,t) = P(x,y,r,\omega) e^{i\omega t}$$

$$P(x,y,r,\omega) = \sum_{m=0}^{\infty} \sum_{n=0}^{\infty} P_{mn}(\omega) X_m(\overline{x}) Y_n(\overline{y}) J_n(\alpha_m \overline{r})$$
 (2)

$$X_{m}(\vec{x}) = \frac{A_{m} \cos (K_{m} L \vec{x}) + B_{m} \sin (K_{m} L \vec{x})}{\left[A_{m}^{2} + B_{m}^{2}\right]^{\frac{1}{2}}}$$
(3)

 $\mathbf{A}_{m}$ ,  $\mathbf{B}_{m}$  = constants to be determined from boundary conditions

 $K_m = \omega_m/c = axial wave number$ 

 $\omega_{iii}$  = axial resonance frequency.

$$Y_n(\overline{y}) = \frac{a_n \cos(2\pi \overline{y}) + b_n \sin(2n\pi \overline{y})}{\left[a_n^2 + b_n^2\right]^{\frac{1}{2}}}$$
(4)

 $a_n$ ,  $b_n = constants$ .

 $J_m(\alpha_m r)$  = n-th order Bessel function of the first kind.

$$\alpha_{III} = R \left[ K^2 - K_{III}^2 \right]^{\frac{1}{2}} = (R/c) \left[ \omega^2 - \omega_{III}^2 \right]^{\frac{1}{2}}$$
 (5)

 $K = \omega/c = wave number$ 

 $\overline{x} = x/L = \text{nondimensional axial coo. `nate; } 0 \le \overline{x} \le 1.$ 

 $\overline{y}$  = y/2 \pi R =  $\varphi/2\pi$  = nondimensional circumferential coordinate;  $0 \le \overline{y} \le 1$  .

 $\overline{r}$  = r/R = nondimensional radial coordinate; 0  $\leq$  7  $\leq$  1 .

 $P_{mn}(\omega) = modal pressure amplitude.$ 

Partial displacements can be obtained from Newton's second law of motion,

$$\rho \frac{\partial^2 \overrightarrow{U}(x,y,r,t)}{\partial t^2} + \overrightarrow{\nabla} P(x,y,r,t) = 0$$
 (6)

 $\vec{U}(x,y,r,t) = \left[U_x, U_y, U_r\right] = particle displacement vector$ 

$$\overrightarrow{\nabla} = \left[ \frac{\partial}{\partial x}, \frac{1}{r}, \frac{\partial}{\partial \phi}, \frac{\partial}{\partial r} \right]$$

For harmonic response, equation (6) reduces to

$$\overrightarrow{U}(x,y,r,\omega) = (\rho\omega^2)^{-1} \overrightarrow{\nabla} P(x,y,r,\omega)$$
 (7)

Substituting (2) into (7) and solving for the particle displacement components gives

$$U_{\mathbf{x}}(\mathbf{x},\mathbf{y},\mathbf{r},\omega) = (\rho \omega^{2})^{-1} \sum_{m=0}^{\infty} \sum_{n=0}^{\infty} K_{m} P_{mn}(\omega) X_{m}^{\dagger}(\overline{\mathbf{x}}) Y_{m}(\overline{\mathbf{y}}) J_{n}(\alpha_{m} \overline{\mathbf{r}})$$
(8)

$$U_{\mathbf{y}}(\mathbf{x},\mathbf{y},\mathbf{r},\omega) = (\rho\omega^2 \mathbf{r})^{-1} \sum_{m=0}^{\infty} \sum_{n=0}^{\infty} m \, P_{mn}(\omega) \, \mathbf{x}_m(\bar{\mathbf{x}}) \, \mathbf{y}_n^{\dagger}(\bar{\mathbf{y}}) \, \mathbf{J}_n(\alpha_m \bar{\mathbf{r}})$$
 (9)

$$U_{\mathbf{r}}(\mathbf{x},\mathbf{y},\mathbf{r},\boldsymbol{\omega}) = (\rho\omega^2 R)^{-1} \sum_{m=0}^{\infty} \sum_{n=0}^{\infty} \alpha_m P_{mn}(\boldsymbol{\omega}) X_m(\tilde{\mathbf{x}}) Y_n(\tilde{\mathbf{y}}) J_n^{\dagger}(\alpha_m \tilde{\mathbf{r}})$$
 (10)

$$X_{m}(\bar{x}) = dX_{m}(\bar{x})/d(K_{m}L\bar{x})$$

$$Y_{\pi}^{+}(\overline{y}) \equiv dY_{\pi}(\overline{y})/d(2\pi \pi \overline{y})$$

$$J_m^i(\alpha_m \bar{\tau}) = dJ_m(\alpha_m \bar{\tau})/d(\alpha_m \bar{\tau})$$

By application of homogeneous (pressure or displacement) boundary conditions at the two ends of the cavity, the function  $X_{772}(\vec{x})$  defined by (3) can be simplified to the following for open-open, closed-closed and open-closed ends:

$$X_{m}(\overline{X}) = \sin (m \pi \overline{X})$$

$$\omega_{m} = c K_{m} = m \pi c/L$$
open-open ends (11)

$$X_{m}(\overline{x}) = \cos(m\pi \overline{x})$$

$$\omega_{m} = c K_{m} = m\pi c/L$$
closed-closed ends
(12)

$$X_{m}(\overline{x}) = \sin \left[ (2m+1) \, \pi \, \overline{x} / 2 \right]$$
 open end at  $\overline{x} = 0$  closed end at  $\overline{x} = 1$  (13)
$$\omega_{m} = c \, K_{m} = (2m+1) \, \pi \, c / 2 \, L$$

For purposes of coupling the cylindrical sound field with an axially symmetric shell, it is sufficiently general to choose  $b_n = 0$  in (4) so that the function  $Y_n(\bar{y})$  can also be

$$Y_{n}(\overline{y}) = \cos(2\pi n \overline{y}) \tag{14}$$

If the enclosing shell is rigid, then  $U_{r}=0$  at  $\vec{r}=1$ ; and hence from (10)

$$J_n'(\alpha_m) = 0 \tag{15}$$

The numerical values of  $\alpha_m$  which are roots of (14) are denoted by the symbol  $\alpha_{ns}$  and are listed in Table I. These allowed values of  $\alpha_m$  define the hard-wall resonance frequencies,  $\omega_{mns}$ , of the cavity, where (m,n,s) refer to the axial, circumferential and radial mode numbers, respectively. Setting  $\omega = \omega_{mns}$  and  $\alpha_{ns} = \alpha_{ns}$  in (5), and solving for  $\omega_{mns}$  gives

$$\omega_{mns} = \left[\omega_{m}^{2} + \omega_{ns}^{2}\right]^{\frac{1}{2}} = \text{hard-wall resonance frequency}$$
 (16)

$$\omega_{ns} = \frac{\alpha}{ns} c/R$$
 = resonance frequency of two-dimensional mode over cylinder cross-section. (17)

From (2), the internal pressure distribution associated with the (m,n,s)-mode is

$$P(x,y,r,\omega_{mns}) = P_{mns} \times_{m}(\bar{x}) \times_{n}(\bar{y}) \cup_{n}(\alpha_{ns}\bar{r})$$
(18)

 $P_{mns}$  = pressure amplitude of the (m,n,s)-mode

Similar expressions are obtainable from (8)-(10) for the particle displacements.

Dynamic coupling of the acoustic field and the shell requires compatibility and equilibrium coupling. Compatibility coupling implies that, at each point on the inner surface of the shell, the radial particle displacement of the acoustic field is equal to the shell deflection. Equilibrium coupling implies that acoustic pressures acting on the shell arebalanced by the elastic and inertia forces in the shell. Consider first the compatibility requirement which for a harmonically vibrating shell can be expressed as

$$\left[U_{r}(x,y,r,\omega)\right]_{r=R}=U(\omega)\,\,\psi(\bar{x},\bar{y})\tag{19}$$

 $U(\omega)$  = radial amplitude of shell vibration

 $\Psi(\vec{x}, \vec{y})$  = deflection distribution function for the shell (assumed to have a maximum value of unity).

Substituting (10) into (19) gives

$$\left(\rho\omega^{2} R\right)^{-1} \sum_{m=0}^{\infty} \sum_{n=0}^{\infty} \alpha_{m} P_{mn}(\omega) X_{m}(\overline{x}) Y_{n}(\overline{y}) J_{n}(\alpha_{m}) = U(\omega) \Psi(\overline{x}, \overline{y})$$
 (20)

Multiplying both sides of (20) by  $X_m(\overline{x}) \ Y_n(\overline{y})$ , integrating over  $0 \le \overline{x} \le 1$  and  $0 \le \overline{y} \le 1$ , and recognizing that each of the sets of functions are mutually orthogonal gives

$$P_{mn}(\omega) = \frac{\rho \omega^2 R U(\omega)}{\alpha_m J_n^{\dagger}(\alpha_m)} S_{mn}$$
 (21)

$$g_{mn} = \frac{\int_{0}^{1} \int_{0}^{1} \Psi(\bar{x}, \bar{y}) \times_{m}(\bar{x}) Y_{n}(\bar{y}) d\bar{x} d\bar{y}}{\left[\int_{0}^{1} X_{m}^{2}(\bar{x}) d\bar{x}\right] \left[\int_{0}^{1} Y_{n}^{2}(\bar{y}) d\bar{y}\right]}$$
(22)

The constants  $g_{mn}$  represent the coefficients in a two-dimensional Fourier series of the normalized shell deflection function  $\psi(x, y)$ ; that is

$$\Psi(\bar{x},\bar{y}) = \sum_{m=0}^{\infty} \sum_{n=0}^{\infty} g_{mn} \times_{m}(\bar{x}) Y_{n}(\bar{y})$$
 (23)

The internal acoustic pressure and the radial particle displacement can now be expressed in terms of  $U(\omega)$  by substituting (21) into (2) and (10) giving

$$P(x,y,r,\omega) = \rho \omega^{2} R U(\omega) \sum_{m=0}^{\infty} \sum_{n=0}^{\infty} \frac{9_{mn}}{\alpha_{m}} X_{m}(\bar{x}) Y_{n}(\bar{y}) \frac{J_{n}(\alpha_{m}\bar{r})}{J_{n}'(\alpha_{m})}$$
(24)

$$U_{r}(x,y,r,\omega) = U(\omega) \sum_{m=0}^{\infty} \sum_{n=0}^{\infty} g_{mn} X_{m}(\overline{x}) Y_{n}(\overline{y}) \frac{J_{n}'(\alpha_{m}\overline{r})}{J_{n}'(\alpha_{m})}$$
(25)

Similar expressions can be obtained for  $U_{\mathbf{x}}$  and  $U_{\mathbf{y}}$  from (8) and (9).

Equations (24) and (15) are quite general in that they describe the undamped interior sound field of an open or closed ended cylindrical cavity for any shell deflection pattern and for any frequency. The deflection distribution function  $\psi(\overline{x}, \overline{y})$  may represent an overall mode of vibration of the shell, a mode of vibration of a localized group of panels or a single panel mounted in the shell wall, or the uniform radial motion of a small piston mounted in the wall.

Using the notation set forth in Section II, the deflection pattern or mode shape of the (m,n)-mode of the overall shell wall, or of a panel segment of the wall is denoted functionally as

$$\varPsi(\bar{x},\bar{y}) = \phi_{m}(\bar{x}) \ \phi_{n}(\bar{y})$$

Since the acoustic mode numbers (m,n) may differ from the structural mode numbers (m,n), it is convenient to introduce the following nore general notation for the constants  $g_{mn}$ , namely,

$$g_{mn}^{mn} = \frac{\left[\int_{0}^{1} X_{m}(\overline{x}) \phi_{m}(\overline{x}) d\overline{x}\right] \left[\int_{0}^{1} Y_{n}(\overline{y}) \phi_{n}(\overline{y}) d\overline{y}\right]}{\left[\int_{0}^{1} X_{m}^{2}(\overline{x}) d\overline{x}\right] \left[\int_{0}^{1} Y_{n}^{2}(\overline{y}) d\overline{y}\right]}$$
(26)

The constants  $g_{mn}^{mn}$  quantitatively express the wavelength coupling between the shell wall and the internal acoustic field, and are thus analogous to the joint acceptances which describe a similar coupling between the external fluctuating pressure field and the shell wall. If  $\psi(\overline{x},\overline{y})$  is normalized to a maximum value of unity, then the constants  $g_{mn}^{mn}$  are also normalized so that  $0 \le \left|g_{mn}^{mn}\right| \le 1$ . Several examples are given below which show the forms of these constants for various acoustic fields and shell wall motions.

### Example 1: Open, Pinned End Cylinder

Consider a uniform, thin cylindrical shell whose ends are tangentially pinned around the circumference, and whose ends are acoustically open. Assuming that the shell is vibrating in the overall (m,n)-mode, the radial mode shape of the shell as defined in Section II is

$$\begin{split} & \Phi_{m}(\overline{x}) = \sin m \pi \overline{x}, & 0 \leq \overline{x} \leq 1, & m = 1, 2, 3, \dots \\ & \Phi_{n}(\overline{y}) = \cos 2n \pi \overline{y}, & 0 \leq \overline{y} \leq 1, & n = 0, 1, 2, \dots \end{split}$$

From (11) and (14), the acoustic field functions  $X_{n}(\overline{x})$  and  $Y_{n}(\overline{y})$  for open ends are

$$X_m(\overline{x}) = \sin(m\pi \overline{x}), \qquad 0 \le \overline{x} \le 1, \qquad m = 1, 2, 3, ...$$

$$Y_n(\overline{y}) = \cos(2n\pi \overline{y}), \qquad 0 \le \overline{y} \le 1, \qquad n = 0, 1, 2, ...$$

Substituting these expressions into (26) and integrating gives

$$g_{mn}^{mn} = 1 \text{ if } m = m \text{ and } n = n$$

$$= 0 \text{ if } m \neq m \text{ or } n \neq n$$
(27)

Thus, the (m,n)-mode of the pinned shell wall couples only with the (m,n)-component of the acoustically open cavity, as discussed in Section III.

### Example 2: Closed, Stiding End Cylinder

Consider a uniform, thin cylindrical shell of length L which is located between two plane, parallel rigid walls that are separated by a distance L, such that the axis of the shell is normal to the wall surfaces. These walls are assumed to provide hard-wall acoustic boundaries at the two ends of the cylindrical cavity, and to provide no radial restraint of the shell wall. The shell is assumed to have sliding ends in the sense that as the ends vibrate radially, there is no axial slope of the shell wall at the two ends. In this case, if the shell vibrates in the (m,n)-mode, the structural deflection shape may be approximated as follows:

$$\begin{split} & \varphi_m(\overline{x}) = \cos m \pi \overline{x}, & 0 \leq \overline{x} \leq 1, & m = 0, 1, 2, \dots \\ & \varphi_n(\overline{y}) = \cos 2 n \pi \overline{y}, & 0 \leq \overline{y} \leq 1, & n = 0, 1, 2, \dots \end{split}$$

From (12) and (14), the acoustic field functions  $X_{nr}(\bar{x})$  and  $Y_n(\bar{y})$  for closed ends are

$$X_{nn}(\overline{x}) = \cos m\pi \overline{x}, \qquad 0 \le \overline{x} \le 1, \qquad m = 0, 1, 2, \dots$$

$$Y_{n}(\overline{y}) = \cos 2n\pi \overline{y}, \qquad 0 \le \overline{y} \le 1, \qquad n = 0, 1, 2, \dots$$

Substituting these functions into (26) and integrating gives

$$g_{mn}^{mn} = 1 \quad \text{if } m = m \text{ and } n = n$$

$$= 0 \quad \text{if } m \neq m \text{ or } n \neq n$$
(28)

Thus, the (m,n)-mode of the sliding end shell wall couples only with the (m,n)-component of the acoustically closed cavity, similar to Example 1.

### Example 3: Closed, Pinned End Cylinder

Consider for this example a uniform, thin cylindrical shell with ends that are tangentially pinned around the circumference to two rigid circular bulkheads, so that the ends are acoustically closed. Then

$$\phi_{\mathbf{m}}(\overline{\mathbf{x}}) = \sin m\pi \overline{\mathbf{x}}, \qquad 0 \le \overline{\mathbf{x}} \le 1, \qquad m = 1, 2, 3, \dots$$

$$\phi_{\mathbf{n}}(\overline{\mathbf{y}}) = \cos 2n\pi \overline{\mathbf{y}}, \qquad 0 \le \overline{\mathbf{y}} \le 1, \qquad n = 0, 1, 2, \dots$$

$$X_{m}(\overline{\mathbf{x}}) = \cos m\pi \overline{\mathbf{x}}, \qquad 0 \le \overline{\mathbf{x}} \le 1, \qquad m = 0, 1, 2, \dots$$

$$Y_{n}(\overline{\mathbf{y}}) = \cos 2n\pi \overline{\mathbf{y}}, \qquad 0 \le \overline{\mathbf{y}} \le 1, \qquad n = 0, 1, 2, \dots$$

Equation (26) yields the following expression for the structure-accustic coupling constants  $g_{mn}^{mn}$ :

$$g_{mn}^{mn} = 0 \quad \text{if } n \neq n, \text{ or if } m = m$$

$$= \frac{4m}{\pi} \frac{1}{m^2 - m^2} \quad \begin{cases} \text{if } m = \text{odd, } m = \text{even, } n = n; \\ \text{or if } m = \text{even, } m = \text{odd, } n = n. \end{cases}$$
(29)

Thus, the (m,n)-mode of the pinned end shell wall couples with half of all the (m,n)-components of the closed acoustic field. A table of values of  $g_{mn}^{mn}$  is given below for limited ranges of the integers m and m.

Table of Numerical Values of  $g_{mn}^{mn}$  for Closed, Pinned End Cylinder

m	0	1	2	.3	4	5	6	7
1 2 3 4 5 6 7	1.275 0 .445 0 .266 0 .190	0 .849 0 .339 0 .218	425 0 .765 0 .303 0 .197	0 510 0 .728 0 .283 0	0845 0 545 0 .706 0 .270	0 121 0 565 0 .695	0364 0 141 0 579 0 .685	0 0566 0 154 0 589

### Example 4: Small Radial Piston Mounted in Rigid Cylindrical Walls

Consider now a relatively small rectangular piston mounted in an otherwise rigid cylindrical wall; and assume that this piston vibrates harmonically in a radial direction. The piston is assumed to be centered at the nondimensional coordinates  $(\overline{x}, \overline{y}) = (\overline{x}_0, 0)$ , and to have nondimensional axial and circumferential lengths  $\Delta \overline{x}$ ,  $\Delta \overline{y}$ . The surface deflection function  $\psi(\overline{x}, \overline{y}) = 1.0$  over the surface of the piston and  $\psi(\overline{x}, \overline{y}) = 0$  off the piston surface so that  $g_{mn}$  as defined by (22) becomes

$$g_{mn} = \frac{\begin{bmatrix} \vec{x}_0 + \Delta \vec{x}/2 \\ \int X_m(\vec{x}) d\vec{x} \end{bmatrix} \begin{bmatrix} \Delta \vec{y}/2 \\ \int Y_n(\vec{y}) d\vec{y} \\ -\Delta \vec{y}/2 \end{bmatrix}}{\begin{bmatrix} \int X_m^2(\vec{x}) d\vec{x} \end{bmatrix} \begin{bmatrix} \int Y_n^2(\vec{y}) d\vec{y} \end{bmatrix}}$$
(30)

For the open end cylinder,  $X_{n_i}(\bar{x}) = \sin m \pi \bar{x}$  and  $Y_n(\bar{y}) = \cos 2 n \pi \bar{y}$  so that from (30),

$$g_{m\pi} = 2 \left[ 2 - \delta(n) \right] \Delta \bar{x} \Delta \bar{y} \cdot \sin(m \pi \bar{x}_0) \frac{\sin(m \pi \Delta \bar{x}/2)}{(m \pi \Delta \bar{x}/2)} \frac{\sin(n \pi \Delta \bar{y})}{(n \pi \Delta \bar{y})}$$
(31)

$$\delta(n) = 1, \quad n = 0$$
  
= 0, \quad n = 1,2,3,...

For the closed end cylinder,  $X_{m}(\bar{x}) = \cos(m \pi \bar{x})$  and  $Y_{n}(\bar{y}) = \cos(2 n \pi \bar{y})$ , and hence

$$g_{mn} = [2 - \delta(m)] [2 - \delta(n)] \Delta \overline{x} \Delta \overline{y} \cos(m \pi \overline{x}_0) \frac{\sin(m \pi \Delta \overline{x}/2)}{(m \pi \Delta \overline{x}/2)} \frac{\sin(n \pi \Delta \overline{y})}{(n \pi \Delta \overline{y})}$$
(32)

$$\delta(m) = 1$$
,  $m = 0$   $\delta(n) = 1$ ,  $n = 0$   
= 0,  $m = 1, 2, 3, ...$  = 0,  $n = 1, 2, 3, ...$ 

Equations (31) and (32) show that the magnitudes of the  $g_{m,n}$  coefficients are proportional to the nondimensional area,  $(\Delta \overline{x} \cdot \Delta \overline{y})$ , of the piston. Except for certain symmetric locations,  $\overline{x}_0$ , the piston drives almost all of the (m,n)-components of the acoustic field,

with the component amplitudes decreasing approximately as 1/(mn) for large integer values of m and n. Also, note that for  $\Delta \overline{x} << 1$  and  $\Delta \overline{y} << 1$ , a large number of low order acoustic components are excited to nearly the same aplitudes. The latter is due to the relatively slow decrease of  $\sin(m\pi \Delta \overline{x}/2)/(m\pi \Delta \overline{x}/2)$  and  $\sin(n\pi \Delta \overline{y})/(n\pi \Delta \overline{y})$  with increasing m and n. Physically, this implies that there are a large number of acoustic components whose wavelengths are greater than the dimensions of the piston. Finally, note that (31) and (32) are essentially the same equation, except for the factors  $\sin(m\pi x_0)$  and  $\cos(m\pi \overline{x_0})$ ; and hence, the small piston drives the acoustic fields for the open and closed cylinders to roughly equal amplitudes.

### Example 5: Two Small Adjacent Radial Pistons Mounted in Rigid Cylindrical Wall

The piston treated in Example 4 acts as a monopole source driving the internal acoustic field. The internal sound field for a dipole wall source is expected to be quite different from that of the monopole because of cancellations due to phasing. It is interesting therefore to extend Example 4 to the case of two, small, adjacent rectangular pistons each having an area  $(\Delta \bar{\mathbf{x}} \cdot \Delta \bar{\mathbf{y}})$ , and each vibrating harmonically with the same amplitude but opposite phase. For convenience, assume that the two pistons are centered at  $(\bar{\mathbf{x}}_0, .25 - \Delta \bar{\mathbf{y}})$  and  $(\bar{\mathbf{x}}_0, .25 + \Delta \bar{\mathbf{y}})$ ; and let the deflection function  $\psi(\bar{\mathbf{x}}, \bar{\mathbf{y}}) = 1.0$  over the surface of the first piston,  $\psi(\bar{\mathbf{x}}, \bar{\mathbf{y}}) = -1.0$  over the surface of these areas. In this case the coefficients g as defined by (22) can be found from the expression

$$g_{mn} = \frac{\begin{bmatrix} \overline{x}_0 + \Delta \overline{x}/2 \\ \int X_m(\overline{x}) d\overline{x} \\ \overline{x}_0 - \Delta \overline{x}/2 \end{bmatrix} \begin{bmatrix} .25 & .25 + \Delta \overline{y} \\ \int Y_n(\overline{y}) d\overline{y} - \int Y_n(\overline{y}) d\overline{y} \\ .25 - \Delta \overline{y} & .25 \end{bmatrix}}{\begin{bmatrix} 1 \\ \int X_m^2(\overline{x}) d\overline{x} \end{bmatrix} \begin{bmatrix} 1 \\ \int Y_n^2(\overline{y}) d\overline{y} \end{bmatrix}}$$

For the closed end cylinder,  $X_{ni}(\bar{x}) = \cos(n_i \pi \bar{x})$  and  $Y_{ni}(\bar{y}) = \cos(2n \pi \bar{y})$  so that

$$g_{mn} = [2 - \delta(m)] [2 - \delta(n)] (2 \Delta \bar{x} \Delta \bar{y}) \cos(m \pi \bar{x}_0) \frac{\sin(m \pi \Delta \bar{x}/2)}{(m \pi \Delta \bar{x}/2)} \frac{1 - \cos(2n \pi \Delta \bar{y})}{(2n \pi \Delta \bar{y})}$$
(33)

where  $\delta(m)$  and  $\delta(n)$  are defined in Example 4.

For small values of  $(2\pi\pi\,\Delta\bar{y})$ , the function  $[1-\cos(2\pi\pi\,\Delta\bar{y})]/(2\pi\pi\,\Delta\bar{y})\approx\frac{1}{2}\,(2\pi\pi\,\Delta\bar{y})^2$ ; and hence, the amplitudes of the low order circumferential components of the acoustic field are quite small, which is expected for the two-piston dipole. Note that the corresponding function,  $\sin(\pi\pi\,\Delta\bar{y})/(\pi\pi\,\Delta\bar{y})$ , in Example 4 is nearly equal to unity for low order values of  $\pi$ .

Consider now the equilibrium coupling between the acoustic field and the shell. For simplicity, it is assumed here that the entire shell is vibrating as a pinned ended cylinder, but that the cavity may have opened or closed ends. If the cylinder vibrates harmonically at frequency  $\omega$  with a radial deflection amplitude of  $q_{vn}(\omega)$  in its (v,n)-mode, then by (24), the internal acoustic pressure generated is

$$P(x,y,r,\omega) = \rho \omega^{2} R q_{vn}(\omega) \sum_{m=0}^{\infty} \sum_{n=0}^{\infty} g_{mn}^{vn} X_{m}(\overline{x}) Y_{n}(\overline{y}) \frac{J_{n}(\alpha_{m}\overline{t})}{\alpha_{m} J_{n}^{+}(\alpha_{m})}$$
(34)

where  $g_{m\pi}^{vn}$  is defined by (26).

It is sufficiently general to assume here that  $Y_n(\overline{y}) = \phi_n(\overline{y})$ . Furthermore, the set of functions  $\phi_n(y)$  are mutually orthogonal and hence from (26),

$$g_{mn}^{Vn} = 0, n \neq n$$

$$= g_m^{V} = \frac{\int_0^1 X_{m}(\overline{x}) \phi_{V}(\overline{x}) d\overline{x}}{\int_0^1 X_{m}^{2}(\overline{x}) d\overline{x}}, n = n$$
(35)

Thus, (34) reduces to

$$P(x,y,r,\omega) = \rho \omega^{2} R q_{yn}(\omega) \sum_{m=0}^{\infty} \sum_{n=0}^{\infty} g_{m}^{v} X_{m}(\overline{x}) \varphi_{n}(\overline{y}) \frac{J_{n}(\alpha_{m} \overline{r})}{\alpha_{m} J_{n}(\alpha_{m})}$$
(36)

Assume that several shell modes are vibrating harmonically at frequency  $\omega$ , with relative phase angles of  $0^{\circ}$  or  $180^{\circ}$ . The total internal pressure field generated by all of these modes is the linear summation of the pressure field due to the individual modes. Thus,

for a fixed circumferential mode number n, and for all shell modes  $\nu=1,2,3,\ldots$ , the pressure field is, from (36),

$$P(x,y,r,\omega) = \rho \omega^{2} R \sum_{v=1}^{\infty} \sum_{m=0}^{\infty} \sum_{n=0}^{\infty} q_{vn}(\omega) g_{m}^{v} X_{m}(\overline{x}) \phi_{n}(\overline{y}) \frac{J_{n}(\alpha_{m}\overline{r})}{\alpha_{m} J_{n}(\alpha_{m})}$$
(37)

Thus, setting  $\bar{r} = 1$  in (37) gives the total acoustic pressure acting on the inner surface of the shell, for a single value of n, namely

$$P(x,y,R,\omega) = \rho \omega^2 R \sum_{v=1}^{\infty} \sum_{m=0}^{\infty} \sum_{n=0}^{\infty} q_{vn}(\omega) g_m^v X_m(\overline{x}) \varphi_n(\overline{y}) \frac{J_n(\alpha_m)}{\alpha_m J_n(\alpha_m)}$$
(38)

The equation of motion for the undamped response of the (m,n)-mode of the shell is

$$M_{mn}\left[\ddot{q}_{mn}(t) + \omega_{mn}^{2} q_{m}(t)\right] = \mathcal{F}_{mn}(t)$$
(39)

 $M_{\text{min}} = \xi_{\text{min}} \mu A = \text{generalized mass}$ 

 $\xi_{\rm mn}$  = generalized mass fraction

 $\mu$  = mass per unit area of shell

A = total area of shell

 $\omega_{mn}$  = resonance frequency of the (m,n)-mode

 $\mathcal{F}_{mn}(t)$  = generalized force due to internal pressure

$$=A\int_{0}^{1}\int_{0}^{1}P(x,y,R,t)\phi_{m}(\bar{x})\phi_{n}(\bar{y})d\bar{x}d\bar{y}$$

P(x,y,R,t) = internal pressure acting on shell

$$\phi_{\mathbf{m}}(\overline{\mathbf{x}}) = \sin \left( m \pi \overline{\mathbf{x}} \right) 
\phi_{\mathbf{n}}(\overline{\mathbf{y}}) = \cos \left( 2 n \pi \overline{\mathbf{y}} \right) = \text{shell mode shape .}$$

If the shell vibrates harmonically at frequency  $\omega$ , all of the above time varying quantities can be replaced by corresponding frequency varying quantities. Then (39) reduces to

$$\mu \, \xi_{mn} \left[ \omega_{mn}^2 - \omega^2 \right] \, q_{mn}(\omega) = \int_0^1 \int_0^1 P(x, y, R, \omega) \, \phi_m(\overline{x}) \, \phi_n(\overline{y}) \, d\overline{x} \, d\overline{y} \tag{40}$$

Substituting (38) into (40), noting the mutual orthogonality of the set of functions  $\phi_n(y)$ , and employing the definition (35) gives

$$\frac{\mu}{\rho R} \xi_{mn} \left[ \left( \frac{\omega_{mn}}{\omega} \right)^2 - 1 \right] q_{mn}(\omega) = \sum_{\nu=1}^{\infty} \sum_{m=0}^{\infty} q_{\nu n}(\omega) g_m^{\nu} g_m^{m} \epsilon_{mn} \frac{J_n(\alpha_m)}{\alpha_m J_n(\alpha_m)}$$
(41)

$$\epsilon_{mn} = \left[ \int_{0}^{1} X_{m}^{2}(\overline{x}) d\overline{x} \right] \left[ \int_{0}^{1} \phi_{n}^{2}(\overline{y}) d\overline{y} \right]$$
(42)

 $=\frac{1}{4}$  for open-open or closed-closed ends.

Equation (41) yields the coupled resonance frequencies of acoustic-structure system modes, and is valid for open-open, closed-closed and open-closed cavities. As shown by Example 1 for an open-open cylinder,  $g_m^m = 0$  if  $m \neq m$  and  $g_m^m = 1$  if m = m; and hence with v = m = m and  $\varepsilon_{mn} = \xi_{mn}$ , (41) reduces to

$$\frac{\mu}{\rho R} \left[ \left( \frac{\omega_{mn}}{\omega} \right)^2 - 1 \right] = \frac{J_n(\alpha_m)}{\alpha_m J_n(\alpha_m)} \quad \text{open-open ends.}$$
 (43)

The essential conclusion that can be drawn from (41) is that for a closed-closed cavity, each shell made is coupled with almost all acoustic modes (having the same circumferential mode number n); and vice versa. Hence, all of the shell modes are coupled by the internal acoustic field and all of the internal acoustic modes are coupled by the shell. Analysis of the internal sound field for a closed-closed cylinder is therefore considerably more complex than for open-apen ends. In the lower frequency range, this mathematical complexity is offset to a degree by the fact that the magnitude of the coupling is probably small for structural and acoustic modes whose resonance frequencies are well separated. On this basis, it is felt that if proper numerical analysis procedures are applied to (41), computations

of coupled resonance frequencies would not be difficult. Some study would be required, however, to determine the accuracy with which these coupled frequencies must be estimated in order to achieve an accurate estimate of the strength of inter-modal coupling.

Once coupled frequencies and coupled mode shapes have been determined for the acoustic structural system, the analysis required to obtain system response to external fluctuating pressures follows the same lines as that presented in Section V. It should be noted finally that the chief reason for investigating the closed-closed cylinder is to obtain more realistic estimates of transmission loss in the low frequency range where the internal sound field may be stiffness controlled. The open-open cylinder follows a mass low below the fundamental cavity resonance and is thus somewhat unrealistic in this frequency range. However, above the first few axial modes, both the open-open and closed-closed cylinders are expected to behave similarly since the effects of acoustic end restraint decrease with increasing order of the axial modes.

In Sections III and V, and in the above, the internal acoustic field quantities, such as pressure and particle displacement, are expressed as doubly infinite series over the axial and circumferential mode numbers (m,n). Examples of these are shown in equations (2), (8)-(10). These series of expressions are modal expressions over the axial and circumferential components of the three-dimensional acoustic modes; however, the countably infinite set of modes associated with the radial components of the acoustic field are all contained within the functions  $J_n(\alpha_n, \overline{\tau})$  and  $J_n^+(\alpha_m, \overline{\tau})$  appearing in (2), (8)-(10). An

alternate functional form for the acoustic field quantitites can be developed as triply infinite series over the axial, circumferential and radial mode numbers (n, n, s). The purpose of the following discussion is to show how this expansion can be accomplished and to present the final series so obtained. Unless otherwise stated, it is assumed that the acoustic field is harmonic at frequency  $\omega$ .

Equation (18) shows the form of the internal acoustic pressure distribution for the (m,n,s)-mode. Following the methods of classical analysis, the net acoustic pressure at any point within the field can be expressed as the summation of the pressures due to the individual modes. Thus,  $P(x,y,r,\omega)$  might be written in the form:

$$P(x,y,r,\omega) = \sum_{m=0}^{\infty} \sum_{n=0}^{\infty} \sum_{s=0}^{\infty} P_{mns}(\omega) X_{m}(\overline{x}) Y_{n}(\overline{y}) J_{n}(\alpha_{ns} \overline{r})$$
(44)

If (44) is substituted into (7), the following comparable expressions are obtained for the modal expressions of the particle displacement components:

$$U_{\mathbf{x}}(\mathbf{x},\mathbf{y},\mathbf{r},\omega) = (\rho\omega^{2})^{-1} \sum_{m=0}^{\infty} \sum_{n=0}^{\infty} \sum_{s=0}^{\infty} K_{m} P_{mms}(\omega) X_{m}'(\bar{\mathbf{x}}) Y_{n}(\bar{\mathbf{y}}) J_{n}(\alpha_{ns}\bar{\mathbf{r}})$$
(45)

$$U_{y}(x,y,r,\omega) = (\rho\omega^{2} r)^{-1} \sum_{m=0}^{\infty} \sum_{n=0}^{\infty} \sum_{s=0}^{\infty} n P_{m\pi s}(\omega) X_{m}(\bar{x}) Y_{n}'(\bar{y}) J_{n}(\alpha_{n} \bar{x})$$
(46)

$$U_{r}(x,y,r,\omega) = (\rho\omega^{2} R)^{-1} \sum_{m=0}^{\infty} \sum_{n=0}^{\infty} \sum_{s=0}^{\infty} \alpha_{m} P_{m\pi}(\omega) X_{m}(x) Y_{n}(y) J_{n}^{1}(\alpha_{n},y)$$
(47)

Thus expanding the acoustic field in terms of the hard wall resonances requires only a knowledge of the modal pressure amplitude  $P_{m_{\overline{n},\overline{n}}}$ . As an example of how these pressure amplitudes can be determined, consider the case of equation (24). To expand (24) in terms of  $(m,\pi,s)$ -modes, equate (24) to (44), multiply both sides of the resulting equation by  $X_m(\overline{x}) Y_n(\overline{y})$ , integrate each term over the range  $0 \le \overline{x} \le 1$ ,  $0 \le \overline{y} \le 1$ , and use the fact that each of these sets of functions  $X_m(\overline{x})$  and  $Y_n(\overline{y})$  are mutually orthogonal. The resulting equation is

$$\rho \omega^{2} R U(\omega) \frac{g_{nm}}{\alpha_{m}} \frac{J_{\pi}(\alpha_{m}\overline{r})}{J_{\pi}^{\prime}(\alpha_{m})} = \sum_{s=0}^{\infty} P_{m\pi s}(\omega) J_{\pi}(\alpha_{n s}\overline{r})$$
(48)

Now let  $\alpha_{nv}$  be a root of the equation

$$J_{\mathbf{g}}^{\prime}(\alpha_{\mathbf{g}_{\mathbf{V}}}) = 0 \tag{49}$$

Multiply both sides of (48) by  $\overline{r} J_n(\alpha_{nv} \overline{r})$  and integrate each term over the range  $0 \le \overline{r} \le 1$ , aiving

$$\frac{\rho \omega^{2} R g_{mn} U(\omega)}{\alpha_{m} J_{n}^{1}(\alpha_{m})} \int_{0}^{1} \bar{\tau} J_{n}(\alpha_{m} \bar{\tau}) J_{n}(\alpha_{n\nu} \bar{\tau}) d\bar{\tau} = 
= \sum_{s=0}^{\infty} P_{mns}(\omega) \int_{0}^{1} \bar{\tau} J_{n}(\alpha_{ns} \bar{\tau}) J_{n}(\alpha_{n\nu} \bar{\tau}) d\bar{\tau}$$
(50)

The following two Bessel function relations, along with (49) are helpful in expanding the two integrals appearing in (50):

$$J_{n}'(z) = \frac{n}{z} J_{n}(z) - J_{n+1}(z)$$

$$J_{n}'(\alpha_{ns}) = \frac{n}{\alpha_{ns}} J_{n}(\alpha_{ns}) - J_{n+1}(\alpha_{ns}) = 0$$
(51)

Based on (51), the two integrals in (50) can be expressed as

$$\int_{0}^{T} \overline{\Gamma} J_{n}(\alpha_{m}\overline{\Gamma}) J_{n}(\alpha_{n}\sqrt{\Gamma}) d\overline{\Gamma} = \frac{\alpha_{m} J_{n}(\alpha_{n}) J_{n+1}(\alpha_{m}) - \alpha_{n} J_{n}(\alpha_{m}) J_{n+1}(\alpha_{n})}{\alpha_{m}^{2} - \alpha_{n}^{2}}$$

$$= \frac{\alpha_{m}}{\alpha_{n}^{2} - \alpha_{m}^{2}} J_{n}(\alpha_{n}) J_{n}^{i}(\alpha_{m})$$
(52)

$$\int_{0}^{1} \overline{r} J_{n}(\alpha_{ns} \overline{r}) J_{n}(\alpha_{nv} \overline{r}) d\overline{r} = \frac{\alpha_{ns} J_{n}(\alpha_{nv}) J_{n+1}(\alpha_{ns}) - \alpha_{nv} J_{n}(\alpha_{ns}) J_{n+1}(\alpha_{nv})}{\alpha_{ns}^{2} - \alpha_{nv}^{2}}$$

$$= \frac{n \left[ J_{n}(\alpha_{nv}) J_{n}(\alpha_{ns}) - J_{n}(\alpha_{ns}) J_{n}(\alpha_{nv}) \right]}{\alpha_{ns}^{2} - \alpha_{nv}^{2}}$$
(53)

= 0 if  $s \neq v$  (orthogonality property)

$$\int_{0}^{1} T J_{n}^{2}(\alpha_{ns}T) dT = \frac{1}{2} \left[ J_{n}^{*}(\alpha_{ns}) \right]^{2} + \frac{1}{2} \left[ 1 - (n/\alpha_{ns})^{2} \right] - J_{n}^{2}(\alpha_{ns})$$

$$= \frac{1}{2} \left[ 1 - (n/\alpha_{ns})^{2} \right] J_{n}^{2}(\alpha_{ns})$$
(54)

Substituting (52)-(54) into (50), setting v = s, and solving for  $P_{max}$  gives

$$P_{mns}(\omega) = \frac{2 \rho \omega^2 R g_{mn} U(\omega)}{\left[\alpha_{ns}^2 - \alpha_m^2\right] \left[1 - \left(\frac{n}{\alpha_{ns}}\right)^2\right] J_n(\alpha_{ns})}$$
(55)

Using (5), (16) and (17), the quantity  $\alpha_{ns}^2 - \alpha_m^2$  can be rewritten in the following form:

$$\alpha_{ns}^{2} - \alpha_{m}^{2} = \left(\frac{R}{c}\right)^{2} \left[\omega_{ns}^{2} - \omega^{2} + \omega_{m}^{2}\right]$$

$$= \left(\frac{R}{c}\right)^{2} \left[\omega_{mns}^{2} - \omega^{2}\right]$$

$$= \left(\frac{R}{c}\right)^{2} \omega_{mns}^{2} \left[1 - \left(\frac{\omega}{\omega_{mns}}\right)^{2}\right]$$
(56)

Substituting (56) into (55) gives

$$P_{mins}(\omega) = 2 p c^{2} \frac{U(\omega)}{R} \frac{g_{min}}{\left[1 - \left(\frac{n}{\alpha_{ns}}\right)^{2}\right] J_{n}(\alpha_{ns})} \frac{\left(\frac{\omega}{\omega_{mins}}\right)^{2}}{1 - \left(\frac{\omega}{\omega_{mins}}\right)^{2}}$$
(57)

Substituting (57) into (44)-(47) gives the desired modal expansion of the internal acoustic field, for an open-open or closed-closed cylindrical cavity, for an arbitrary known wall motion. The resulting modal expressions are convenient in that damping of the acoustic field can be introduced in the conventional manner used in structural analysis. Let Q<sub>mass</sub> denote the dynamic magnification factor at resonance for the (mms)-mode.

Then with an equivalent linear viscous damping introduced, the expression for (57) can be rewritten in the alternate more general form:

$$P_{mns}(\omega) = 2 pc^{2} \frac{U(\omega)}{R} \frac{g_{mn}}{\left[1 - \left(\frac{n}{\alpha_{ns}}\right)^{2}\right] J_{n}(\alpha_{ns})} \left(\frac{\omega}{\omega_{mns}}\right)^{2} H\left(\frac{\omega}{\omega_{mns}}\right) e^{-i\theta_{nms}}$$
(58)

$$H\left(\frac{\omega}{\omega_{mns}}\right) = \left[\left\{1 - \left(\frac{\omega}{\omega_{mns}}\right)^{2}\right\}^{2} + \frac{1}{Q_{mns}^{2}}\left(\frac{\omega}{\omega_{mns}}\right)^{2}\right]^{-\frac{1}{2}}$$
(59)

$$\theta_{mins} = \tan^{-1} \left[ \frac{\frac{1}{Q_{mins}} \left( \frac{\omega}{\omega_{mins}} \right)}{1 - \left( \frac{\omega}{\omega_{mins}} \right)^2} \right]$$
 (60)

It is now a relatively straightforward exercise to study the internal sound field generated by a known wall motion, such as for a piston or an overall shell made.

#### APPENDIX II

#### THE COMPUTER PROGRAM

## 1. GENERAL

The equations and expressions given in the foregoing sections of this report have been programmed in the FORTRAN IV language for evaluation by a digital computer. The programs have been written according to the requirements of the IBM 7094 FORTRAN IV implementation and are intended to be run on the coupled IBM 7094-7044 computer system installed at the Digital Computation Division, Wright-Patterson AFB.

A diagrammatic representation of the overall program organization is shown in Figure 53; the program has been divided into five independent sections, but with some common parts, as indicated in Section 5 of this Appendix, for convenience of handling.

This Appendix defines the input data requirements and formats, defines the remaining COMMON storage variables, provides a brief description of each routine comprising the programs and the method of sub-division into five separate programs. A description of the output from each program is given together with computer output examples, and finally indications are given of changes necessary to expand the programs to deal with different ranges of various parameters.

## 2. DEFINITION OF INPUT DATA

## a. Variable Parameters Required by the Programs

The following table contains a list of all the input parameters required by the various programs together with units and dimensions, the FORTRAN variable name, the FORTRAN card punching format, units of the parameter within the program, the data card number and columns on the card occupied by the item of data.

The input parameters have been divided for convenience of description into sub-sections as indicated in the list, but this has no effect on the punching format. It should be noted that all five program sections do not use all the data listed in the table, but to maintain continuity the input routines of all the programs use the same read statements for this data and thus require the same cards. Parameters which are not used by a particular program may be left blank in the parameter input cards for that program (see 2 d.).

	ПЕМ	INPCT UNITS	VARJABLE NAME	PROGRAM UNITS	FORMAT	CARD	CARD COLS.
3	Structural Configuration						
<u>-</u>	Length of cylinder representing the fuselage	Ė	12	÷	F10.5	_	1-10
<u>~</u>	Radius of fuselage	Ė	œ	÷.	F10.5	_	11-20
<u>ښ</u>	Frame pitch	. <b>ċ</b>	FL	÷.	F10.5	_	21-30
4.	Stringer pitch	ë	SL	fi.	F10.5	_	31-40
<u>ئ</u>	Cross-sectional area of frames	in2	FA	f1.2	F10.5	_	41-50
<u>.</u>	First moment of area of frame about skin center line	<u>"-</u>	AF 1	<u>ي</u>	F10.5	-	51-60
<u>'</u>	Second moment of area of frame about skin center line	ë.	AF2	ŧ	F10.5	_	61-70
ထ်	Second moment of area of frame about a polar axis through center of area of cross-section	Ē	FMIT	Œ	F10.5	-	71-80
<u>°.</u>	Cross-sectional area of stringers	 	ν	fi.	F10.5	~	1-10
<u>.</u>	First moment of area of stringer about skin center line	e.	ASI	ŧ	F10.5	8	11-20
<u>:</u>	Second moment of area of stringer about skin center line	<u></u>	AS2		F10.5	8	21-30
2.	Second moment of area of stringer about a polar axis through cross-section center of area	ţ.	SMIT	<b>*. ±</b>	F10.5	8	31-40

	ITEM	INPUT	VARIABLE NAME	PROGRAM UNITS	FORMAT	CARD NUMBER	CARD COLS.
Ξ	Structural Configuration (Continued)						
.5	Warping constant for stringers about center of area of cross-section	ů. E	CWARP	÷÷	F10.5	8	41-50
4.	St. Venant torsion constant for stringers	<b>↓</b> .	CTOR	fi.4	F10.5	2	51-60
15.	Product of second moment of area about perpendicular axes through stringer center of area normal and parallel to skin.	ž:	SMICR	<b>‡</b> :	F10.5	2	61-70
.9	Fuselage skin thickness	. <u>:</u>	<b>-</b>	ft.	F10.5	2	71-80
17.	Initial load/unit length in skin panels in axial direction	lb/ft.	STRSSX	lb/ft.	F10.5	m	01-1
8.	Initial load/unit length in skin panels in circumferential direction	lb/fì.	STRSSY	lb/ft.	F10.5	က	11-20
.61	Initial shear load/unit length in skin panels	lb/fn.	SHEAR	lb/ft.	F10.5	ო	21-30
હ	Number of windows in cross-section considered at high frequency	1	WWN	1	0 1	ო	31-40
2.	Window dimension in axial direction	Ë	XWNDW	ft.	F10.5	က	41-50
22.	Window dimension in circumferential direction	ë.	WWW	ŧ	F10.5	က	51-60
23.	Window thickness	<u>.</u> <u>.</u> <u>.</u>	TWNDW	÷	F10.5	ဇာ	61-70
24.	Initial load/unit length in window in axial direction	1b/ft.	WSTRX	lb/ft.	F10.5	ო	71-80

	ITEM	INPUT	VARIABLE NAME	PROGRAM UNITS	FORMAT	CARD NUMBER	CARD COLS.
=	Structural Configuration (Continued)						
25.	Initial load/unit length in window in circumferential direction	lb/ft.	WSTRY	lb/ft.	F 10.5	4	01-1
36.	Initial shear/unit length in window	16/ft.	WSHR	lb/ft.	F 10.5	4	11-20
27.	Double skin indicator (0 for no double skin, 1 for double skin)	1	ZSX	ı	0 1	4	21-30
<u>.</u> 28.	Inner skin thickness	ë	Z	#	F 10.5	4	31-40
29.	Inner wall indicator for fastening to stringers (1 for fastening, 0 for non- fastening)	•	KAYı	•	01 1	4	41-50
30.	Inner wall indicator for fastening to frames (1 for fastening, 0 for non- fastening)	ı	KAY2	1	01	4	51-60
31.	Stringer depth (from inside skin)	Ë	DEPTHS	÷	F 10.5	4	61-70
32.	Frame depth (from inside skin)	<u>.ċ</u>	DEPTHF	ft.	F 10.5	4	71-80
33.	Dynamic magnification factor at resonance for the structure	1	Ø	•	F 10.5	ĸ	1-10
34.	Skin damping material loss factor	,	ETA	ı	F 10.5	Ŋ	11-20
Ξ	Structural Material Properties						
35.	Young's modulus for shell material (assumed the same for stringers, frames and skin)	lb/in?	ESY EY	16/ft?	F 10.5	ις.	21-30

	ПЕМ	INPUT	VARIABLE NAME	PROGRAM UNITS	FORMAT	CARD	CARD COLS.
	Structural Material Properties (Cont'd)						
8	Young's modulus for window material	lb/in?	EWW	lb/ft.²	F10.5	ις;	31-40
37.	Poisson's ratio for shell	•	SHNU	ı	F10.5	'n	41-50
38.	Shell material density	lbwt/ft³.	SKDENS FDENS STDENS	lb wr/fr³.	F10.5	ĸ	21-60
39.	Window material density	lbwt/ft3.	WDENS	lb wr/ft3.	F10.5	ĸ	02-19
6.	Skin damping material surface density	lbwt/ft?	DMPDEN	lb wt/ft?	F10.5	'n	71-80
	(iii) External Aerodynamic Conditions						
41.	Forward speed conircraft	ft./sec.	Z 5	ft./sec.	F10.5	•	1-10
42.	Ambient air density	slugs/ft³.	ROIN	slugs/ft3.	F10.5	v	11-20
<del>.</del> 63	Ambient speed of sound	ft./sec.	2	ft./sec.	F10.5	•	21-30
4.	Viscosity of air	slugs/ft.	EMU	slugs/ft.	£10.5	•	31-40
45.	Ambient atmosphere pressure	16/41?	NI N	1b/ftt <sup>2</sup>	F10.5	•	41-50
3	(iv) Internal Air Conditions						
<del>.</del> 6	Internal static pressure	1b/ft?	PSTI	1b/ft <sup>2</sup> .	F10.5	•	21-60
47.	Speed of sound inside fuselage	ft./sec.	CSPD	ft./sec.	F10.5	•	02-19
		_					_

	ITEM	INPUT	VARIBALE NAME	PROGRAM UNITS	FORMAT	CARD NUMBER	CARD COLS.
(2)	(iv) Internal Air Conditions (Cont'd)						
48.	Density of air inside fuselage	slugs/ft³.	800	slugs/fr³.	F10.5	9	71-80
3	Engine Layout (Jet)						
<del>6</del>	Distance from front of cylinder (fuselage) to the inboard jet exhaust in axial direction	æ	XJET 1	æ:	F10.5	^	0-1
50.	Distance from front of cylinder (fuselage) to the autboard jet exhaust in axial direction	ŧ	XJET2	<b>.</b>	F10.5	٨	1-8
51.	Distance from fuselage center line to inboard jet center line	ŧ	YJETI	fì.	F10.5	7	21-30
52.	Distance from fuselage center line to outboard jet center line	ŧ	YJET2	Ĥ.	F10.5	^	31-40
53.	Velocity of jet at exit	ft./sec.	VJET	ft./sec.	F10.5	۸	41-50
54.	Speed of sound in jet at exit	ft./sec.	CJET	ft./sec.	F10.5	2	21-60
55.	Radius of jet at exit	÷	RADJET	÷	F10.5	7	61-70
3	(vi) Acoustic Treatment					-	
38	Number of layers of treatment		z	ı	0 -	<b>6</b>	01-1
57.	Equivalent surface area for internal absorption by furnishings, etc.	£;	AOVS	ft?	F10.5	∞	11-20
Note:	N cards are now required, each containing		_		_	_	_

Note: N cards are now required, each cantaining Items 58 - 64 as appropriate.

	ITEM	INPUT	VARIABLE NAME	PROGRAM UNITS	FORMAT	CARD NUMBER	CARD COLS.
Ē	Acoustic Treatment (Continued)						
58.	Type of treatment (1 for airgap, 2 for pareus blanket, 3 for septum, 4 for panel)	1	NLRS	ı	01 1	9, 10,	1-10
59.	Density of material (surface density for septa and volume density for blanket)	lbwr/ft? Ibwr/f;3	DENSLR	slugs/ft <sup>2</sup> . slugs/ft <sup>3</sup> .	F10.5	9, 10,	11-20
8	Thickness of layer	ë	DIHICK	÷	F10.5	9, 10,	21-30
For Por	For Porous Blankets the Following is Required:						
61.	Flow resistance	lb sec./	RFI	lb sec./	F10.5	9, 10,	31-40
62.	Volume coefficient of elasticity for air	lb/ft <sup>2</sup>	BKA	1b/ft?	F10.5	9, 10,	41-50
83.	Porosity (see Appendix IV)	1	YBI	1	F10.5	9, 10,	21-60
64.	Structure factor (see Appendix IV)	1	SKB	ŧ	F10.5	9, 10,	61-70
<u> </u>	(vii) Frequency Ranges						
65.	Lowest frequency for the complete cylinder model	cbs	 *	rad/sec.	F10.5	Z 6	1-10
. 99	Upper frequency for the complete cylinder and starting frequency for the panel group	sdo	W2	rad/sec.	F10.5	Z 6	11-20
67.	Upper frequency for the panel group and starting frequency for the single panel model	cps	%	rad/sec.	F10.5	Z *	21-30

İ	ITEM	INPUT	VARIABLE NAME	PROGRAM UNITS	FORMAT	CARD NUMBER	CARD COLS.
Frequ	Frequency Ranges (Continued)						
Uppe	Upper frequency for the single panel model	<b>s</b> dɔ	W4	rad/sec.	F10.5	N+6	31-40
Initio	Initial frequency intervalfor frequencies between W1 and W2(doubled every octave)	cps	DELW	rad/sec.	F10.5	Z č	41-50
Initi	Initial frequency intervalfor frequencies between W2 and W3 (doubled every octave)	cps	DELX	rad/sec.	F10.5	Z č	21-60
Initi	Initial frequency interval for frequencies between W3 and W4 (doubled every octave)	Sdo	DELY	rad/sec.	F10.5	Z č	61-70
Mod	Mode Number Control						
Numb panel field.	Number of axial modes for cylinder and panel response and internal acoustic field,	1	\$	ı	01 1	Z *	71-80
Z 2 5 5 5 5 5 5 5 5 5 5 5 5 5 5 5 5 5 5	Number of circumferential modes for cylinder and panel response and internal radial acoustic modes	1	Ī	. 1	0 -	N+01	1-10
Z Z Z	Number of circumferential internal acoustic modes	ı	NS1	1	1 10	Z + 0.	11-20
Exte	External Field Control						
Leng for o	Length from front of fuselage to position for calculation of boundary layer thickness for total cylinder case	Ė	ВІСУІ	<u></u>	F10.5	Z+01	21-30

	ПЕМ	INPUT UNITS	VARIABLE NAME	PROGRAM UNITS	FORMAT	CARD NUMBER	CARD COLS.
E	External Field Control (Continued)						
76.	Length from front of fuselage to center of panel in panel group and single panel case	Ŧ.	BLX	÷	F10.5	N+01	31-40
77.	Angle around fuselage from horizontal nearest the jet to the points at which jet noise is to be determined	degrees	PHIFUS	degrees	F10.5	Z 6	41-50
_ <b>78</b>	Number of points on fuselage at which jet noise is to be determined	ı	Z.T.P		01 1	N+01	51-60
79.	First position from front of cylinder at which jet noise is to be determined	ŧ	XJTFUS(1)	÷	F10.5	Z +	1-10
<u>8</u>	Second position as in 79	÷	XJTFUS(2)	÷	F10.5	Z +	11-20
81.	Third position as in 79	ft.	XJTFUS(3)	£.	F10.5	Z ±	21-30
82.	Fourth position as in 79	÷	XJTFUS(4)	£	F10.5	Z <del>-</del>	31-40
83.	Fifth position as in 79	÷	XJTFUS(5)	÷.	F10.5	N+ +	41-50
3	Acoustic Dynamic Magnification Factor						
84.	Acoustic dynamic magnification factor at resonance	ı	OMEG		F 10.5	Z+:	51-60

#### b. Tabulated Functions

In addition to the foregoing parameters, tables of various functions are required as follows:

(1) Jet Noise Calculation

## Table DIRTBL

Table of directivity function as a function of directivity angle  $\theta$  in degrees and modified axial Strouhal number, as given in Figure 30. This table of values is stored in a two-dimensional array named DIRTBL with dimensions 11, 25. From Figure 30 a set of values of 10 log f ( $\theta$ ) are provided for the 11 values of  $\theta$  which are given on the figure and for 25 values of  $x/\lambda_0$  starting at 0.5, with initial interval 0.1, and going to 100.0 on a logarithmic scale. The interval in  $x/\lambda_0$  is multiplied by 10.0 in each decade.

If it is desired to replace the directivity function provided, the new values are punched in the format 11F 7.2 per card, with one card corresponding to each value of  $x/\lambda_0$  and the 11 numbers corresponding to the 11 values of  $\theta$  given in Figure 30.

#### **Table ACPOW**

One-dimensional array of maximum dimension 33 containing overall acoustic power per unit value of jet exhaust as a function of ratio of downstream distance to jet exit radius on a logarithmic scale. The table layout is given below. A set of values is provided based on Figure 28.

## Table CORPOW

One-dimensional array of maximum dimension 33 containing normalized acoustic power as a function of axial Stroubal number, for the core region of the jet, on a logarithmic scale. The table layout is given below. A set of values is provided based on Figure 26.

## Table DOWPOW

One-dimensional array of maximum dimension 33 containing normalized acoustic power as a function of axial Strouhal number, for the region of the jet outside the core, on a logarithmic scale. Table layout is given below. A set of values is provided based on Figure 27.

# Format of Tables ACPOW, CORPOW, DOWPOW

First value in table: Starting value of independent variable (logarithmic scale)

Second value in table: Interval in independent variable in decade 1-10 (multiplied by

10 in each subsequent decade and divided by 10 in each prior

decade)

Third value in table: Number of values of dependent variable in table

Fourth and subsequent: Dependent variable corresponding to the independent variable

values val

The above tables are punched on cards in the format 11 F 7.2 per card. Three cards must be provided for each table.

(2) Absorption Coefficients for Interior Surfaces

## Table ABSCOF

This table contains values of the fuselage interior absorption coefficient as a function of frequency. The table contains 10 values of absorption coefficients specified at the following frequencies (in cycles/second):

100, 300, 500, 1000, 2000, 3000, 4000, 5000, 6000, 7000.

The table is punched as one card in the format 10 F 7.2. Input parameter number 57 is the absorbing area associated with these coefficients. Some typical values of absorption coefficient are given in Table IV.

#### c. Notes on Input Data

- Item 20 is the number of windows in the particular fuselage cross-section used for the high frequency model. The number will normally be 2 or 0; if 0 then items 21-26, 39 will also be zero.
- (2) If item 27 is 0 then items 28-32 are also zero.
- (3) Modulus of rigidity for the shell material is calculated from E/2(1 + v).
- d. Input Data Set-up for the Various Programs
  - (1) Tabulated functions DIRTBL, ACPOW, CORPOW and DOWPOW are required only for the jet noise calculation program, the principal routine of which is JTNSE, in which case the data set-up is at follows:

- 1. 25 cards for DIRTBL
- 2. 3 cards for ACPOW
- 3. 3 cards for CORPOW
- 4. 3 cards for DOWPOW
- Parameter cards as given in 2a. Of these parameters only those numbered 1, 41, 49, 50 through 55, 65 through 71, and 77 through 83 are used by the jet noise program.
- (2) Tabulated function ABSCOF is required only for the acoustic treatment noise reduction program and the one card containing the coefficients precedes the parameter cards described in 2a. The number of elements (or layers) in the acoustic treatment must not exceed 10 of which no more than 5 are porous blankets. Only parameters numbered 1, 2, 3, 4, 16, 27, 28, 33, 34, 35, 38, 19, 46, 47, 48 and 56 through 71 are used by the acoustic treatment noise reduction program.
- (3) The three structural interior response programs require only the parameter cards. The value of item 57 may be 0 in which case cards containing items 58 through 64 are not required. Other parameters which are not used by these programs are 49 through 55, 57 and 77 through 83. In addition, parameters numbered 13 through 15 are used only by the intermediate frequency, panel group program and parameters 17 through 26 are used only by the high frequency, single panel program.

# 3. COMMON VARIABLES

All the FORTRAN variables defined in 2 as input data are also defined as numbered common variables. In addition, the following list of variables are defined as common. Arrays are indicated by their dimensions.

# a. Numbered (Blank) Common

Variable Name	Definition
NPTSW	Number of frequency values, and hence the number of results in the low frequency range.
NPTSX	Number of frequency values in the intermediate frequency range.
NPTSY	Number of frequency values in the high frequency range.

Variable Name	Definition
FJ(5)	Array used to return values of Bessel functions of the first kind of integer order from routine BSSLJ.
TEMP1,TEMP2,TEMP3 TEMP4	Locations used as general purpose temporary storage locations.
QIN	Dynamic pressure, calculated in routine INTIL.
RECYL	Reynolds number for the total fuselage (low frequency) case based on length BLCYL.
REX	Reynolds number for the panel (intermediate and high frequency) cases based on length SLX.
CONST 1, CONST 2, CONST 3, CONST 4	Variables pre-set in routine INITL for subsequentuse by routine BLNOIS.
EM	Mach number
FMIB	Frame second moment of area about center of area in bending (i.e., axis parallel to skin)
SMIB	Stringer second moment of area about center of area in bending (i.e., axis parallel to skin)
DPANEL	Panel flexural rigidity Et3/12(1-v)
DWNDW	Window panel flexural rigidity
XPANEL	Individual skin panel length in the axial direction (i.e., between frames)
YPANEL	Individual skin panel width in the circumferential direction (i.e., between stringers)
SMASS	Mass of the cylindrical shell and stiffeners
NPANEL	Number of skin panels around the cylinder circumference
SBAR	Parameters for computing frequencies of stiffened shell in routine APPEND - (from Equation 2.24).
RBAR	a trail and a finantial and a

Variable Name		Definition
ZSQ	$L_{\times}^4 (1-v^2)/R^2$	t <sup>2</sup> from Equation (2.24)
ZSOVR	Distance from :	skin center line to stringer center of area
ZROVR	Distance from s	kin center line to frame center of area
BARM	Cylinder mass/	unit area multiplied by $L_{x}^{4}/\pi^{4}D$
PTERM	(PSTI-PIN) mul	tiplied by $L_x^2/\pi^2D$
PART	E I Dd	
PAR2	G <sub>s</sub> J <sub>2</sub> /Dd	Parameters for computing natural frequencies of stiffened shell in
PAR3	G <sub>s</sub> J <sub>2</sub> /Dd G <sub>r</sub> J <sub>2</sub> /Dd	routine APPEND - Equation (2.22)
PAR4	EI /D/	
FREQ (100)	Values of frequ	ency at which results are calculated
SWBL (100)	fuselage model:	density of structural response of the various s to boundary layer excitation divided by value of boundary layer pressure p.s.d. (SP)
SWRF (100)		density of structural response of the various s to a reverberant sound field divided by the pressure p.s.d.
(001) NLW2	fuselage model:	density of structural response of the various s to jet engine noise divided by the value of jet noise pressure spectrum
SPIBL (100)	•	e spectral density due to boundary layer ded by boundary layer pressure p.s.d. (SP)
SPIRF (100)		e spectral density due to reverberant field ded by the external pressure p.s.d.
SPUN (100)		e spectral density due to jet noise excita- the jet noise pressure p.s.d.

Variable Name	Definition
SPWSBL (50)	Internal pressure spectral density due to window response to boundary layer noise, non-dimensionalized as for SPIBL (high frequency model).
SPWS, 'N (50)	Internal pressure spectral density due to window response to jet noise, non-dimensionalized as for SPLIN (high frequency model)
SPWSRF (50)	Internal pressure spectral density due to window response to a reverberant field, non-dimensionalized as for SPIRF (high frequency model).
SWSBL (50)	Structural response spectral density of windows to boundary layer noise ratioed as for SWBL (high frequency model).
SWSJN (50)	Structural response spectral density of windows to jet noise ratioed as for SWJN (high frequency model).
SWSRF (50)	Structural response spectral density of windows to reverberant field ratioed as for SWRF (high frequency model).
ICOUNT	Frequency term counter.
R1 BAR (5)	The part of the dynamic flow resistance independent of frequency is calculated for each porous blanket in routine INIII and stored here.
RQ1 BAR (5)	The part of effective air density independent of frequency is calculated for each porous blanket in routine INITL and stored here
PRR (10)	Real part of pressure ratio across acoustic treatment.
PRI (10)	Imaginary part of pressure ratio across acoustic treatment.
TRL (100)	Transmission loss of the structure, with all responses converted to equivalent reverberant field.
TRLAT (100)	Transmission loss due to acoustic treatment, function of frequency.
TRLWS (50)	Transmission loss due to windows.

Variable Name	Definition
TRF (100)	Noise reduction due to absorption by interior furnishings.
SPJET (100)	Sound pressure level in dB relative to 0.0002 dynes/cm <sup>2</sup> at the chosen point on the fuselage due to jet engine noise.
WST	Weight of the structure.
WAT	Weight of acoustic treatment
OMEG	Frequency: used in the acoustic treatment routines.
THETA	Sound wave incidence angle for acoustic treatment transmission loss calculation.
AOVS	Interior absorption equivalent area divided by surface area of the cylinder
PBDENS (5)	Densities of porous blankets involved in the acoustic treatment (obtained from input parameter cards).

# b. Labeled Common

Labelled common variables are used by the routines which calculate the natural frequencies and modes for the groups of panels in the intermediate frequency case. The variables are defined as follows:

Variable Name	Definition
A (2,2,161)	Three-dimensional array of coefficients of the frequency Equation (2.48). Zeros of this determinant give the natural frequencies.
STR (6)	Stringer force and moment terms (other than those involving frequency) which are used by routine FORMTX in forming A.
ANIT (3)	Array containing stringer and panel constants.
STOR	Elements of transfer matrix R <sub>2</sub> evaluated in routine SPASET (see Equation (2.40).
xM	Elements of matrix F evaluated in routine SPASET.
OMEGA	Frequency in rads/sec.

PBL  $\left( \frac{m \pi b}{L_{\chi}} \right)^{2}$  used in Equation (2.36)  $b^{2} \sqrt{h/D p}$  Modal constants  $A_{1}$ ,  $A_{2}$ ,  $A_{3}$ ,  $A_{4}$  for each panel in the group (see Equation 2.35).

# 4. DESCRIPTION OF THE ROUTINES COMPRISING THE PROGRAMS

This section contains a brief description of each of the subroutines which comprise the five computer programs.

## a. Main Program

The main program in each case reads the input parameters and tables as specified in 2, converts the units where necessary and calls the various other routines as required. The input data is transmitted to the other routines via common storage.

## b. Routine WTANSS

This routine calculates the weight of the structure and acoustic treatment, calculates the various structural constants and the modifications due to a double skin, where appropriate, according to Equations (2.2) to (2.9). Panel density, stiffness and damping are modified to allow for addition of damping material if this is specified in the input data.

The input parameters (for the three structural - interior response programs) are added to the printed output, identified by their parameter numbers.

## c. Routine INITL

This routine calculates various constant terms used at a later stage in the program; these constants include Reynolds number, boundary layer thickness, Mach number, dynamic pressure and the structural constant terms used in the calculation of shell natural frequencies. The constant parts of R 1BAR and RO1 BAR, used in calculating the acoustic impedance of porous blankets, are also calculated (see Equations (6.26) and (6.27)).

Reynolds numbers, boundary layer thickness, dynamic pressure and structural weight and mass are printed.

#### d. Routine CYLRES

This routine calculates the structural and internal pressure response for the low frequency, complete fuselage case. The steps in the routine are as follows:

- (1) A pair of nested loops with loop variables NN and M control the summation of modes n and m respectively, according to Equation (5.59).
- (2) Routine APPEND is called to calculate shell natural frequency and coupled natural frequencies and generalized masses according to Equations (2.22), (3.30) and (3.42). The required number of frequencies are calculated as specified by input item 73- number of circumferential acoustic modes.
- (3) For each frequency in the range W1 to W2 the contribution to the structural response is calculated and summed. Routines BLNOIS, JMSQJN, JNSQJN, JMSQBL, JNSQBL, JMSQRF, JNSQRF are called to calculate the joint acceptance to the various environments.
- (4) An inner loop with toop variable I is used to sum over the acoustic mode number is according to Equation (5.26).
- (5) Contributions to the summation term of the internal response Equation (5.28) are calculated.
- (6) The frequency is incremented by DELW (or 2<sup>n</sup> DELW where n is the octave number starting from W1) and if the frequency is less than W2 the procedure is repeated from (3).
- (7) At the end of the two loops mentioned in (1) a further loop is used to multiply the summation terms by the appropriate constants.
- (8) The number of frequencies at which results are obtained is stored in NPTSW and the frequencies in array FREQ.

# e. Routine APPEND

This routine calculates the shell natural frequencies, the coupled cylinder-air natural frequencies and generalized masses.

Formal parameters are:

NN mode number in circumferential direction

M mode number in longitudinal direction

WMNS

array for return of coupled natural frequencies

**GENM** 

array for return of generalized masses.

The steps in the program are:

- (1) Calculate the shell natural frequency according to Equation (2.22) using the constants SBAR, RBAR, ZSQ, ZSOVR, ZROVR, BARM, PTERM, PAR1, PAR2, PAR3 and PAR4 calculated in routine INITL and stored in common area.
- (2) For the NS1 mode numbers calculate coupled natural frequencies by an iterative solution of Equation (3.30) using routine REGFAL and NATF1 and also store the result in array WMS.
- (3) Calculate generalized masses from Equation (3.42) and store in array GENM.

#### f. Routine BLNOIS

This routine calculates the boundary layer turbulence convection velocity and turbulent pressure power spectral density.

Formal parameters are:

**CMEGA** 

frequency

UCV

convection velocity

Convection velocity is calculated from Equation (4.15) depending on the Mach number and pressure power spectral density from Equation (4.5). Constant terms which depend on Reynolds number and Mach number are calculated by routine INITL and stored in common area.

# g. Routine NATF1

This routine is used in the iterative solution of Equation (3.30). The expression on the left hand side of the equation is evaluated using routines BSSLI or BSSLI to calculate unmodified or modified Bessel functions of the first kind and integer order, depending on whether the acoustic axial natural frequency  $\omega_{\rm m}$  is greater than or less than  $\Omega$ , and returned in formal parameter FX. Formal parameter X contains, on entry to the routine, a value of the variable  $\Omega$ .

Entry points NATFE2 and NATFE3 are used to pre-set values of shell frequency and mode numbers m and n.

## h. Routine JTACSQ

Formal parameters are:

OMEGA

frequency

UCV

boundary layer pressure fluctuation convection velocity

Μ

mode number

XJM

joint acceptance squared returned as the output term.

The various entry points are used as follows:

**JMSQBL** 

The joint acceptance to boundary layer noise in the axial direction (mode number m) is calculated according to Equations (5.47) and (5.48).

**JNSQBL** 

The joint acceptance to boundary layer noise in the circumferential direction (mode number n) is calculated according to Equation (5.49).

MLDSWL

The joint acceptance to jet noise in the axial direction is calculated according to Equation (5.53).

JNSQJN

The joint acceptance to jet noise in the circumferential direction is calculated according to Equation (5.54) and (5.55).

## i. Routine LMSQRF

This routine calculates joint acceptance squared for the total cylinder to a reverberant acoustic field. Simple support end conditions to cylinder.

Format parameters are:

**OMEGA** 

frequency

UCV

speed of sound

XLENG length in axial or circumferential direction

mode number in axial or circumferential direction

XJ value of joint acceptance returned.

Entry point JMSQRF:

M

Joint acceptance is evaluated for the axial direction according to Equation (5.50) and routine ONEFV is used to evaluate the cosine and sine integrals.

Entry point JNSQRF:

Joint acceptance is evaluated for the circumferential direction according to Equation (5.51). Routine ONEFV is used to evaluate the cosine and sine integrals.

# . Routine PLRSEP

This routine calculates the structural and internal pressure response for the high frequency, single panel case. The steps in the procedure are:

- (1) An outer loop with loop variable M controls the summation of the axial direction modes.
- (2) Values of n and R/c are transmitted to routine BSLRT via entry BSLRT2.
- (3) For each n the required number of values of  $\alpha$  are calculated by solving Equation (3.66) using REGFAL and BSLRT;  $\alpha_{ns}$  and corresponding values of  $\omega$  are stored in arrays ALPHMS and WMS respectively.
- (4) The next loop, with loop variable NN controls the structural response summation in the circumferential direction. This loop is skipped if either m or n are zero. Skin panel and window response is calculated according to Equation (3.84).
- (5) In this loop the frequency control is set up starting at W3 and incrementing by 2<sup>n</sup> \* DELY where n is the octave number commencing from W3. An inner loop to calculate the summation terms for the internal field (Equation (3.90)) is only traversed for the first value of NN and for each frequency.
- (6) Routines BLNOIS (ENTRY BLNSPL), JABLPL, JAJNPL, and JARFPL are called to calculate aerodynamic data and joint acceptance for the various excitation pressure fields.

(7) Finally, the structural and pressure response summations are multiplied by their respective constants and the internal response summation by the structural response term.

## k. Routine BLSRT

This routine defines the left hand side of Equation (3.65) for use by REGFAL in obtaining an iterative solution. Routine BSSLJ is used to calculate Bessel functions of the first kind and integer order.

Entry BSLRT2 is used to pre-set the value of n.

#### I. Routine JABLPL

This routine calculates joint acceptance squared of a simply-supported flat plate to boundary layer turbulence and jet noise.

#### Formal parameters are:

OMEGA	frequency
UCV	convection velocity in boundary layer
N	mode number in circumferential direction
M	mode number in axial direction
XJ2MN	joint acceptance squared.

For the boundary layer entry the joint acceptance is calculated according to Equations (5.68) and (5.70). For jet noise the entry point is JAJNPL and joint acceptance is obtained from Equations (5.75) and (5.77).

#### m. Routine JARFPL

This routine calculates joint acceptance squared in one modal direction of a simply-supported flat plate to a reverberant acoustic field according to Equations 5.72-5.74.

## Formal parameters are:

OMEGA	frequency in rad/sec		
UC	speed of sound		

XL length of plate along one edge

N mode number along this edge

XJMN joint acceptance squared.

The total joint acceptance squared for the plate is obtained as the product of joint acceptances in each of the two directions.

## n. ONEFV

This routine is used to evaluate cosine and sine integrals by the methods defined in Equations (5.52).

Formal parameters are:

x value of input variable. Cosine integral returned by this parameter

Y sine integral returned on exit from routine

The three parts of the routine are:

Ent.y ONEFV calculates Cin(x) and Si(x) by rational fraction approximation (smell values of x).

Entry SIXSEV calculates Cin(x) and Si(x) by power series summation (intermediate values of x).

Entry TWELVE calculates Cin(x) and Si(x) from an asymptotic expansion (large values of x).

## o. Routine BSSLi

This routine calculates Bessel functions of the first kind and of integer order.

# Formal parameters are:

X argument of Bessel functions required

N order of Bessel functions; positive of value n or oFJ results array of dimension 5 where the Bessel functions  $J_{n-2}(x), J_{n-1}(x), J_{n}(x), J_{n+1}(x), J_{n+2}(x)$  are resumed

The method of calculation is a recursion starting from  $J_{n+2}(x)$  and calculating with decreasing n down to n=0. Only the upper five values are returned in FJ. The argument giving the order N must be zero or positive. The recursion procedure is defined in M.T.A.C. VII, 1957. The procedure is repeated until the maximum difference between any pair of functions is less than  $10^{-6}$ .

## p. Routine BSSLI

This routine calculates modified Bessel functions of the first kind and of integer order.

Formal parameters are:

X argument of Bessel functions required

N order of Bessel functions; positive of value n or o

NJ results array of dimension 5 where the modified Bessel functions  $I_{n-1}(x)$ ,  $I_n(x)$ ,  $I_{n+1}(x)$  are returned.

The method of calculation is as follows:

when x > 12 and x > n the function is calculated from an asymptotic expansion

$$I_n(x) = \frac{e^x}{\sqrt{2\pi x}} \left[ 1 + \sum_{r=1}^{\infty} \frac{\left(\frac{1}{8x}\right)^r \left(2r-1\right)^2 - 4n^2\right)}{r!} \right]$$

and otherwise

$$I_n(x) = \sum_{r=0}^{\infty} \frac{\left(\frac{1}{2}x\right)^{n+2r}}{r! (n+r)!}$$

In both cases the summations are restricted to either 30 terms or until a particular term is found to be less than  $10^{-6}$ .

## q. Routine REGFAL

This routine is used for the iterative solution of equations of the form f(x) = G.

## Formal parameters are:

STEP	increment	in variable	×	when	looking	for a	root
------	-----------	-------------	---	------	---------	-------	------

FUNC subroutine name which when called returns a value of 
$$f(x)$$
 for a given  $x$ .

The routine increases the value of x by STEP (or 2\* STEP if the initial value of  $|f'(x)| < \frac{1}{2}$ ) until a change of sign of f(x) is detected. Let the values of x and f(x) on either side of the change of sign be  $x_a$ ,  $f_a$  and  $x_b$ ,  $f_b$  respectively. A linear interpolation gives:

$$x_{c} = \frac{x_{a}f_{b} - x_{b}f_{a}}{f_{b} - f_{a}}$$

and the function is evaluated to give  $f_c$ . If  $f_a$  and  $f_c$  have the same sign then new values  $x_a^i$ ,  $f_a^i$ ,  $x_b^i$  and  $f_b$  are assigned as

$$f_b^i = \frac{f_a f_b}{f_a + f_c}$$

$$x_p' = x^p$$

$$f^{\bullet} = f$$

If  $f_{\mathbf{a}}$  and  $f_{\mathbf{c}}$  have opposite sign then

$$f'_{a} = \frac{f_{a}f_{b}}{f_{a} + f_{c}}$$

$$x'_{a} = x_{a}$$

$$f'_{b} = f_{c}$$

$$x'_{b} = x_{c}$$

and the process is repeated by calculating a new value of  $x_c$ . The process terminates with  $x_c$  as the root when  $\left|x_a^t - x_b^t\right| < \epsilon$  or  $f_c = 0$ .

# r. Routine PLGRP

This routine calculates the structural and internal pressure response for the intermediate frequency, panel group case. Steps in the procedure are:

- (1) Calculate the mass of one panel and one stringer
- (2) Set structural and geometrical constants in arrays AIN and SAB.
- (3) DO loop with loop variable M (= 1,2 and 3) controls the number of half waves between frames.
- (4) Set starting frequency to W2 and call routine PANLNO to calculate the number of panels in a group depending on the correlation length and also the frequency OMEGL at which the number in the group reduces.
- (5) DO loop with loop variable I to calculate the natural frequencies of the panel group and the contribution at each frequency to the response. Routine FLATTX is called to calculate natural frequencies and modes.
- (6) Calculate mode shape squared in PHISQ by summing over the individual panel mode shape squared in DO loop which terminates on label 80; see Equation (5.83).
- (7) Calculate structural response summation terms for the frequency range up to OMEGL. Joint acceptance squared is calculated by calling routines

JNSQGR,JMSQBL and JMSQRF. Frequency is incremented by  $2K \star DELX$  where k is the octave number starting from W2.

- (8) When frequency exceeds OMEGL calculate new number of panels and continue from (5). When the frequency exceeds W3 the outer loop terminates.
- (9) The final section of the routine calculate the internal response as in routine PLRESP, using REGFAL to calculate values of  $\omega_{\rm mn}$  and  $\alpha_{\rm mn}$ . Summation over M1 and NS1 modes is controlled by a pair of nested loops; the same frequency values are used as those calculated in (3) and stored in array FREQ.

## s. Routines FLATTX, TMVRSA, FORMTX, DETMTX, MODFLT, SPASET and COEF

This group of routines calculates panel group modes and natural frequencies for the structural configuration outlined in Section 11-2c. by solving Equation (2.48).

## Formal parameters throughout are:

AKI	value of k returned for the natural frequency
AK2	value of k <sub>2</sub> returned for the natural frequency
FREQ	starting value of frequency search in c.p.s. The calculated natural frequency is returned in this parameter on exit.
DFREQ	increment in frequency (c.p.s.) when searching for a natural frequency
NST	number of incremental steps to be covered in the search for a natural frequency
NSPA	number of panels in the group
М	number of half waves between frames
AIN	array containing panel geometry and structural constants, set by calling routine
SAB	array containing stringer geometrical constants, set by calling routine
NFL	indicator whose value on exit indicates whether a natural

frequency has been found (0 for no frequency found, 1 for successfully finding a natural frequency)

NMAX 8 + (2 + NSPA + 1) - 7

value of the determinant (Equation 2.48)) for a given IDET frequency expressed as DET \* 10.0IDET

two-dimensional array obtained after back substitution in the frequency determinantal equation when a natural frequency is obtained in order to obtain the modal coefficients A<sub>1</sub>, A<sub>2</sub>, A<sub>3</sub> and A<sub>4</sub> for each panel.

The routines are used as follows:

X

FLATTX calculates structural and geometrical terms from AIN and SAB and stores them in labeled common arrays STR and STOR and also PBL and D1.

TMVRSA controls the frequency searching procedure. An initial loop increments FREQ until a change in sign of the value of the determinant (evaluated by FORMTX and DETMTX) is detected or until NST increments have been covered, in which case NFL is 0 and exit from the routine occurs. When a change in sign is detected an iterative procedure, similar to that defined for REGFAL, is used to find a root of Equation (2.48). However, because of the nature of the determinantal function (very large values with extremely abrupt change in sign) the function used in the iteration is the term IDET but made positive or negative according to the sign of DET. This has been found to give very satisfactory convergence and frequencies correct to seven decimal places easily obtained.

FORMTX forms the matrix of coefficients, in labeled common array A, whose determinant is required. The coefficients are determined from the frequency and the structural terms calculated in FLATTX. Routine SPASET is called to calculate  $k_1$ ,  $k_2$  and the terms of the matrix F (Equation (2.46)).

DETMTX is used to evaluate the determinant of the matrix formed by FORMTX by the method of Gaussian elimination. The value is formed as a mantissa and exponent (power of 10) because of the large numbers encountered.

MODELT carries out the back substitution in array A in order to obtain the modal vector. Routine COEF is called to calculate the values of the coefficients for each panel which are returned in array XCOEF (equivalenced to part of A since the latter is no longer needed).

## t. Routine PANLNO

This routine calculates the number of panels in a group, depending on the maximum correlation length for the three excitation types. Correlation lengths are calculated according to Equations (4.23) for boundary layer, (4.49) for jet noise and (4.56) for reverberant field.

## Formal parameters are:

OMEGA	frequency in radians/sec.
OMEGL	frequency at which the panel group is reduced by 1 panel
N	number of panels in a group.

The minimum value of  $\,N\,$  is 3, in which case  $\,OMEGL\,$  is  $\,W3\,$  and the maximum value has been chosen as  $\,10\,$  because of storage limitations.

#### u. Routine JNSQGR

This routine calculates joint acceptance squared for the panel group in the circumferential direction to boundary layer noise, jet noise and reverberant acoustic field.

## Formal parameters are:

OMEGA	frequency in radians/sec.
AK1	k <sub>1</sub> as defined by Equation (2.36)
AK2	k <sub>2</sub> as defined by Equation (2.36)
XN	number of panels
UCV	boundary layer convection velocity
XJNBL	joint acceptance squared for boundary layer
NINIX	joint acceptance squared for jet noise
XJNRF	joint acceptance squared for reverberant field.

Joint acceptance squared is evaluated by numerical integration using the trapezoidal rule. A total of sixty stations across the panel group is used. In matrix notation the expression for joint acceptance calculated numerically may be written

$$J_{n}^{2}(\omega) = \frac{1}{(m-1)^{2}} \left[ \phi(x_{i}) \right] \left[ c(\omega, x - x^{i}) \right] \left[ \phi(x_{i}^{i}) \right]^{*}$$

where  $\phi(x_i)$  is the mode shape evaluated at m stations,  $x - x^i$  is the separation distance and \* means the transpose.

 $\left[ \varphi\left(x_{i}^{*}\right) \right] \text{ and } \left[ \varphi\left(x_{i}^{*}\right) \right] \text{ are column vectors and } \left[ c \right] \text{ is a square matrix af correlation coefficients for separation } x - x^{*}. \text{ The first and last terms of } \varphi \text{ are divided by 2, as required by the trapezoidal integration rule.}$ 

Correlation coefficients are defined for the three excitation environments by Equations (4.12), (4.45) and (4.54). Joint acceptance is evaluated by forming  $[\phi(x)]$  and one column of [c] at a time; a pair of nested loops are used to carry out the multiplications and summations in forming the matrix product.

### v. Routines TRLSS, ACTREA, AIRGAP, SEPTUM, PORBLT, and PANEL

This group of routines calculates the transmission loss due to the acoustic treatment applied to the interior wall of the fuselage.

Formal parameters throughout the group are:

RZŢ	real part of acoustic terminal impedance
XZT	imaginary part of acoustic terminal impedance
Κ	layer counter (i.e., the $k^{th}$ treatment layer from the outer side)
I	porous blanket layer counter (i.e., the i <sup>th</sup> porous blanket layer from the outer side).

TRLSS is the control routine for calculation of transmission loss. A loop with loop veriable ICOUNT sets frequency OMEG for each value of the FREQ array and an average value of transmission loss for varying incidence sound waves is calculated from Equation (6.2) using a Simpson rule numerical integration procedure for which routine SMPINT is called with ACTREA as a routine to evaluate transmission loss.

After a value of transmission loss due to the acoustic treatment has been determined the noise reduction due to internal absorption is calculated according to Equation (6.26). The appropriate value of absorption coefficient is determined by interpolation in the table stored in array ABSCOF; the frequency intervals are given in 2b. ATL due to acoustic treatment is calculated by subtracting from the total TL that due to the skin alone, treated as a single panel.

ACTREA is the routine used to control the evaluation of  $\bar{\tau}$  from Equation (6.6). The formal parameters X and FX represent values of P (input) and  $\tau$ - $\frac{1}{2}\sin 2\theta$  (return). For each layer of acoustic treatment for which an indication is stored in array NLRS an appropriate routine is called to evaluate input impedance, given a terminal impedance, and complex pressure. After each layer has been dealt with, including the skin, the value of  $\tau$  is calculated from the overall pressure ratio. The initial value of terminal impedance is set at  $\rho c$ .

AIRGAP calculates the input impedance and pressure ratio across an airgap (part of acoustic treatment) according to Equations (22) and 23 of Appendix IV.

SEPTUM calculates the input impedance and pressure ratio across a septum layer according to Equations (5) and (6) of Appendix IV.

PORBLT calculates the input impedance and pressure ratio across a porous blanket according to Equations (15) to (20) of Appendix IV.

PANEL calculates the input impedance and pressure ratio across a panel (considered as part of the acoustic treatment) according to Equations (2) and (3) of Appendix IV.

### w. Routine JTNSE

A STATE OF THE PROPERTY OF THE

This routine calculates the sound pressure level at a point on the aircraft fuselage allowing for scattering and pressure doubling. There are two entry points, used as follows:

Entry point JTNSE. The actual parameter in this case is the distance from the forward end of the fulselage at which the s.p.l. is required. The near field sound pressure is calculated according to Equation (4.28), and using Figures 26, 27, 28 and 30 for a range of 9 octave band center frequencies starting at 26.3 cps routine LOGINT is used to interpolate in the tables representing Figures 26, 27 and 28 routine DIRECT is used to calculate the directivity function by interpolating in a table representing Figure 30. It should be noted that the position down the fuselage is controlled by a maximum of 5 stations read from input cards, and an angular position around the fuselage, (i.e. al! stations are at the same angular position). The program accepts two engines on each side of the fuselage.

After calculating the free field sound pressures (and forming the summation if there are two engines per side of the aricraft) the pressure levels and frequencies are printed, and the sound pressure level on the fuselage for each octave and each jet segment is calculated from Equation (4.35) if the distance from the jet to the fuselage exceeds three jet siameters. The summations defined by Equation (4.36) are carried out for 13 terms and routines BSSLJ and BSSLY are used to determine Bessel functions of the first and second kinds respectively.

If the distance from the jet to the fuselage is less than three jet diameters the sound pressure is calculated according to the Equation (4.37). Results are printed for the nine octave band center frequencies.

Entry point JTSPL. The actual parameter in this case is frequency in cps. The pressure level (in dB relative to 0.0002 dynes/cm<sup>2</sup>) on the fuselage (at the current position) is obtained by linear interpolation in the table of sound pressure levels calculated at entry point JTNSE.

Entry point OUTPIN. This entry point produces the printing of the input data as described below in Section 6.

### x. Routine DIRECT

This routine is used to interpolate in the table representing the directivity function in Figure 30.

Formal parameters are:

ANGL angle  $\theta_i$  in degrees

X number of wavelengths downstream from nozzle of the

source.

RESUT directivity function returned on exit.

Tabulated values correspond to those shown on the curves, with the independent variables taking the same values, i.e.  $x/\lambda_0$  starts at 0.4 and follows a logarithmic increase.

Angle  $\theta_i$  has values 10, 40, 80 and thereafter increments by 10 up to 160. The two way interpolation procedure first of all determines that the independent variables are within the range abulated; if this is so then interpolation in the  $x/\lambda_0$  direction is qua-

dratic, to give two values of  $f(\theta_i)$  for the given X corresponding to the tabulated  $\theta_i$  which lie either side of the value of ANGL. Linear interpolation between the two values of  $f(\theta_i)$  then gives a value to RESLT for return to the calling program.

If either of the independent variable values provided by ANGL and X are outside the tabulated range then the value of  $f(\theta_i)$  on the edge of the table nearest to the out-of-range variable is assigned as the interpolated value for that direction.

If a different table of values for  $f(\theta_i)$  is provided then  $x/\lambda_0$  and  $\theta_i$  must have the same starting value and increments as described above.

### y. Routine LOGINT

This routine is used for interpolating in the tables representing Figures 26, 27 and 28.

### Formal parameters are:

X independent variable value

N table number (1 for Figure 28, 2 for Figure 26, 3 for

Figure 27, 4 for absorption coefficient)

RESLT interpolated result on exit.

The laybut of the tables is described in Section 2 of this Appendix. Interpolation is quadratic in the logarithmic X axis, and if the value of X is outside the tabulated range the value in the table nearest to X is assigned as the result.

### z. Routine SMPINT

This routine carries out Simpson rule integration and is used by routine TRLSS.

### Forma parameters are:

A lower limit of integration

B upper limit of integration

HI initial step length

S result of integration

FUNC subroutine name, which when called returns a value of the integrand function.

The number of integration steps is calculated from A, B and HI and is made even, as required by Simpson rule integration. A new step length is calculated and the even and odd steps carried out, each time calling the routine FUNC to determine the value of the function for each value of the variable, which is the angle of incidence of sound waves impinging on the structure. The angle of incidence is transmitted via common storage variable THETA and the actual parameter corresponding to FUNC is ACTREA which returns  $\tau$  sin  $\theta$  cos  $\theta$  as the function value. The value of the integral S is calculated from

$$S = \frac{h}{3} \left\{ f(A) + f(B) + 2 \sum_{n=1}^{N/2} f(2nh) + 4 \sum_{n=1}^{N/2} f(2n+1) h \right\}$$

where f(A) and f(B) are values of the function at A and B and N is the number of integration steps.

### α. Routine BSSLY

This routine evaluates Bessel functions of integral order of the second kind.

Formal parameters are:

X argument of the required Bessel function

N order of the Bessel function

BY calculated value of the Bessel function returned on exit from the routine.

The method of calculation is as follows:

 $Y_{i}(x)$  and  $Y_{i}(x)$  (Second kind Bessel functions of orders 0 and 1 respectively) are obtained from a polynominal approximation as described in M.T.A.C. VII, 1957, and values for other orders are obtained from the recurrence relation:

$$Y_{n+1}(x) = \frac{2n}{x} Y_n(x) - Y_{n-1}(x)$$

### β. Routine STRRSP

This routine is used by the response programs to check the values of upper and lower frequency limits and set the initial values of the response summation variables to zero.

Entry OUTP is used to print the results of the response calculation.

### γ. Routine TLCNTL

This routine forms the acoustic treatment transmission loss control program. The input data used by this phase of the calculation is printed and the required values of frequency are generated in array FREQ. Routine TRLSS is called to calculate transmission loss and noise reduction at the required frequencies; the results are then printed.

### δ. Routine JNCNTL

This routine forms the jet noise calculation control program. The required values of frequency are generated in array FREQ and routine OUTPJN is called to print the input data used in the jet noise calculation. For each of the specified positions on the fuselage routine JTNSE is called to calculate sound pressure level as a function of frequency, and routine JTSPL is called to interpolate in this array for each required frequency. Interpolated sound pressure levels and frequencies are printed.

### 5. FORMATION OF THE PROGRAMS

The five separate programs are formed from the routines described in 4. above as follows:

- (1) Low frequency response of total cylinder comprises mutines MAIN, WTANSS, INITL, STRRSP, CYLRES, APPEND, BLNOIS, NATFI, JTACSQ, JMSQRF, ONEFV, REGFAL, BSSLI, BSSLI.
- (2) Intermediate frequency response of panel group comprises MAIN, WTAINSS, INIT 2, STRRSP, PLGRP, PANLNO, JNSQGR, FLATTX, TMVRSA, FORMTX, DETMIX, MODELT, SPASET, COEF, JTACSQ, JMSQRF, ONEFV, REGFAL, BSSU.
- (3) High frequency response of single panel comprises MAIN, WTANSS, INITL, STRRSP, PLRESP, BLNOIS, BSLRT, JABLPL, JARFPL, ONEFV, REGFAL, SSSLI.
- (4) Acoustic treatment transmission loss comprises MAIN, INITL, TICNTL, TRLSS, ACTREA, AIRGAP, SEPTUM, PANEL, PORBLT, SMPINT. In this case routine MAIN is modified to read table ABSCOF.
- (5) Jet noise sound pressure level comprises MAIN, JNCNIL, JTNSE, DIRECT, LOGINT, BSSLJ, BSSLY. In this case MAIN is modified to read tables DIRECT, ACPOW, CORPOW and DOWPOW.

### DESCRIPTION OF THE OUTPUT.

a. Structural - Interior Response Programs.

Examples of the output are shown at the end of this Appendix. In all cases the first sheet of output contains the input data identified by its number in the input parameter table given in Section 2; this sheet also contains the aerodynamic environment constants calculated in routine INITL and the structural and acoustic treatment weight calculated in routine WYANSS.

The second section of the output represents the various natural frequencies, as a function of mode numbers, used in the analysis. These natural frequencies are defined as follows:

- (1) Low frequency total cylinder program The structural natural frequencies for structural modes m, n are printed together with coupled air-structure natural frequencies from Equation (3.30) for coupled modes m, n, s. The generalized mass associated with each mode is also printed.
- (2) Intermediate frequency panel group program The number of panels in the group is printed followed by the structural natural frequencies for modes m, n. For each frequency the modal coefficients A<sub>1</sub>, A<sub>2</sub>, A<sub>3</sub>, A<sub>4</sub> for each panel in the group are also printed.

(3) High frequency single panel program - For each pair of coupled circumferential acoustic mode numbers n and radial acoustic mode numbers s the natural frequency is printed together with the term ω /Rc.

The third section of the output contains the power spectral density ratios of structural and internal pressure response for the required frequency range. Also included is the boundary layer pressure fluctuation power spectral density. The columns of printed results and their units are identified at the head of the first sheet of the output section. The fourth section contains the interior pressure spectral density ratios converted to transmission losses. For the single panel program output Sections 3 and 4 are repeated for windows where these are specified in the input data.

### b. Acoustic Treatment

The first part of the output is a description of the acoustic treatment and the associated input data. Continuing on the same sheet are the results as described in the heading. The transmission losses through the fuselage wall with and without acoustic treatment are calculated and the difference represents the effect of the acoustic treatment. The final column contains the noise reduction due to absorption by the fuselage interior.

### c. Jet Noise

The first part of the output contains the input data relating to the jet noise calculation and a reference to the origin of the tabulated functions. Then for each position, up to limit of five, on the fuselage specified in the input data the following is printed:

- (1) nine values of octave band centre frequencies
- (2) free field sound pressure level in dB (relative to  $.0002 \text{ dynes/cm}^2$ ) at each centre frequency, corresponding to the position on the fuselage
- (3) sound pressure level in dB at each centre frequency allowing for the presence of the fuselage
- (4) a linear interpolation in the sound pressure levels described in (3) above for each frequency generated from the input data.

### 7. EXPANSION OF THE PROGRAM

Various program parameters have been given arbitrary values based on considerations of computer storage space. The following is a list of changes which are necessary when expanding the program to deal with extended values of some input parameters:

Soutine CYLRES. If NS1 (input parameter number 74) is greater than 20 dimensions
of arrays WMNS and GENM must be increased to the value of NS1.

- b. Routine PLRESP. If NS1 is greater than 20 dimensions of arrays WMS and ALPHMS m must be increased to the value of NS1.
- c. If the total number of frequency points generated by the frequency controlling input parameters exceed 100 the dimensions of the common storage arrays which hold the structural-interior response ratios, acoustic treatment transmission losses and interpolated jet noise sound pressure levels must be increased accordingly.
- d. If the tabulated functions described in 2 b are changed and exceed the array sizes given there the array dimensions must be increased accordingly, and also the input instructions must be amended to read the extra terms.

IPPUT DATA (IN THE CROER LISTEC IN APPENDIX II OF AFFOL-TREGU-2) CONVERTED TO FT. LO. SECOND UNITS,

12 , 22E - 05	*	36 1,006 00	4.30E-08
7 1 2 3 4 5 6 7 8 8 9 10 11 12 10 12 10 12 10 12 10 12 10 12 13 10 13 10 13 10 13 10 13 13 13 13 13 13 13 13 13 13 13 13 13	21 22 23 24 .653 1,125 ,617 0	29 30 31 38 33 34 39 36 9	37 36 39 40 41 42 43 44 45 46 47 46 17 48 48 47 48 48 47 48 48 45 46 47 48 48 48 48 48 48 48 48 48 48 48 48 48
3,325.09	128	<b>*</b>	3000
6.40F.03	20 40 40 40 40 40 40 40 40 40 40 40 40 40	33	20 45 60 0000
5,05E=05	**	<b>4</b>	.906.07
7 6.78E=05	81	31.	1120,0 1
4,42E-04	81 81	80	42 2,386=03
3,00 E-03	<b>.</b>	Ф ©	390,0
4.	3, 33k-03	2	ç°
7,000	<b>6</b> 7	Ph CO Og	200.0
5.42	14 1,096•04	<b>*</b> •	36
90,0	2,176,08	<b>5</b> , 0	000
ITEM AUPBER VALUE	17EW NUMBER 13 14 15 16 17 18 19 28 VALUE 2:17E+0# 1,09E+04 0 3,33E+03 0 0 0 8	17EF AUPUER 25 26 VALUE 0 0	ITEM AUPBER Value

2. #22 25 CO	9,1
•••••	•
REVACIDS AUMBER FOR CVI, AUFR REVACIDS NUMBER FOR PARE, HOUNDARY LAYER TAICKARSW FOR FARE, VYARIC PARSSURE WIFEL FASS STRUCTURES WIFEL FASS STRUCTURES	

SAMMLE OUTPUT - FIRST PAGE COMMON TO STRUCTURAL-INTERIOR RESPONSE PROGRAMS

MATURAL FREGUENCIES IN CYCLES/SECOND FOR SHELL NOGES IN AND M

The second of the second representation of the second seco

PRESENT PRESENT ALL ALL ALL ALL ALL ALL ALL ALL ALL AL	SECOND CONTRACT CONTR	SHELL FREGUENCY 415,432		SHELL FREDUENCY 413,445		SOR'DIE AUROCESES SIN'ROS		WEELL PRECERTY AND. 50%	284 286 00-90.40 286 00-90.40 286 00-00
 	OBERTAL OF STATE OF S		COUNTY OF THE COUNTY OF T	"	SALP CONTRACTOR CONTRA	•	CONTROL CONTRO	n •	COCHEC, 600,004 040,000 040,000 040,000 040,000 040,000
•		• •		•		•		e *	

SAMPLE OUTPUT - NATURAL FREQUENCIES AND GENERALIZED MASS FOR CYLINDER

and de company and the

RESPONSE RESULTS FOR TOTAL CYLINDER CASE

COLUMN 1, FREGUENCY IN CYCLES/SECOND,

COLUMNS 2, 3, AND 4 ARG MATIOS OF AVERAGED STRUCTURAL MOTION PSO TO THE EXCITATION PRESSURE PSD FOR BOUNDARY LAYER,
LET HOUSE AND REVERBERANT ACOUSTIC FIELD RESPECTIVELY, UNITS ARE FIX-X/(LG/IT++2)-+2)

COLUMNS S. 6. AND 7 ARE NATIUS OF INTERNAL PRESSURE PSD TO EXCITATION PRESSURE PED FOR SOUNDARY LAYER, JET NUISE, And neverbenant acquestic field medpectively.

COLUMN 8, HOUNDARY LAYEN PRESSUME PSD IN (LW/FT002) 002/MAD, PER SECOND

## RESPONSE

1000	70/ 1770	45/4745		827 14148	98 (107.108	46194	ā
10,000	1,5772448=09	4,754014k-06	1,3149196-87	9.649044.9	2, 3699654-01	4.040000-01	1,0743756-04
11,000	1,7408116-09	3,642796E-0A	10-309655-17	1,1946746-02	2 . 6385934 - 6X	9,4975616.81	1,0750446-64
12,000	1,9761518-09	3, V99147E-08	1,6056334-07	#0-3640844 N	4,99854411-05	2,4013976 90	ての - 単の がわせんの * ゼ
13,000	2,297272±-09	4,24#3voh+0n	1,6353996-07	1,1628245+01	2,156432k 00	+, H+0349E 0+	1,0748806-44
14,000	2,7687976.09	4,6641568-03	2,1450641-07	2,2939796 01	3.064288£ 02	1,7037605 69	1.0747446-04
19,000	3,5067066-39	5,337720t-08	2,666266E+D7	2,6927616-01	4,0064406 00	2,046229E 01	1.074206E-94
14,000	4,7870026-09	6,424807E-08	5,487992b-07	1,2836776-05	1,728869k 08	+,379160E 89	1.6741696-64
17,000	7,346497k-09	6,180798k-08	>, C626566-07	1,3479206-01	1,523276h 00	9,4639466 90	1,8741216.04
16,009	1,389061k+08	1,144929k-09	8,932659k-07	2,7525386+01	2,2670134 00	1,7699566 01	1.0740756-64
38,046	3,9299692-08	2,44971116-07	2,336418E-06	1,320512E 00	0,2331616 08	7,4923986 81	1,0746246-04
20,000	9.6094476-08	4,992550t-07	5,7429926-04	1,1898406 81	6,109766k 01	7,135230R B2	1,0730746.44
22,000	1,714426-48	1,7889436-07	2,4657446-04	2,7950436 00	2,917533k 01	4,4212936 62	1.8746686.84
24,000	40-468846D, D	5,944912k-07	6.436741E-DA	1,244073E 00	1,4866592 01	2,5010478 02	1,073741E-84
26,000	6,616740k-09	6.488845k=08	9,1462496-07	4,2445476-01	4,1547686 00	S,034519E 61	1.0736006.04
20,000	1,4256096+46	1,0028456-07	1,2944176=06	2,1419406 01	1,6990914 02	1,9691666 03	1,073466.04
30,000	6,121A23E-09	3,4177116-08	5,84682TE-07	5,7971246.01	3,2141074 00	5,4065126 01	1.0 7331 2E-04
32,000	1.690ABB-69	1,619988E-09	1,6310766-07	1,1181646.01	9,0484088-01	1,0791216 01	1.0731486-84
34,000	V,934219k+10	90-4868468.5	E JANNORE-DA	3,6921466+01	1,4762316 00	3,4674226 01	1,072974E-04
34,000	9,419574ce10	2,9764136.09	6,201577k-08	4,0859546.63	1,2911746 00	2,4002056 01	1,0727896-04
30,100	1,454805b=09	3,6846601-09	7,4524096.08	1,4248096+61	3,0292176=01	4,4687936 00	1,0725936-84
40,000	J, 8245276+09	5,0865/2k-09	1,7832338.07	6,1459976-01	6,2066974-01	2,4740715 41	1,072387E-04
44,000	2,4604802-09	7.400573k=09	1,6827694.07	5,1413536+01	1,5464046 00	3,6341046 01	1,0719446-04
48,000	1.021413K-U9	6,4372606+09	1,6805528+07	1,579446E 00	4,840649£ 00	1,2487966 02	1.871498E-04

SAMPLE OUTFUT FOR TOTAL CYLINDER RESPONSE

ROIE REDUCTION OF STRUCTURE IN DO

FOR BOUNDARY LAYEN, JET WOISE AND ASVERBENANT ACOUSTIC FIELD RESPECTIVELY.	54.	•••	90°			64. Ga	96.04				86,12	84 an		99.7 Val		70.40		50.61	20° 120 1		P-1	(C)	#20.09	•20,47	00 to 10 to		60°018	- A-10-10		\$ PT •				100 00 00 00 00 00 00 00 00 00 00 00 00	F6.4.				• •		<b>**</b> 9	10 To	P. G. G. P.		A. 1	15,92
LAYER, JET WOTHE AND AL	97.0			10 m 4 m 4 m 4 m 4 m 4 m 4 m 4 m 4 m 4 m			10 · 10 ·	4 h		4C-110	47.40	COLUMN TO SERVICE SERV	10°E	1012	7		•	-1.69	K-1-0-1				101	50.40	44.10	66.0°	.2.0	# 60 P		60.1	29.01	7 0 0	100	A BOOM O	200		711			000	94.9		W C		90 of -	7,56
FOR BDUNBARY I	20.13	19.22	10.07	47. 47.	10001	26. R	99.0	9.6	4,49	.1.02	10.7	67'710	2	16.5			3.50	5	£7'7.	6,0				7	×	7.33	20.2			99.4	66.7		07.7	2	10.50	97.78	A	10.10		27,53	76.2	20,	76.17	26.28	20.00	41,22
COLUMN 1, FREDURNCY IN CYCLES/BEGGNU, COLUMNS 2: 3: AND 4 NOINE MEDUCTIONS	50.01	00 1	C - C - C - C - C - C - C - C - C - C -	93+94		22.00	07.64	00 · 6 · 6 · 6 · 6 · 6 · 6 · 6 · 6 · 6 ·			23	67.98	0 7 0 0 0 0 0 0 0 0 0 0 0 0 0 0 0 0 0 0				777	07:44	07.07					03.00	63.00	07.70	D		207.44	D - 804	07 .				OD STORY						00.469	07 087			ロコ、マナマ	E>"067

SAMPLE OUTPUT - TOTAL CYLINDER NOISE REDUCTION

SAMME OUTPUT - COUMED ACOUSTIC NATURAL FREQUENCIES FOR SINGLE PANEL CASE

# RESPONSE RESULTS FOR SINGLE PANEL HETMOD

THE PROPERTY OF THE PROPERTY O

COLUMN 1, FREDURNCY IN CYCLES/SECOND,

The state of the s

COLUMNS 2: 5: AND 4 ARE MATIOS OF AVERADED STRUCTURAL MOTION PSD 10 THE EXCITATION PRESSURE PRO FOR BOUNDARY LAVER.

COLUMNS 9, 6, AND 7 ARE RATIOS OF INTERNAL PRESSURE PSD TO EXCITATION PRESSURE PSD FOR BOUNDARY LAYER, JET HOLBE.

COLUMN F, BOURDARY LAYEN PRESSURE PSD IN (LAFFT--2) -- 2/RAD PER SECOND

			Ť	E STORES			
1000.000	SHUL/8P 6.1709#9h-13	803N/8P 1.1105346-11	1.043249E11	\$PIFL/8P 1,464676E-04	#F1JM/SF #.001922k=63	1,6701476.03	96 4,3679708-99
1025,000	6.1298786-13	8,5496206-12	7,5973946-12	1.0473356.04	1,5845616-03	1,3937646.03	4,2224598.09
000.0461	4,8252136-13	7,6033636-12	4.2033096-19	P.9948506.05	1.5749456-03	1,2044416-03	4.8818498.89
900 6201	5,999631k-13	6,3614066-12	5,0742566-12	6,469407E-05	1,030020£-03	B, 216085k-94	3,9491848.09
1100.000	2,7438914-13	4,9600814-12	J.SE46226-12	6,5627346.05	1,1649426-03	40-3684417 B	1,0132496-09
1129,000	2,2264874-13	4,2064006-12	3,1361496-12	3,749518E-09	7,0796136-04	9,279795£=04	3,6696148+09
1150,000	2,2924948-53	3,0573036-12	2,8619416-12	4,7728006+85	0.2368654.04	9,098346E-04	1.562449E+19
1179,000	1,0422728413	J, 367559E-12	2,4442096-12	4,0433166.05	7,0184006-04	5,0687216-64	3,443698-69
1300,000	1,421964#=13	2,7445816-12	2,0414966-12	3,0408256.05	\$.46044E.04	+0.45Venob,+	3.3204748-69
1229,000	1,2746724-13	2,400964E-12	1,8043296-12	2,6336186.05	9,16J068k-04	50-3484E865	3,2164786.09
290,000	1,1933366-13	2,1201496-12	1,632131E-12	2,5846896.09	4,7555176.04	3,4606256-04	3,111170E-05
1275,000	1,1036096-13	1,9686318+12	1,5521276=12	2,246044E.US	4,0065346-04	3,1560706-04	3,00864R
1300,000	0.565059k-14	1.8061206-12	1,5622316-12	2,228A95E-05	4,4240146-04	3,4411466-04	2.90069E-8
1329,000	6,5326912-14	1,0104146-12	1,6258636-12	1,9640796-09	4,4282066-04	3,7441916-64	1,1120406-05
1356,600	7,0724126-14	2,014043k-12	1,6520665-12	1,6804356.69	4,818820£-04	3,946188E-04	8,7205338-05
1375,000	6,3874618=14	2,4349346+12	1,6398576-12	2,0313316.03	9,8970846.04	4,455RB76-04	8.6319402.6
400,000	9.9905306-14	おでも当日ものするの。つ	2,3165016-17	2,3525946-05	7,9985336-04	9,4946266-04	2,5457656-05
1425,000	1,1507098-13	4,6696294+12	2,6948846-12	2,7905396-05	1,1322144.03	7.0267304-04	2,4431886-89
1490,000	1,1823526-13	4,895096-12	2,0511716-12	5,037080E=09	1,2573706-03	40-3487686.V	2,3639926-09
1479.000	1,0791596-13	5,9471128-12	2,1746076-12	2,941379E=09	1,0798035-03	40-3860000 B	2,3069296-69
900,000	9,5945468=14	3,0101826-12	4. \$2000 SE . 1	2,3082896.05	7,2420026-04	5.67470nk-04	2,2330726-65
1525,000	8,456074E*14	2,3789966-12	1,106400E-12	2,347557E=05	6.602408E-04	3,0719626-64	2,1619336-09
009'0661	7,088679E-14	1,9208035-12	6,4612326-13	1,8366276-85	4,9772094-04	2,1924856-04	2,093407E-05

TRANSMISSION LOSSES OF STRUCTURE IN DB

COLUMN 1, FREDUENCY IN CYCLES/SECONU, COLUMNS 2, 3, AND 4 THANSHISSION LOSSES FUR BOUNDARY LAYEM, "ET HOISE AND REVERBEHANT ACOUSTIC FIELD RESPECTIVELY,

7.2	4:						•	:	3	ŗ	2.	7	:				?	7	:			:	•	•	2	3	3	~	-	-		3		•	•		`:	3	•	7.
;							:	:	2	٠ <u>.</u>			-		•	2	:	3	•			;	;	;	•	;	3.	3	:	2	`			3	2			7	-	すん。あり
2.0					-	•		:		3	3	2	2		:		ŝ	3	7			:-	?		7	2		9	9						•	Ž			7	-
0.000	025.4	0.650	0.540	0.00	196				0.0	275 te	300.0	325.0	150.4	, 36		2	22.5	450.0	475.0	800.0	22.0			0,570	2004	25,0	9000	975.0	700.0	725.0	750.0	7.4			200	578,0	0.000	125.0	150.0	1979,00

SAMPLE OUTPUT - TRANSMISSION LOSS FOR SINGLE PANEL CASE

	4.567479	4,222499	4,001949	3.945184	3.013899	1,68981	3,562649	7.443698	3,326174	3.21.0070	3,11117	200000	2,900095	2,012400	2,720533	2,631546	2,545793	201190.	2,343592	2,306425	2,233072	2,1-1-63	2,093467	2,027567	00000	1,902552	V60048.4	1,7900//	060182°	5.06.0° C	1,02621	7,27,27	1,931,907	POPOST .	1,442396	1,400024	1,35915	1,319741	1,261713	1,245621	
	3,1244176-06	2.0291206-04	1, 3721936-06	9.940F30ts 07	1,1616546-06	6,961169E-07	7,4717416-67	6,9366776-07	6,44276E-87	7,0004696-07	6.2373838-07	9.249175E-07	1 . 4 7 4 4 4 6 K - De	2.108770K=06	10-2125044	2.0041E41-04	1.700526E-04	1.912ng4x-04	2.254044E-06	サロールノロッのかだ。 的	1,4443676-06	7.110000 - 06	7,3924196-07	6.666284E-07	4,91720AE-07	7,489676E-07	5,4716416-07	7,256437E+07	9.954976t-07	4,0775356-07	10-20-15-01-1-1-1-1-1-1-1-1-1-1-1-1-1-1-1-1-	LO-MENUTED OF	20 - 40 T 32 S E = 0 X	2.408605E-07	2, 392FE9E - 07	2,9649551-07	3.149.430 k= 07	3, 35 66 47 F-07	2,754410E-07	2,973646E-07	
	8.671823k-07	サロー 場の行む人となって	1.027657k-06	1.234384E+04	1.5101524-06	0,743572k=07	9.078A01E-07	7.674006E-07	7,4687476-67	7,3127706-07	8.247629t-07	O NO BENEVILLO	7, 499969E-06	2.094844H-06	2.4348491-06	2,0093646-06	1,7566016-06	2,267138t-06	20-900000000	4,1545396+06	2,862726E=86	2,2490625-06	1,457644E=06	1,2023576-04	7,9325966-07	7,4957746=67	5,900726E=07	6.444105E-07	4,7723625-07	トローリイのハトサーサ	3,0678214-07	POTENTO PROPERTY	V0-24040010	3. 568675E-07	3,5251196.07	トジャンのコンロのマ・マ	4.748484E-07	5,174922E-07	4,814949k-07	人の七川の内の行のす。中	
	2,607A34E.08	1 595929E. 18	1.257095E-06	7.256981E.00	d. 4610376.09	4,964107E-09	7.467050E=00	9,1340206-09	7,266936E-09	5,44808BE-09	6.659241E-09	7,945757E-09	1,2635476:06	1.625F¥6E=08	2,1134526+08	1 790622E=08	1,6483526-04	1,0393646.08	2.164R04E-DA	1.9430726-06	1,1489445-08	8,532119E-D	\$ 468677E-DP	4 932370E-09	3,746722E-09	4,440859E-19	4,728577E-00	0 - 40704 4E - DO	4,8833656-09	00-30-00-0	4. 638929E - 09	2,4537176-09	1,9364216-09	%,028082E.09	2,0840666-09	2,7914176-09	J. 1303105-09	3, 327424E . 09	2,657489E.09	2,342288E . 09	•
	4.1839766*13	2 70564 Shank	1.937482E-13	1.476442E=13	1.1697076-13	4. 959732E-14	6.728603E-14	7, 4964566-14	7,700L78E-14	7,913213E-14	0.0140706-14	1,0907116-13	1,5162646-13	2,197700E-13	2.4646866-23	1.9460916-13	1, 700409E=10	1,725796-13	2,11,37026-13	1.9861.376-15	1,440646-15	9.6637956-14	6.0140486-14	5, 3231,526-14	4,628007E-14	4,525140E-14	4,924964E-14	5,342202E+14	4,820068E-14	J, 706682E-14	2, 8306156-14	2,2999461-14	2,010459E-14	1,892426E-14	1,9244516-14	2,1640728+14	2,3557746014	2,4109B5E-14	2,137665E-14	1.004816E-14	•
STRUCTUME,	1.461003km13	F	#	何の日本の一名の行動		1.247400k-13	1.045776E-13	9.0611168-14	41-104-10F-14	6,161313k-14	8,822034E-14	1,07/4316-19	1,498847E-13	2.179008E-13	2.4504498.43	1.9872786-13	1.79u687t-13	2.184714k+15	4.104239E+13	3. 422986kv13	2.455763E-13	1.914916E-13	1.315032E+13	9.5981316-24	7.4660396-14	6.142345E-14	5.316374k-14	4,74/9006-14	4.193550E-14	4,9440976-14	3,1179826-14	2,8457876-14	2,7071806-14	2,6975226=14	サイニ 日本ののののので	3.1459464-14	6.3644B7E1A	5.761084E-14	3.507615E=14	5.104040E	
SOLUHA BEFINITIONS AS FOR STRUCTUME	3. 401427ka15	90 - 4000 CAR	20140700F	8-1404V4C	A	7.110723k-16	6. 30.531.6E+10	9.916903E+15	5.911069k-16	6.325790k-16	7. 3394476-15	9.370029k-10	1,321692k=15	1.9028476-15	2,124007t=15	1.7744596-15	1.680260E-19	1.919663Ea15	2.02264Bks15	1.720550ce15	1.1601111-15	7.375998E+16	D-042349E-16	3.037393E+16		3.860997e-16	4.2501418-16	4,7754616-10	4,8296956-16	3,0910256-10	2,24333BE+16	1,774089E-16	1,562663k-16	1.530017#-10	1.6761966-16	1.980927k-16	2.343999E-10	2.416908E=16	2.062475E+34	1.642572E+16	•
COLUMN CEF	2000	200				000	1150.000	1175.000	1208.600	1229,000	1250.000	1279.000	1300.000	1329,000	1390.000	1379.000	1400.000	1429.000	400.000	1474,000	1566.000	1525,000	1994 . 100	1575.000	1600.000	1625.000	1656.000	1679,000	1700,000	1727,000	1750,000	1779,000	1600,000	1625.000	1650,000	1675. 000	1904.000	1925, 600	1950.000	1975.000	

THE REPORT OF THE PROPERTY OF

		41194		4.6+23		4. 7295		7,6137			4044.4	
		. S.		* 2¥		£2 =		×			£2 =	
FUR PANEL GANUP	15jûgele CoPoSo	4,993;	-0.3291465E-02 -0.4764639E-02 -0.3338699E-02	5.0116	-, 334, 625F+(2 -, 4617F+1F-C2 , 3253223E+12	6.1925	2. 96683.51-04 (-3194236-03 -0.43741316-03	7. 8444	4471715-03 10491995-02	15 Jec. 5 Calleson	62,4363	A4 2.29E3282E-12 3.4174396E-12
NATURAL FREDUENCIES F	1 01 9U	. IX	S	¥	5 6.37293596-72 43541.35-02 1.3.872586-72	* 17	S A3 C.4710825E-f4 -i.2992613E-C3 0.3419686E-C2	Ž.	6 4346525E-63 6-9623453E-63 6-5637126E-63	3	ž	\$ A3 \\2266582F=(2 -(.3198385E=(2 '.2266522E=C
NATURA	IN GAÜUP 3	. 134,568	CDEFFICIENTS A2 C=3C41326-C2 C=4353226-C2 U=3C395226-(2	* 136.233	COSFFICIEN A2 2-3C565GFF L2 -0-4274631E-72 -3C11364E-L2	= 141.76	CCEFFICIEN A2 C-89737718-C4 C-4C547538-C2	* 348. A05	COEFFICIEN A2 A2 A2 A2 L-136475E-(3 C-167172E-C3	PAVELS IN GRJJP 3	. 157,221	COEFFICIES A2 1.22514418-C2 1.321514118-C2 0.22456726-C3
	YUMBER OF PAYELS	NATURAL FREQUENCY	41 -0.3:87635-02 -0.4413398E-02 -0.3131550E-02	NATURAL FREQUENCY	A1 	NATURAL FREGUENCY	A1 - C = 30464254: - 74 - 13464254: - 13 - 13464254: - 13	NATUHAL FREGUENCY	A1 C.7132459F=.3 = -0.105835E=.2 C.7071579E=.33	NIMBER OF PAVELS	NATURAL FACOURACY	41 
	-			7		<b>~</b>		•		7		
	• #	•		•		Z		2		x .	2	

# SAMPLE OUTPUT - NATURAL FREQUENCIES FOR PANEL GROUP

THANSMITTING STRUCTURE .

/ff**3, T**3, /fT**2,	
172,00 LB, 1,00 LB/F1 1300 1300 04 LB/	
AT DENSITY OF LY SECONSES SEFECTION OF THE SECONSES SECON	
CHES AND MEIGHTONES, WEIGHTONES, WEIGHTONES	. DAG . 42/FT
THICKNESS , U40 INCHES AND MEIGHT DENSITY 172,00 LUFF10-3, 2,000 INCHES MIDE, THICKNESS 3,000 INCHES MEIGHT DENSITY 1,50 LB/F10-83, SPECIFIC FLOW MFFISTANCE 3000,00 LB SECOND/F10-83, FORMSITY 1,000 MEIGHT DENSITY 1,500 LB/F10-83, COLFFICIENT OF ELSTICITY OF AIR 3,000 E 04 LB/F10-82, CHINER COLFFICIENT OF ELSTICITY OF AIR 3,000 E 04 LB/F10-82, CHINER COLFFICIENT OF ELSTICITY OF AIR 3,000 E 04 LB/F10-82, CHINER COLFFICIENT OF ELSTICITY OF AIR 3,000 E 04 LB/F10-82, CHINER COLFFICIENT OF ELSTICITY OF AIR 3,000 E 04 LB/F10-82, CHINER COLFFICIENT OF ELSTICITY OF AIR 3,000 E 04 LB/F10-82, CHINER COLFFICIENT OF COL	
AIR DAP POROUS BLANNET TE SP SEPTIN	

FULIVALENT INTERIOR ABSURPTION AREA \* 5000.0 SQUARE FEET,

# GESULTS .

UTEH SKIN),	
אם כואכו חחואם ס	
H INCIDENCE SOU	ON TABLE ATED AT
IN DB FOR RANDO IR RANDOM INCIDE	BSORPTION HASED
ND. S OF STRUCTURE N ONLY IN DB FO	E TO INTERIOR A
COLUMN 1, FREUDLYCY IN CYCLES/SECUND, COLUMN 2, DYFHALL THANSMISSION LOSS OF STRUCTURE IN DB FOR RANDOM INCIDENCE SOUND (INCLUMING OUTER SKIN), COLUMN 3, TGANSMISSION LOSS OF SKIN ONLY IN OB FOR RANDOM INCIDENCE SOUND, COLUMN 4, COLUMN 2 & COLUMN 3,	COLUMN 5, NOISE MEDUCATION IN DR DUE TO INTERTOR AUSOMPTION HASED ON TARILLATED ALGEBRAGE CONTINUES.
COLUMN 1. COLUMN 3. COLUMN 3.	COLUMN 5,

O O O O O O O O O O O O O O O O O O O	97.46
	23,44
	37.60
	P
	,

SAMPLE OUTPUT FROM ACOUSTIC TREATMENT PROGRAM

AUPHER OF ENGINES PER SIDE # 2
LET EXIT DISTANCES FRUM FROMT OF FUSFLAUR # 35,0 FT AND 40,0 FT.
LET CENTER LINES FROM FUSELAUE CENTER LINE # 28,0 FT AND 34,0 FT.

AIRCRAFT FORMARU SPEED a .350,0 FT/SEC.

LET EXIT VELOCITY 3 1850,0 FT/SEC.
TABLES OF OVERALL ACOUSTIC POWEN, NORMALIZED POWER FOR CORE AND DOWNSTREAM REGIONS AND DIMECTIVITY FUNCTION FAOM FIGURES 28, 26, 27, AND 30 OF AFFDL-FR-68-2 UNLESS OTHERWISE SPECIFIED.

A, B, ALL FAEDUFACIES IN THE FULLOWING ALSULTS AME IN CYCLES/SECOND.

	8164,000 141,777 145,747													
	000°,000 140°040 150°,47													
	2016,000 151,293 156,233													
6E1	000 000 000 000 000 000 000 000													
20.0 FEET	504,000 142,474 144,571	8.9,1, (00)		27,74	26.24	9	126,73	24.42	29.47	48.40	56.85	11000	00.00	
FUSEL AGE	252,000 126,474 129,979	40	3 33	-	-	•	<del></del> 0		<del>-1</del>	1 <del>at</del>	<b>~</b>	-1	rd <b>v</b>	•
POSITION DOWN FUSELAGE	120,130 121,900 121,500													
ě	63,000 119,900 117,605	FREGUENCY	e 0	50.0	-07	900	100.0		0.0	20.05	90'8	0,5	9.5	• • • • • • • • • • • • • • • • • • • •
	31,500 112,247 115,247	FRE		-	e4 •	4 -4	-1 ·	4-4	-17	<b>3</b> 74	.76	~	Cu *	7
	FREE FIELD S.P.L (DM) S.P.L (DM)													

SAMPLE OUTPUT FROM JET NOISE PROGRAM

### APPENDIX III

### **DESIGN CHARTS**

In this appendix, a number of simple design charts are presented to serve as a guide for preliminary design prior to detailed calculations. Essentially, the charts provide the necessary data for making engineering estimates of the anticipated fluctuating pressure environments, sound attenuation through various acoustic treatments and the expected noise reduction inside the cabin. Also included are charts which provide data on the weight of damping treatments versus their corresponding loss factors and an abstract from a Military specification for internal noise level criteria.

### 1. THE ENVIRONMENT

### a. Aerodynamic Turbulence

### (1) Overall Level

The overall level for an attached boundary layer is shown in Figure 54 as a function of Mach number. For structural areas where  $p_{rms}/q$  does not follow the relationship in Equation (4.3), the overall level may be determined by use of Figures 55 and 56 which show typical values of  $p_{rms}/q$  at various positions on the aircraft structure, and overall sound pressure levels as a function of  $p_{rms}/q$ , respectively.

### (2) Frequency Spectra

The octave band sound pressure levels are determined from the non-dimensional spectrum shown in Figure 58 after first calculating the boundary layer thickness from Figure 57 and the dynamic head, q, from the relation;

$$q = 0.5 \rho U_0^2$$

where

p = fluid density

and

 $U_0$  = free stream velocity.

It should be noted that in practice the effective boundary layer noise pressures are lower than the measured surface pressures due to the lower structural coupling efficiency (i.e., joint acceptance of the turbulent boundary layer pressure fluctuations). This is accounted for in detail in the computer program and is accounted for approximately in Figure 58 by decreasing the true Octave Band Levels at a rate of 6 dB/Octave below a cut-off

frequency  $f_c = 0.4 \frac{U_0}{\delta_b}$ . The corrected or effective octave band levels are shown

in Figure 58 by the dashed line. The corrected levels will thus provide values of overall noise reduction in reasonable agreement with values measured in the laboratory for reverberant acoustic excitation.

### b. Jet Noise

The jet noise design charts are based on the measurements carried out by Hermes and Smith (Reference 67) for the J57-P21 Turbojet engine operating at 100 percent military power for which the jet exit diameter and jet exit velocity were 1.85 feet and 1920 ft./sec. respectively.

### (1) Overall Level

The overall sound levels for the near field are obtained from Figure 59, which shows the overall level contours as a function of the number of jet exit diameters from the nozzle exit plane.

### (2) Frequency Spectra

To account for the variation in octave band levels with position relative to the nozzle exit, average sound pressure spectra in the near field have been established for the regions identified by the grid shown in Figure 60. The octave band sound pressure levels shown in Figures 61(a) through 61(x) represent typical smoothed spectra for the 24 regions identified by the grid. To allow for intensity doubling at the surface of a structure placed in the immediate vicinity of the nozzle exit plane, the overall sound pressure level should be modified by adding a maximum increment of 6 dB for positions directly opposite the nozzle exit plane.

To account for the change in overall levels for jet engines having different jet exit velocities, the relationship derived by Hermes and Smith (Reference 67) should be used, as follows:

$$SPL_{1} - SPL_{2} = 10n \left[ log_{10} V_{1} - log_{10} V_{2} \right]$$
 (1)

where

$$SPL = 10 \log_{10} \frac{\vec{p}^2}{\vec{p}^2}$$

V<sub>1</sub> = Jet exit velocity for engine 1

 $V_2$  = Jet exit velocity for engine 2

n = Velocity exponent, determined from Figure 62.

The effects of a change in jet velocities on the frequency spectrum are accounted for by simply shifting the peak of the spectrum by the ratio of the jet exit velocities.

### 2. TRANSMISSION LOSS

### a. Single Fuselage Panel

The variation in effective transmission loss of a mass-controlled panel for random incidence conditions as a function of frequency times surface density is shown in Figure 63. The effective transmission loss is defined as relative difference in sound level that would be observed on each side of the panel when it is in place. In general, the transmission losses predicted by this figure lie about 5 dB below normal incidence transmission loss curves. A design chart for single mass-controlled panels, proposed by Beranek (Reference 60), is shown in Figure 64 for use when a reverberant sound field is assumed to act on one side of the panel. The procedure for computing the transmission loss through a panel of thickness h and specific surface density  $\bar{\mathbf{w}}$  is carried out with the aid of Figures 63 and 64 as follows:

(1) Determine the surface density Wn from the relation

$$W_0 = h\overline{w}$$

using the value of w given in the table of Figure 64.

- (2) Determine the effective random incidence transmission loss for a particular value of frequency, f', by reading off the value in Figure 63 corresponding to f'Wa. Plot this point and draw a line of 6dB/Octave slope through it.
- (3) Determine the height, A, in dB from the table in Figure 64 for the particular panel material and construct a horizontal line such that it intersects the 6 dB/Octave line at the point x. Increase the plateau height by 6 dB if the panel area is less than 5 sq.ft.
- (4) Having obtained the point x, determine the position of point y by multiplying by the frequency ratio (i.e., dimension B tabulated in Figure 64).
- (5) Extend the line above point y at 10 dB/octave for the first octave and 6 dB/octave thereafter.

(6) To allow for the change in transmission loss at low frequency due to the combined stiffness effects of the structure and the air cavity inside the fuselage, add the following corrections to the values determined from the preceding steps

Frequency Hz. Cylinder Diameter	25	50	100	200
3 - 6 ft.	15 dB	15 dB	9 dB	3 dB
6 - 12 ft.	12 dB	9 dB	3 dB	c
12 - 24 ft.	9 d3	3 dB	0	0

### b. Incremental Transmission Loss Due to Treatment

The increment in transmission loss due to acoustic treatment may be estimated from the design charts shown in Figures 65(a) through 65(e). These curves are essentially simplified versions of curves computed by Beranek and Work (Reference 62). Where an air gap is present in the system, the incremental transmission loss will depart from the basic mass law trend at the double-wall resonance frequency, which is given by; (References 61 and 68)

$$f_0 = 170 \left[ \frac{W_1 + W_2}{d(W_1 W_2)} \right]^{\frac{1}{2}}$$
 Hz. (2)

where

d = air gap length - inches

 $W_1, W_2 =$  surface weight densities of each wall.

The curves represent the average over the range of air gap thickness and double-wall surface weights indicated by the figures. Two values of specific flow resistance for the acoustical blankets have been chosen as representative of maximum and minimum values encountered in practice, namely 250 rayls per inch (of material thickness) and 25 rayls per inch. Specific flow resistance is defined as

$$R_1 = \frac{\Delta p}{\Delta T u}$$
 c.g.s. rayls/cm. (3)

where

 $\Delta p$  = sound pressure differential across thickness  $\Delta T$  of porous material, measured in direction of particle velocity, dynes/cm<sup>2</sup>

u = particle velocity through the porous material, cm/sec.

ΔT = incremental thickness, cm.

(Note: To convert c.g.s. rayls/cm to c.g.s rayls/inch, multiply by 2.5.)

Two values of blanket thickness are included in each design chart, enabling interpolation to be carried out during design. The density of the septum,  $\sigma_s$ , is assumed to be 0.06 lb./ft? throughout and changes in attenuation due to different values of  $\sigma_s$  are determined

by adding 20  $\log_{10}\left[\frac{\sigma_s}{0.6}\right]$  to the incremental attenuation, where  $\sigma_s$  is the actual surface density of the septum. The double-wall configurations illustrated in Figure 65 are representative for many of the aircraft in current service where the inner wall is very light. Advanced performance aircraft may utilize a heavier inner wall with thinner blanket material for both acoustic and thermal protection. An approximate upper bound to the incremental transmission loss  $\Delta TL$  for configurations not covered by Figure 65 may be estimated as follows

- (1) Estimate the double-wall resonance frequency for using Equation (2).
- (2) For  $f < f_0$ , the incremental transmission loss will be approximately

$$\Delta TL = 10 \log \left[1 + \frac{W_2}{W_1}\right]^2 \tag{4}$$

where  $W_2$  = total surface density of added treatment

W<sub>1</sub> = total surface density of outer skin.

- (3) For  $f = f_0$ , the incremental transmission loss may decrease by 5 to 10 dB below the value determined in Step 2 depending on the damping provided for the panels and the geometry of the air space (Reference 68).
- (4) For  $f_0 < f < 6700/d$  (where d = air gap thickness = inches)

Add 40  $\log [f/f_0]$  to the estimate made in Step 2. This is an upper bound for the increase in transmission loss due to de-coupling of the outer and inner walls above the double-wall resonance frequency.

### (5) For f > 6700/d

The incremental transmission loss may be estimated by adding the random incidence transmission loss given by Figure 63 for the inner wall only. In this frequency range, the incremental loss may exhibit dips due to standing wave resonances within the air gap. These resonances can normally be suppressed by proper acoustic lining of the air gap. The total estimated transmission loss is the sum of the absolute values determined for the single fuselage panel (determined in part 20) and the incremental attenuation due to the acoustic treatment.

### 3. NOISE REDUCTION

Cabin noise reduction may be defined as (Reference 69)

N.R. = dB sound reduction = 
$$10 \log_{10} \left[ 1 + \frac{A}{T} \right]$$
 (5)

where A = Total number of absorption units in the cabin

and T = Total number of transmission units of the bounding surfaces.

The absorption and transmission units are defined by;

$$A = S\bar{a}$$

$$T = S\bar{\tau}$$
(5)

and  $I = 5\bar{\tau}$ 

where  $\overline{\alpha}$  and  $\overline{\tau}$  are the average sound absorption and transmission coefficients, respectively, of the bounding surfaces of the cabin. These coefficients are determined from the relations;

$$\bar{\alpha} = (S_1 \alpha_1 + S_2 \alpha_2 + S_3 \alpha_3 + ----)/S$$
 $\bar{\tau} = (S_1 \tau_1 + S_2 \tau_2 + S_3 \tau_3 + ----)/S$ 
(7)

where  $S_1$ ,  $S_2$ ,  $S_3$  --- are the areas of portions of the boundaries having the same construction and  $\alpha_1$ ,  $\alpha_2$ ,  $\alpha_3$ ,  $\tau_1$ ,  $\tau_2$ ,  $\tau_3$ , ---- are the particular  $\alpha$ 's and  $\tau$ 's for these areas, respectively.

Further,

$$S = S_1 + S_2 + S_3 + ---- = Total boundary area.$$

A design chart relating noise reduction, average transmission coefficient, average transmission loss, and average absorption coefficient is shown in Figure 66. This figure is based on Equation (5) and (6) where the average transmission loss is  $10 \log_{10} (1/\bar{\tau})$ .

Some typical values for the absorption coefficients of various structural items and structuretreatment configurations are listed in Table IV.

The procedure for calculating noise reduction is as follows:

- a. Determine the average transmission losses for the whole structural area under consideration. Using Figure 66 to convert from transmission loss to transmission coefficient, determine an average transmission coefficient, 7, by summing the products of the area and the transmission coefficient for each area and dividing by the total area.
- b. Similarly determine the average absorption coefficient, \(\overline{\alpha}\), by summing the products of the area and the absorption coefficient for each area and dividing by the total area.
- c. Determine the noise reduction from Figure 66 by entering the corresponding values of the average transmission and average absorption coefficients.

For the special problem of estimating noise transmission between adjacent compartments (such as transmission between a baggage compartment and the cabin), an additional computation is necessary in order to establish the effective sound transmission coefficient for this flanking path. First, the noise reduction  $NR_2$  for the adjacent compartment, (2), is determined for the exterior sound field in the same way as outlined above. Next, the transmission loss,  $TL_{12}$  of the sound field within the adjacent compartment to the cabin (1), is determined according to the methods given in Section 2 above. Finally, the total transmission loss is determined by the sum of  $NR_2$  and  $TL_{12}$ . This overall flanking path transmission loss is then included in the overall noise reduction calculation for the primary cabin according to the methods specified earlier.

### 4. THE EFFECTS OF A DAMPING TREATMENT

A further significant point concerning the noise reduction in aircraft cabin structures involves the reduction in resonant responses of the fuselage panels by the addition of damping treatment. Referring back to Figure 64, it should be noted that the finite resonances of the panel have been ignored and have effectively been replaced by a single line of slope 6 dB/octave; in practice, this single line will have discrete resonances superimposed. Since the addition of damping treatment to a bare panel contributes to the noise reduction, it is worthwhile to consider how the additional damping is affected by the geometry and properties of the treatment. The two different types of damping treatment commonly employed in light structures are;

- (i) unconstrained layer treatment consisting of one or more layers of damping material applied to one side of a panel, and
- (ii) constrained layer damping treatment which involves two metal layers and an intermediate layer of damping material.

The effects of three different types of unconstrained layer damping treatment, applied to an aluminum plate, on the combined loss factor are shown in Figure 67 as a function of the weight ratio  $W_2/W_1$ . The surface weight of the aluminum plate is denoted by  $W_1$ , and the surface weight of the treatment is denoted by  $W_2$ . The relevant properties of the three representative damping treatments, namely, loss factor, real part of the complex modulus of elasticity and density, are indicated in the figure.

Secondly a design chart is shown in Figure 68 for the optimum configuration of a constrained layer damping treatment (i.e.,  $\eta_{max}$ ) as a function of; (i) a modified shear parameter ( $\gamma$ ), (ii) the ratio of constraining thickness to basic panel thickness ( $h_3/h_1$ ), and (iii) the ratio of constrained layer thickness to basic panel thickness ( $h_2/h_1$ ). For this particular chart it has been assumed that the real parts of the complex modulii of elasticity for the basic panel and constraining layer are identical and that the shear loss factor of the constrained layer (i.e.,  $\beta$ ) is equal to unity. The modified shear parameter,  $\gamma$ , is defined by;

$$\gamma = \frac{1.03 \, C_n \, E_1}{\sqrt{1 + 8^2} \cdot G_2} \, \left(\frac{h_1}{\sigma}\right)^2 \tag{8}$$

where

a = plate span

E, = Young's modulus for the basic plate.

 $\beta$  = loss factor of the constrained layer.

G<sub>2</sub> = shear modulus of the constrained layer.

hi = basic plate thickness

C<sub>n</sub> = a frequency constant for the n-th mode(tabulated in Reference 70).

Finally, a design chart for the combined loss factor,  $\eta_{\text{max}}$ , of an aluminum plate (treated with a constrained layer), as a function of the treatment weight to plate weight ratio, is shown in Figure 69. The subscripts 1,2, and 3 in this figure refer to the basic plate, constrained layer and constraining layer respectively, h denotes thickness and p denotes density. The value of the loss factor for the constrained layer has again been assumed equal to unity.

The design charts for damping layers are based on refinements to analytical methods developed by Ungar (Reference 71) and Oberst (Reference 72).

### 5. NOISE CRITERIA

The criteria for internal noise levels within an aircraft cabin normally differ depending on the particular location considered and the aircraft mission. The primary objectives associated with the acoustic treatment in a passenger aircraft cabin are to maintain passenger comfort, avoid hearing damage, and interference with speech communication, while retaining privacy and the ability to hear the communication system. For military command and communications aircraft, minimum speech interference levels are a primary concern. Speech interference level (S.I.L.) is defined as the arithmetic average of the octave band sound pressure levels in the octave bands 600–1200 Hz., 1200–2400 Hz. and 2400–4800 Hz. (The octave band levels in the new preferred octave band frequency scale with center frequencies of 1000, 2000 and 4000 Hz. will provide essentially equivalent results.) The required SIL values for effective speech communication are tabulated below at a function of voice e.fort and listener-speaker separation distance. (Reference 73).

TABLE OF MAXIMUM SPEECH INTERFERENCE LEVELS FOR EFFECTIVE VOICE COMMUNICATION – dB re: 0.0002 Microbar

D4		Voice Level (Average Male)					
Distance (fr.)	Normal	Raised	Very Loud	Shouting			
0.5	71	77	83	89			
3	65	<i>7</i> 1	77	83			
2	59	65	71	77			
3	55	61	67	73			
4	53	59	65	71			
5	51	57	63	69			
6	49	55	61	67			
12	43	49	55	61			

As an example of current noise criteria for military aircraft, an abstract from the Military Specification MIL-A-8806 A is attached below.

### ABSTRACT FROM MILITARY SPECIFICATION MIL-A-8806A, 11 July 1966

Superseding MIL-A-8805(ASG), 25 October 1956

### ACOUSTICAL NOISE LEVEL IN AIRCRAFT, GENERAL SPECIFICATION FOR

This specification has been approved by the Department of Defense and is mandatory for use by the Departments of the Army, the Navy, and the Air Force.

### SCOPE

1.1 This specification covers the general requirements for the control of acoustical noise in occupied spaces of aircraft, including the acceptable noise levels and the texting requirements for determining conformance to these levels.

### 2. APPLICABLE DOCUMENTS

2.? The following documents of the issue in effect on date of invitation for bids or request for proposal, form a part of this specification to the extent specified herein.

### **SPECIFICATIONS**

Military
----------

MIL-S-3151 Sound-Level-Measuring Equipment

MIL-S-6144 Soundproofing for Aircraft; General

Specification for Installation of

MIL-1-7171 Insulation Blanket, Thermal-Acoustical

(When requesting specifications, refer to both title and symbol. Copies of specifications may be obtained upon application to the Commanding Officer, Naval Supply Depot, 5801 Tabor Avenue, Philadelphia, Pennsylvania, 19120, Attention: Code 105).

### MIL-A-8806A

### 3. REQUIREMENTS

### 3.1 Acoustical noise levels -

3.1.1 Maximum continuous power – The acoustical noise level in any part of the aircraft (see 6.2.2) intended for occupancy by the crew or other personnel shall not exceed the values specified in Table IA (preferred) or Table IB during conditions of MAXIMUM CONTINUOUS POWER.

TABLE 1. - Maximum acceptable noise level at maximum continuous power

IA.								
	Free	Max . accept-						
Bond			Center	level (db)				
0	ABIC	al l		113				
22.4	<b>.</b> -	45	31.5	111				
45	-	90	63	111				
90	-	180	125	111				
180	-	355	250	111				
355	-	710	500	105				
710	-	1400	1000	99				
1400	-	2800	2000	93				
2800	-	5600	4000	87				
5600	-	11200	8000	87				

IB.					
Frequency bands (cps)	Max. accept- able noise level (db)				
Overall	113				
37.5 - 75 75 - 150 150 - 300 300 - 600 600 - 1200	111 111 111 105 99				
1200 - 2400 2400 - 4800	93 87				
4800 - 9600	87				

3.1.2 <u>Short duration conditions</u> - For takeoff, afterburner operation and other conditions normally not exceeding 5 minutes continuous duration the acoustical noise level in any part of the aircraft (see 6.2.2) intended for occupancy by the crew or other personnel shall not exceed the values specified in Table IIA (preferred) or Table IIB.

TABLE 11. - Maximum acceptable noise level under short duration conditions

IIA.								
	Frequency (	Max. accept- able noise						
	Band	Center	level (db)					
С	verall		120					
22.4	4 - 45	31.5	118					
45	- 90	63	118					
90	- 180	125	118					
180	- 355	250	118					
355	- 710	500	112					
710	- 1400	1000	106					
1400	- 2800	2000	100					
2800	- 5600	4000	94					
5800	- 11200	8000	94					

IIB.						
Frequency bands (cps)	Max . accept- able noise level (db)					
Overall	120					
37.5 - 75 75 - 150 150 - 300 300 - 600 600 - 1200	1 18 1 18 1 18 1 12 106					
1200 - 2400	100					
2400 - 4800	94					
4800 - 9600	94					

3.1.3 <u>Protective helmets</u> – In aircraft in which personnel must necessarily wear helmets at all times and communicate by electronic means (e.g., single place fighter aircraft), the acoustical noise level (see 6.2.2) shall not exceed the values specified in Table IIIA (preferred) or Table IIIB during conditions of MAXIMUM CONTINUOUS POWER.

Table III. - Maximum acceptable noise level with protective helmets or devices

HIA.								
	Fre	Max. accept-						
	Ban	d	Center	level (db)				
	Over	ali		113				
22.4	4 -	45	31.5	171				
45	-	90	63	111				
90	-	180	125	111				
180	-	355	250	111				
355	-	710	500	109				
710	-	1400	1000	106				
1400	-	2800	2000	190				
2800	-	5600	4900	94				
5600	-	11200	8000	94				

ItiB.					
Frequency bands (cps)	Max. accept- able noise level (db)				
Overal:	113				
37.5 - 75 75 - 150 150 - 300 300 - 600 600 - 1200 200 - 2400 400 - 4800 4800 - 9600	111 111 111 109 106 100 94 94				

3.1.4 Normal cruise power – The acoustical noise level in any part of the aircraft (see 6.2.2) intended for occupancy by the crew or other personnel shall not exceed the values specified in Table IVA (preferred) or Table IVB, during conditions of NORMAL CRUISE POWER. Tables IVA and IVB are applicable to all Naval aircraft procurement; and to Air Force and Army aircraft procurement when so stated in the aircraft detail specification.

TABLE IV. - Maximum acceptable noise level at normal cruise power

	IVA.								
	Fn	Max. accept- able noise							
	Ba	ınd	Center	level (db)					
С	)verc		Ţ <u>-</u> -	106					
22.4	4 -	45	31.5	104					
45	_	90	63	104					
90	_	180	125	104					
180	_	355	250	104					
355	-	710	500	96					
710	-	1400	1000	90					
1400	_	2800	2000	86					
2800	-	5600	4000	75					
5600	_	11200	8000	75					

I∨B.	
Frequency bands (cps)	Max. accept- able noise level (db)
Overall	126
37.5 - 75 75 - 150	104 104
150 - 300 300 - 600 600 - 1200	104 96 90
1200 - 2400 2400 - 4800	86 75
4800 - 9600	75

### MIL-A-8806A

- 3.1.5 Auxiliary systems The auxiliary systems which normally operate for longer than 5 minutes shall not produce an increase in noise levels in occupied compartments above the tables herein. Short duration noise levels shall not exceed levels in Table IIA or Table IIB unless specifically approved.
- 3.1.6 Special missions For special missions such as Anti-Submarine Warfare (ASW), Aircraft Early Warning (AEW), and Electronic Counter Measures (ECM) which may require noise levels lower than those required by this specification, me i souirements will be so stated in the detail specification.

### 6.2 Definitions -

- 6.2.1 Acoustic reference level The reference sound pressure level for measurements made in accordance with this specification will be the level produced by a sound pressure of 0.0002 dyne/cm $^2$ .
- 6.2.2 Acoustical noise level The acoustical noise level of the aircraft shall be considered to be the numerical average of the measured minimum and maximum levels, provided this average is not less than 3 db below the maximum. In the latter case the reported level shall be the maximum less 3 db.
- 6.2.3 Overall acoustical noise level The term overall acoustical noise level will be interpreted as including all noise within the frequency range from 22.4 to 11200 cycles per second.
- 6.2.4 Maximum continuous power Maximum continuous power is the maximum power that the engine can develop for continuous operation in level flight at the altitude where measurements are to be taken.
- 6.2.5 Normal cruise power Normal cruise power is the power the engine can develop for maximum range in level flight at the altitude where measurements are to be taken.
- 6.?.6 Auxiliary systems An auxiliary system is any mechanism or structure other than the airframe or power plant which performs a function at some time during the operation of the aircraft, e.g., heat and vent, pressurization, defrost and defog, inverters, pumps, Auxiliary Power Unit (APU), etc.

### APPENDIX IV

### PRESSURE RATIOS AND INPUT IMPEDANCES FOR ACOUSTIC TREATMENT

### I. INTRODUCTION

In Section VI expressions for the complex pressure ratios and input impedances for the various types of acoustic treatment are stated. In this Appendix the equations are re-arranged into forms more suitable for computational purposes. Symbols used below are those defined in Section VI except where given here.

### 2. PANEL

The pressure ratio is given by the ratio of input and terminating impedances. The characteristic impedance is given by

$$Z = \omega_0 m \eta + \frac{\omega^3 D}{c^4} \eta \sin^4 \theta + j \left( \omega_m - \frac{\omega_0^2 m}{\omega} - \frac{\omega^3 D}{c^4} \sin^4 \theta \right)$$
 (1)

and thus the input impedance which is the sum of characteristic and terminating impedances is

$$Z_{i} = Z + Z_{f} \tag{2}$$

The pressure ratio across the panel is given by

$$\frac{p_1}{p_2} = 1 + \frac{X_t \left(\omega_m - \frac{\omega_o^2 m}{\omega} - \frac{\omega^3 D}{c^4} \sin^4 \theta\right) + R_t \left(\omega_o m \eta + \frac{\omega^3 D}{c^4} \eta \sin^4 \theta\right)}{\left|Z_t\right|^2}$$

$$+\frac{j}{\left|Z_{t}\right|^{2}}\left\{R_{t}\left(\omega_{m}-\frac{\omega_{o}^{2}m}{\omega}-\frac{\omega^{3}D}{c^{4}}-\sin^{4}\theta\right)-X_{t}\left(\omega_{o}m\eta+\frac{\omega^{3}D}{c^{4}}\eta\sin^{4}\theta\right)\right\} (3)$$

where  $Z_t = R_t + jX_t$  is the terminating impedance.

### 3. SEPTUM

The characteristic impedance is given by

$$Z = j\omega m$$
 (4)

and thus the input impedance is

$$Z_{i} = R_{i} + j (X_{i} + \omega m)$$
 (5)

The pressure ratio is

$$\frac{P_1}{P_2} = 1 + \frac{X_t \omega_m \cos \theta}{\left|Z_t\right|^2} + \frac{j R_t \omega_m \cos \theta}{\left|Z_t\right|^2}$$
 (6)

### 4. POROUS BLANKET

From Equations (6.11) and (6.12) of Section VI it is seen that to determine the pressure in a porous blanket it is necessary to know the complex propagation constant b. This propagation constant is a function of the material properties of the blanket; Reference 63 shows that the following are the important properties governing the acoustical performance of porous blankets:

- a. K volume coefficient of elasticity of air in  $10^6$  or dynes/cm² (in c.g.s. units varying from  $1.0 \times 10^6$  to  $1.4 \times 10^6$  as compression varies from isothermal to adiabatic).
- b. Q volume coefficient of elasticity of the solid material in the blanket.
- c. R unit area acoustic resistance in "Rayls" (see Reference 63) which has units of lb sec/ft<sup>3</sup>. A Rayl is the unit for the ratio of sound pressure to particle velocity and is thus the unit of specific acoustic impedance.
- d. R' specific flow resistance of a unit cube of blanket in Rayls/ft.
- e. R<sub>1</sub> alternating specific viscous resistance per unit volume of air, due to difference in velocity of air particles and solid particles in the material. Units in Rayls/ft.
- f. R<sub>2</sub> alternating frictional resistance per unit volume due to friction caused by relative motion of solid particles in the material. Units are mechanical ohms per unit area.
- g. X unit area acoustic reactance in Rayls.
- h. Y porosity; ratio of volume of air to total volume of material including the air.
- i. k structure factor to allow for the effect of ablique and non-uniform passages for the moving air particles. k is greater than 1 and is dimensionless.

A soft acoustical blanket is defined as one in which K > 20 Q, and this generally includes acoustical blankets used in aircraft fuselage sound proofing. Sound waves in the blanket are propagated through both the air and the material in the blanket; however, the sound wave in the solid material will travel slowly and be highly attenuated, under the above assumption of "softness," and may thus be neglected.

It is found from experiment that  $R_1$  is reasonably constant with frequency, and is approximately equal to  $R^1$ . The propagation constant b can be expressed in terms of K, k,  $R_1$  and Y plus the air and material densities and sound wave frequency as

$$b = i\omega \left(\frac{\overline{\rho_1} Y}{K} \left(1 - \frac{i\overline{R_1}}{\rho_1 \omega}\right)\right)^{\frac{1}{2}}$$

where

$$\overline{\rho}_{1} = \rho k - \frac{B (Y/k + \rho_{m}/\rho k) + \frac{1 + \rho Y (k - 1)/\rho_{m} k}{1 + \frac{\rho}{\rho_{m}} (k - 1)}}{1 + B}$$
(8)

$$\overline{R}_{1} = \frac{R_{1} \left(1 - \frac{\rho}{\rho_{m}} (1 - Y)\right)}{\left(1 + B\right) \left(1 + \frac{\rho}{\rho_{m}} (k - 1)\right)^{2}}$$
(9)

$$B = \frac{R_1^2}{\rho_m^2 \omega^2 \left(1 + \frac{\rho}{\rho_m} (k-1)\right)^2}$$
 (10)

 $\overline{P}_1$  may be regarded as an effective density of the material and  $\overline{R}_1$  as a dynamic resistance, both varying with frequency.

The material constants used above must be determined by measurements on samples of particular blankets being considered. Typical results are given in Reference 63 where the propagation constant b and the impedance of various materials were measured directly and the material properties obtained from equations given above.

If the further assumption is made that the blanket porosity  $\,Y\,$  is greater than 0.95 the characteristic impedance of an acoustic blanket is

$$Z = \frac{j Kb}{\omega Y}$$

and the blanket input impedance becomes (from Equation (6.11) of Section VI)

$$Z_{i} = \frac{j \, Kb}{\omega \, Y} \, \coth \left( \frac{bd}{\cos \phi} + \coth^{-1} \frac{Z_{t} \omega \, Y}{j \, Kb} \right) \tag{11}$$

The complex propagation constant may be written

$$b = \alpha + j \beta \tag{12}$$

where  $\alpha$  may be regarded as an attenuation constant and  $\beta$  as a phase constant for the material. In order to compute  $Z_i$  and b they may be re-arranged into the following forms:

since 
$$b = j\omega \left(\frac{\overline{\rho}_1 Y}{K} \left(1 - \frac{j\overline{R}_1}{\overline{\rho}_1 \omega}\right)^{\frac{1}{2}}\right)$$

then 
$$\alpha = \sqrt{\frac{\omega Y}{2K}} \left\{ \sqrt{\omega^2 \, \overline{\rho}_1^2 + \overline{R}_1^2} - \omega \rho_1 \right\}^{\frac{1}{2}}$$
 (13)

and 
$$\beta = \sqrt{\frac{\overline{R}_1 \sqrt{\frac{\omega Y}{2K}}}{\sqrt{\omega^2 \,\overline{p}_1^2 + \overline{R}_1^2} - \omega \,\overline{p}_1}}}$$
 (14)

$$Z_{i} = \frac{\kappa}{\omega Y \left(L_{R}^{2} + L_{I}^{2}\right)} \left\{ \alpha \left(U_{R}L_{I} - U_{I}L_{R}\right) - \beta \left(U_{R}L_{R} + U_{I}L_{I}\right) \right.$$

$$\left. + j \left[\alpha \left(U_{R}L_{R} + U_{I}L_{I}\right) - \beta \left(U_{I}L_{R} - U_{R}L_{I}\right)\right] \right\}$$

$$(15)$$

where

$$L_{R} = \frac{K}{\omega Y} (\alpha^{2} + \beta^{2}) (1 + \tan h^{2} \times \tan^{2} y) + (R_{t} \alpha + X_{t} \beta) \tan y \operatorname{sech}^{2} x$$

$$+ (X_{t} \alpha - R_{t} \beta) \tan h \times \operatorname{sec}^{2} y$$
(16)

$$L_{I} = (X_{t}\alpha - R_{t}\beta) \text{ fan y sech}^{2} \times -(R_{t}\alpha + X_{t}\beta) \text{ fan h x sec}^{2} y$$
 (17)

$$U_{R} = \frac{K}{\omega Y} (\alpha^{2} + \beta^{2}) \tanh^{2} x \sec^{2} y + (X_{t} \alpha - R_{t} \beta) (1 + \tanh^{2} x \tan^{2} y)$$
 (18)

$$U_{I} = \frac{K}{\omega Y} (\alpha^2 + \beta^2) \tan y \operatorname{sech}^2 \times - (R_{t} \alpha + X_{t} \beta) (1 + \tan h^2 \times \tan^2 y)$$
 (19)

and 
$$x = \frac{\alpha d}{\cos \phi}$$
  $y = \frac{\beta d}{\cos \phi}$ 

The pressure ratio across the blanket may be written as

$$\frac{P_1}{P_2} = 1 + \frac{K}{\omega Y \left| Z_{\uparrow} \right|^2} \left\{ X_{\uparrow} \tanh x - R_{\uparrow} \tan y \right\}$$

$$+ j \left\{ \tanh x \tan y + \frac{K}{\omega Y \left| Z_{\uparrow} \right|^2} \left( X_{\uparrow} \tan y + R_{\uparrow} \tanh x \right) \right\}$$
(20)

where x and y are defined above.

## 5. AIR GAP

The input impedance for an airgap of width d is given by

$$Z_{i} = Z_{o} \coth \left( \frac{j \omega d}{c \cos \theta} + \coth^{-1} \frac{Z_{i}}{Z_{o}} \right)$$
 (21)

The characteristic impedance for air is  $Z_0 = \rho c$  and writing

$$v = \frac{\omega d}{c \cos \theta}$$

the input impedance becomes

$$Z_{i} = \frac{\rho c}{V^{2} + W^{2}} \left\{ R_{i}W + V (X_{i} + \rho c tan u) + j \left[ W (X_{i} + \rho c tan u) - R_{i}V \right] \right\}$$
 (22)

where

$$V = R_t tan v$$

$$W = \rho c - X_t tan v$$

and the pressure ratio is given by

$$\frac{P_1}{P_2} = \cos u + \frac{\rho e X_t}{\left|Z_t\right|^2} \sin u + j \frac{\rho e R_t}{\left|Z_t\right|^2} \sin u$$
 (23)

## REFERENCES

- Corcos, G. M., and Liepmann, H. W., "On the Transmission Through a Fuselage wall of Boundary Layer Noise," Douglas Report No. SM-19570, December 1955.
- Ribner, H. S., "Boundary Layer Induced Noise in the Interior of Aircraft", UTIA Report No. 37, April 1956.
- Kraichnan, R. H., "Noise Transmission from Boundary Layer Pressure Fluctuations," Jour. Acoustical Soc. of Amer., Vol. 29, No. 1, January 1957.
- Davies, D. E., "The Radiation Sound Field of a Rectangular Panel Set in an Infinite Wall and Excited by a Turbulent Boundary Layer," R.A.E. Tech. Note Structures 355, April 1964.
- White, P. H., "The Transduction of Boundary Layer Noise by a Rectangular Panel," Presented at the Meeting of Acoustical Society of America, October 1964.
- Maestrello, L., "Use of Turbulent Model to Calculate the Vibration and Radiation Responses of a Panel, with Practical Suggestions for Reducing Sound Level," Journ. Sound and Vibration, Vol. 5, No. 3, 1967.
- Junger, M., "Sound Scattering by Thin Elastic Shells," Journ. Acoust. Soc. of America, Vol. 24, p. 367, 1952.
- Foxwell, J. H., and Franklin, R. E., "The vibrations of a Thin-Walled Stiffened Cylinder in an Acoustic Field," The Aeronautical Quarterly, February 1959.
- Clarkson, B. L., and Ford, R., "The Response of a Typical Aircraft Structure to Jet Noise," J. Roy. Aero. Soc., 66, 31, 1962.
- McElmon, J. A., and Mikulas, M. M., "On Free Vibrations of Eccentrically Stiffened Cylindrical Shells and Flat Plates," NASA TND-3010, 1965.
- 11. Den Hartog, J. P., "Mechanical Vibrations," McGraw-Hill Book Company, 1956.
- Timoshenko, S., and Woinowsky-Krieger, S., "Theory of Plates and Shells," McGraw-Hill Book Company, 1959.
- Mercer, C. A., and Seavey, C., "Prediction of Natural Frequencies and Normal Modes of Skin-Stringer Panel Rows," Jour of Sound and Vibration, Vol. 6, No. 1, 1967.

- 14. Morse, P. M., "Vibration and Sound," McGraw-Hill Book Company, 1948 \_
- 15. Lowson, M. V., "Prediction of Boundary Layer Pressure Fluctuations," Wright-Patterson Report AFFDL-TR-67-157, October 1967.
- 16. Eldred, K. McK., Roberts, W. H., and White, R. W., "Structural Vibrations in Space Vehicles," Wright Patterson Report WADD-TR 61-62, December 1963.
- 17. Lilley, G. M., "Wall Pressure Fluctuations Under Turbulent Boundary Layers at Subsonic and Supersonic Speeds," AGARD Report 454, April 1963.
- Lowson, M. V., "Pressure Fluctuations in Turbulent Boundary Layers," NASA IND-3156, December 1965.
- 19. Bull, M. K., "Properties of the Fluctuating Wall Pressure Field of a Turbulent Boundary Layer," AGARD Report 455, April 1963.
- Markovin, M. V., "Effects of Compressibility on Turbulent Flows," Mecan sque de la Turbulence, CRNS, p. 369, 1962.
- 21. Bies, D. A., "A review of Flight and Wind Tunnel Measurements of Boundary
  Layer Pressure Fluctuations and Induced Response," NASA CR-626, October 1966.
- 22. Hodgson, T. H., "Pressure Fluctuations in Shear Flow Turbulence," Ph.D. Thesis University of London, 1962.
- 23. Gibson, J. S., "Boundary Layer Noise Measurements on a Large Turbofan Alicra Ft," Paper No. 110, 70th Meeting A.S.A., November 1965.
- 24. Maestrello, L., "Use of a Turbulence Model to Calculate Vibration and Residutional Responses of a Panel with Practical Suggestions for Reducing Sound Level," Jour \_ Sound and Vibration, Vol. 5, pp 407-448, 1967.
- 25. Speaker, W. V., and Ailman, C. M., "Spectra and Space-Time Correlations of the Fluctuating Pressures at a Wall Beneath a Supersonic Turbulent Boundary Layers Perturbed by Steps and Shock Waves," NASA CR-486, 1965.
- Gardner, S., "On Surface Pressure Fluctuations Produced by Boundary Layer Turbulence," Accustica, Vol. 16, No. 2, 1965/66.
- 27. Willimarth, W. W., and Wooldridge, C. E., "Measurements of the Fluctuating Pressure at the Wall Beneath a thick Turbulent Boundary Layer," J. Fluid Mech. Vol. 14, Part 2, October 1962.
- 28. Kistler, A. L., and Chen, W. S., "A Fluctuating Pressure Field in a Supersonic Turbulent Boundary Layer," J. Fluid Mech., Vol. 16, Part 1, May 1963.

- Clarkson, B. L., "Scaling of the Near Field Pressure Exhaust," <u>Acoustical Fatigue</u> in <u>Aerospace Structures</u>, ed. Trapp and Forney, Syracuse University Press, (1965).
- 30. Lighthill, M. S., "Jet Noise," AGARD Report 448, April 1963.
- Lighthill, M. J., "On Sound Generated Aerodynamically, 1 General Theory," Proc. Roy. Soc. A, Vol. 211, 1952.
- Lighthill, M. J., "On Sound Generated Aerodynamically, 2 Turbulence as a Source of Sound," Proc. Roy. Soc. A, Vol. 222, 1954.
- 33. Ribner, H. S., "The Generation of Sound by Turbulent Jets," Advances in Applied Mechanics, Vol. 8, p. 104, Academic Press, 1964.
- Atvars, J., et al., "Refraction of Sound by Jet Flow or Jet Temperature," UTIAS Tech. Note 109, May 1965.
- Rollin, V. G., "Effect of Jet Temperature on Jet-Noise Generation," NACA TN 4217, 1958.
- 36. SAE, "Jet Noise Prediction," Aerospace Information Report Number AIR 876, 1965.
- Eldred, K. McK., "Review of Noise Generation of Rockets and Jets," Jour. Acoust. Soc. Am., Vol. 32, p. 1502, 1960.
- Ffowcs-Williams, J. E., "The Noise from Turbulence Convected at High Speed," Phil., Trans. Roy. Soc. A., Vol. 255, p. 469, 1963.
- Lighthill, M. J., "Sound Generated Aerodynamically," Proc. Roy. Soc. A., Vol. 267, p. 147, 1962.
- 40. Howes, W. L., "Similarity of the Far Noise Fields of Jets," NASA TR R-52, 1960.
- Eldred, K. McK., et al., "Suppression of Jet Noise with Emphasis on the Near Field," ASD-TRD-62-578, 1963.
- 42. Potter, R. C., "Correlation Patterns of the Acoustic Pressure Fluctuations on the S-IC Vehicle Due to the Exhaust Noise at the Test and Launch Stand," Wyle Research Staff Report WR 66-15, 1966.
- 43. Ribner, H. S., "On the Strength Distribution of Noise Sources Along a Jet," ASTIA AD-154264, April 1958.
- Dyer, I., et al., "Jet Noise Reduction by Induced Flow," Jour. Acoust. Soc. Am., Vol. 30, No. 8, 1958.

- Wenzel, A. R., "Surface Pressure Correlation Function for a Cylinder in a Diffuse Reverberant Sound Field," Wyle Laboratories Research Staff Report WR 66-14, 1966.
- Howes, W. L., et al., "Near Noise Field of a Jet Engine Exhaust," NACA Report 1338, 1957.
- Cax, R. J., et al., "A Study of the Characteristics of Modern Engine Noise and the Response Characteristics of Structures," Wright Patterson Air Force Base, WADC TR-60-220, 1961.
- 48. Clarkson, B. L., and Ford, R. D., "An Experimental Investigation of the Random Excitation of a Tailplane Section by Jet Noise," Wright Patterson Air Force Base, ASD-TDR-62-680, 1962.
- Crocker, M. J., and White, R. W., "Response of the Lockheed L-2000 Supersonic Transport Fuselage to Turbulence and to Reverberant Noise," Wyle Laboratories Consulting Report No. WCR 66-11, September 1966.
- 50. Eckart, C., "The Theory of Noise in Continuous Media," Journ. of the Acoustical Soc. of America, Vol. 25, No. 2, pp 195–199, March 1953.
- 51. Bakewell, H. P., Jr., "Wall Pressure Correlation in Turbulent Pipe Flow," U. S. Navy Sound Laboratory Report No. 559 (AD 283 683), August 1962
- Corcos, G. M., "The Structure of the Turbulent Pressure Field in Boundary Layer Flows," University of California, Institute of Engineering Research Report, Series 183, No. 4, 1963.
- 53. Belcher, P. M., "Predictions of Boundary Layer Turbulence Spectra and Correlations for Supersonic Flight," 5th International Acoustic Congress, Liege, Belgium, Sept. 1965.
- 54. Shattuck, R. D., "Sound Pressures and Correlations of Noise on the Fuselage of a Jet Aircraft in Flight," NASA TN-D 1086, August 1961.
- Williams, D. J. M., "Measurements of the Surface Pressure Fluctuations in a Turbulent Boundary Layer in Air at Supersonic Speeds, University of Southampton AASU Report No. 162, December 1960.
- 56. White, R. W., "Predicted Vibration Responses of Apollo Structure and Effects of Pressure Correlation Lengths on Response," Wyle Laboratories Research Staff Report WR 67-4, March 1967.
- Powell, A., "On the Response of Structures to Random Pressures and to Jet Noise in Particular," Random Vibration, edited by S. H. Crandall, Chapter 8, John Wiley and Sons, Inc., 1958.

- 58. Wilby, J. F., "Response of Panels to Random Pressure Fields," University of Southampton A.A.S.U. Report No. 243, July 1963.
- Abramowitz, M., and Stegun, I. A., "Handbook of Mathematical Functions,"
   U. S. Department of Commerce, National Bureau of Standards, American Mathematical Series 55, November 1964.
- 60. Beranek, L., "Noise Reduction," McGraw-Hill Book Company, 1960.
- Cremer, L., "Insulation of Air-borne Sound by Rigid Partitions and Insulation of Impact Sound," Ch. 11.2, WADC Tech. Report 52–204, Vol. 1, Supplement 1, Wright Patterson Air Force Base, Ohio, 1955.
- 62. Beranek, L. L., and Work, G. A., "Sound Transmission Through Multiple Structures Containing Flexible Blankets," J.A.S.A. Vol. 21, No. 4, pp 419–428, July 1949.
- Beranek, L. L., "Acoustical Properties of Homogeneous Isotropic Rigid Tiles and Flexible Blankets," J.A.S.A. Vol. 19, No. 4, pp 556–568, July 1947.
- Ross, D., Kerwin, E. M., "Damping of Flexural Vibrations in Plates by Free and Constrained Viscoelastic Layers," BBN Report 632, May 1959.
- Oberst, H., "Ueber die D\u00e4mpfung der Biegeschwingungen d\u00fcnner Bleche durch fest haftende Bel\u00e4ge," Acustica, Vol. 2, No. 4, 1952.
- 66. Kerwin, E. M., "Damping of Flexural Waves by a Constrained Viscoelastic Layer," J.A.S.A., Vol. 31, No. 7, 1959.
- 67. Hermes, P.H., and Smith, D.L., "Measurement and Analyses of the J57-P21 Noise Field," AFFDL-TR-66-147, November 1966.
- 68. London, A., "Transmission of Reverberant Sound Through Double Walls," J. Acoust. Soc. Am. 22:2, pp. 270-279, March 1950.
- 69. Rudmose, H. W. and Beranek, L. L., "Noise Reduction in Aircraft," Jour. of Aeron. Sciences, February 1947.
- Macduff, J. N. and Feigar, R. P., "Vibration Design Charts," Transactions of the ASME, pp. 1459–1475, October 1957.
- 71. Ungar, E. E., "Lass Factors of Viscoelastically Damped Beam Structures," J. Acoust. Soc. Am., Vol. 34, pp. 1082–1089, August 1962.
- Oberst, H. and Schammer, A., "Optimization of Viscoelastic Damping Materials for Specific Structural Composite Applications," Acoustical Fatigue in Aerospace Structures, Syracuse University Press, 1965.

- 73. Beranek, L. L., "Acoustics," McGraw-Hill Book Company, New York, 1954.
- Nichols, R. H., et al, "Acoustical Materials and Acoustical Treatments for Aircraft,"
   J. Acoust. Soc. Am., Vol. 19, No. 3, May 1947.
- 75. Acoustical Materials Assoc., "Architectural Acoustic Materials," A.I.A. Number 39-B, Bulletin Number XXV, 1965.

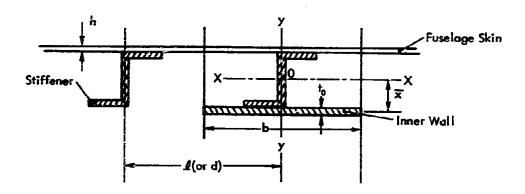


Figure 1. Double-Wall Fuselage; Low Frequency Model

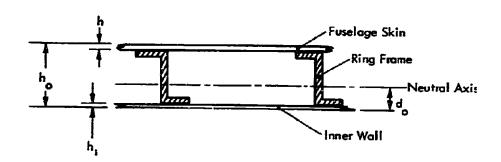
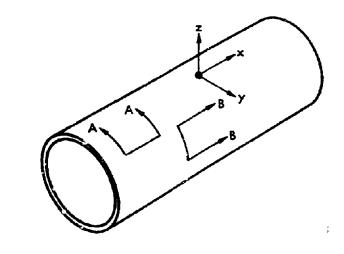
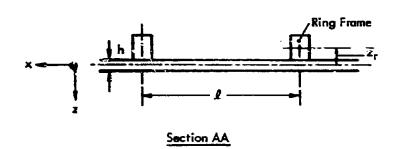


Figure 2. Double-Wall Fuselage; High Frequency Model





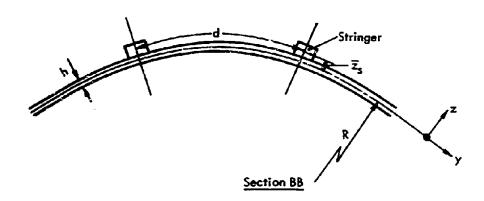


Figure 3. Geometry of the Reinforced Cylindrical Shall

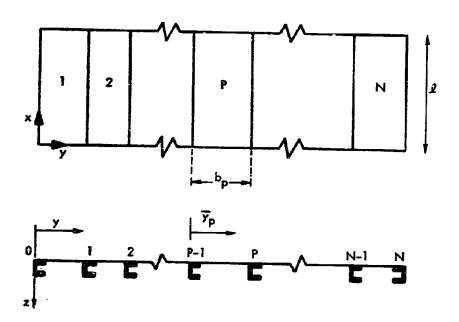


Figure 4. Geometry and Coordinate Axes of the Panel Group

S Skin

Figure 5. Panel Group - Stringer Details

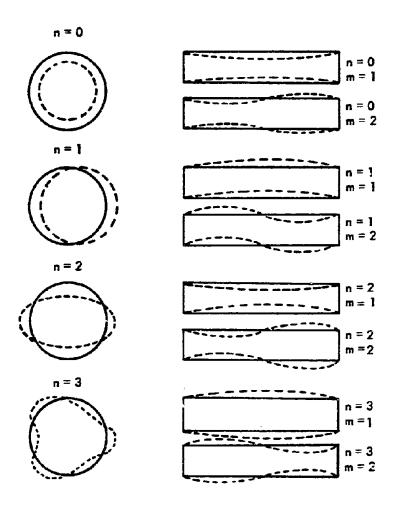


Figure 6. Resonant Deflection Shapes of a Cylindrical Shell

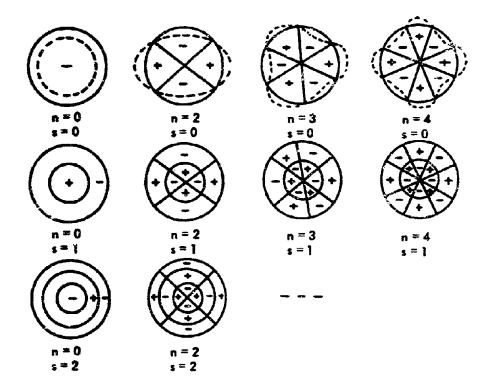


Figure 7. Typical Circumferential and Radial Acoustic Wave Patterns and the Corresponding Circumferential Structural Wave Patterns.

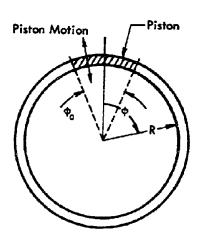


Figure 8. Rigid Shell with a Single Radial Piston

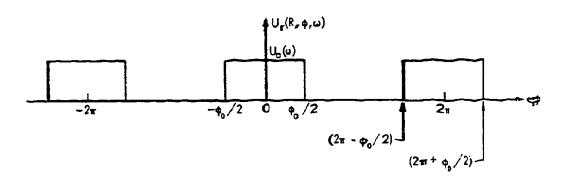


Figure 9. Graph of Radial Displacement of Rigid Shell with Radial Piston

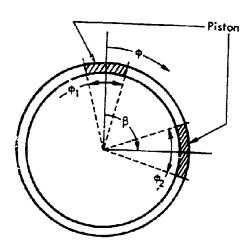


Figure 10. Rigid Shell with Two or More Radial Pistons

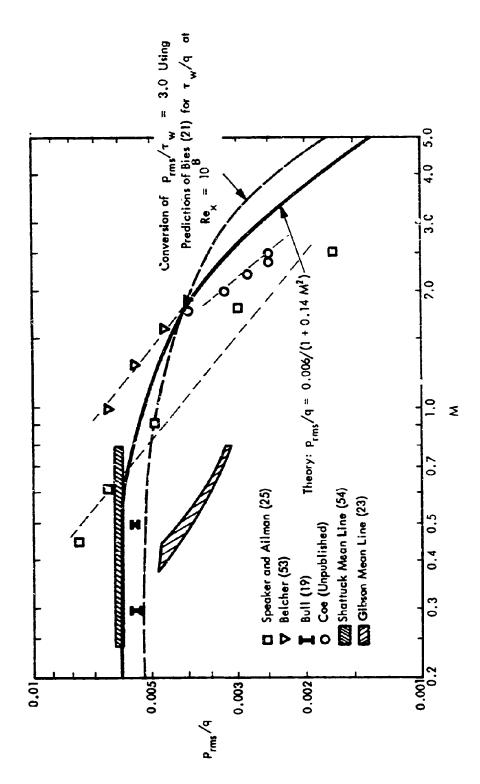


Figure 11. Fluctuating Pressure Non-dimensionalized by Dynamic Huad versus Mach Number

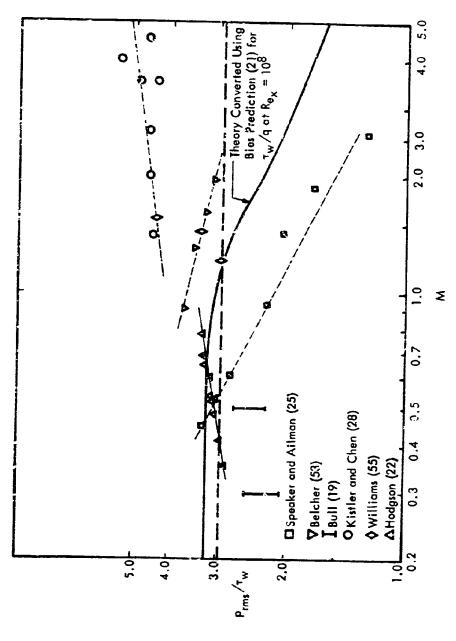


Figure 12. Fluctuating Pressure Non-dimensionalized by Wall Shear Stress versus Mach Number

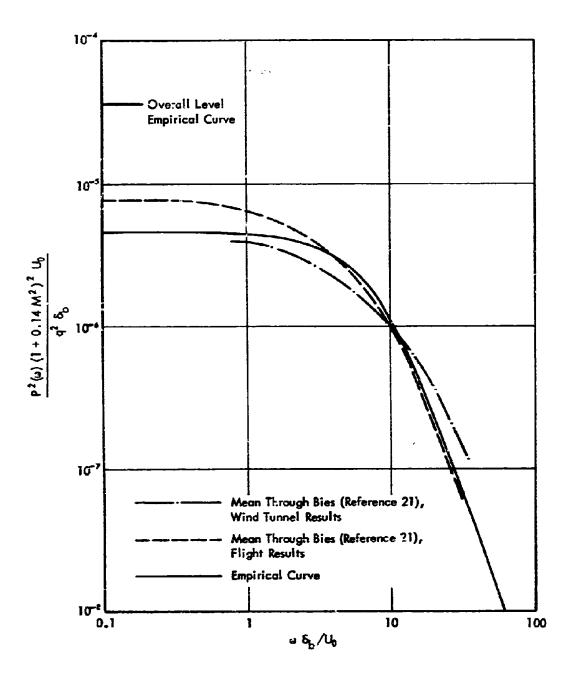


Figure 13. Comparison of Empirical Curve with Data from Bies (Reference 21)

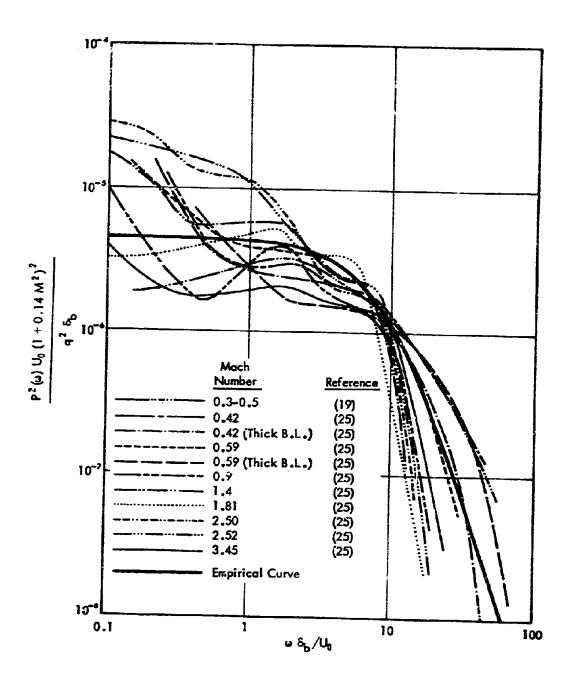


Figure 14. Comparison of Pressure Fluctuation Spectra (References 19 and 25)

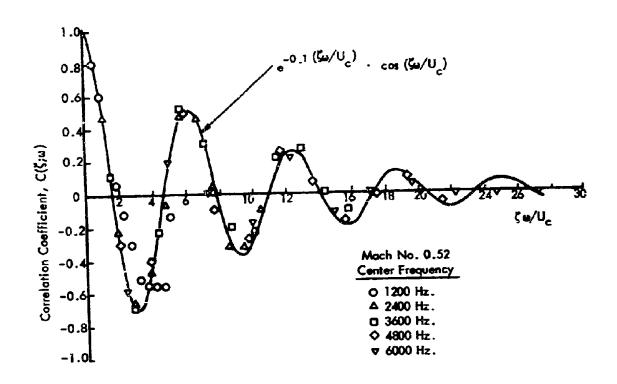
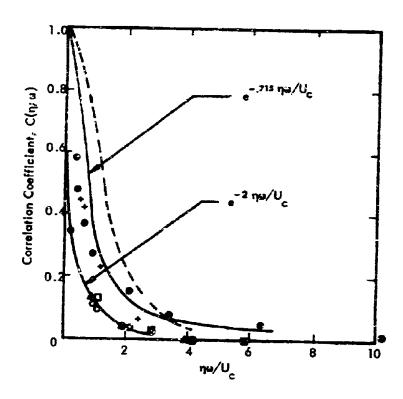


Figure 15. Narrow-Band Longitudinal Space Correlation Coefficient for Boundary Layer Turbulence (Reference 24)



---- Gardner, (Theoretical), (Reference 26)

- Maestrello, Center Frequency 1200 Hz, (Reference 24)
- Δ Maestrello, Center Frequency 2400 Hz, (Reference 24)
- Maestrello, Center Frequency 3500 Hz, (Reference 24)
- Willmorth and Wooldridge, Center Frequency, 500 Hz, (Reference 27)
- Bull, Center Frequencies at 1260, 2000, 3200, and 5000 Hz, (Reference 19)

Figure 16. Narrow-Band Lateral Space Correlation Coefficient for Boundary Layer Turbulence

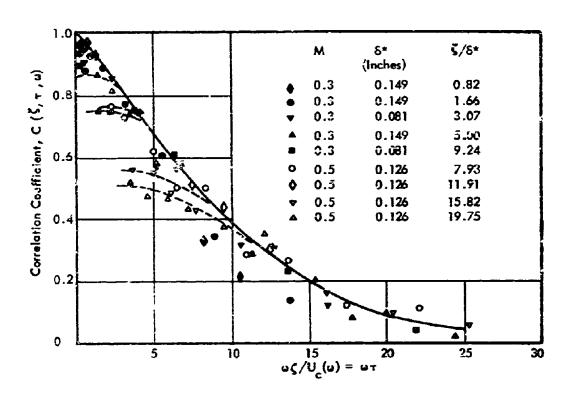


Figure 17. Narrow-Band Longitudinal Space-Time Correlation Coefficients for Wall Pressure Field from Boundary Layer Turbulance (Reference 19)

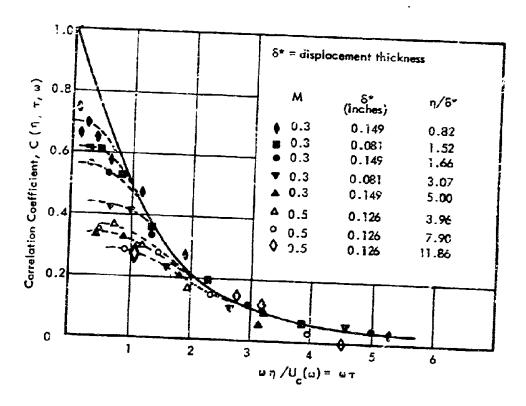


Figure 18. Narrow-Band Lateral Space-Time Correlation Coefficients for Wall Pressure Field from Boundary Layer Turbulence (Reference 19)



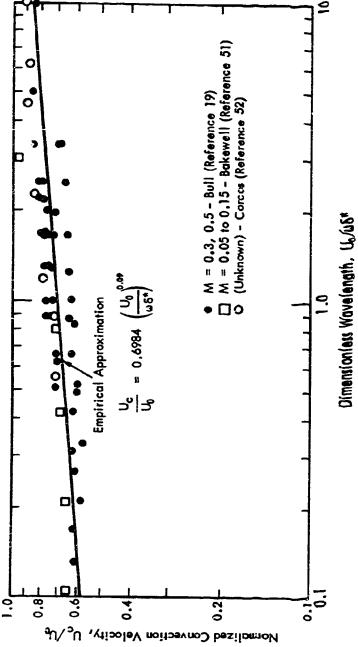


Figure 19. Turbulent Boundary Layer Convection Velocity Derived from Narrow-Band Longitudinal Space-Time Correlation Measuroments (After Bies, Reference 21)



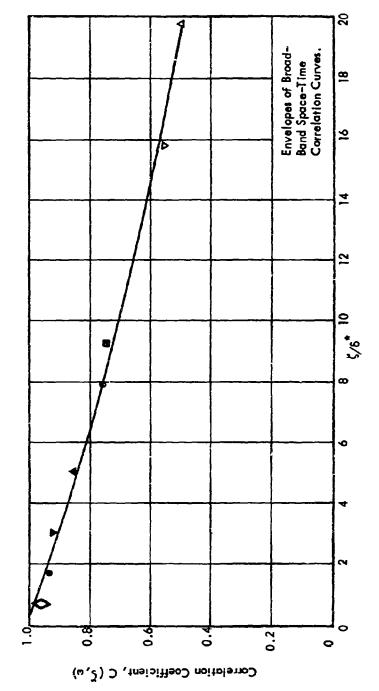


Figure 20. Asymptotic Values of Narrow-Band Longitudinal Pressure Correlation Coefficient at [ $\omega^2/U_c(\omega)$ ] = 0 (Reference 19)

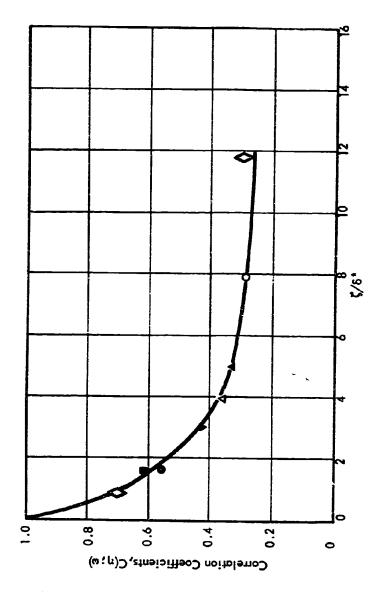


Figure 21. Asymptotic Values of Narrow-Band Lateral Pressure Correlation Coefficient at  $\left[\omega\,\eta/U_c(\omega)\right]=0$  (Reference 19)

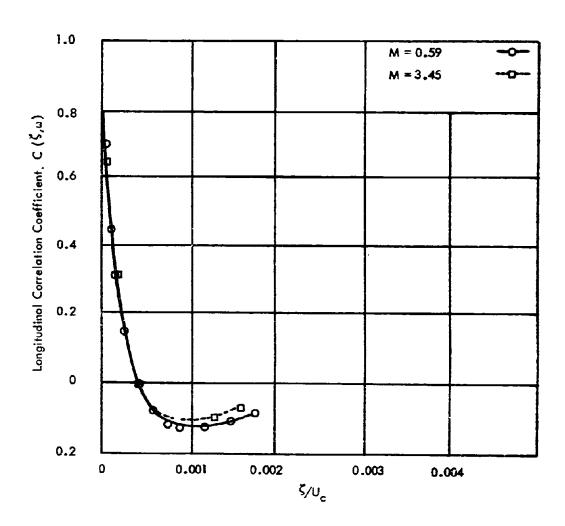


Figure 22. Comparison of Longitudinal, Broadband Correlation Coefficients at Two Mach Numbers (Reference 28)

The property of the second cold and the state of the state

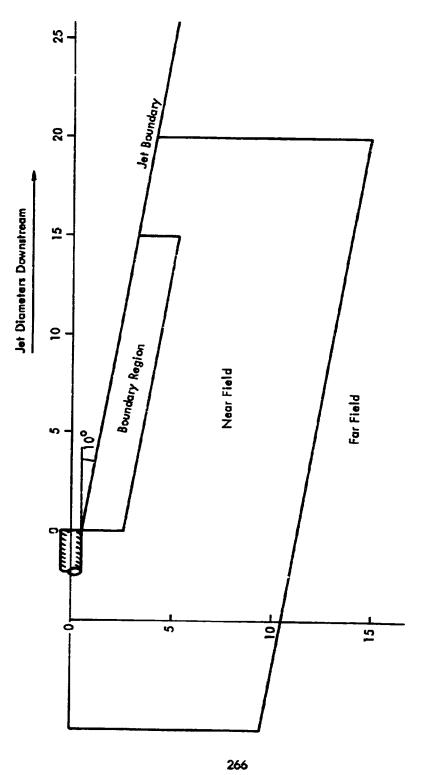


Figure 23. Jet Noise Fields

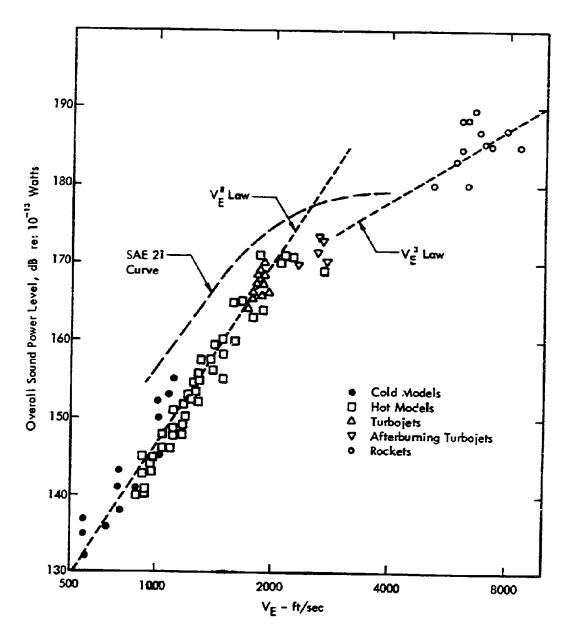


Figure 24. Overall Jet Sound Power Per Unit Nozzle Area Versus Exhaust Velocity (from Reference 37)

THE PROPERTY OF THE PROPERTY O

Figure 25. Spectrum of Overall Sound Produced by a Jet

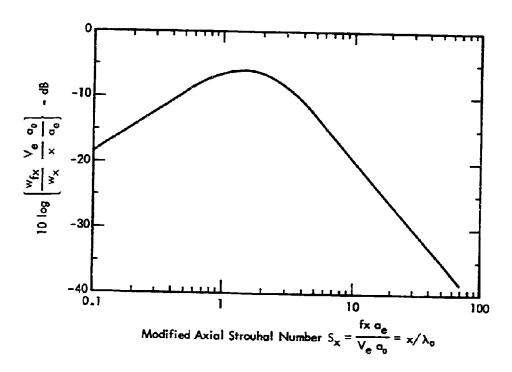


Figure 26. Normalized Power Spectra in Care Region (from Reference 41)

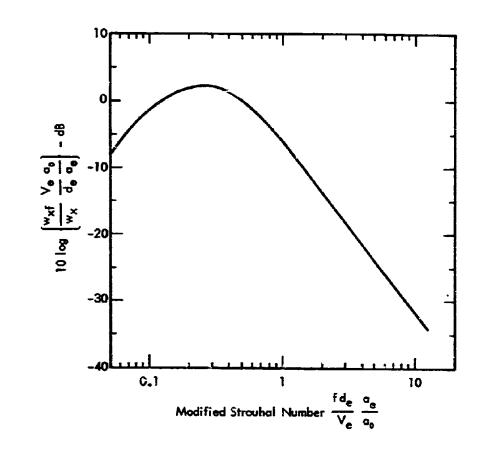


Figure 27. Normalized Power Spectra in Downstream Region (from Reference 41)

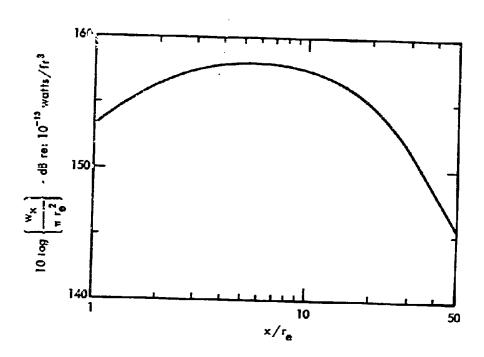
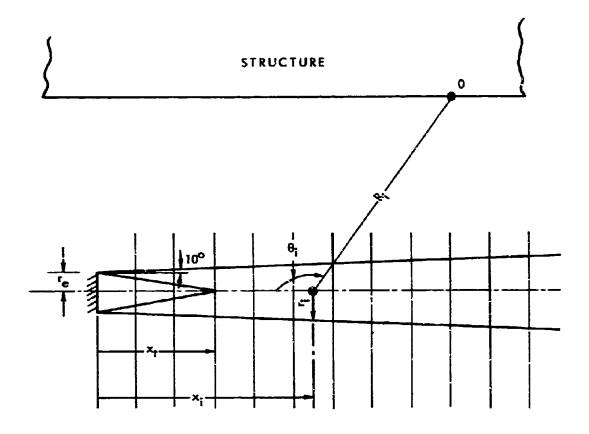


Figure 28. Overall Acoustic Power Per Unit Axial Distance and Per Unit Nozzle Area (from Reference 41)



The state of the s

Figure 29. Jet Geometry

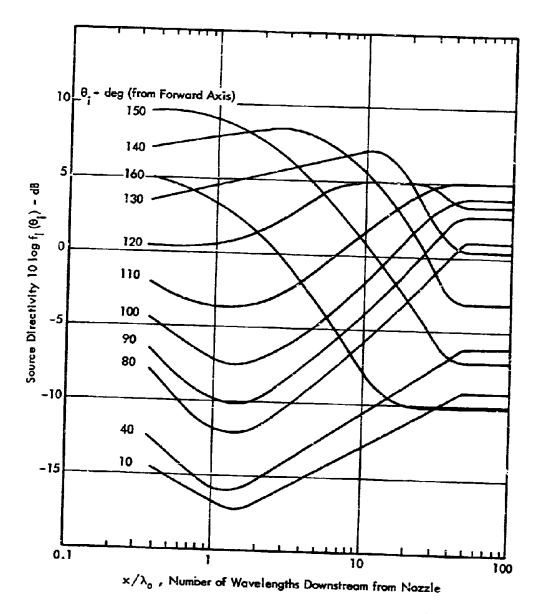


Figure 30. Calculated Directivity as a Function of Position in the Jet with 6, the Angle from Upstream, as a Parameter

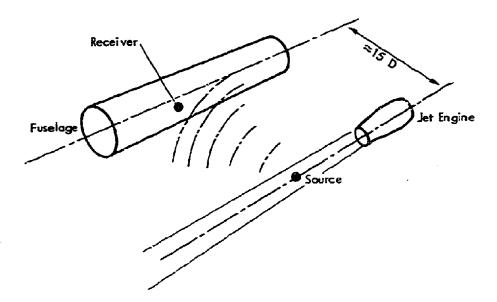


Figure 31. Fuselage and Engine

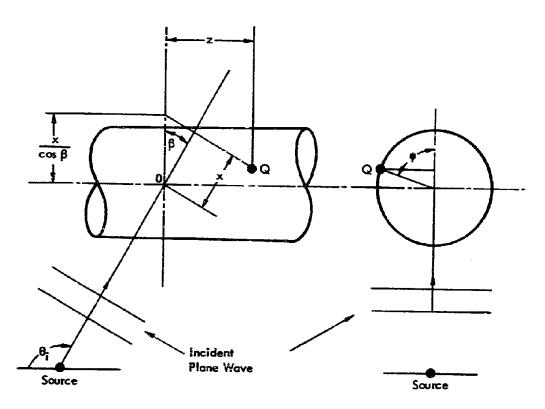


Figure 32. The Coordinate System; Wing-Mounted Engine

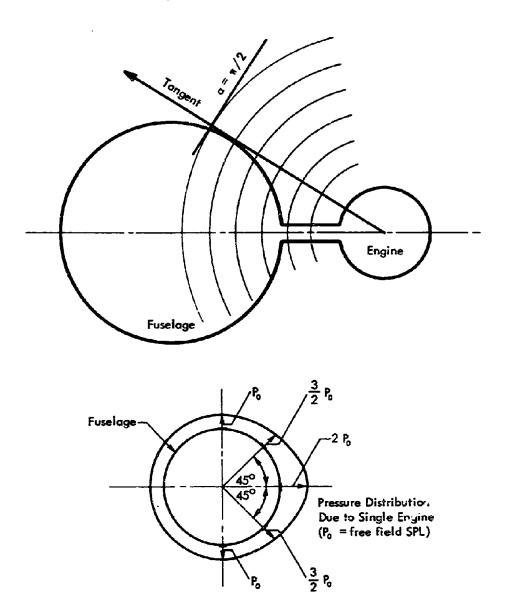
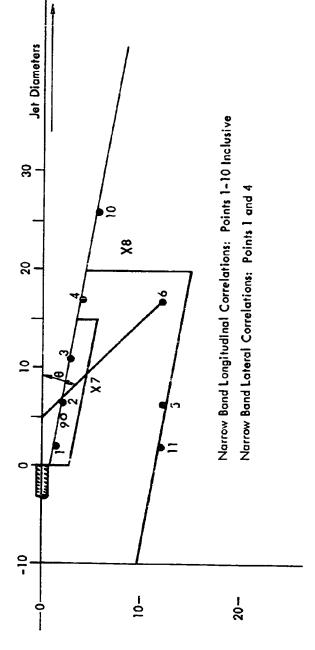


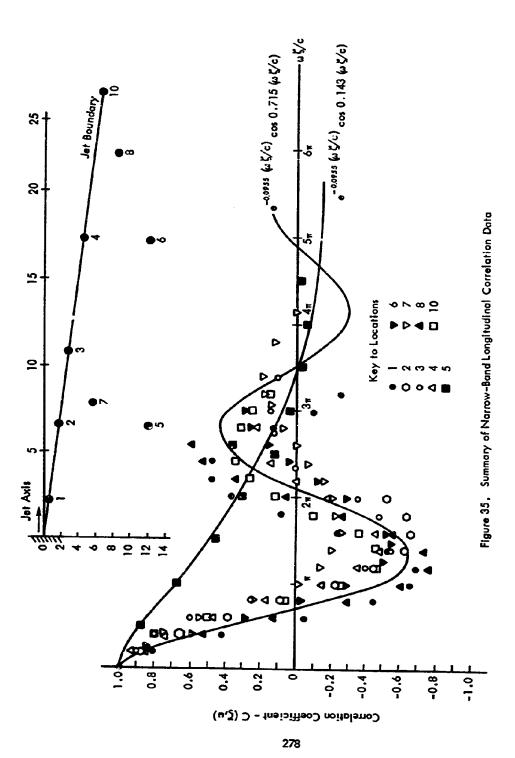
Figure 33. Geometry and Pressure Distribution; Fuselage-Mounted Engine





277

Figure 34. Narrow-Band Pressure Correlation Points





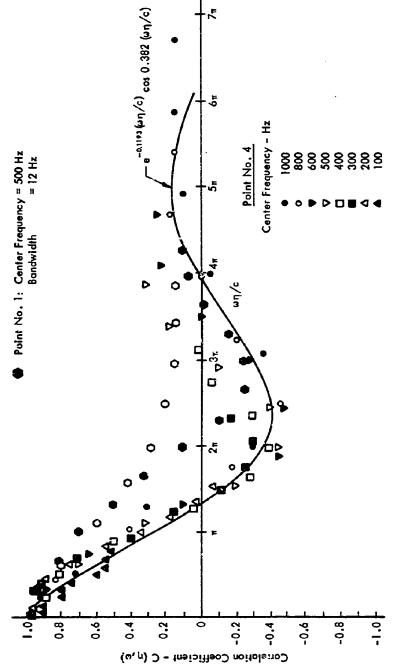


Figure 36. Summary of Narrow-BandLateral Correlation Data

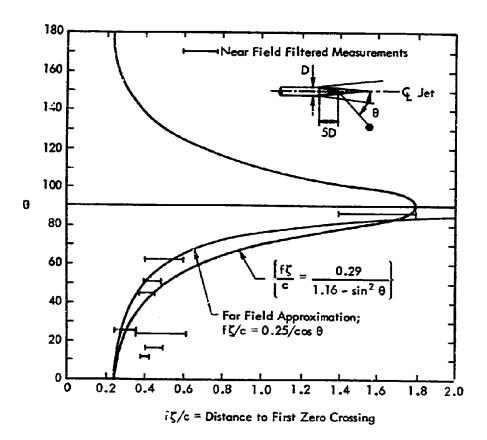


Figure 37. Near Field Longitudinal Correlations (References 46, 47 and 48)

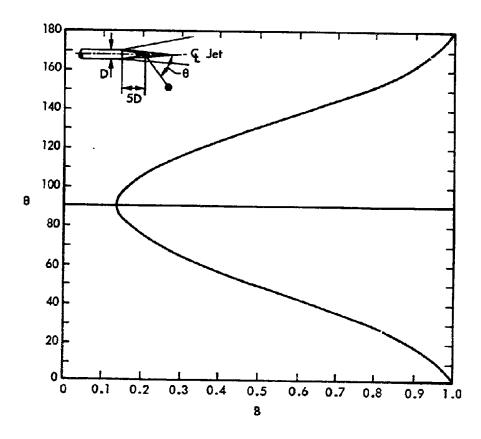
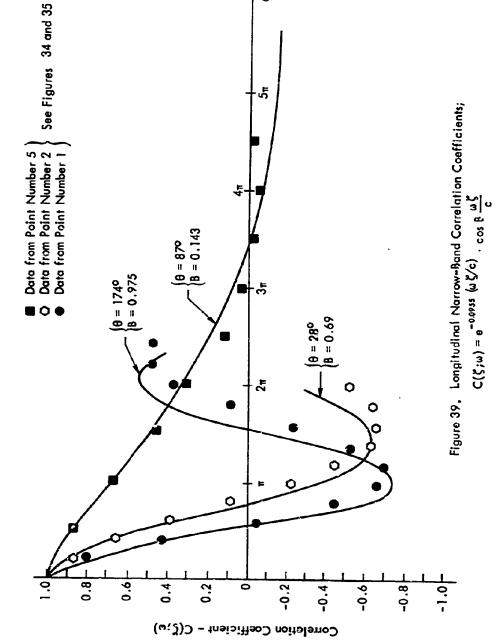


Figure 38. Numerical Values of the Constant B Appearing in the Longitudinal Correlation Coefficient  $C(\zeta,\omega)=\exp\left[-0.0955\frac{\omega\zeta}{c}\right]\cos\left\{8\frac{\omega\zeta}{c}\right\}$ 



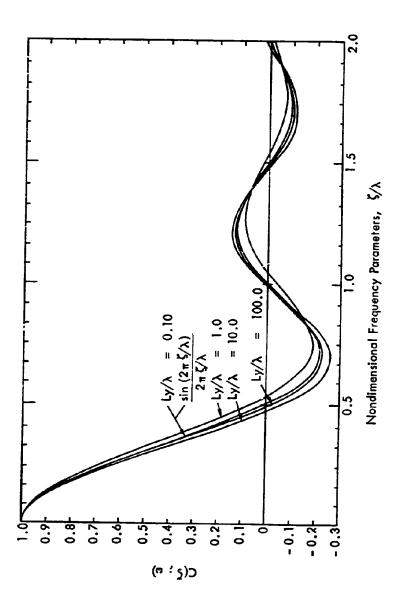


Figure 40. Narrow-Band Longitudinal Space Correlation Coefficient on the Surface of a Cylinder Immersed in a Reverberant Acoustic Field (Reference 45)

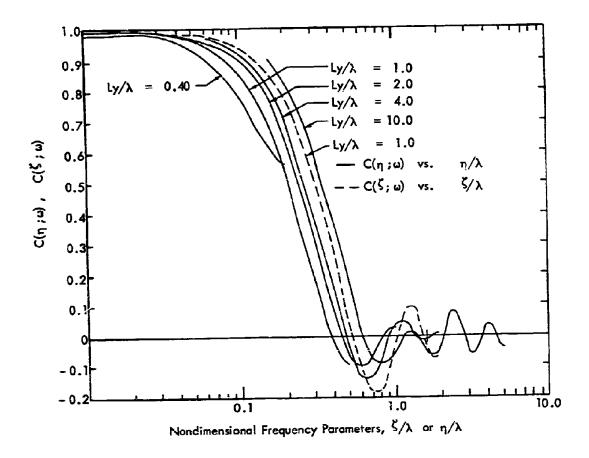


Figure 41. Narrow-Band Longitudinal and Lateral Space Correlation Coefficients on the Surface of a Cylinder Immersed in a Reverberant Acoustic Field (Reference 45)

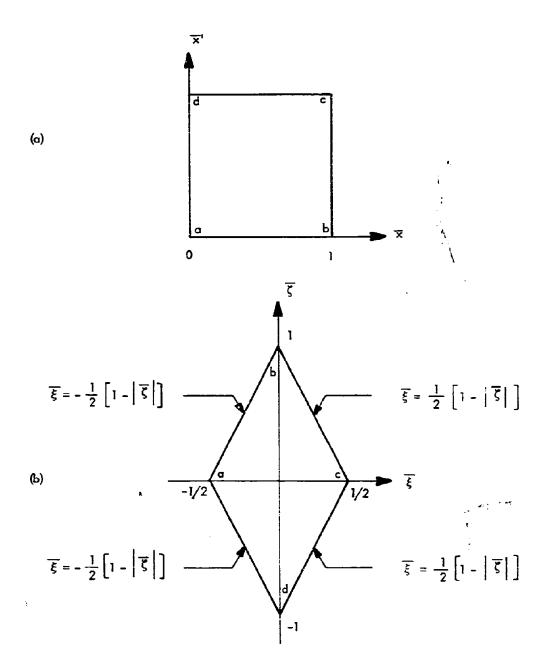


Figure 42. Transformation of the Region of Integration for Joint Acceptances

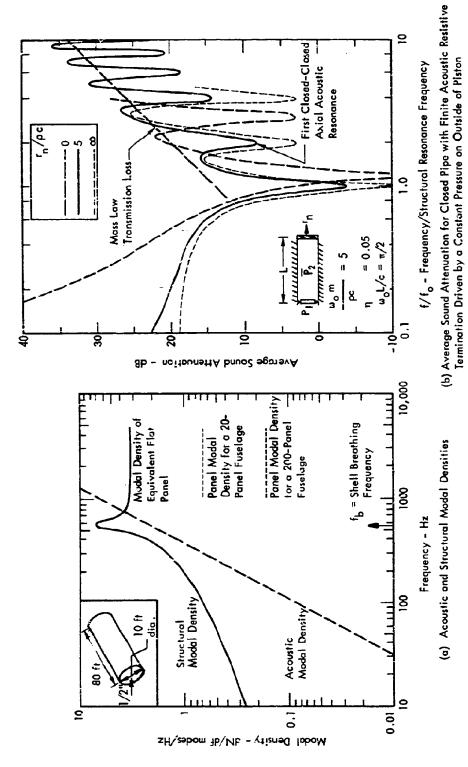


Figure 43. Separation of the Behavior of a Typical Structure into Three Frequency Regions

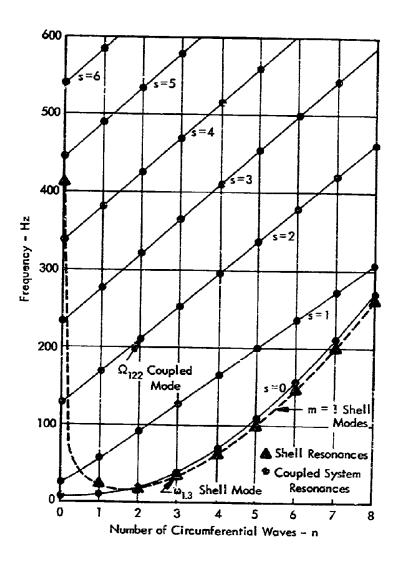


Figure 44. Shell Resonances,  $\omega_{mn}$ , and Coupled System Resonances,  $\Omega_{mns}$ , for Axial Mode Number m = 1

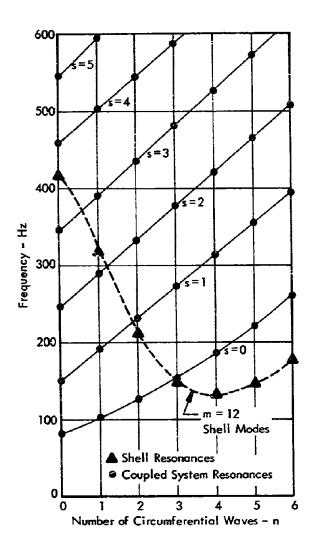


Figure 45. Shell Resonances,  $\omega_{mn}$ , and Coupled System Resonances,  $\Omega_{mns}$ , for Axial Mode Number m = 12

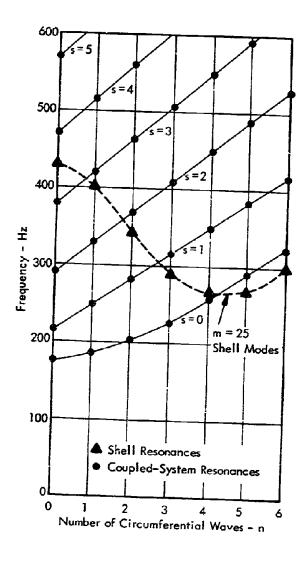
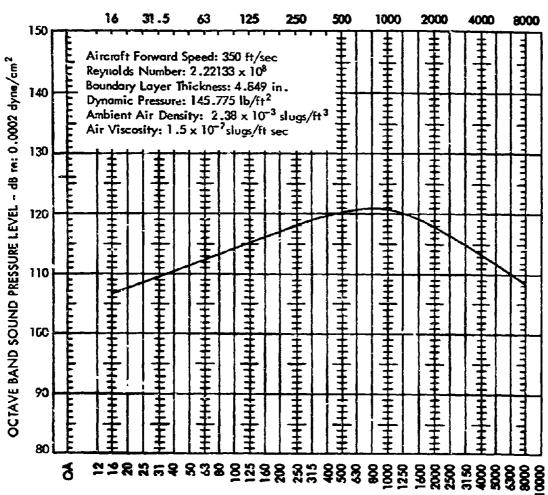


Figure 46 . Shell Resonances,  $\omega_{mn}$  , and Coupled System Resonances,  $\Omega_{mns}$  , for Axial Mode Number m = 25

# OCTAVE BAND CENTER PREQUENCIES

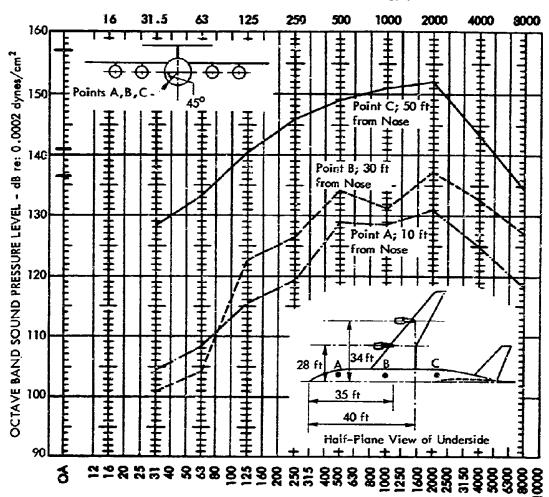
A CONTRACT OF THE PROPERTY OF



# ONE-THIRD OCTAVE BAND CENTER FREQUENCIES - Hz.

Figure 47. Boundary Layer Noise at a Position 40 Feet Along Fuselage

#### OCTAVE BAND CENTER REQUENCIES



# ONE-THIRD OCTAVE BAND CENTER FREQUENCIES - Hz

Figure 48. Jet Exhaust Noise Variation Along the Fuselage

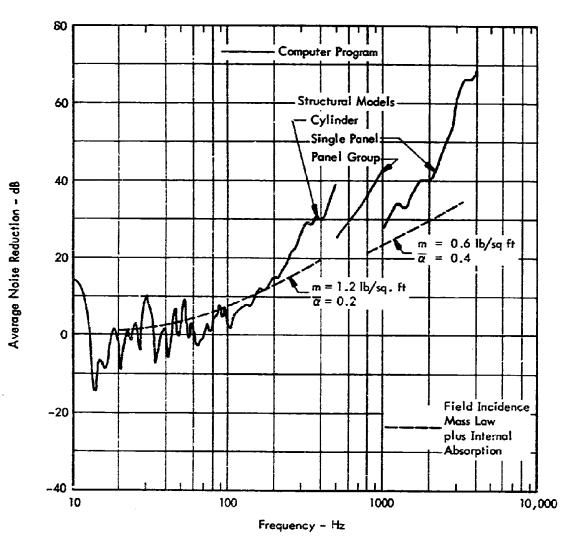
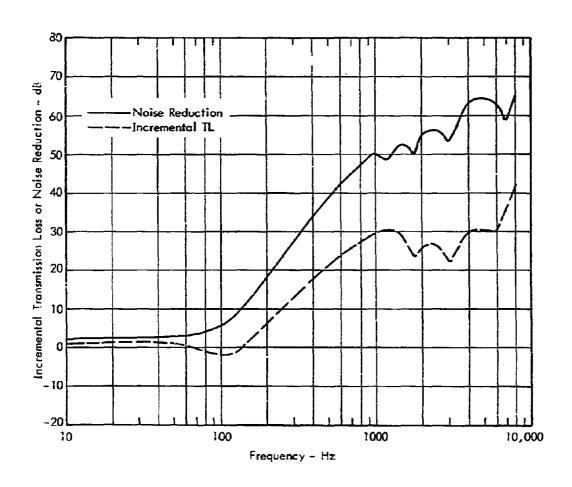
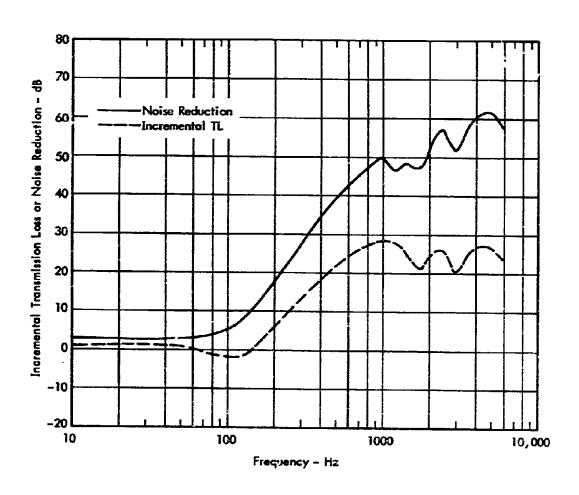


FIGURE 49: Noise Reduction for the Untreated Fuselage



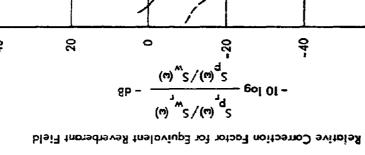
(a) Airgap, Septum, Porous Blanket, Septum

Figure 50. Incremental Transmission Loss of Acoustic Treatment and Interior Noise Reduction.



(b) Airgap, Porous Blanket, Septum

Figure 50. Incremental Transmission Loss of Acoustic Treatment and Interior Noise Reduction

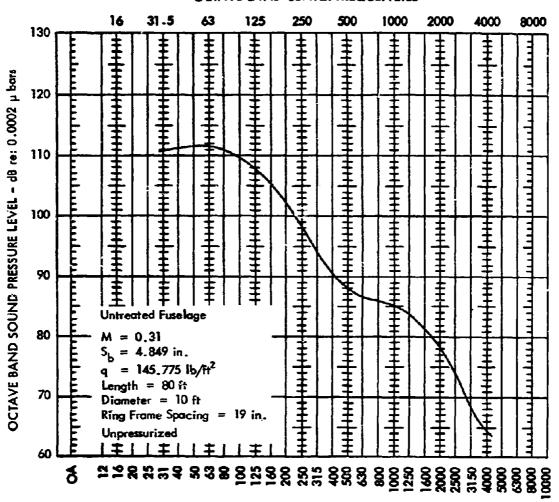


Boundary Layer Turbulence at 350 ft/sec, Sea Level 9 <del>\$</del>

FIGURE 51: Equivalent Reverberant Field for Jet Notse and Boundary Layer Turbulence

Frequency - Hz

# **OCTAVE BAND CENTER FREQUENCIES**



# ONE-THIRD OCTAVE BAND CENTER FREQUENCIES - Hz.

Figure 52. Fuselage Internal Noise Levels due to Transmitted Boundary Layer Noise.

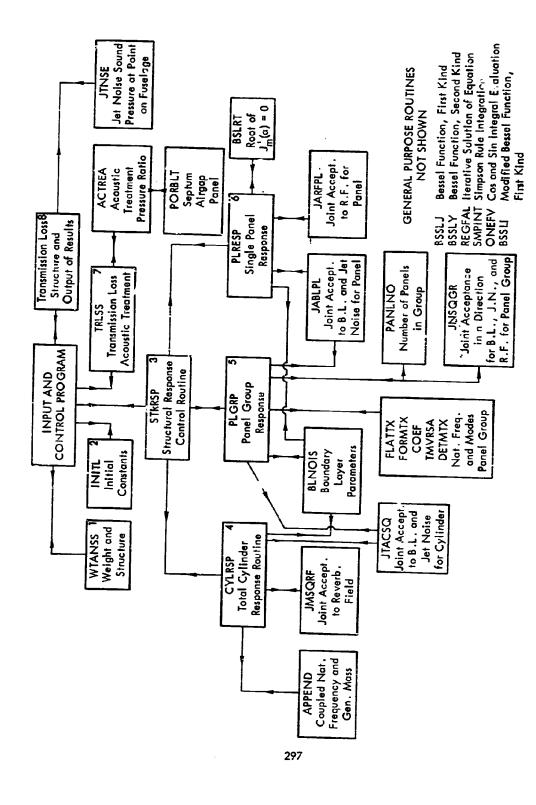


Figure 53. Computer Program Organization

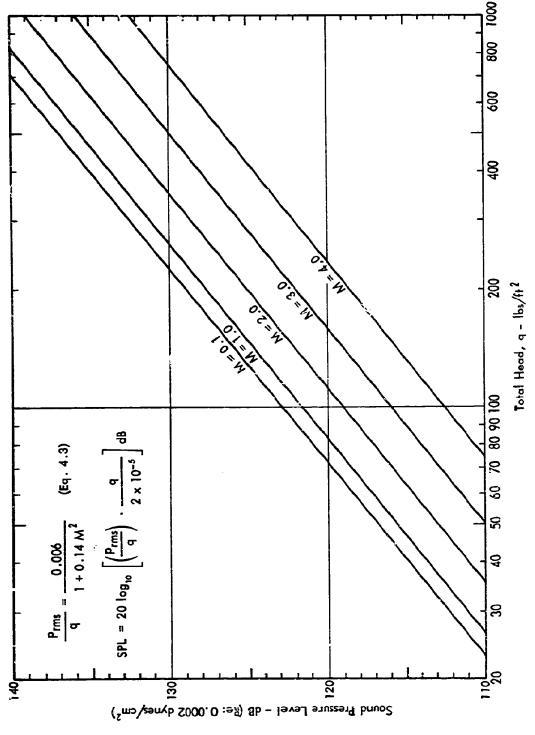


Figure 54. Conversion Chart for p /q to dB as a Function of Mach Number

· · · · · ·			<b></b>	0	<u> </u>		
Speed Range	Supersonic	150 - 160 dB (Exhaust Only)	160 ~ 165 dB	$p_{ms}/q \simeq 0.10$	None		
	Transonic	8P 091 - 051	160 - 165 dB	$p_{rms}/q \simeq 0.10$	P <sub>rms</sub> /q ≃ 0.20	SEE FIGURE 54.	
	Subsonic	150 - 160 dB	160 - 165 dB	$p_{rms}/q \simeq 0.10$	None		
Unsteady Aerodynamic Phenomena		A - Radiated Campressor Noise	B - Jet Exhaust Noise at Exit	C - Turbulent Wakes	D - Oscillating Terminal Shock Waves	E - Attached Turbulent Boundary Layers	

Figure 55. Noise Sources as a Function of Aircraft Geometry and Speed

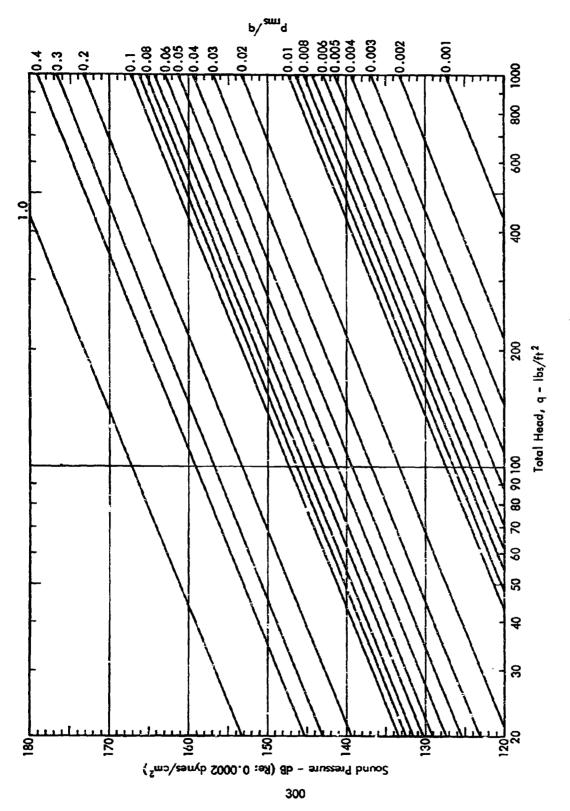
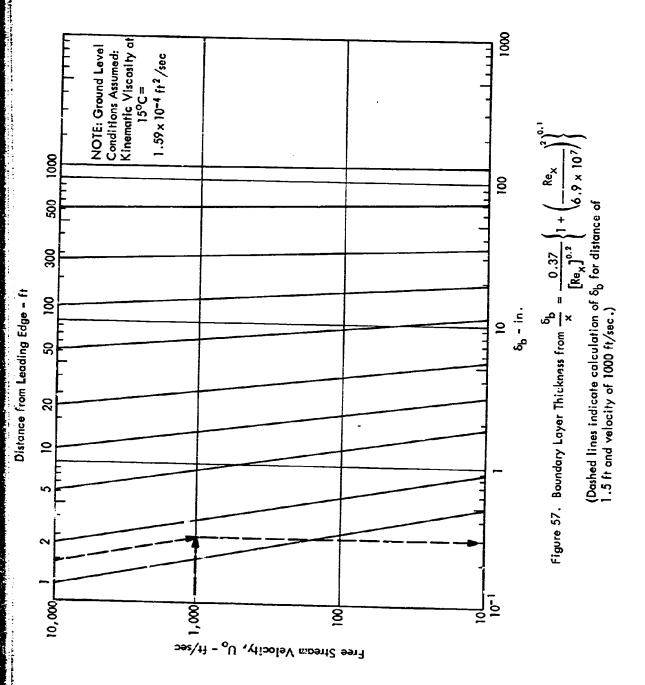
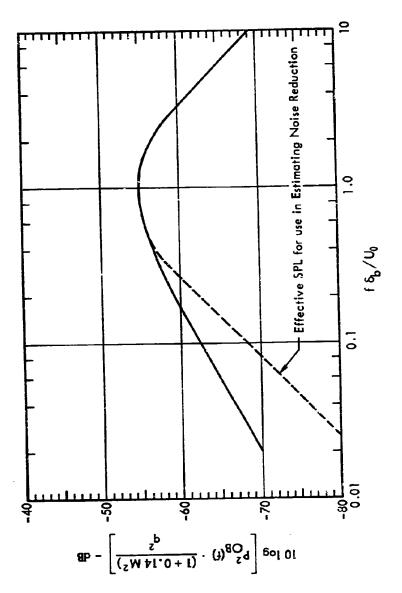


Figure 56. Conversion Chart for p<sub>rms</sub> /q to dB





COMPANY OF THE PROPERTY OF THE

Figure 58. Design Chart for Octave Band Sound Pressure Level Versus Nondimensional Center Frequency - Turbulent Boundary Layer Pressure Fluctuations

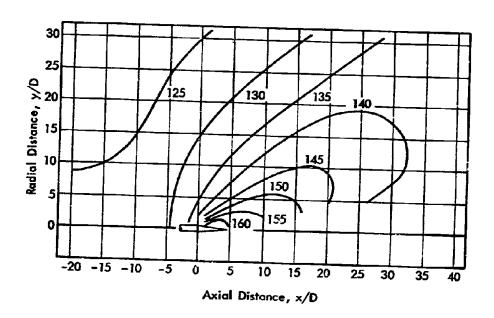


Figure 59. Overall Sound Field for J57-P21 Turbojet Engine at 100 Percent Military Power - dB re: 0.0002 dynes/cm² (After Hermes and Smith, Reference 67)

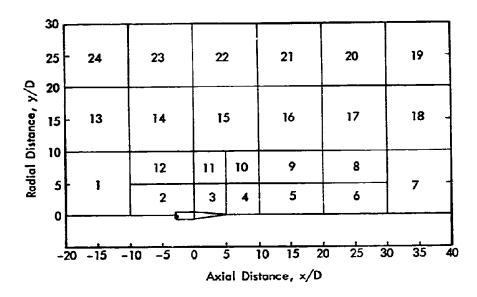
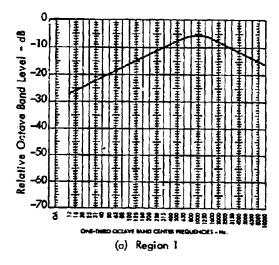
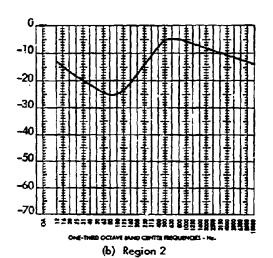
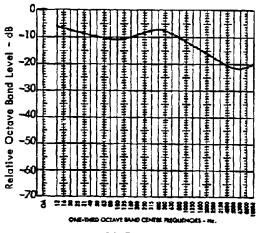
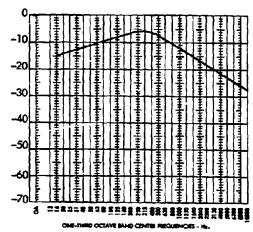


Figure 60. Sound Field Grid in Nozzle Diameters for J57-P21 Turbojet Engine.
(To be used with Figures 59 and 61 for estimating relative octave band spectra for near field jet engine noise)





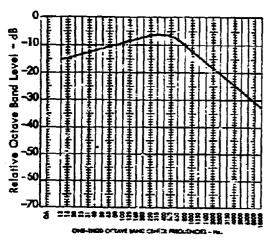




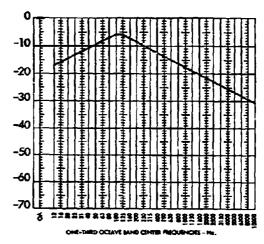
(c) Region 3

(d) Region 4

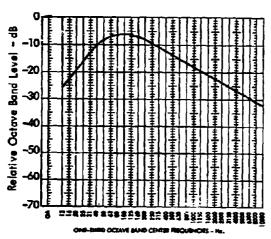
Figure 61. Relative Sound Pressure Levels in Octave Bands for J57-P21 Turbojet.
(To be used in conjunction with Figures 59 and 60 for estimating octave band spectra for near field jet engine noise)



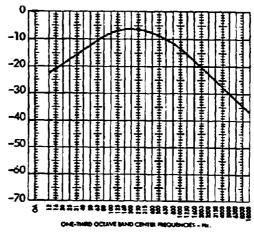




(f) Region 6

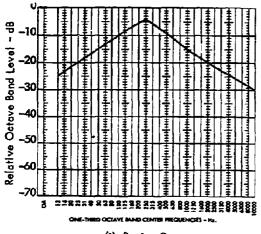


(g) Region 7

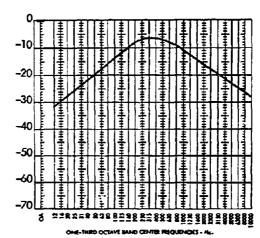


(h) Region 8

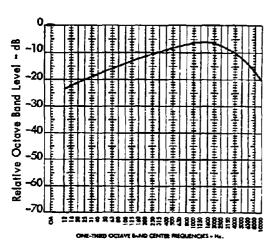
Figure 61. (Continued)



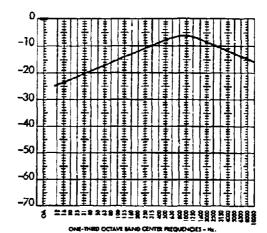
(i) Region 9



(j) Region 10

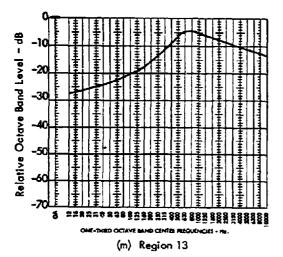


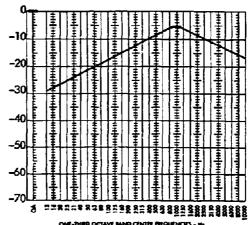
(k) Region 11



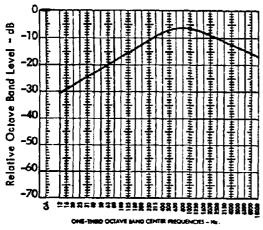
(1) Region 12

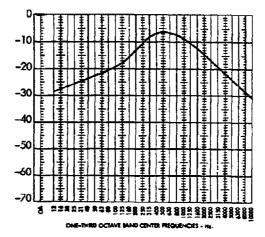
Figure 61. (Continued)





(n) Region 14

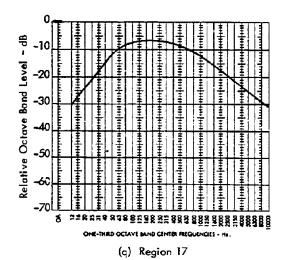


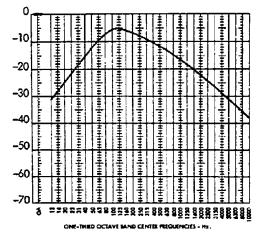


(a) Region 15

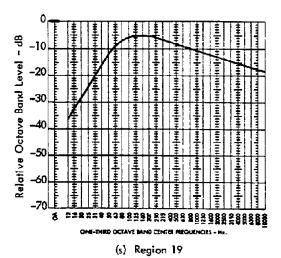
(p) Region 16

Figure 61. (Continued)





(r) Region 18



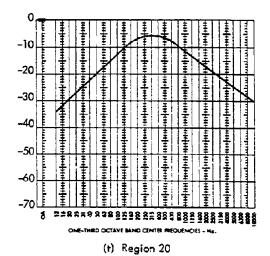
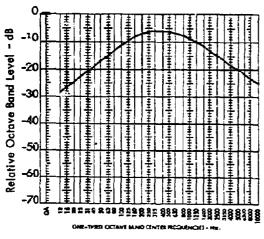
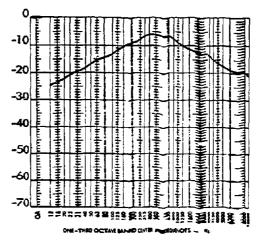


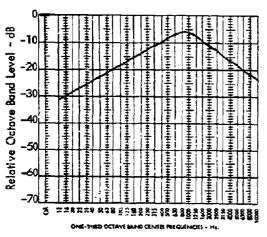
Figure 61. (Continued)



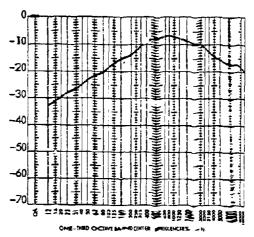




(v) Region 22



(w) Region 23



(x) Region Z4

Figure 61. (Concluded)

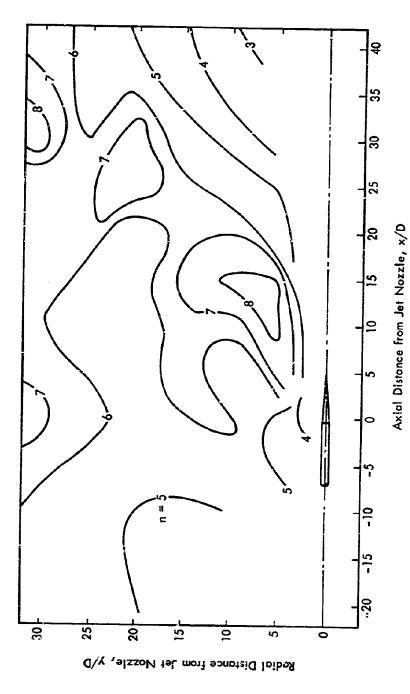


Figure 62. Overall SPL Velocity Expanent Field (After Hermes and Smith, Reference 67)

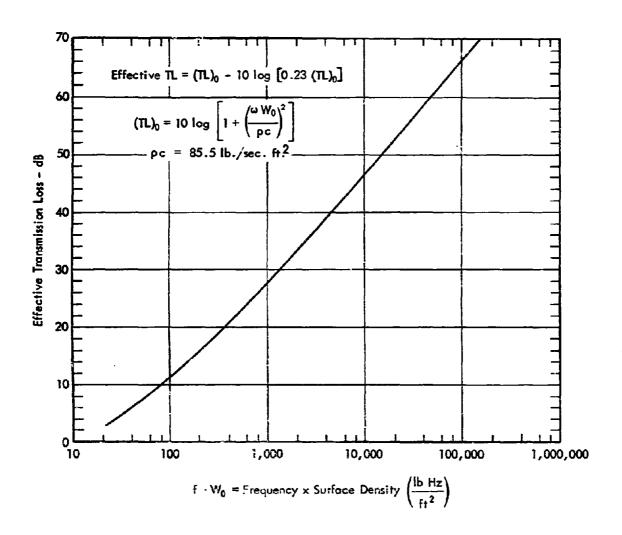


Figure 63. Effective Transmission Loss (Random Incidence). (This curve is approximately 6 dB higher than the usual "limp-wall random incidence mass-law transmission loss" since the loss is based on the observed pressure on the source side of the wall with the wall in place).

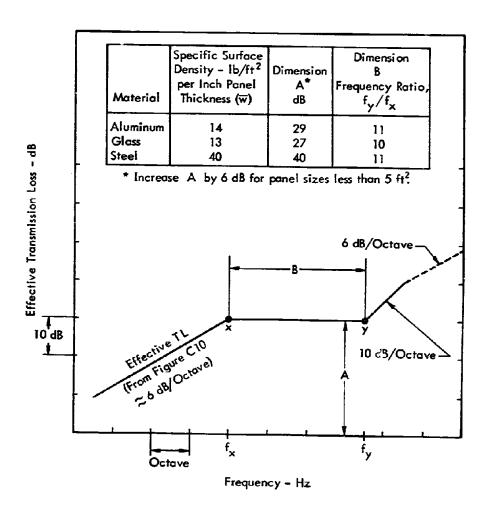


Figure 64. Design Chart for the Change in Effective Transmission Loss of Single Untreated Panels to Include the Effect of Coincidence (Modified from Beranek, Reference 60)

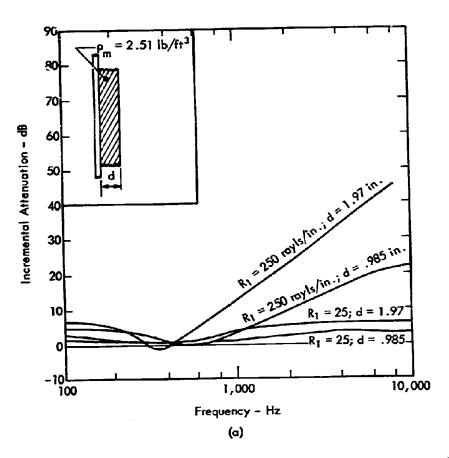


Figure 65. Incremental Attenuatic Due to Adding the Absorbing Structure to the Basic Plate (After Beranek and Work, Reference 62)

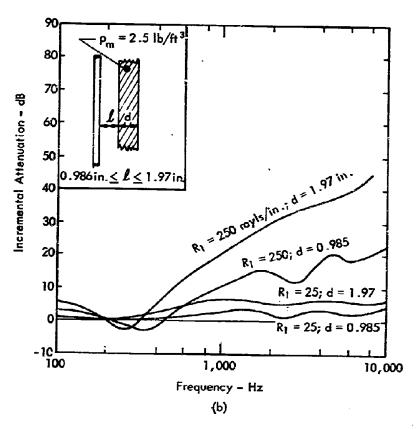


Figure 65. (Continued)

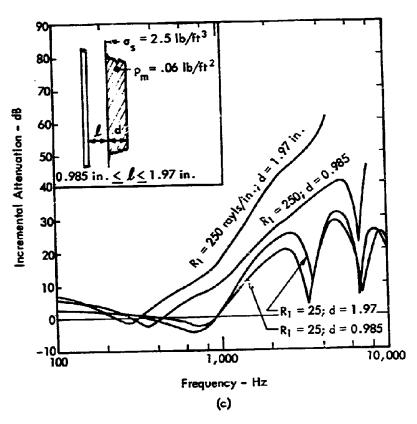


Figure 65. (Continued)

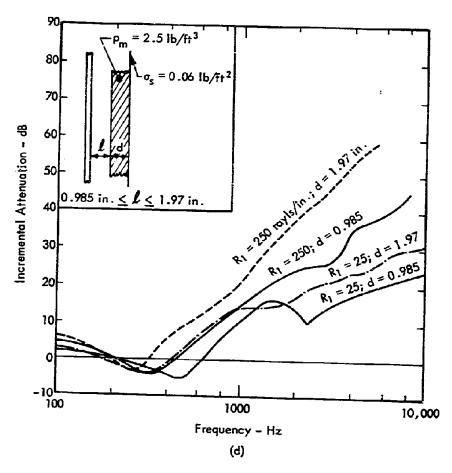


Figure 65. (Continued)

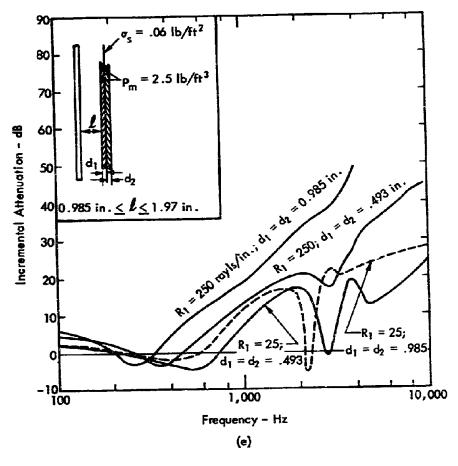


Figure 65. (Concluded)

### 〒 - Average Transmission Coefficient

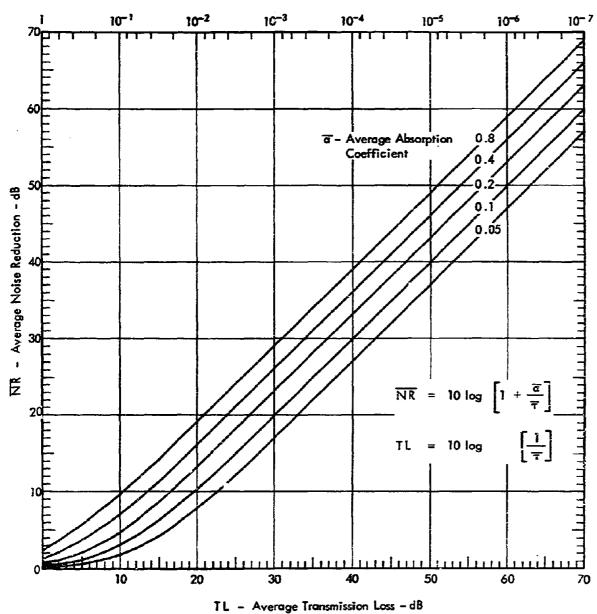


Figure 66. Noise Reduction Versus Absorption Coefficient and Either Average
Transmission Coefficient or Average Transmission Loss of Cabin Walls

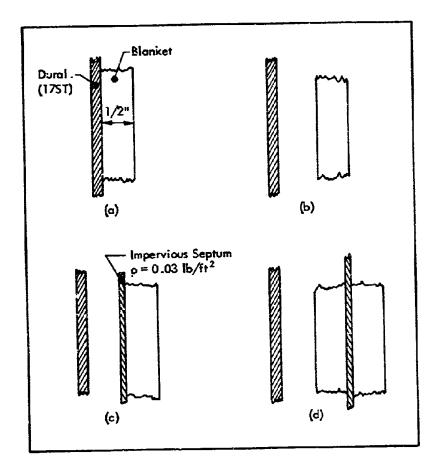


Figure 67. Typical Acoustic Treatments (as Listed in Table IV)

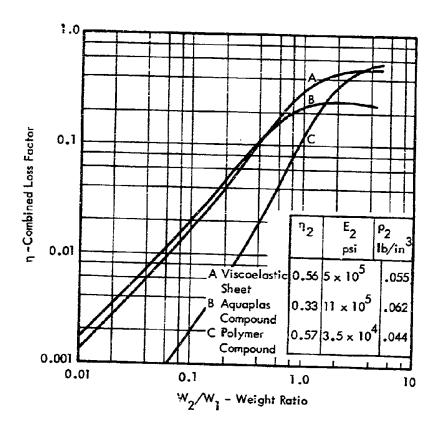


Figure 68. Calculated Combined Loss Factors for Three Typical Unconstrained Commercial Damping Materials Applied to a Uniform Aluminum Plate (Temperature  $\approx 65^{\circ}\text{F}$ , Frequency  $\simeq 75 \text{ Hz}$ 

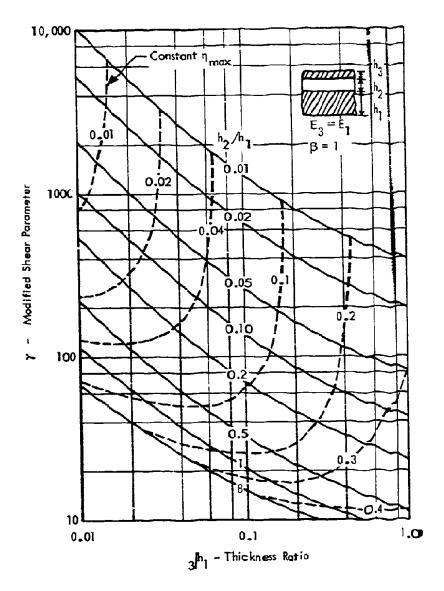


Figure 69. Design Chart for Optimum Constrained Layer
Damping Treatment Based on Modified Shear
Parameter Y

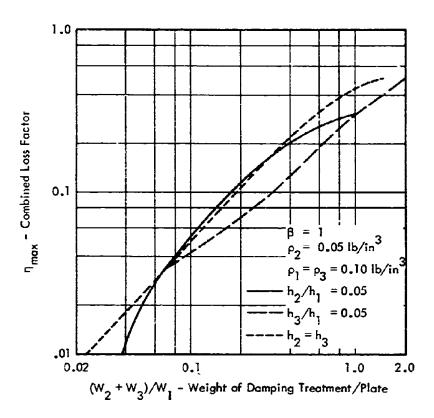


Figure 70. Variation of Combined Loss Factor With The Ratio; Weight of Treatment to Weight Of Basic Plate.

TABLE i

NUMERICAL VALUES OF  $\frac{\overline{R}}{\pi}$  FOR  $J_n'(\overline{R}_{ns}) = 0$ 

s n	0	1	2	3	4
0	0000.0	1.2197	2.2331	3.2383	4.2411
1	0.5861	1.697	2.714	3.7261	4.7312
2	0.9722	2.1346	3.1734	4.1923	5.2036
3	1.3373	2.55!3	3.6115	4.6428	5.6624
4	1.6926	2.9547	4.0368	5.0815	6.1103
5	2.0421	3.3486	4.4523	5.5108	6.5494
6	2.3877	3.7353	4.86	5.9325	6.9811
7	2.7304	4.1165	5.2615	6.3477	7.4065
8	3.0709	4.4931	5 .6576	6.7574	7 .8264

TABLE II

COEFFICIENTS OF THE RATIONAL FRACTION APPROXIMATIONS
FOR SINE AND COSINE INTEGRALS

i	a;	Þ,	c,	ď
8	1.0	1.0	1.0	1.0
6	38.027	40.021	42.243	48.197
4	265.187	322.625	302.758	482.486
2	335.677	570.236	352.018	1114.979
0	38.102	157.105	21.822	449.690

# TABLE III. TEST CASE INPUT DATA

1.	Length of Fuselage	80 ft
2.	Radius of Fuselage	5.42 ft
3.	Frame pitch	19.2 in.
4.	Stringer pitch	8.16 in.
5.	Frame sectional area	0.432 in. <sup>2</sup>
6.	ist moment of area of frame about skin c/l	0.764 in. <sup>3</sup>
7.	2nd moment of area of frame about skin c/l	0.9902 in. <sup>4</sup>
8.	2nd polar moment of frame section	1.0466 in. <sup>4</sup>
9.	Stringer sectional area	0.2302 in. <sup>2</sup>
10.	1st moment of stringer area about skin c/1	0.0574 in. <sup>3</sup>
11.	2nd moment of stringer area about skin c/l	0.1794 in. <sup>4</sup>
12.	2nd polar moment of stringer section	0.254 in. <sup>4</sup>
13.	Stringer warping constant	0.0649 in. <sup>6</sup>
14.	Stringer forsion constant	2.263 in. <sup>4</sup>
15.	Stringer product of inertia	0.0
16.	Fuselage skin thickness	0.04 in.
17.	Lood/unit length (longitudinal)	
18.	Load/unit length (circumferential)	0.0
19.	Load/unit length (shear) in skin	0.0
20.	Number of windows in cross section	2
21.	Window axial length	10.0 in.
22.	Window circumferential length	13.5 in.
23.	Window thickness	0.2 in.
24. 25.		0.0
26.		
27.	Double skin indicator	0
28. 29. 30. 31.	Double skin details	o

## TABLE III. TEST CASE INPUT DATA (Continued)

33.	Dynamic magnification factor			50		
34.	Ski damping treatment material loss fact			9		
35.	Young's modulus for fuselage shell	O!		10.5×106 lb/in.2		
35. 36.	•			7.5 x 10 <sup>6</sup> lb in. <sup>2</sup>		
	Young's modulus for window					
37.	Paisson's Ratio			0.3		
38.	Fuselage shell material density			172.0 lb/ft <sup>3</sup>		
39.	Window material density			200.0 lb/ft <sup>3</sup>		
40.	Skin damping treatment material density			0.0		
41.	Forward speed of aircraft			350.0 ft/sec.		
42.	Air density			0.00238 slugs/ft <sup>3</sup>		
43.	Speed of sound			1120.0 ft/sec.		
44.	Air viscosity			$1.5 \times 10^{-7}$ slugs/ft sec.		
45.	Air pressure			2080 lb/ft <sup>2</sup>		
46.	Internal static pressure			2080 lb/ft <sup>2</sup>		
47.	Internal speed of sound			1120 ft/sec.		
48.	Internal air density	.00238 slugs/ft <sup>3</sup>				
49.	Front of fuselage to jet exit I	35.0 ft				
50.	Front of fuselage to jet exit 2	40 ft				
51.	Fuselage c/l to jet c/l 1			28.0 ft		
52.	Fuselage c/l to jet c/l 2			34 ft		
<i>5</i> 3.	Jet exit velocity			1850 ft/sec.		
54.	Speed of sound in jet			1850 ft/sec.		
55.	Radius of jet			0.925 ft		
56.	Number of layers of acoustic treatment			3 and 4		
<i>57</i> .	Equivalent surface area for internal absor	ption	า	3000 ft <sup>2</sup>		
58.	Type of treatment:	(b) (c)	Airgap Septum Porous blanket density air volume coefficient flow resistance porosity structure factor Septum	2 in. deep 0.06 lb/ft <sup>2</sup> 3.0 in. thick 1.5 lb/ft <sup>2</sup> 30,000 lb/ft <sup>2</sup> 3,000 lb sec/ft <sup>3</sup> 0.9 1.3 0.06 lb/ft <sup>2</sup>		
	2	27				

TABLE IV. ABSORPTION COEFFICIENTS

	-					requer	Frequency - Hz	z			
Type of Structure	6	1 06	125	16.0	250	360	200	720	1000	2000	4000
1 - Figure 67 (a) (b)	£666	000	.33	0.25 0.37 0.33 0.49 0.33 0.54	0.13 0.65 0.65 0.78	0.23 0.83 0.77 0.74	0.4 0.89 0.64 0.59	0.65 0.8 0.53 0.45	0.82 0.75 0.6 0.37	0.9 0.8 0.8	
Nithout Trim Nithout Trim Nithout Trim	(2) (2) (3) (3)	0.03	0.09	0.18	0.09 0.18 0.27 0.48 0.15 0.31 0.52 0.79 0.27 0.62 0.78	0.48 0.79 0.76	0.65 0.84 0.84	0.87 0.91 0.91	0.92 0.92 0.92	0.87 0.87 0.87	0.78 0.78 0.78
Trim Cloth (Impervious) Trim Cloth (Perforated)	<del></del>				0.72		0.73		0.57	0.28	0.13
ft?)	(3) (3) (3) (5) (5)	0.02	7.75	0.15 0.12 0.02 0.02 0.15 2.7 0.7	0.0 0.03 3.0 0.6		0.2 0.02 0.02 3.2 0.6		0.25 0.01 0.005 3.2 1.2		0.35 0.005 0.001 3.2 1.5
Air Absorption (lotal sq. 17 per Unit Volume – ft <sup>-1</sup> )									0.0015	0.0031	0.0015 0.0031 0.0078

<sup>(1)</sup> Reference 74 (2) Reference 60 (3) Reference 75

### Security Classificatio

Security Classification			<del></del>
Security classification of title, body of abetract and index	NTROL DATA - R&!		he overell report te classizied)
1 DRIGINATING ACTIVITY (Corporate author)			T SECURITY CLASSIFICATION
-Wyle Laboratories, P.O. Box 1008		Un	classified
Huntsville, Alabama 35800		25 GROUP	
			/A
3. REFORT TITLE Structural-Acoustic Response,	Noise Transmissio	n Losses	and Interior Noise
Levels of an Aircraft Fuselage Excited by I	Random Pressure F	ields.	
			<b> </b>
4. DESCRIPTIVE NOTES (Type of report and inclusive detec)	<del></del>		
Final January 1967 to January 1968			
5. AUTHOR(S) (Lest name, first name, initial)			<del></del>
Cockburn, James A., and Jolly, Alex C.			
Cockborn, Junes A., and Johy, Alex C.			
6. REPORT DATE	78 TOTAL NO. OF P.	ACEB	78. ND. OF REFS
August 1968	328		75
BE CONTRACT OF GRANT NO.	94 CHISHATOR'S RE		ez#(S)
F33(615)-67-C-1287	AFFDL-TR-6	8-2	
b. PROJECT NO.	}		
c. 1471	SO. OTHER REPORT	HO(3) (Any	other numbers that may be assigned
a. 147102	1		
10. AVA ILABILITY/LIMITATION NOTICES	WR 67-16		
This document is subject to special export	controls and each	n transmî	ttal to foreign govern-
ment or foreign nationals may be made onl			
Laboratory (FDDA) WPAFB, Ohio	y will prior appr	OV G1 O1 7	vii i riigin bynames
11. SUPPLEMENTARY NOTES	12. SPONSORING MILI	TARY ACT	VITY
			mics Laboratory
	Wright-Patter	son AFB,	, Ohio 45433
	<u> </u>		
13. ABSTRACT			
A theoretical and empirical study of the st	ructural –accustic	respons	e and sound transmission
properties of fuselage structures is describe	ed. The external	fluctuat	ing pressure environments
discussed are boundary layer turbulence, j			• •
to investigate the complete behavior of the			
analyzed whose combined characteristics r			
the entire frequency response range of inte			
treated throughout as a coupled dynamic s	•		
system's normal modes. Prediction method			
reduction and internal acoustic fields of u		•	•
tures. The results of this study have been			
the significant parameters affecting sound	transmission to be	e determ	ined. In addition to the
computer programs, empirical design chart	s are presented fo	or carryi	ng out pre-design esti-
mates of the external fluctuating loads due			
overall noise reduction of typical acoustic			•
,,,,,,,,,,,,,,,,,,,,,,,,,,,,,,,,,,,,,,,			
Distribution of this Abstract is Unlimited.			
5 - String of the Control of Children			
DD FORM 1473		1 t.	nclassified

Security Classification

14 KEY WORDS	LINK A		LINX &		LINKC	
KEY WORDS	HOLE	#1	ROLT	#T	ROLE	₩T
Structural-Acoustic Response			i			•
Noise Transmission Losses			1		1 1	
Aircraft Fuselage Soundproofing			!		1	
					1	
	İ		1			
	[ ]		1			
	İ					
	]		1 [			
	i		li			
			1 1			
			1		i 1	
			i i			
	1		j			

#### INSTRUCTIONS

- ORIGINATING ACTIVITY: Enter the name and address of the contractor, subcontractor, grantee, Department of Defense activity or other organization (corporate author) insuing the report.
- 2a. REPORT SECURITY CLASSIFICATION: Enter the overall security classification of the report. Indicate whether "Restricted Data" is included. Marking is to be in accordance with appropriate security regulations.
- 2b. GROUP: Automatic downgrading is specified in DoD Directive 5200. 10 and Armed Forces Industrial Manual. Enter the group number. Also, when applicable, show that optional markings have been used for Group 3 and Group 4 as authorized.
- 3. REPORT TITLE: Enter the complete report title in all capital letters. Titles in all cases should be unclassified. If a meaningful title cannot be selected without classification, show title classification in all capitals in parenthesis immediately following the title.
- 4. DESCRIPTIVE NOTES: If appropriate, enter the type of report, e.g., interim, progress, summary, annual, or final. Give the inclusive dates when a specific reporting period is covered.
- 5. AUTHOR(S): Ester the name(s) of author(s) as shown on or in the report. Ester test name, first name, middle initial. If military, show rank and branch of service. The name of the principal author is an absolute minimum requirement.
- REPORT DATE: Enter the date of the report as day, month, year, or month, year. If more than one date appears on the report, use date of publication.
- 7a. TOTAL NUMBER OF PAGES: The total page count should follow normal pagination procedures, i.e., enter the number of pages containing information.
- 76. NUMBER OF REFERENCES: Enter the total number of references cited in the report-
- ds. CONTRACT OR GRANT NUMBER: If appropriate, enter the applicable minder of the contract or grant under which the report was written.
- 8b, &, & 8d. PROJECT NUMBER: Enter the appropriate military department identification, such as project number, subproject number, system numbers, task number, etc.
- 9s. ORIGINATOR'S REPORT NUMBER(3): Enter the official report number by which the document will be identified and controlled by the originating activity. This number must be unique to this report.
- 9h. OTHER REPORT NUMBER(S): If the report has been assigned any other report numbers (either by the originator or by the sponsor), also enter this number(s).
- 10. AVAILABILITY/LIMITATION NOTIGES: Enter any line itations on further dissemination of the report, other than those

imposed by security classification, using standard statements such as:

- (1) "Qualified requesters may obtain copies of this report from DDC."
- (2) "Foreign announcement and dissemination of this report by DDC is not authorized."
- (3) "U. S. Government agencies may obtain copies of this report directly from DDC. Other qualified DDC users shall request through
- (4) "U. S. military agencies may obtain copies of this report directly from DDC. Other qualified users shall request through
- (5) "All distribution of this report is controlled. Qualufied DDC users shall request through

If the report has been furnished to the Office of Technical Services, Department of Commerce, for sale to the public, indicate this fact and enter the price, if known

- 12 SUPPLEMENTARY NOTES: Use for additional explanatory notes.
- 12. SPONSORING MILITARY ACTIVITY: Enter the name of the departmental project office or laboratory spomsoring (paying for) the research and development. Include address.
- 13. ABSTRACT: Enter an abstract giving a brief and factual summary of the document indicative of the report, even though it may also appear excewhere in the body of the technical report. If additional space is required, a continuation sheet shall accordingly.

It is highly desirable that the abstract of classified reports be unclassified. Each paragraph of the abstract shall end with an indication of the military security classification of the information in the paragraph, represented as (T3), (5), (C), or (U).

There is no limitation on the length of the abstract. However, the suggested length is from 150 to 225 words.

14. KEY WORDS: Key words are technically meaningful terms or short phrases that characterize a report and may be used as index entries for cataloging the report. Key words must be selected so that no security classification is required. Identifiers, such as equipment model designation, trade name, military projets colon name, geographic location, may be used as key words: but will be followed by an indication of technical context. The assignment of links, rules, and weights is optional.

Unclassified

Security Classification